The University Of Sheffield.

Improving the Diagnostic Pathway of Pulmonary Hypertension using Cardio-Pulmonary Magnetic Resonance Imaging

By:

Dr Christopher Samuel Johns

A thesis submitted in partial fulfilment of the requirements for the degree of Doctor of Philosophy

Co-supervised by:

Prof J.M. Wild

Dr AJ Swift

The University of Sheffield

Faculty of Medicine

Department of Infection, Immunity and Cardiovascular Sciences

Academic Unit of Radiology

Submission Date: March 2018

SYNOPSIS

Whilst pulmonary hypertension is a relatively uncommon condition, it is associated with a poor quality of life and poor survival. It is therefore important that we correctly identify patients who suffer from pulmonary hypertension, assess the underlying cause (an essential step for treatment) and seek those who are at risk of death. Current guidelines centre on right heart catheterisation as the recommended tool to answer these important clinical questions.

Since it was first described in the mid-1950s, there have been significant improvements in the survival of patients with pulmonary hypertension, mainly due to the introduction of vasodilator therapies and surgical procedures. There have been parallel improvements in imaging technologies, the most tangible of which is cardiac MRI, allowing time resolved assessment of cardiac structure and function. Despite these improvements in non-invasive methodologies, there remains heavy reliance upon invasively measured pressures and flow for the diagnosis, phenotyping and assessment of risk in patients with pulmonary hypertension.

The aim of this PhD thesis is to evaluate, and hopefully increase, the role of cardio pulmonary vascular MRI in the non-invasive assessment of pulmonary hypertension. I show that cardiac MRI metrics, particularly when combined in a regression model, are able to predict mean pulmonary arterial pressure. Such models are able to identify with reasonable accuracy the presence of pulmonary hypertension in patients referred to a tertiary referral centre. The role of cardio-pulmonary MRI in the assessment of the underlying group of pulmonary hypertension, such as chronic thrombo-embolic pulmonary hypertension and PH-left heart disease, is then explored as identification of patients who may respond to PH specific therapy is an important step. Finally, the role of MRI in the assessment of prognosis, concentrating specifically on patients with PH left heart disease and PH in patients with chronic obstructive pulmonary disease is assessed.

ACKNOWLEDGEMENTS

First and foremost, I would like to thank my joint supervisors, Prof Jim Wild and Dr Andy Swift for their guidance and support. Jim has provided the perfect environment for accomplishing a period of dedicated research and has been pivotal for technological insights. Andy has been a fantastic example of how a radiologist can successfully brave a research career, and has provided exceptional advice and input into the work within this project.

Further thanks are also extended to David Kiely for his enthusiastic input into the clinical context of the work in this thesis, and to the other consultants in the Sheffield Pulmonary Vascular Disease Unit: Robin Condliffe, Charlie Elliot, Ian Sabroe and Thanos Charalampopoulos, for their clinical insights and guidance.

Next, I would like to thank Dan Connolly, who has been my educational supervisor for the last 5 years of Radiology training. Without Dan's helpful "encouragement" I would not have had the opportunity to undertake a period of academic activity. I would also like to thank Professors Paul Griffiths and Nigel Hoggard, who have provided useful guidance along the way. I would also like to thank the thoracic and cardiac radiology department for their help and understanding whilst I have been out of programme.

Finally, I would like to thank my parents and sister who have been supportive since I first told them that I was going back to medical school! In addition, a special thanks to my wife, Gloria, for her understanding of multiple trips away on conferences and late nights writing followed by even later on call shifts.

LIST OF FIGURES

LIST OF TABLES

LIST OF ABBREVIATIONS

AIF	Arterial Input Function
ANOVA	Analysis Of Variance
ASL	Arterial Spin Labelling
ASPIRE	Assessing The Spectrum Of Pulmonary Hypertension Identified At A Referral Centre
AUC	Area Under The Curve
CASL	Continuous Arterial Spin Labelling
CI	Cardiac Index
CMR	Cardiac MRI
PARV$_{CMR}$	Pulmonary Artery And Right Ventricle Model For mPAP Prediction
RVBB$_{CMR}$	Pulmonary Artery And Black Blood Model For mPAP Prediction
RV$_{CMR}$	Right Ventricle Model For mPAP Prediction
CO	Cardiac Output
COPD	Chronic Obstructive Pulmonary Disease
Cpc-PH	Combined Pre And Post PH
CPFE	Combined Pulmonary Fibrosis And Emphysema
CT	Computed Tomography
CTEPH	Chronic Thrombo-Embolic Pulmonary Hypertension
CTPA	Computed Tomography Pulmonary Angiography
CXR	Chest Radiograph
DAP	Diastolic Systemic Arterial Pressure
DCE-MRI	Dynamic Contrast Enhanced Magnetic Resonance Imaging
DECT	Dual Energy Computed Tomography
DIR-FSE	Dual Inversion Recovery Fast Spin Echo
DLCO	Diffusing Capacity For Carbon Monoxide
dPAP	Diastolic Pulmonary Arterial Pressure
DPG	Diastolic Pressure Gradient
DVT	Deep Vein Thrombosis
ECG	Electrocardiogram
Echo	Echocardiogram
ESC	European Society Of Cardiology
FDG	Fluorodeoxyglucose
FEV1	Forced Expiratory Volume In 1 Second
FEV1/FVC	Forced Expiratory Volume In 1 Second/Forced Vital Capacity
FIESTA	Fast Imaging Employing Steady-State Acquisition
FOV	Field Of View
FVC	Forced Vital Capacity
FWHM	Full Width Half Maximum
HIV	Human Immunodeficiency Virus
HP	Hypersensitivity Pneumonitis
HRCT	High Resolution Computed Tomography
IPAH	Idiopathic Pulmonary Arterial Hypertension
Ipc-PH	Isolated Post Capillary Pulmonary Hypertension
IPF	Idiopathic Pulmonary Fibrosis
ISWT	Incremental Shuttle Walk Test
UIP	Usual Interstitial Pneumonitis
IV	Intravenous
IVC	Inferior Vena Cava
IVS	Interventricular Septal Angle
LA	Left Atrium
LAP	Left Atrial Pressure
LHD	Left Heart Disease
LIFOF	Left Ventricular Inflow Outflow
LV	Left Ventricle
LVEDV	Left Ventricular End Diastolic Volume
LVEF	Left Ventricular Ejection Fraction
LVESV	Left Ventricular End Systolic Volume
LVLA	Left Ventricle Left Atrium
MAA	Macro-Aggregated Albumin
MAP	Mean Arterial Pressure
mPAP	Mean Pulmonary Arterial Pressure
MRA	Magnetic Resonance Angiography
MRI	Magnetic Resonance Imaging
MTT	Mean Transit Time
NPV	Negative Predictive Value
NSIP	Non-Specific Pneumonitis
OCT	Optical Coherence Tomography
PA	Pulmonary Artery
PAH	Pulmonary Arterial Hypertension
PASL	Pulsed Arterial Spin Labelling

PAWP	Pulmonary Arterial Wedge Pressure
PBF	Pulmonary Blood Flow
PBV	Pulmonary Blood Volume
pCASL	Pseudo-Continuous Arterial Spine Labelling
PE	Pulmonary Emboli
PET	Positron Emission Tomography
PH	Pulmonary Hypertension
PPV	Positive Predictive Value
PTT	Pulmonary Transit Time
PVR	Pulmonary Vascular Resistance
PVRI	Pulmonary Vascular Resistance Index
RA	Right Atrium
RAC	Relative Area Change
RF	Radiofrequency
RHC	Right Heart Catheterisation
RIFOF	Right Ventricle Inflow Outflow
ROC	Receiver Operator Characteristics
ROI	Region Of Interest
RV	Right Ventricle
RVEDV	Right Ventricular End Diastolic Volume
RVEF	Right Ventricular Ejection Fraction
RVESV	Right Ventricular End Systolic Volume
RVOT	Right Ventricular Outflow Tract
SA	Short Axis
SAP	Systolic Systemic Arterial Pressure
SEEPAGE	Spin-Echo Entrapped Perfusion Image
SNR	Signal To Noise Ratio
sPAP	Systolic Pulmonary Arterial Pressure
SPECT	Single Photon Emission Computed Tomography
SPVDU	Sheffield Pulmonary Vascular Disease Unit
SSFP	Steady State Free Procession
SvO2	Mixed Venous Oxygen Saturations
TAPSE	Tricuspid Annular Plane Systolic Excursion
TE	Echo Time
TLCO	Transfer Factor Of Carbon Monoxide
TOF	Time Of Flight
TPG	Trans-Pulmonary Gradient
TR	Repetition Time
TRICKS	Time Resolved Imaging Of Contrast Kinetics
UK	United Kingdom
VMI	Ventricular Mass Index
WHO	World Health Organisation
WU	Woods Units

1 PULMONARY HYPERTENSION

Pulmonary hypertension is a heterogenous collection of disorders that are characterised by elevated mean pulmonary arterial pressure (mPAP). Whilst considered to be relatively rare (in the UK the prevalence is 97 cases per million) (1), it is associated with a poor quality of life and survival: Median survival in untreated idiopathic pulmonary arterial hypertension is 2.8 years (2). The "abnormal muscularisation" of the pulmonary arterial wall was first described in 1957 by Sheffield pathologist Donald Heath (3) and medical interest in the condition grew in the 1970s due to an epidemic of "primary pulmonary hypertension" (now replaced by the term pulmonary arterial hypertension) due to Aminorex, an appetite suppressant (4,5). Since then, a number of therapies that reverse pulmonary arterial remodelling have significantly improved outcomes in certain forms of the disease; however, there remains poor survival and quality of life in selected patient groups.

1.1 THE PULMONARY CIRCULATION

The human cardiovascular system comprises two circuits in series: the systemic and pulmonary circulations. The main role of the pulmonary circulation is gas exchange; carrying oxygen absorbed by the lungs to the rest of the body and returning carbon dioxide to be expired.

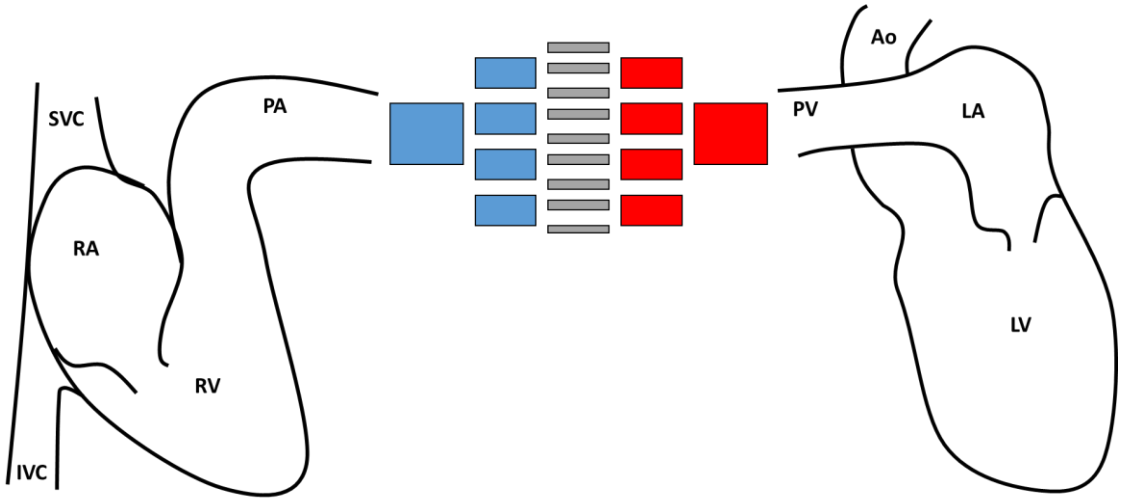

Figure 1.1: Diagrammatic representation of the cardiopulmonary circuit.
SVC: Superior vena cava, RA: Right atrium, IVC: Inferior Vena Cava, RV: Right ventricle, PA: Pulmonary artery, PV: Pulmonary veins, Ao: Aorta, LA: Left atrium, LV: Left ventricle.

In health, the pulmonary circulation is a low pressure, low resistance, highly compliant system, with a normal mean pulmonary arterial pressure of 14±3mmHg (6). Pulmonary hypertension may be caused by increased pulmonary vascular resistance or high pulmonary venous pressures (pulmonary venous hypertension), which can be idiopathic or related to multiple cardiac, respiratory or systemic diseases. These increased pulmonary arterial pressures cause increased right ventricular afterload, leading to right ventricular dysfunction, remodelling, failure and eventual death.

Right ventricular and pulmonary arterial pressures and flows are measured on right heart catheterisation, an invasive technique that uses a balloon tipped thermodilution catheter inserted into the jugular (or less commonly femoral) vein (7). The tip is then advanced into the pulmonary artery, pulmonary artery wedge position, right ventricle and right atrium (1). It has a 1.1% risk of morbidity and 0.06% risk of mortality (8).

From the pulmonary arterial pressure waveform, the systolic pulmonary arterial pressure (sPAP) and diastolic pulmonary arterial pressure (dPAP) can be measured. The mean pulmonary arterial pressure (mPAP) is then defined as $mPAP = \frac{sPAP+2.dPAP}{3}$. The upper limit of normal is considered 20mmHg, but PH is defined as a resting mPAP ≥25mmHg. Interestingly, patients with mPAP 21-24mmHg are followed up closely due to a potential increase in mortality rates, although there is little evidence for how to treat these patients and the term "borderline pulmonary hypertension" is currently not used in guidelines (6).

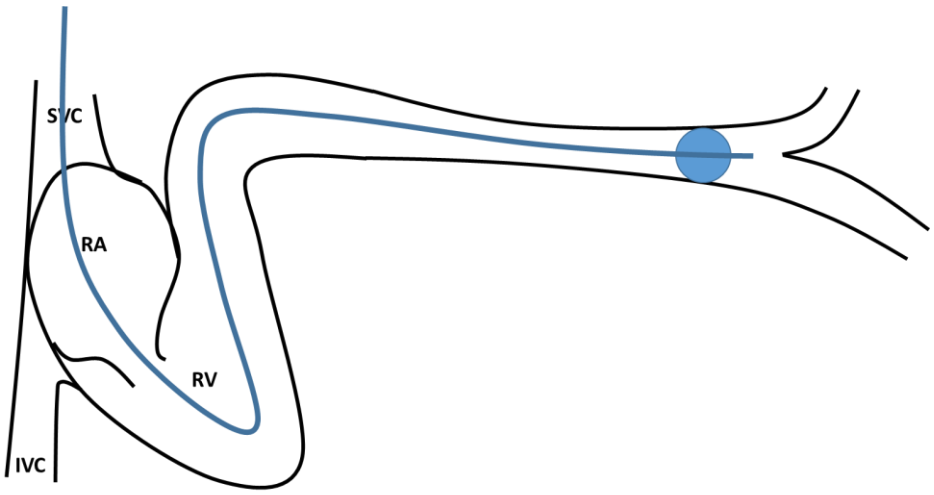

Figure 1.2: Diagrammatic representation of the PAWP measurement.

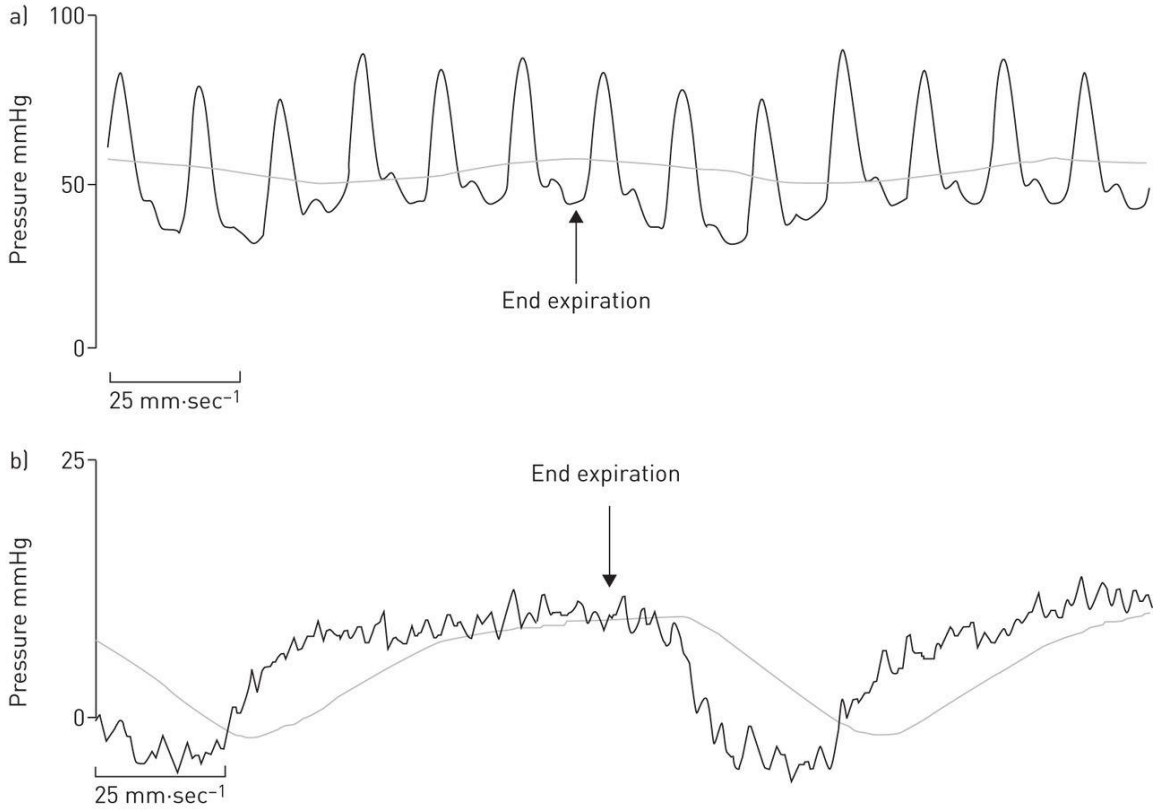

Figure 1.3: The typical pulmonary arterial and pulmonary arterial wedge pressure waveforms. Note the degree of variation with the respiratory cycle. Reproduced under creative commons license from Rosenkranz S, Preston IR. Right heart catheterisation: best practice and pitfalls in pulmonary hypertension. Eur Respir Rev. 2015 Dec;24(138):642–52.

Making assumptions that exclude compliance of the vasculature, Poiseuille's law describes the relationship between resistance (R), length (L) and radius (r) of a cylinder and viscosity of the fluid (μ), in this case blood: $R \propto \frac{8\mu L}{\pi r^4}$. Thus, small changes in vessel radius have a large impact on resistance. In the lung, this resistance can be characterised as the pulmonary vascular resistance $PVR\ (WU) = \frac{mPAP-LAP}{CO}$. Where CO is cardiac output (L/min) and LAP is left atrial pressure (mmHg), estimated through measuring pulmonary arterial wedge pressure (PAWP). Left atrial pressure is estimated using PAWP, where a threshold of >15mmHg defines the presence of left heart disease.

1.2 THE DIAGNOSIS OF PULMONARY HYPERTENSION

Pulmonary hypertension (PH) is defined at right heart catheterisation as a mean pulmonary arterial pressure (mPAP) ≥25mmHg (1). It ranges from mild elevations of pulmonary artery pressure, frequently due to cardiac and respiratory disease, to often severe elevations of pressure in patients with a pulmonary arterial vasculopathy (9). Regardless of aetiology, it has a significant negative impact on both quality of life and survival. The current classification identifies 5 groups with similar clinical and pathological characteristics; Group 1: Pulmonary arterial hypertension (PAH), Group 2: PH due to left heart disease (PH-LHD), Group 3: PH due to lung disease and/or hypoxia (PH-lung), Group 4: Chronic thrombo-embolic PH (CTEPH), and Group 5: PH with unclear/multifactorial mechanisms, which are outlined below (1). Key aspects of PH management include establishing the diagnosis, identifying the form of PH (which defines the optimal treatment strategy) and the serial assessment of disease severity.

The diagnosis of PH is usually suggested by an echocardiogram performed in the breathless patient (9). However, the diagnosis is increasingly suggested following other imaging investigations, such as computerised tomography (CT) (10), which may identify a dilated pulmonary artery or right ventricle.

Once a diagnosis of PH is suspected it is important to identify the cause as this defines the optimal treatment strategy (1). Forms of PH (PAH and CTEPH), for which therapies directed at the pulmonary vasculature have been proven effective are uncommon, whilst for commoner forms (PH-LHD and PH-resp), treatment is currently aimed at the underlying cardiac or lung disease.

As the diagnosis is made using invasive methodologies, diagnostic strategies are dependent on the physician ensuring that further investigation is in the best interests of the patient. An important part of this strategy is an appreciation of factors that increase the pre-test probability of identifying forms of PH for which therapies directed at the pulmonary vasculature are likely to be beneficial. Features from the history are important; a previous history of thromboembolic disease raises the probability of CTEPH. Alternatively, features known to increase the likelihood of PAH, such as the presence of an underlying connective tissue disease (e.g. systemic sclerosis, with a prevalence of PAH 9% (11)), portal hypertension (prevalence of PAH

2-6%(12–14)) and HIV (prevalence of PAH 0.5%(15)) should also be sought. In contrast, mild elevation of pulmonary artery pressures, in patients with severe respiratory or cardiac disease, may not require further investigation where there are no red flag features (such as, severe elevation of pulmonary artery pressures or severe impairment of right ventricular function).

1.3 The Classification of Pulmonary Hypertension

Pulmonary hypertension is classified in 5 groups based upon shared clinical features, pathological findings, haemodynamics, and management decisions (1,16,17).

1.3.1 Group 1: Pulmonary arterial hypertension (PAH)

Group 1 pulmonary arterial hypertension (PAH) may be idiopathic (IPAH), heritable (such as BMPR2 mutation), associated with drugs/toxins or due to an underlying condition (connective tissues disease, HIV, portal hypertension, congenital heart disease or schistosomiasis) (1,16,17). These conditions are all characterised pathologically by remodelling of the precapillary arterioles, and respond to treatment with pulmonary vasodilator therapy (see treatment of PH section on page 26).

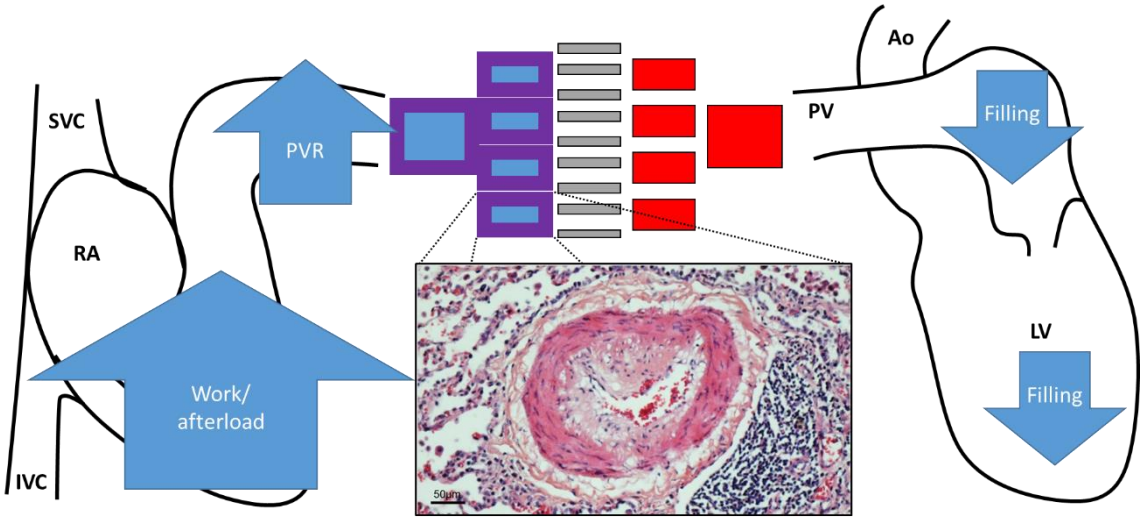

Figure 1.4: Diagrammatic representation of the haemodynamic effects of group 1: PAH.
Pre-capillary pulmonary arteriolar remodelling leads to increased pulmonary vascular resistance (PVR). This increases the load on the right ventricle and also reduces pulmonary venous flow to the left atrium, impairing LV filling. Inset, is a histopathology slide of a vessel with severe neo-intimal formation, there is thickening of the smooth muscle layer. Histology reproduced with permission from Wolters Kluwer Health. Rabinovitch et al, Inflammation and Immunity in the Pathogenesis of Pulmonary Arterial Hypertension Circulation Research, 115, 2014. http://circres.ahajournals.org/content/115/1/165

The underlying pathological mechanism of elevated pulmonary vascular resistance in patients with PAH is due to a number of pathological processes (**Figure 1.5**) (18):

- Sustained pulmonary vasoconstriction
- Obliteration of small and large arteries and arterioles
- Formation of plexiform lesions
- In situ thrombosis
- Concentric thickening of arteriolar wall from
    - Smooth muscle proliferation (Medial hypertrophy)
    - Intimal fibrosis

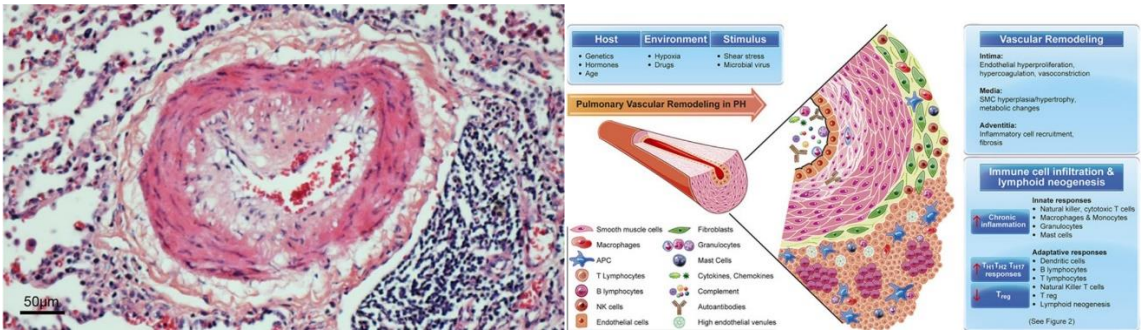

Figure 1.5: *The pathophysiological changes of pulmonary vascular remodelling in PAH.*
Reproduced with permission from Wolters Kluwer Health. Rabinovitch et al, Inflammation and Immunity in the Pathogenesis of Pulmonary Arterial Hypertension Circulation Research, 115, 2014.
http://circres.ahajournals.org/content/115/1/165 (19)

1.3.2 Group 2: Pulmonary hypertension due to left heart disease (PH-LHD)

Pulmonary hypertension is most commonly seen in patients with left heart disease (1,9,20,21), defined on right heart catheter by mPAP ≥25mmHg and a pulmonary arterial wedge pressure >15mmHg (22). It is being increasingly recognised (23), and is associated with a poor prognosis (24–27) and high levels of health care utilisation.

Patients with left heart disease due to valvular disease, systolic, or most often diastolic dysfunction may develop pulmonary hypertension (28). This initially results from passive backward transmission of high left ventricular filling pressures through the pulmonary circulation, previously termed "passive" or "pulmonary venous" pulmonary hypertension (29). Where the pulmonary hypertension is solely due to passive backwards transmission of high left ventricular filling pressures, it is now termed isolated post capillary pulmonary hypertension (Ipc-PH).

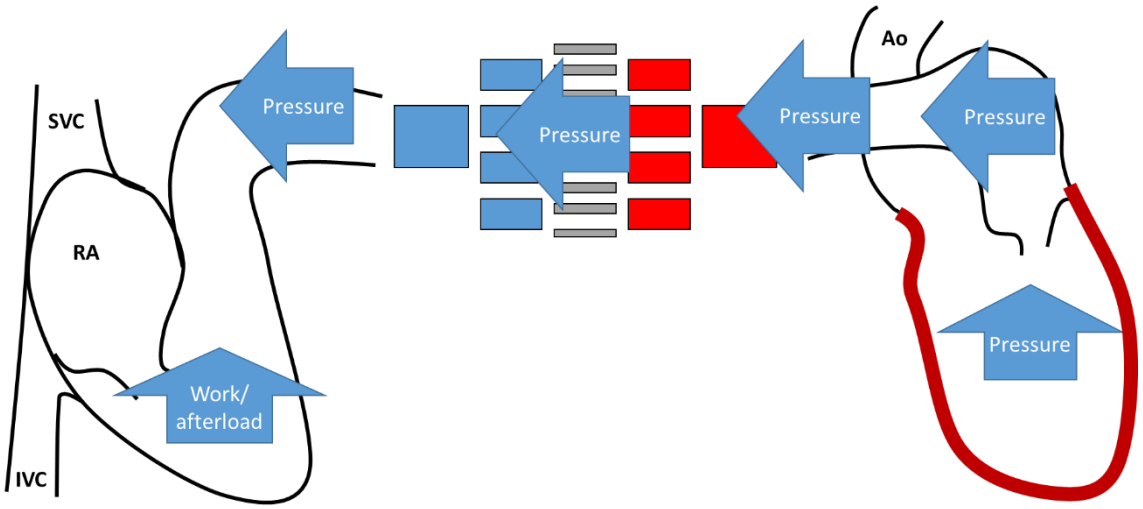

Figure 1.6: Isolated post capillary pulmonary hypertension *(Ipc-PH).*
This results from the backward transmission of high left ventricular filling pressures. It is defined on right heart catheter as PAWP >15mmHg and a diastolic pulmonary gradient (DPG) ≥7mmHg or PVR ≥3WU.

Some patients with post-capillary pulmonary hypertension may develop a degree of pre-capillary vascular remodelling. It is likely that this is due to prolonged elevation of pulmonary arterial pressures (22,30–37) causing stress related pulmonary capillary endothelial injury (38,39). Previously, the difference between mPAP and PAWP (the trans-pulmonary gradient, TPG) was used to identify patients with PH "out of proportion" to left heart disease. A study by Gerges et al identified the diastolic pulmonary pressure gradient (DPG = diastolic pulmonary artery pressure - mean PAWP) as a superior prognostic parameter in patients with post-capillary disease, as

it is not dependent upon cardiac output (30). The 5th world PH symposium, therefore, introduced the classification of combined pre and post capillary pulmonary hypertension (Cpc-PH), defined as mPAP ≥ 25mmHg, PAWP >15 mmHg, DPG of ≥7 and/or pulmonary vascular resistance (PVR) >3 WU (22).

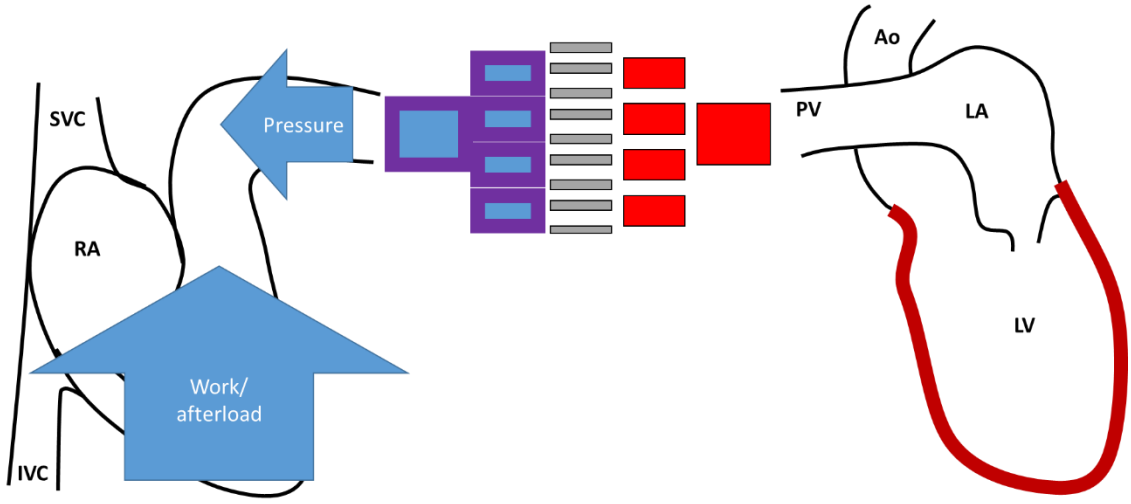

Figure 1.7: Combined pre and post-capillary pulmonary hypertension *(Cpc-PH).*
This results from precapillary pulmonary vascular remodelling in the presence of high left ventricular filling pressures.

Patients with Cpc-PH are at greater risk of deterioration than those with isolated post-capillary PH (Ipc-PH), but may benefit from PAH-specific therapy, especially in the context of randomized controlled trials (37,40,41) (also see ClinicalTrials.gov identifier: NCT02070991). It would be of clinical benefit to increase the role of non-invasive identification and phenotyping of this patient group for identification of potential vasodilator responsive cases in randomised control trials.

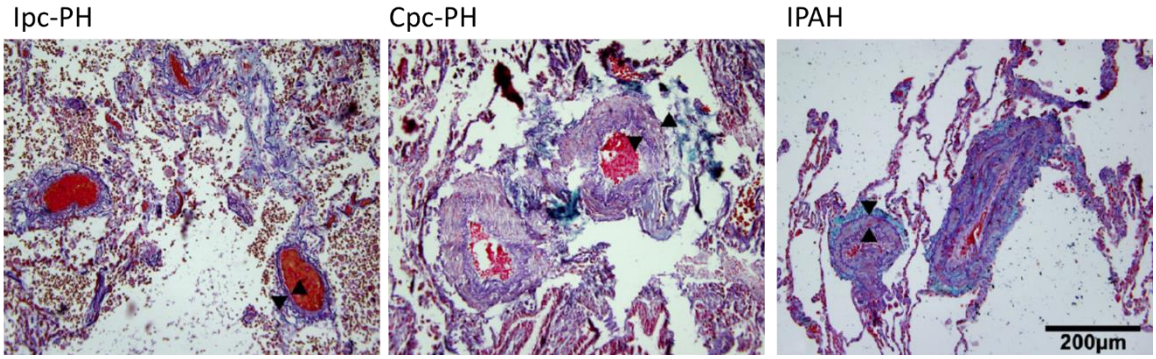

Figure 1.8: Histology from a patient with Ipc-PH (left), Cpc-PH (middle) and IPAH (right*).*
The patient with Cpc-PH has precapillary remodelling that is similar to that in IPAH. Reprinted from Diastolic Pulmonary Vascular Pressure Gradient, Chest 2013, Gerges C, Gerges M, Lang MB, Zhang Y, Jakowitsch J, Probst P, et al, with permission from Elsevier.

1.3.3 Group 3: Pulmonary hypertension due to lung disease or hypoxia (PH-Lung)

There is strong interaction between lung and heart disease, mediated by the pulmonary vascular system. This is particularly evident in patients with chronic obstructive pulmonary disease (COPD), where the presence of pulmonary hypertension is a predictor of death and hospitalisation (42–46). There is an inverse relationship between mPAP and survival and COPD patients with mPAP ≥25mmHg have a 5-year survival rate of only 36% (47). Furthermore, patients with COPD are more likely to die or be hospitalised due to cardiovascular rather than respiratory complications (48).

The prevalence of pulmonary hypertension in lung disease is difficult to assess, but it is likely that there is a high prevalence of patients with "mild" pulmonary hypertension in COPD: reportedly 90% of patients with Gold stage IV COPD have mPAP 20-35mmHg. A significantly lower proportion of patients with COPD have severe pulmonary hypertension, reported to be around 5% of GOLD stage IV COPD patients (44,49,50). Pulmonary hypertension in COPD is thought to result from multiple different mechanisms: hypoxic pulmonary vasoconstriction, polycythaemia (from chronic hypoxia), destruction of the pulmonary vascular bed by emphysema, hyperinflation causing high intrathoracic pressures (above pulmonary venous pressure) and endothelial dysfunction and remodelling (43,51,52).

Idiopathic pulmonary fibrosis (IPF) is a condition with median survival of only 3-5 years (53). The incidence of pulmonary hypertension in interstitial lung disease increases with severity: up to 60% of end-stage idiopathic pulmonary fibrosis patients have pulmonary hypertension (54). Again, increasing mean pulmonary arterial pressure has been shown to be associated with poor outcome in IPF (53).

Patients with combined pulmonary fibrosis and emphysema (CPFE) are also at significantly increased risk of developing pulmonary hypertension. Interestingly, these patients have severe PH and impaired diffusing capacity of the lungs for carbon monoxide (DLCO) but relatively normal lung volumes and little or no airflow obstruction (55).

Pulmonary hypertension in lung disease is categorised into three distinct categories:

1. COPD/IPF/CPFE without PH: mPAP <25mmHg
2. COPD/IPF/CPFE with PH: mPAP ≥25mmHg
3. COPD/IPF/CPFE with severe PH: mPAP ≥35mmHg or mPAP ≥35mmHg with low cardiac index (CI ≤2.0) (50)

This classification is used, as there are important, clinically relevant differences between patients with mPAP 25-35 and ≥35mmHg. The severe pulmonary hypertension group represents the minority of patients, so the majority of cases fall into the 25-35 group. There is an important physiological difference between patients in each group: patients with COPD-PH show a respiratory limitation to exercise ($PaCO_2$ elevation), whereas patients with severe PH have a cardiovascular limitation to exercise (SvO_2 reduction with normal $PaCO_2$) (56).

These differences raise interesting possibilities regarding the phenotyping of lung disease associated with pulmonary hypertension. The first possibility is whether these patients represent a different response to COPD with more cardiovascular involvement. COPD patients show a rapid elevation in mPAP with moderate exercise, suggesting a loss of pulmonary vascular distensability and vessel recruitment (57), similar to patients with idiopathic pulmonary arterial hypertension. The other possibility is that these patients may actually have pulmonary arterial hypertension and coexistent lung disease mislabelled as pulmonary hypertension due to lung disease (50). Both of these arguments raise a possible role for vasodilator therapy, although so far no survival advantage has been shown (58). As such, the identification of PH in COPD is made from a prognostic viewpoint, so reducing the requirement for invasive investigation would be useful in this regard.

Assessment of outcome may be challenging in patients with COPD and lung disease as a whole as they are a heterogenous cohort. Evidence of PA dilatation on CT has been linked with increased risks of exacerbation (59) and patients with COPD have increased levels of coronary heart disease (60), making assessment of the cause of death potentially erroneous.

1.3.4 **Group 4: Chronic thromboembolic pulmonary hypertension (CTEPH)**

Chronic thromboembolic pulmonary hypertension (CTEPH) is a potentially curable form of pulmonary hypertension (PH) (61). The diagnosis requires a mean pulmonary artery pressure (mPAP) ≥25 mmHg at right heart catheterization (RHC), in the presence of at least one segmental defect on perfusion imaging or filling defects on computed tomography pulmonary angiography (CTPA), after at least 3 months of effective anticoagulation (62). The true incidence and prevalence of CTEPH is not known, but the cumulative incidence of CTEPH after survival from an acute pulmonary embolus is reported as 3.8% at 2 years (63). The pathological process is thought to be due to incomplete lysis of the acute pulmonary embolus. The subsequent organisation of the obstructing thrombus leads to obstruction of the pulmonary vascular bed (64). This ultimately causes increased pulmonary arterial pressure, right ventricular dysfunction and, untreated, the prognosis is poor (65).

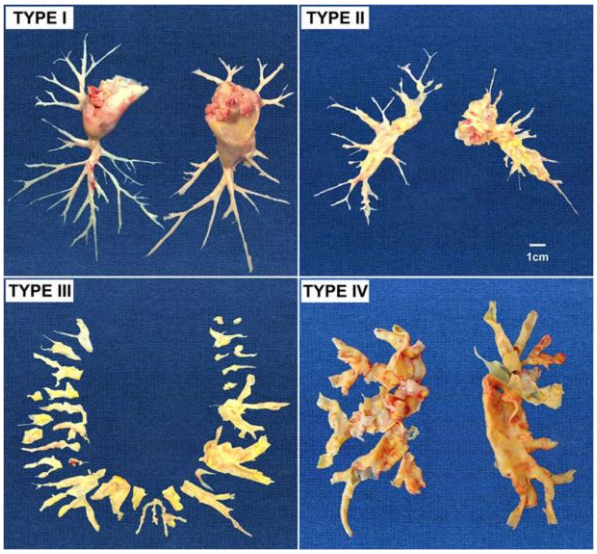

Figure 1.9: *Pulmonary end arterectomy specimens from CTEPH.*
This shows the different patterns of clot that are surgically operable.
Reproduced with permission from Wolters Kluwer Health. Lang IM, Madani M. Update on chronic thromboembolic pulmonary hypertension. Circulation. 2014;130(6):508–18. (314)

Patients with CTEPH usually have a history of either pulmonary embolism (PE) or deep venous thrombosis (DVT) although, a significant proportion may present with unexplained breathlessness or pulmonary hypertension of unknown cause (66,67). It is important that the diagnosis of CTEPH is made as pulmonary endarterectomy is associated with increased survival and a favourable functional outcome in CTEPH (61).

1.3.5 Group 5: Pulmonary hypertension due to unclear or multifactorial mechanisms

This is a heterogenous group of pulmonary hypertension with multiple pathologies and aetiologies, including haematological disorders, systemic disorders, metabolic disorders and other rare causes of pulmonary hypertension. These are grouped together as they share poorly understood mechanisms of development of PH and there is no evidence for the use of pulmonary vasodilators in this group.

1.4 TREATMENT OF PULMONARY HYPERTENSION

The treatment of pulmonary hypertension is related to the underlying cause, so it is important that once the diagnosis of PH is made, the correct group is identified to ensure timely and effective treatment.

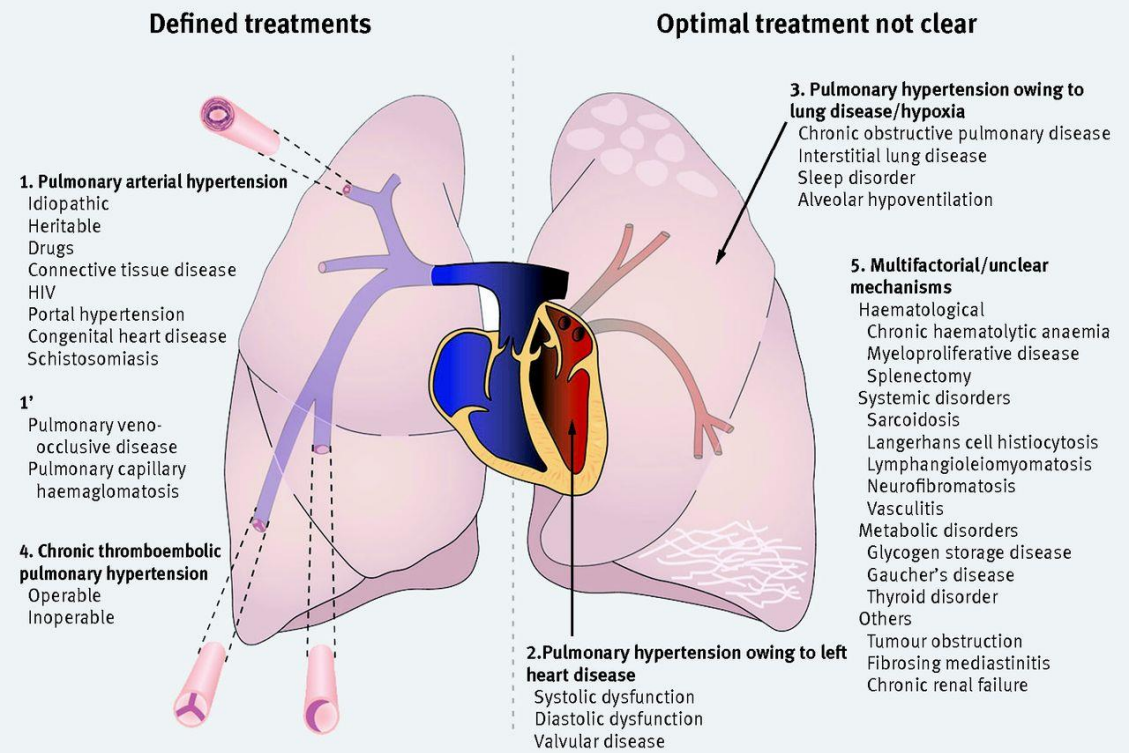

Figure 1.10: A diagrammatic representation of the causes of pulmonary hypertension.
Those on the left have therapies directed at the pulmonary vasculature, in distinction to those on the right. Reproduced from Pulmonary hypertension: diagnosis and management, Kiely et al, BMJ, 2013 with permission from BMJ Publishing Group Ltd. (9)

There are a number of facets to the treatment of patients with PH in addition to the pulmonary vascular therapies outlined below, which include psycho-social support regarding a life threatening disease, supervised rehabilitation and supportive therapy with oxygen and long term O_2. The pulmonary vascular therapies used in PAH are outlined below (1,9,68,69).

1.4.1 Pulmonary vascular therapies

1.4.1.1 High dose calcium channel blockers

Approximately 10% of patients with IPAH show positive vasoreactivity to inhaled nitric oxide, which is defined as a reduction in mPAP ≥10mmHg to an absolute value

≤40mmHg. Of these patients a small number will respond to long term calcium channel blocker, and those that do have a significantly improved prognosis (70,71).

1.4.1.2 Endothelin receptor antagonists

Endothelin receptor antagonists lead to vasodilatation, acting on the pulmonary vascular smooth muscle, and have been shown to improve exercise status and prolong the time to clinical deterioration (72).

1.4.1.3 Prostanoids

Prostacyclin causes vasodilatation and reduces precapillary remodelling. These are generally given either intravenously (iloprost) or subcutaneously (Trepostinil) (73)(74).

1.4.1.4 Phosphodiesterase inhibitors

Phosphodiesterase-5 inhibitors (sildenafil or tadalafil) cause pulmonary vascular dilatation via cyclic GMP and also reduce cellular proliferation (75).

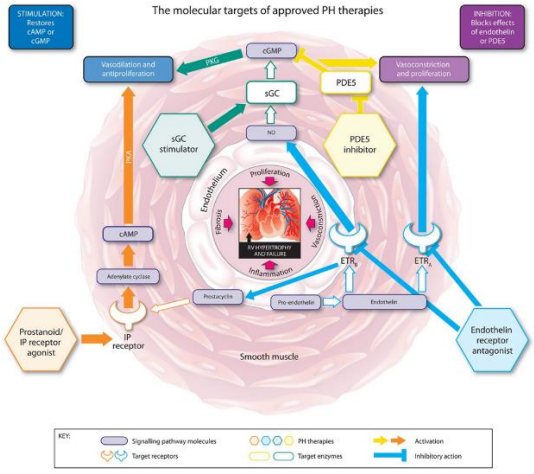

Figure 1.11: *The mechanism of PAH therapies that are currently approved.*
(PDE-5: Phosphodiesterase 5 inhibitors)
Reproduced with permission from Humbert M, Ghofrani H-A. The molecular targets of approved treatments for pulmonary arterial hypertension. Thorax. 2016 Jan;71(1):73–83.

1.4.2 **CTEPH**

Patients with CTEPH have a significant improvement in survival from pulmonary endarterectomy, when surgically accessible. For those who do not have surgically accessible disease, medical therapy as outlined above has also been shown to confer an improvement in survival (61).

1.4.3 **Other causes of Pulmonary Hypertension**

There is currently no body of evidence to support the use of pulmonary vascular specific therapies in the other causes of PH, although there is specific interest in

certain groups of PH-lung and in PH-left heart disease in the context of clinical trials. The current roles of therapy in these groups is directed at the underlying disease.

2 IMAGING OF THE CARDIOPULMONARY CIRCULATION: THE CURRENT CLINICAL PICTURE

The following chapter summarises the imaging methodologies that are currently used in the investigation of pulmonary hypertension[i].

2.1 CHEST RADIOGRAPHY (CXR)

The chest radiograph is a well-established first line imaging technique for the assessment of known or suspected lung disease, providing a general overview of the lungs and pulmonary vasculature. It is helpful in providing a guide to further investigation in patients with unexplained breathlessness, but is insensitive for the detection of pulmonary hypertension, particularly, where pulmonary artery pressure elevation is modest. It provides limited information on causes of pulmonary hypertension, but may identify the presence of significant lung disease such as emphysema, pulmonary fibrosis or sarcoidosis. It has the advantage that is widely available, utilises minimal doses of radiation and is easily interpreted by medical practitioners. Typical findings in pulmonary hypertension are shown in Figure 2.1, these include dilatation of the pulmonary arteries, right atrium and ventricle, although the latter are features of severe disease. In a historical study of patients with IPAH, an abnormality on CXR or ECG was found in 90% of patients at diagnosis (76), however, this represents a highly selected population of patients with severe disease and the accuracy of CXR in an unselected population of patients with suspected pulmonary hypertension has not been evaluated.

[i] This chapter has been published as two review articles: "Current and Emerging Imaging Methodologies in the diagnosis and investigation of Pulmonary Hypertension" in *Expert Review of Respiratory medicine* (313), and "Pulmonary MR angiography and perfusion imaging—A review of methods and applications" in *European Journal of Radiology* (90).

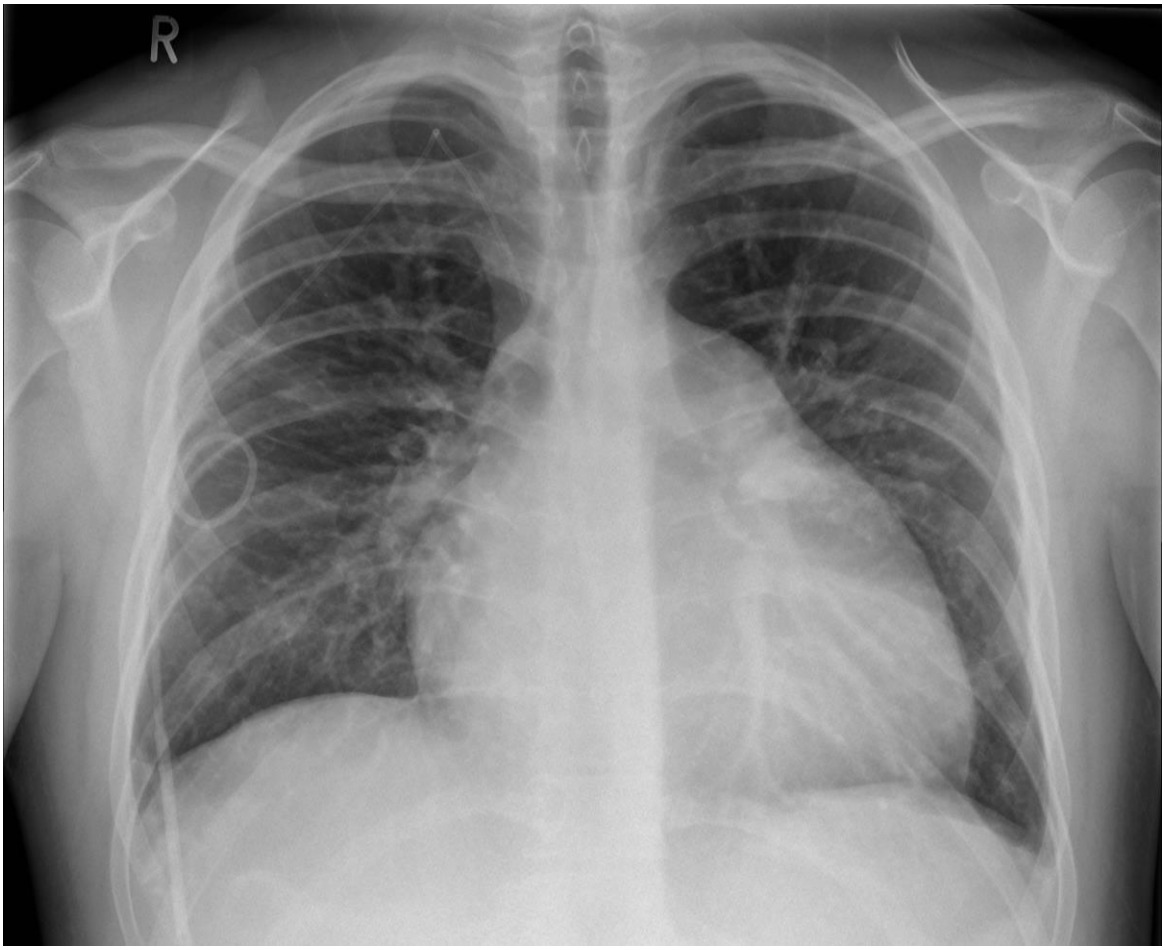

Figure 2.1: The typical chest radiographic features of pulmonary hypertension in a patient with IPAH. *The chest radiograph shows cardiomegaly with dilatation of the main pulmonary artery. There is a tunnelled central line for intravenous delivery of iloprost.*

2.2 ECHOCARDIOGRAPHY (ECHO)

Echocardiography is widely available and is usually the first non-invasive imaging investigation to suggest a diagnosis of pulmonary hypertension. It has the advantage of being portable and easily performed at the bedside. Echocardiography has high temporal resolution, with direct visualisation of cardiac motion, allowing assessment of right and left ventricular function and estimation of pulmonary artery pressure. Systolic pulmonary artery pressure can be measured using Doppler echocardiography; the peak tricuspid regurgitant jet velocity (v), measured from Doppler echocardiography, is used to calculate the trans-tricuspid gradient (TG) (pressure difference between right ventricle and right atrium) using the modified Bernoulli equation, $TG=4v^2$ (77). This is added to an estimate of right atrial pressure to give right ventricular systolic pressure, which, in the absence of pulmonary valvular disease, should be equivalent to systolic pulmonary artery pressure. Right atrial pressure is estimated as either 5, 10 or 15mmHg based on the diameter and respiratory variation of the inferior vena cava (78).

Currently, the non-invasive estimation of pulmonary arterial pressure is made using Doppler echocardiography. Whilst this has the advantage of being cheap and portable, it has a number of limitations, which include inter-operator variability, a requirement for tricuspid regurgitation and over-estimation of pulmonary arterial pressures in certain patients groups. Several studies have identified a strong correlation of echo derived sPAP and right heart catheter measured mPAP in cardiac disease (79,80), however, the diagnostic utility of echocardiography derived pulmonary artery pressure is less accurate in pulmonary hypertension in certain conditions, particularly in the presence of respiratory disease. A prospective study of unselected patients with PH, identified the inaccuracies of Doppler echocardiography derived mPAP, with limits of agreement ranging from -40 to 38.8 mmHg (81). Echocardiographic estimation of sPAP can only be performed in the presence of tricuspid regurgitation and where this is absent, mean pulmonary artery pressure may be estimated using systolic time intervals, such as pulmonary acceleration time (77,82).

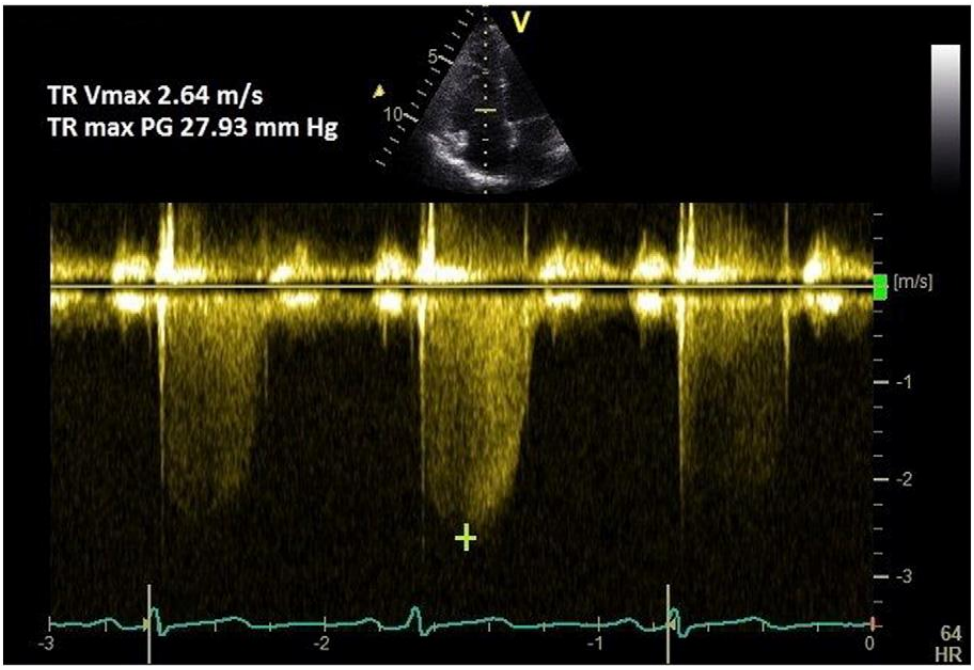

Figure 2.2: Echocardiographic assessment of PH.
Doppler echocardiograph showing the peak tricuspid regurgitant velocity, which can be used to estimate sPAP. Reproduced under creative commons license from (77).

Echo can identify morphological characteristics of chronic right ventricular pressure overload including flattening of the inter-ventricular septum (IVS), increased thickness of the right ventricular free wall and increased left ventricular eccentricity. In addition, tissue Doppler is helpful in the assessment of left ventricular diastolic function (83). Echocardiography also allows an assessment of the cardiac valves and may identify congenital heart defects. Injections of agitated saline (bubble echo) can be used to look for right to left shunting and can identify whether this occurs at an intra-cardiac or pulmonary level (84,85). Trans-oesophageal echocardiography is particularly helpful in the assessment of suspected intra-cardiac defects such as atrial septal defects, often not well visualised on transthoracic echocardiography (86).

2.3 RADIONUCLIDE IMAGING

2.3.1 Ventilation/Perfusion single photon emission tomography (SPECT)

Ventilation/perfusion (V/Q) SPECT is currently recommended by the European Society of Cardiology (ESC) as the first line screening test for chronic thromboembolic pulmonary hypertension (CTEPH) (1). The perfusion image entails injection of 100MBq of 99mTc labelled macroaggregated human albumin, exposing the patient to ionising radiation with an effective dose of approximately 0.017mSv/MBq (87). The macro-aggregated albumin is trapped within the small pulmonary arterioles, and a 3D image of pulmonary perfusion is acquired over around 10 minutes.

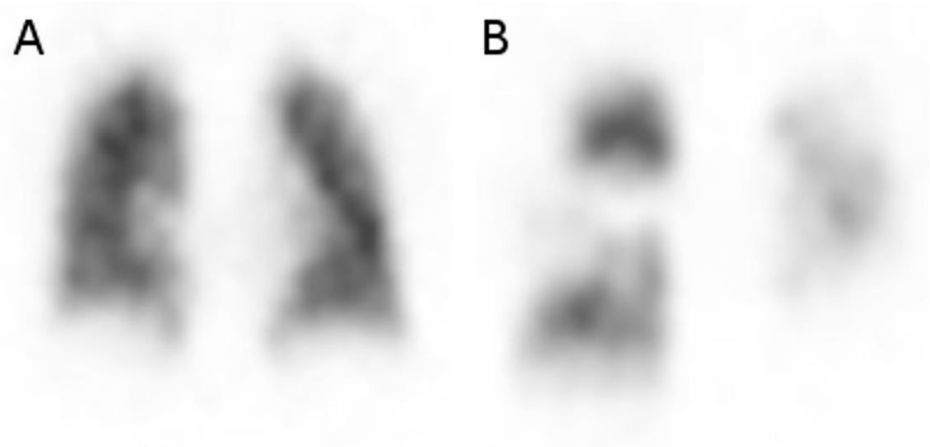

Figure 2.3: *Single coronal slice from perfusion SPECT.*
Patient A has a normal SPECT, patient B has CTEPH. Note the typical wedge shaped perfusion defects that are seen in patient B. If ventilation imaging is performed these are mis-matched.

In CTEPH, there are characteristic wedge shaped perfusion defects (Figure 2.3). When ventilation imaging is performed, the perfusion defects are mismatched to the ventilation. Whilst the recommendation from the ESC/ERS is to perform V/Q scanning, many centres (including Sheffield) have removed the ventilation portion of the V/Q scan, relying on the assumption of normal ventilation from a normal chest radiograph or CT. Ventilation MRI using hyperpolarised gas and perfusion lung imaging (as outlined later in this chapter) provides the potential to image both ventilation and perfusion in a single scan (88).

The advantage of this V/Q scanning over CT is that image interpretation is relatively straightforward, and a normal scan essentially excludes the diagnosis of CTEPH. In contrast, the absence of perfusion due to attenuated vessels and the presence of endo-luminal chronic thromboembolic disease may not be appreciated on CT by less experienced observers. Initial studies demonstrated that scintigraphy was significantly more sensitive than CT, although, more recent studies have demonstrated that in expert hands that CT and 3D MR perfusion techniques are equally sensitive when compared with scintigraphy (89–91). In addition, imaging of systemic vascular beds (kidneys or brain) can be used to quantify the size of a right to left shunt and can be considered in a patient with unexplained hypoxemia and pulmonary hypertension (86).

2.4 COMPUTED TOMOGRAPHY (CT)

Computed tomography (CT) is the main imaging modality for the assessment of pulmonary parenchymal abnormalities (1). CT can be performed either unenhanced, or after the administration of intra-venous contrast. The intravenous contrast, which may be iodinated or less commonly gadolinium based, increases the density of the blood. Depending upon the delay after the injection, the scan may be performed with the contrast in the pulmonary arterial, arterial, venous or excretory phase.

2.4.1 Computed Tomography Pulmonary Angiography (CTPA)

In suspected pulmonary hypertension, a CT pulmonary angiogram (CTPA) is usually performed: a bolus of iodinated contrast is administered into a large proximal vein (typically into a vein in the antecubital fossa) and the scan is acquired at the point of optimal opacification of the pulmonary arteries. In Sheffield, CTPA is performed with 100mls of Iopamidal ("Niopam") 300 injected at a rate of 5mls/second using an injector pump. The national diagnostic reference level (DRL) for CTPA is a dose length product (DLP) of 440 mGy cm (92).

CTPA provides information on the pulmonary vasculature and the size of cardiac chambers, and aids identification of the form of pulmonary hypertension. In patients with PAH there are characteristic CT findings, which reflect disease severity. In a large cohort of patients with pulmonary arterial hypertension a systematic assessment of vascular, cardiac, parenchymal and mediastinal features demonstrated characteristic features of various forms of PAH and also identified important prognostic markers, outlined below (93).

A well-established feature of pulmonary hypertension is increased pulmonary artery (PA) size. A number of thresholds have been used to identify the presence or absence of pulmonary hypertension. In one study, a transverse PA diameter of >29 mm on CT was shown to have a high positive predictive value (97%) (94), whereas another study used a value of 33 mm (95), and a pulmonary artery with a larger diameter than the adjacent ascending aorta (pulmonary artery-aorta ratio >1) has also been shown to be predictive of PH (94). In patients where there is a high prevalence of pulmonary hypertension, such as systemic sclerosis, interrogation of the CT can be helpful, as an enlarged PA may be the first indicator of the presence of pulmonary hypertension. Dilatation of the PA in this setting, in particular a pulmonary to aortic ratio of >1.0,

can be highly predictive (96,97). Serpiginous vessels within the pulmonary parenchyma are seen in severe pulmonary hypertension (Figure 2.4), particularly Eisenmenger's syndrome and IPAH, and are thought to represent neovascularity (98).

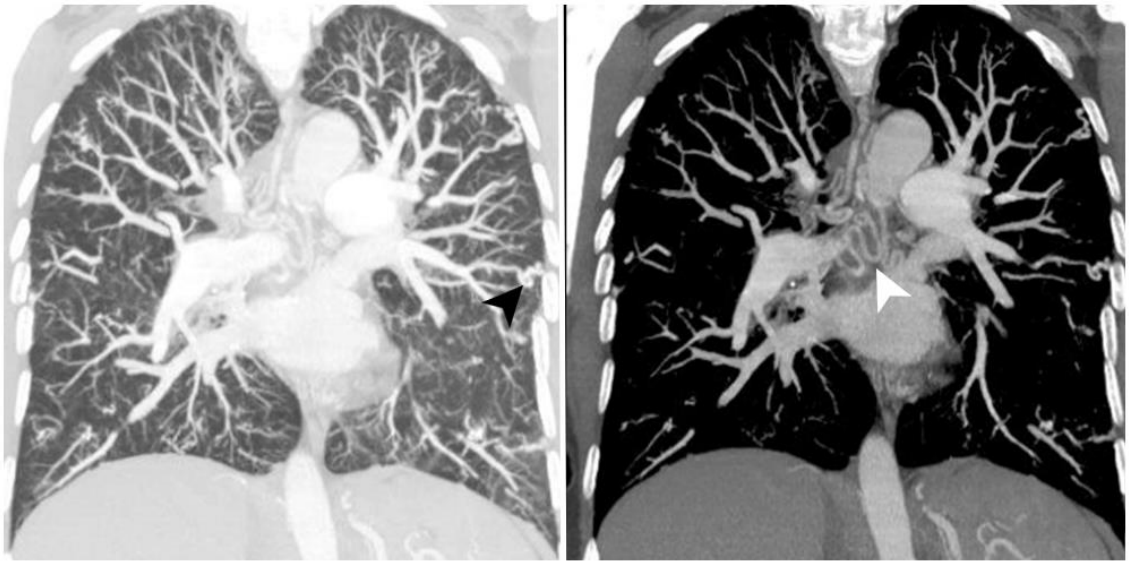

Figure 2.4: *Coronal reconstruction of a CTPA from a patient with Eisenmenger syndrome.*
The left image is presented in lung windows and shows corkscrew neovascularity (black arrow) that can be seen in patients with group 1 PAH. The right image is presented in soft tissue windows and shows dilatation of the bronchial arteries (white arrow).

CTPA is particularly useful in CTEPH, where the distribution of vascular webs, stenosis and mural thrombus allows for treatment planning and assessment of suitability for pulmonary endarterectomy. Figure 2.5 shows the typical CT findings in a patient with CTEPH. CTPA is sensitive to the diagnosis of CTEPH in expert hands (99,100), although there are concerns regarding lower sensitivity with less

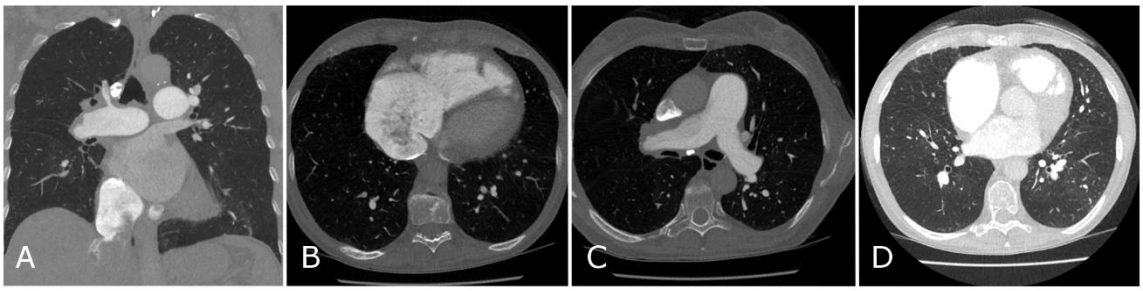

Figure 2.5: *Selected images from a CTPA, showing the typical features of CTEPH.*
Coronal reconstruction of a CTPA, showing mural thrombus in the right pulmonary artery and reflux of contrast into the IVC. B shows marked dilated of the RA and RV. C shows a dilated pulmonary artery with

experienced radiologists (1,101). It can also be used to assess the burden of clot (102)(103).

Pulmonary hypertension causes remodelling and eventual failure of the right ventricle. Whilst right ventricular dilatation and features reflecting its failure are visible on CTPA, these are not features of early disease. CTPA findings of right ventricular compromise include dilatation of the right heart chambers, right ventricular hypertrophy (wall thickness >4mm) and displacement of the interventricular septum towards the left ventricle (104). Changes of right ventricular hypertrophy are usually best appreciated in the right ventricular outflow tract, likely reflecting the reduced quantity of trabeculation. Reflux of contrast into the inferior vena cava and hepatic veins on contrast enhanced CT has been considered to be a marker of the severity of tricuspid regurgitation, commonly seen in pulmonary hypertension (105), often in PH-LHD, although anecdotally, it correlates poorly with the severity of pulmonary hypertension. In severe pre-capillary pulmonary hypertension such as PAH, CTEPH and PH associated with respiratory disease (where there is severe pulmonary hypertension) the left ventricle is under filled and compressed by the dilated RV, causing a small volume left atrium and ventricle. There may also be features of cardiac decompensation visible on CT, such as pleural and pericardial effusions, and an increase in inferior vena cava size, all of which are associated with a poor prognosis (93).

After the administration of IV contrast, 4D (time resolved) CT has the potential to provide detailed information about lung perfusion (106,107), and has been shown to identify abnormal perfusion after acute PE, despite apparent resolution of clot burden (108). Technologies such as iodine mapping have the potential to allow for CT assessment of a single time point of perfusion, without significant increases in dose (109).

2.4.2 **Unenhanced Computed Tomography**

Pulmonary parenchymal changes may help to identify the cause of pulmonary hypertension, and can be assessed on CTPA or non-contrast enhanced volumetric computed tomography (HRCT). In patients with pulmonary hypertension due to lung disease, CT can identify the underlying lung disease and monitor changes in severity. Patients with PAH including IPAH, PAH with systemic sclerosis and PAH associated with congenital heart disease often have centrilobular ground glass opacities (110) (**Figure 2.6**). This is also described in patients with pulmonary veno-occlusive disease, where additional features, such as septal lines and lymphadenopathy, may also be present (111). Patients with CTEPH often have regions of sub-pleural scarring from infarction, and a mosaic pattern of lung attenuation due to perfusion heterogeneity. Although not in routine clinical use, more specialized methodologies in CT such as ECG gating (112) and dual energy CT for perfusion imaging are useful tools for phenotyping disease (113–115).

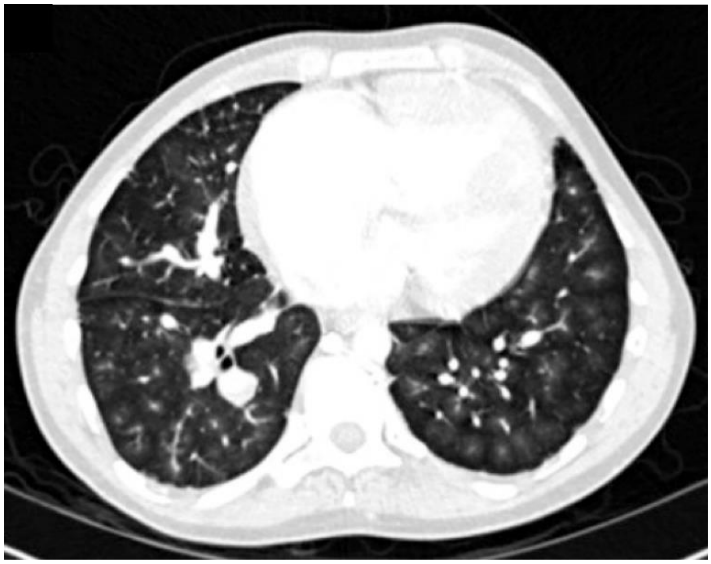

Figure 2.6: *Selected CTPA image showing centrilobular ground glass opacities in a patient with PAH.*

In patients with PAH, CT imaging may also give a clue as to the aetiology of the PAH (93). Features seen in patients with systemic sclerosis and PAH include dilatation of the oesophagus and a ground glass pattern that frequently spares the periphery of the lung. Patients with congenital heart disease frequently have very significant pulmonary artery enlargement (often with mural thrombus and calcification of the pulmonary vasculature) and abnormalities such as pulmonary anomalous venous drainage (frequently associated with a sinus venosus defect) may be identified.

Dilatation of the left atrium is also suggestive of the presence of left heart disease (116).

2.4.3 **Dual Energy Computed Tomography (DECT)**

With dedicated dual or multi-energy CT scanners, it is possible to simultaneously image the lungs and pulmonary vasculature at different kVp, either using different x-ray tubes (115), or oscillating kVp systems (117). This allows images of low and high kV spectra to be produced and can "weight" the image to the k-edge of different materials (118,119). Scanning at 80kV and 120kV after the administration of intravenous (IV) iodinated contrast medium can be used to provide iodine maps, as a marker of pulmonary blood volume at the time point of the scan (120), which may be useful in the assessment of patients with chronic thrombo-embolic pulmonary hypertension (121,122). Dual energy CT may also increase the opacification of the pulmonary arteries as it produces photons with kinetic energy closer to the k-edge of iodine (122) and provide insights into the perfusion of the left and possibly right ventricle (118,120,123). Despite these promising applications in patients with pulmonary hypertension, routine clinical use of dual energy CT is limited by requirement of expensive specialist CT systems.

2.5 MAGNETIC RESONANCE IMAGING (MRI)

MRI is considered the gold standard for functional and morphological assessment of the heart. Standard sequences implemented in pulmonary hypertension include two and four chamber cardiac cine steady state free precession imaging (SSFP), black blood imaging (dual inversion recovery fast spin echo), contrast enhanced MR angiography and 3D dynamic contrast enhanced MR imaging. Cardiac MRI can be used to diagnose pulmonary hypertension (124,125), assess prognosis and serial measurements can be used to assess response to therapy.

2.5.1 The Principles of MRI

2.5.1.1 The MRI signal

Magnetic resonance imaging uses the inherent spin properties of protons to generate images. The patient is placed inside the bore of a large magnet, which generates a strong, constant magnetic field (B_0), in this case at 1.5T. Each proton within the magnetic field have their own magnetic moment, which aligns with the the B_0 field, either parallel or antiparallel (although a slight majority will lie parallel, as this requires less energy). When placed in an external magnetic field all of the protons precess around their own axis, in a similar motion to a spinning top, at a speed that is specific to each nuclear species (the Larmor frequency, in this case protons, which spin at 42.6MHz/T). At this point, the sum magnetisation is parallel to the B_0 field as the transverse moments are random and cancel each other out, this state is termed longitudinal magnetisation.

Radiofrequency (RF) energy is emitted by the RF coils within the scanner. When the RF pulse has the same frequency as the precession of the protons it can deposit energy in them (resonance). This energy deposition causes some protons to flip to the higher energy state of being anti-parallel, and also causes the protons to precess in phase (in the same direction simultaneously). As the protons are precessing in phase, there is a magnetisation vector in the transverse direction, which moves with the precession of the protons.

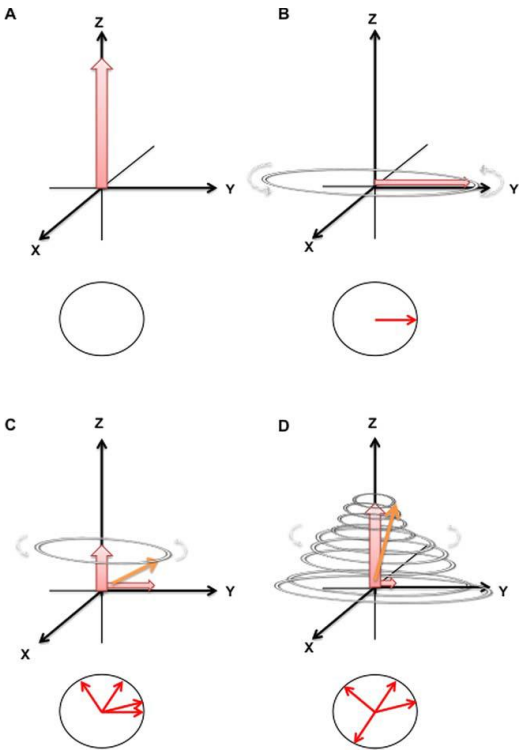

Figure 2.7: *Magnetisation recovery after a 90° RF pulse.*

A. B_0 produces a net magnetisation vector in a longitudinal direction

B. The RF pulse creates transverse magnetisation and reduces longitudinal magnetisation

C. Dephasing reduces the transverse signal as longitudinal magnetisation increases

D. Longitudinal recovery (T1 relaxation)

Images reproduced Reproduced from Understanding MRI: basic MR physics for physicians. Currie S, Hoggard N, Craven IJ, Hadjivassiliou M, Wilkinson ID, 2013 With permission from BMJ Publishing Group Ltd.

As this is a moving magnetisation vector, a current will be generated in any receiver coil near the precessing protons, alternating at the Larmor frequency, forming the MR signal. After the RF pulse switches off there are 2 relaxation processes that take place: the transverse magnetisation disappears (transverse or T2 relaxation) and the longitudinal magnetisation returns to it's original value (longitudinal or T1 relaxation).

T1 relaxation occurs due to energy deposition in the surroundings of the protons, which results in a return to their original parallel magnetization, and this occurs at different rates for different molecules. The T1 time is the length of time for longitudinal magnetisation to return from 0 to $1-e^{-1}$. T2 relaxation is due to the protons falling out of phase, which results from inhomogeneity in the magnetic field due to the inherent properties of the B_0 field and interaction with the magnetic fields from neighbouring nuclei. T2 time is the time taken for transverse magnetisation to return to e^{-1}.

After the RF pulse, the net magnetisation decays following a spiral path, which creates a signal in the RF receiver coils. The signal received is termed the free induction decay (**Figure 2.8**, next page), which has a constant frequency (Larmor), initial magnitude related to longitudinal relaxation and reducing magnitude due to transverse

relaxation (T2* effects). These T2* effects can be counteracted by using 180˚ refocussing echoes, such as in gradient echo imaging.

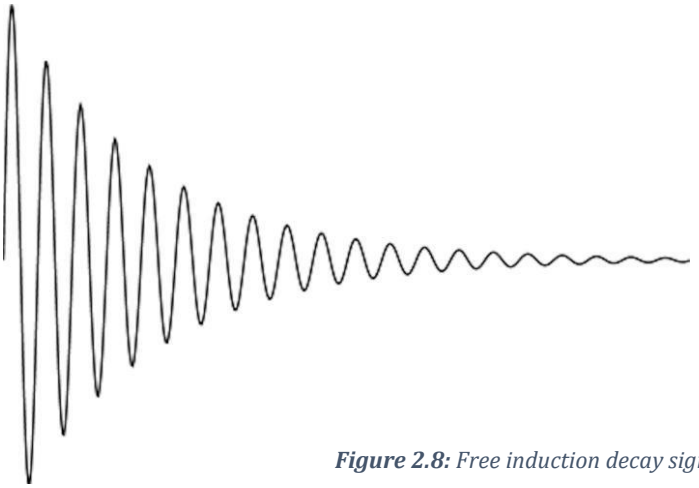

Figure 2.8: *Free induction decay signal*

2.5.1.2 Image reconstruction

The MR signal is localised in 3D space using 3 magnetic field gradients: the slice selection gradient, the phase encoding gradient and the frequency encoding gradient. The slice is selected through applying a gradient in the z direction (parallel to B_0), altering the Larmor frequency of the protons in the z axis, so only the protons in the selected slice are excited by the RF pulse. The slice thickness can be manipulated by adjusting the RF pulse bandwidth or the steepness of the gradient. A gradient applied in the phase encoding direction causes the spin phase to vary linearly and the frequency encoding gradient causes the protons to spin at different frequencies, allowing spatial position of the signal to be assessed.

Whilst all protons in the selected slice are simultaneously excited by the RF pulse, only a single echo signal is recorded for each phase encoding step. In order to complete the image for each slice, the pulse sequence, therefore, has to be repeated many times. During this repetition, the slice selection and frequency encoding are kept the same, but the phase encoding gradient is incrementally increased. Each of these repetitions creates a signal echo, which is stored in a data matrix referred to as k-space. k-space is used to store the data of the MR signal in the signal domain. The data stored in k-

space is converted to an image (in the spatial domain) using Fourier transformation, as demonstrated by an image of the Polaris team in **Figure 2.9**, below (126,127).

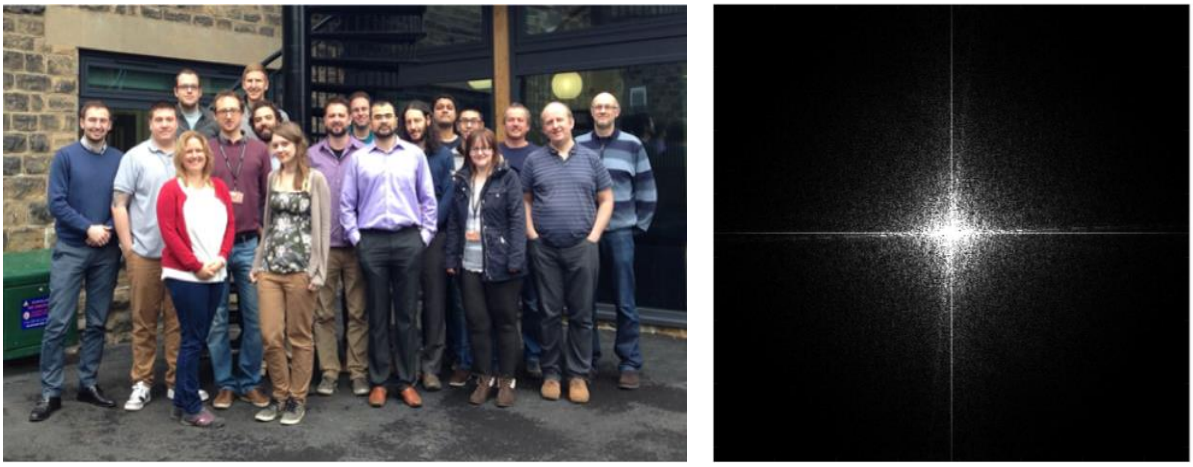

Figure 2.9: *A demonstration of the spatial and the frequency domains.*
Left is an image of the Polaris team demonstrated in the spatial domain. Right is the same image in the frequency domain (after Fourier transformation). k-space is the placeholder for the frequency information acquired by the MRI scanner.

2.5.2 **Cardiac Cine MR Imaging**

Retrospectively ECG gated cardiac cine steady state free procession imaging (SSFP) in the two and four chamber views allow for qualitative and quantitative assessment of the structure and function of the ventricles (128). Segmentation of the ventricular endocardium quantifies the right and left ventricular end-diastolic and end-systolic volumes from which stroke volume and ejection fraction can be calculated. Baseline RV end-diastolic volume and RV ejection fraction and the change in RV ejection fraction over time are both predictive of outcome (129,130). RV stroke volume measured using cine imaging is less reproducible due to inaccuracies in contouring the ventricles (131), although new software allowing for thresholding of trabeculation may improve reproducibility (132). In addition, due to the variable nature of tricuspid regurgitation, RV stroke volume measured by volumetry is a poor reflector of forward pulmonary arterial flow (131).

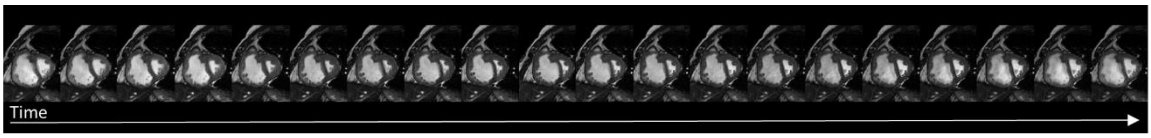

Figure 11: The 20 phases from a mid-chamber slice of the short axis SSFP cine *images*
This patient has IPAH: note the flattening of the interventricular septum and dilatation of the right ventricle.

The myocardium of the left and right ventricles can be segmented, giving right and left ventricular mass. The ratio of these is the ventricular mass index (VMI = RV mass / LV mass), which correlates with mean pulmonary arterial pressure in patients with pulmonary hypertension (133).

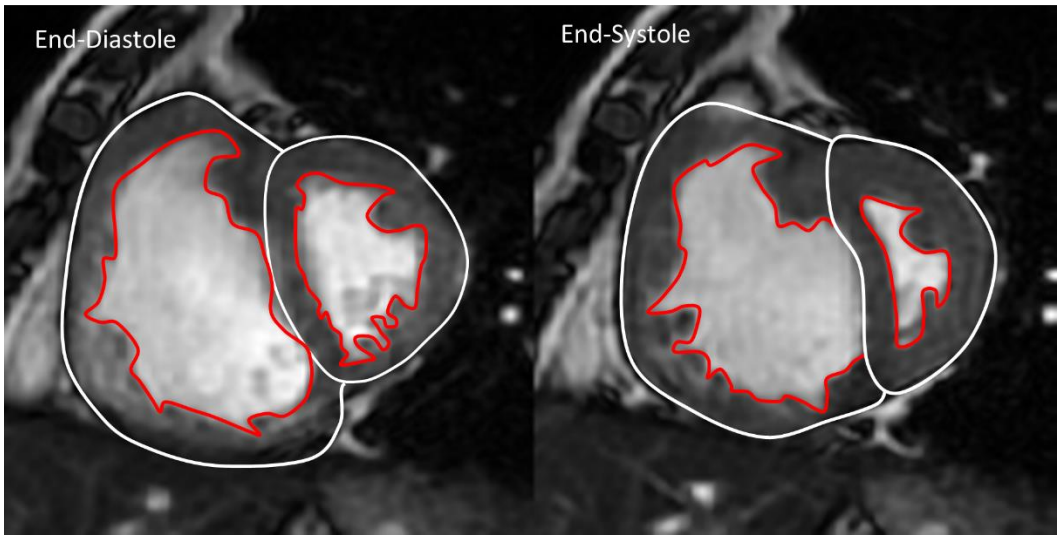

Figure 2.11: Measurement of the epicardial and endocardial contours.
Diagrammatic representation of the endocardial (white) and epicardial (red) contours from the short axis images at end diastole and systole. In this patient with IPAH, the muscle mass of the right ventricle is significantly thickened.

In health, left ventricular pressure is significantly greater than right ventricular pressure, giving a characteristic circular shape to the left ventricle, and a crescentic shape to the right ventricle on short axis views. The angle of the inter-ventricular septum can be measured, it is increased (deviating towards the LV) in patients with pulmonary hypertension (134). This has been shown to correlate with pulmonary artery pressure although in the presence of left heart disease septal angle measurements are less accurate due to the confounding effect of elevated left ventricular diastolic pressures.

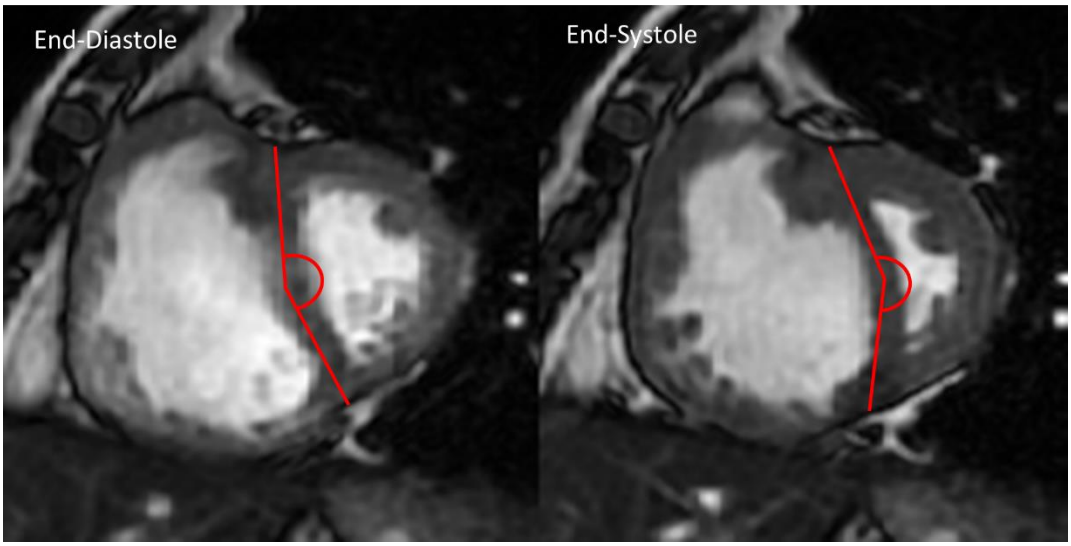

Figure 2.10: Measurement of the interventricular septal angle.
Single slice form a patient with IPAH, left at end diastole and right, at end systole showing the septal position.

2.5.3 **Functional Imaging of Pulmonary Arterial Flow and Motion**

Dual inversion recovery fast spin echo (DIR-FSE) Black blood imaging is used to provide a morphological assessment of the pulmonary arteries and aorta. The protons within the field of view are excited. Any spins that remain in the field of view return signal, any protons that flow out of the field of view are replaced by non-excited protons and return no signal. In health, this results in high contrast between the flowing blood in the pulmonary arteries (no signal/black) and the pulmonary artery wall (high signal/white). A reduction in blood velocity and turbulent flow results in high signal within the pulmonary arteries, a strongly diagnostic and prognostic feature of PH, described as black blood flow artefact (135). Black blood slow flow artefact imaging is potentially limited; as the degree of artefact may be related to the slice thickness, angle of acquisition and field strength, although these are all controllable variables. Care is also required as thrombus also returns high signal, so it is important to look at other sequences to ensure that the signal is due to slow flow rather than clotted blood.

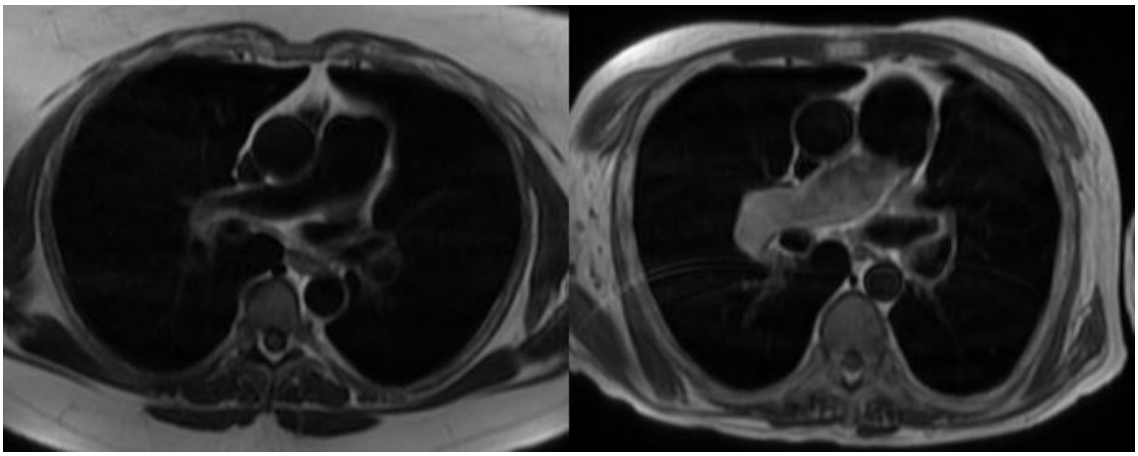

Figure 2.12: Two examples of black blood imaging.
The image on the left is a patient with very mild black blood flow artefact in the lobar artery on the right (grade 1), the image on the right is a patient with severe black blood flow artefact (grade 4).

Phase contrast MRA with velocity sensitising gradients can be used to quantitatively map the blood flow in the major vessels in the lungs in 3-dimensions and can provide insight in to pulmonary vascular resistance and non-steady and turbulent flow in the pulmonary arteries (136,137). Typical velocity encoding settings of Venc 150cm/s would be used to map flow in the pulmonary artery but this may need adjustment for

slower flow in diseases such as pulmonary hypertension where flow velocity is slower and directionality is helical. Pulmonary arterial flow, velocity and area change can be calculated and have been shown to have clinical value in the assessment of patients with PH.

Recent developments with 3D view shared phase contrast methods allow for the acquisition of 4D flow in the pulmonary arteries (138,139). This can be retrospectively interrogated to analyse flow in multiple regions of interest in the heart or pulmonary vasculature. In pulmonary hypertension, vortices can be seen within the pulmonary artery (140), and the duration of these vortices have been shown to be predictive of the presence of PH (141,142). Further research examining the clinical utility of 4D flow MRI is warranted.

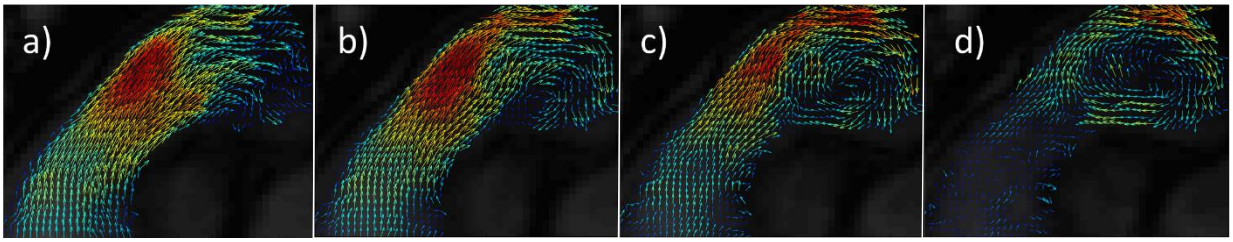

***Figure 2.13*:** Vortical flow in the main pulmonary artery.
Sequential images from 2D phase contrast imaging of the main pulmonary artery in a 63 year old patient with pulmonary hypertension (mPAP = 51mmHg). a), b), c) and d) are from cardiac phases = 5, 8, 11 and 14 respectively. Images courtesy of Dr G Collier and Prof JM Wild.

2.5.4 **Magnetic Resonance Angiography and Perfusion Imaging**

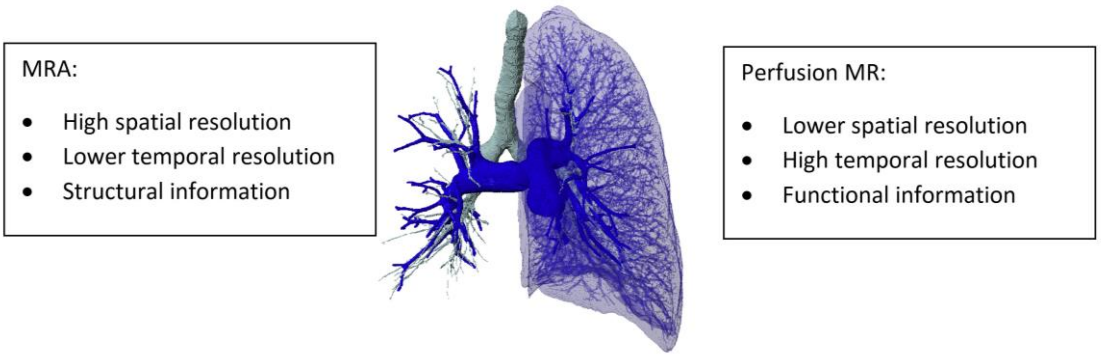

Figure 2.14: *A diagrammatic representation of the basic principles of MR angiography against perfusion MR*

2.5.4.1 Contrast Enhanced MR Angiography

T1 shortening contrast agents can be used to produce high spatial resolution images of the pulmonary arteries and veins with 3D acquisitions within a single breath-hold. Currently, this method is the mainstay of pulmonary MRA in the clinical setting. Typically, a bolus of gadolinium-chelated agent is administered into a large vein, usually in the antecubital fossa followed by a saline flush. Typical contrast doses are 0.1 mmol/kg body weight Gadovist followed by a 20ml saline flush injected at 5ml/sec. In order to reduce venous contamination and gain greatest arterial and venous separation, a single dose of gadolinium at a high injection rate should be used.

The contrast administration is followed by acquisition of a T1 weighted 3D gradient echo dataset. Typical imaging parameters are: TR=2.5-3 ms, TE=1.0-1.5 ms, α=30-40°, matrix=40×192×256, FOV=460 mm, parallel imaging factor R=2 (143). In order to synchronise image acquisition with peak contrast enhancement in the pulmonary vessels, a bolus tracking technique can be employed: a test bolus with a time resolved test scan is used to assess the optimal time from injection to acquisition of central k-space, resulting in images from a single time point (143). An important consideration in pulmonary MRA is the rapid transit of blood through the lungs (3-5 seconds). Centric elliptic phase encoding, with the scan acquisition starting at peak enhancement ensures maximum SNR and optimal separation of arterial and venous phases.

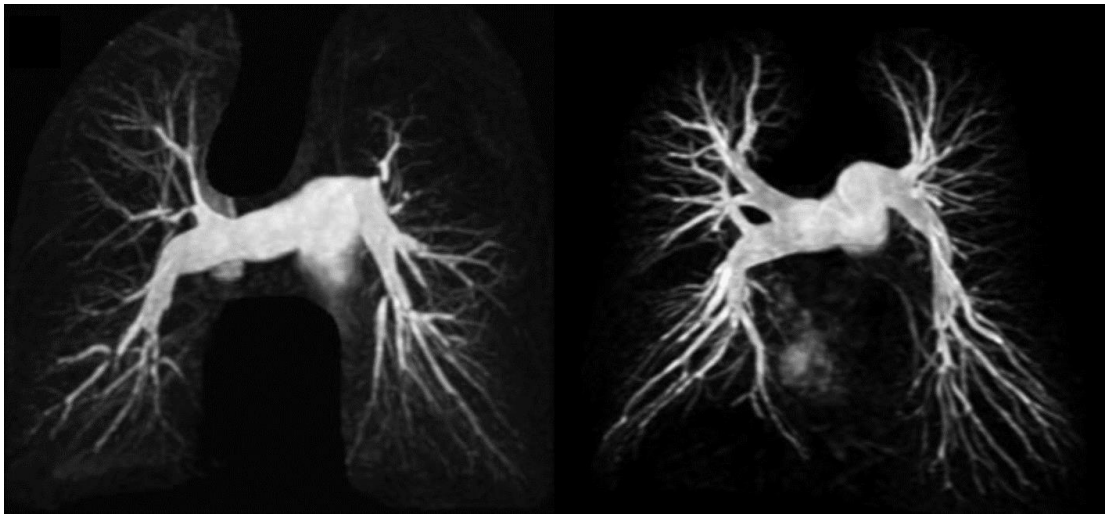

Figure 2.15: Examples of Magnetic Resonance Angiography.
These are reconstructed as a maximum intensity projection (MIP) in a patient with CTEPH (left) and a normal example (right). Reprinted with permission from European Society of Radiology: Springer. European Radiology. Diagnostic accuracy of contrast-enhanced MR angiography and unenhanced proton MR imaging compared with CT pulmonary angiography in chronic thromboembolic pulmonary hypertension, Rajaram et al. 2012.

The contrast bolus passage may also be imaged with time resolved 3D view sharing acquisitions, such as TRICKS (Time Resolved Imaging of Contrast KineticS), allowing for haemodynamic assessment of the pulmonary circulation (Figure 2.16). These view-sharing methods under-sample k-space and share missing k-space between datasets, giving a higher nominal temporal resolution, albeit with the risk of spatio-temporal interpolation artefacts. Other methods for k-space sampling, such as spiral acquisition and view sharing can further reduce scan times, with some centres producing high spatial resolution MRA images with temporal resolution of 1 second through spiral-TRICKS acquisition (144). These methods are useful in the assessment of shunting.

Whilst the majority of clinical MRA is currently performed using extracellular contrast media such as gadobutrol (Gadovist TM) and gadobenate dimeglumine (Multihance TM), there is also the potential to perform pulmonary MRA using intravascular (blood pool) media such as Gadomer-17, Gadofosveset trisodium and ferumoxytol (145). The long residency time of these agents can enable high SNR and spatial resolution with averaging over several breath-holds, however arterial and venous phase separation is sacrificed (145). Blood pool agents for clinical pulmonary MRA are very

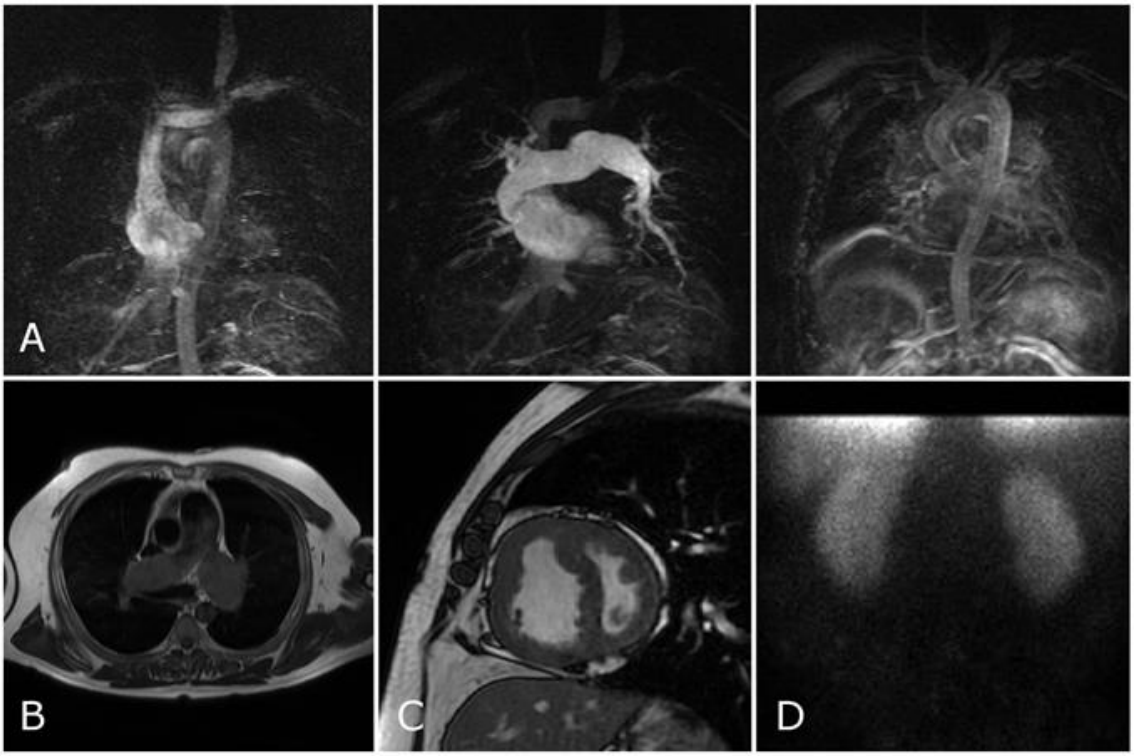

Figure 2.16: Selected images from a patient with IPAH with a patent foramen ovale.
The top row (A) shows the images from the time resolved TRICKs (time resolved contrast kinetics), with increasing time to the right of the image. On the early images, there is contrast within the aorta at a time point before filling of the pulmonary arteries, in keeping with a right to left shunt. This was confirmed with quantitative perfusion single photon emission tomography (SPECT) over the kidneys (D), which shows uptake of tracer in the capillary bed of both kidneys. The black blood imaging (B) shows dilated pulmonary arteries with slow flow/turbulent blood artefact and the 2-chamber image (C) shows significant flattening of the interventricular septum.

helpful in patients that cannot hold their breath as non-breath hold, heavily averaged MRA acquisition methods can be used.

2.5.4.2 Dynamic Contrast Enhanced Perfusion MRI

With a similar methodology to contrast enhanced MRA, but using lower spatial and higher temporal resolution image acquisitions, T1-weighted dynamic contrast enhanced (DCE) perfusion images of the first pass of a gadolinium contrast bolus can be performed. Typical imaging parameters would be: TR=2.0-2.5ms, TE=0.8- 1.0ms, α=30-40°, matrix=32×96×128, FOV=460mm. A lower dose of contrast is needed e.g. 0.05ml per kg patient weight of gadobutrol (Gadovist TM). Again, the nominal temporal resolution of the acquisition can be increased with parallel imaging and view sharing (136) but this can result in spatio-temporal blurring of the signal. In

clinical practice, images acquired with a frame rate of around 0.5 s per 3D lung volume can preserve spatial resolution sufficient for diagnostic purposes. This data is often presented as the peak signal for each voxel, after the original 'unenhanced' dataset has been subtracted, giving a peak perfusion image (90). This is particularly useful in the assessment of CTEPH and has been shown to be of equivalent sensitivity to perfusion SPECT imaging (89). Dynamic contrast enhanced MRI can also be quantified (143,146–148), potentially allowing for easier longitudinal follow up of perfusion abnormalities in pulmonary hypertension (131).

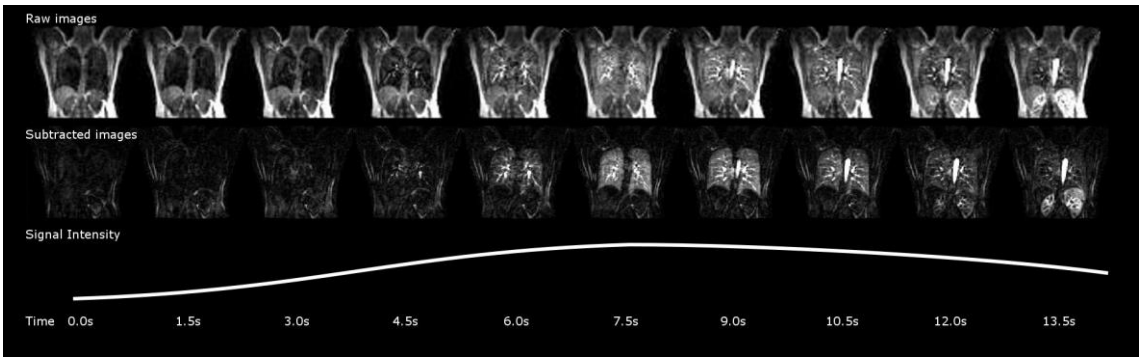

Figure 2.17: The time-course of DCE-MRI showing a single coronal slice in a healthy volunteer.
The top row of images shows the non-subtracted "raw" images, the second row shows the subtracted images and the bottom row shows the pulmonary parenchymal signal change over time. Please note that the images were acquired with a temporal resolution of 0.5 seconds per 3D dataset, but are displayed with a temporal resolution of 1.5 seconds.

Perfusion images can be qualitatively assessed by subtraction of the baseline dataset from the peak enhancement dataset, allowing for a rapid assessment of perfusion defects and their anatomical location. With more detailed post-processing of the entire time resolved data, quantitative assessment of contrast passage kinetics can be made. Pulmonary blood flow (PBF), pulmonary blood volume (PBV) and mean transit time (MTT) can then be quantified and parametric maps of these metrics can be generated from voxel-wise analysis. For absolute quantitative analysis an arterial input function (AIF) is measured in a large feeding artery, often the main pulmonary artery for lung imaging (143). Once the AIF has been established, the signal time curve of a voxel can be converted to concentration time course from the assumption of a linear relationship between signal intensity and contrast concentration. A model free approach using the following equation can be used:

$$C(t) = k\ \frac{S(t) - S_0}{S_0}$$

Where S(t) is the signal time-course, S0 is the mean signal before contrast enhancement and k is an unknown constant. For absolute quantitative analysis, T1 mapping is required in order to convert signal intensity to contrast agent concentration (mmol/litre (mM)). One method of T1 mapping used in quantitative perfusion analysis is the variable flip angle approach. Using a Levenberg-Marquardt fitting algorithm tissue density at equilibrium (m0) and T1 relaxation at equilibrium can be calculated on a voxel-by-voxel basis via:

$$s(\alpha) = m_0 \sin\alpha\ \frac{1 - E1_0}{1 - \cos\alpha\ .E1_0}$$

Where $E1_0$ = exp(-TR.R1$_0$). TR = repetition time used in acquiring the T1-weighted flip angle images. Most commonly three values of flip angle (α) are used generally in the range of 2-35˚. 4D post-injection longitudinal relation rates R1(t) are then calculated:

$$R1(t) = -\left(\frac{1}{TR}\right).ln\frac{1 - (A + B)}{1 - \cos\alpha\ .(A + B)}$$

Where α = flip angle, A = [S(t) – S(0)]/(M$_0$sin α), B = (1 - $E1_0$)/(1 – cosα $E1_0$). Gadolinium concentration maps can then be calculated using the equation:

$$C(t) = \frac{R1\ (t) - R1_0}{\Re 1}$$

Where $\Re 1$is the experimental relaxivity of Gadolinium (4.39 s-1 mM-1 at 37 ˚C) (149). Following contrast concentration mapping the concentration time-curves are fitted using the Gamma variate function:

$$C(t) = K(t - AT)ae - (t - AT)b$$

Where K is a constant scale factor, t is time after injection, AT is appearance time of the contrast agent in the voxel and a/b are arbitrary parameters. It is worthwhile noting that for gadolinium based contrast agents, unlike iodinated contrast agents, contrast concentration and signal intensity are not linearly related at higher concentrations. Constant *K* is related to tissue density, imaging sequence parameters, contrast agent and inspiration level. Hence, it is important that these are kept constant during the experiment (147).

Following the indicator dilution theory (150), once the concentration time course of the AIF is known, $C_{AIF}(t)$, pulmonary blood flow (PBF) can be calculated:

$$C_{VOI}(t) = PBF \int_0^t C_{AIF}(\tau).R(t-\tau)d\tau = PBF\,[C_a(t) \otimes R(t)]$$

Where $C_{VOI}(t)$ is the contrast time course of the region of interest, R is the concentration of contrast remaining at time t and $\otimes$ denotes the convolution integral (146,147). Pulmonary blood volume (PBF) and mean transit time (MTT) are defined as (146):

$$PBV = \frac{\int_0^\infty C_{VOI}(t)dt}{\int_0^\infty C_{AIF}(t)dt} \text{ and } MTT = \frac{PBV}{PBF}$$

Noise filtering is required before these calculations can be reliably made (147) since the inherent image SNR is low. In order for perfusion quantification, it is assumed that there is a linear relationship between signal and concentration. This is not a true assumption and linearity is only seen in a small range of low concentrations of contrast. This is a particular problem for the AIF as the contrast passes in a compact bolus (i.e. high concentration) (151). A robust contrast administration protocol is therefore paramount. One method for overcoming this is to use a smaller dose of contrast such as 0.05ml/kg at a rate of 4ml/second as suggested above. This has the advantage of only requiring a single injection, but with a reduction in SNR in the perfusion image. Another method is to use 2 boluses: a low dose injection to calculate the AIF and a second larger dose to give better SNR in the lung perfusion image (152). When using this split bolus technique the AIF must be recalculated to match the bolus used in the lung imaging part of the sequence. As contrast kinetics are involved, the bolus used to calculate the corrected AIF is shifted by injection duration τ (148):

$$C_{AIF}(t) = \sum^{V/V_p} C_p\,(t + q\tau)$$

It is also important to ensure that there is sufficient time between the first and second bolus to allow for washout of contrast.

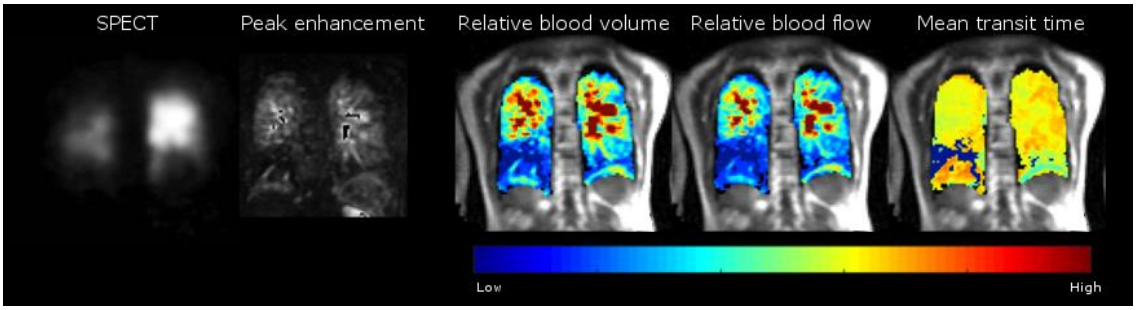

Figure 2.18: Quantitative analysis of Perfusion imaging.
Matched slices from a single patient with CTEPH showing the SPECT and the peak enhancement image from a DCE perfusion MRI scan used clinically, alongside semi-quantitative perfusion maps (pulmonary blood volume, flow, and mean transit time) from a DCE perfusion MRI.

2.5.4.3 Non-contrast enhanced MRA and Perfusion imaging

Long acquisition times and problems with artefacts, such as motion, have limited the use of non-contrast enhanced MRA. Improving MR technologies, concerns about the use of gadolinium from the risk of nephrogenic systemic fibrosis (153) and the desire for non-invasive techniques for paediatrics have increased the motivation for non-contrast enhanced methodology for MR perfusion and angiography.

ECG gated 3D partial-Fourier Fast Spin Echo (FSE) sequences utilise the difference between fast flow and slow flow on T2 signal. In systole, arterial flow is fast and causes a void of T2 signal, whereas in diastole, flow is reduced and returns high T2 signal. Venous systems have slow flow in systole and diastole. Hence, a subtraction image of the systolic from diastolic image gives high T2 signal in the arterial system (137). This method requires ECG gating to allow separation of the diastolic and systolic images, and brings with it the risk of mis-registration.

Balanced steady-state free procession (bSSFP) produces images with the signal proportional to the T2/T1, through refocusing gradient echoes and alternating phases of RF pulses to create a coherent steady state. The TR must be kept very short as bSSFP is susceptible to field inhomogeneity (154). bSSFP is particularly useful in imaging the blood, which has long T2 when compared to the surrounding tissues (143) and has short acquisition times allowing for short breath-holds (154). The high contrast between pulmonary blood pool and lumen make bSSFP an effective tool for assessment of thrombus when MRA and CTPA are inconclusive (155) and a fast 3D bSSFP acquisition provides a quick and contrast free means of generating a pulmonary angiogram (156).

Arterial spin labelling (ASL) images are produced by radiofrequency excitation of the water protons in blood upstream of the imaging field of view through an inversion pulse. These "tagged" protons then flow into the field of view to be imaged (137,151,157). A control image is also taken and the images tend to be presented as a subtraction of the control image from the tagged image. ASL in the lungs is challenging as ECG gating requires a regular heartbeat (151) and spin tagging with selective radiofrequency pulses is confounded by B_0 and B_1 field inhomogeneity. Newer labelling techniques including continuous arterial spin labelling (CASL), pulsed arterial spin labelling (PASL) and a combination as pseudo-continuous arterial spin labelling (pCASL) have the potential to increase the use of ASL in thoracic imaging (158). ASL using the spin echo entrapped perfusion image (SEEPAGE) allows for a single shot acquisition within 5 seconds. SEEPAGE completely supresses the background tissue, so only the "tagged" protons flowing into the field of view return signal. This has the advantage of requiring no subtraction (so no mis-registration) and allows rapid acquisitions within short breath-holds (159). All of these spin-labelling techniques are by nature slice selective methodologies, and therefore are currently limited in terms of lung volume coverage.

Time of flight (TOF) MRA is commonly used in neurovascular and peripheral vascular imaging, but poor spatial resolution, sensitivity to motion (cardiac or respiratory), multi-planar flow directionality, insensitivity to slow flow and sensitivity to susceptibility artefacts limits the utility of TOF MRA in the lungs (160).

Time resolved imaging of the lungs during free breathing with Fourier decomposition (FD) analysis has also been used as a surrogate method to image lung perfusion without the need for contrast or ECG gating. Fourier decomposition has recently been applied to lung ventilation and perfusion imaging (161). During inspiration, the lungs increase in volume, reducing parenchymal signal, increasing again in expiration. During systole, high blood velocity causes dephasing of the MR signal, reducing signal. The respiratory changes occur at a rate of 12-20 beats per minute and the cardiac changes at a rate of 60-80 beats per minutes on average. The difference in frequencies allows for separation using Fourier Decomposition (FD), to give ventilation weighted or perfusion weighted images (162) which have been used for perfusion quantification (163).

2.5.5 **Magnetic Resonance Imaging Tissue Characterisation**

Late gadolinium imaging is in common usage in the assessment of patients with myocardial infarction, to identify myocardial scar tissue (164). The technique utilizes an ECG gated T1-weighted inversion recovery sequence performed 10 to 15 minutes after injection of gadolinium (a T1 shortening agent). Normal myocardial tissue enhance early, but wash-out. Abnormal cardiac muscle traps gadolinium, remaining enhanced on delayed imaging either due to an increase in the extra-cellular space or a break down in the cell membrane of myocytes (164,165). In patients with pulmonary hypertension, late gadolinium enhancement is seen in the right ventricular insertion points and in the interventricular septum (166). It is likely that these areas are exposed to mechanical stress. The extent of right ventricular insertion point and interventricular septum late gadolinium enhancement has been shown to correlate with right ventricular function (167).

A similar pattern of disease can be seen on native T1 mapping (i.e. non contrast enhanced T1 values), with high native T1 values in the RV insertion points (168), which correlates with right ventricular dysfunction (169). This allows the potential to characterize myocardial tissue, without the use of contrast media and provide a method for the identification of patients at risk of adverse right ventricular remodelling and right ventricular failure.

2.5.6 **Reproducibility of Cardio-Pulmonary Vascular MRI metrics**

Measures of the structure and function of the right ventricle, left ventricle and the pulmonary artery have been shown to have high inter and intra-observer reproducibility. **Table 2.1** summarizes the previously calculated inter and intra-observer reproducibility metrics for commonly measured MRI metrics of the right and left ventricle and the pulmonary artery in 30 patients with pulmonary hypertension (170).

Table 2.1: *Reproducibility of cardio-pulmonary vascular MRI metrics in pulmonary hypertension.*

	Inter		Intra	
	ICC	95% CI	ICC	95% CI
Right Ventricle				
RVEDV	0.988	0.974 - 0.994	0.996	0.991 - 0.998
RVESV	0.991	0.981 - 0.996	0.988	0.974 - 0.994
RVEF	0.957	0.910 - 0.979	0.940	0.875 - 0.972
RVSV	0.928	0.848 - 0.966	0.990	0.979 - 0.995
RV mass	0.947	0.763 - 0.980	0.990	0.979 - 0.999
VMI	0.959	0.910 - 0.981	0.984	0.966 - 0.992
Left Ventricle				
LVEDV	0.991	0.981 - 0.996	0.996	0.992 - 0.998
LVESV	0.959	0.810 - 0.986	0.986	0.970 - 0.993
LVEF	0.918	0.718 - 0.968	0.973	0.942 - 0.987
LVSV	0.979	0.922 - 0.992	0.973	0.903 - 0.990
Interventricular Septal Position				
IV septal angle systole	0.972	0.907 - 0.989	0.988	0.975 - 0.995
Pulmonary Arterial Structure/Function				
PA systolic area	0.995	0.990 - 0.998	0.996	0.992 - 0.998
PA diastolic area	0.986	0.957 - 0.995	0.986	0.957 - 0.995
Phase contrast MRI forward flow	0.999	0.997 - 0.999	0.999	0.997 - 0.987
Phase contrast MRI backward flow	0.902	0.795 - 0.953	0.997	0.992 - 0.999

Reproduced with permission from Dr AJ Swift (170).

2.6 DIGITAL SUBTRACTION PULMONARY ANGIOGRAPHY (DSA)

Digital subtraction angiography (DSA) of the pulmonary artery is an invasive test, in which iodinated contrast is administered through a catheter in the pulmonary artery under fluoroscopic visualisation. DSA is used in many centres in patients with chronic thromboembolic disease to guide surgical intervention (171) and is currently recommended in the ESC guidelines as a final step in the surgical assessment of CTEPH. It can be performed in conjunction with balloon pulmonary angioplasty, a treatment methodology for non-surgical CTEPH which has increasing interest (172–175). The advent of CTPA and MR angiographic techniques provide an alternative non-invasive approach to assess suitability for pulmonary endarterectomy. As a result, digital subtraction angiography is reserved for problem solving in the Sheffield Pulmonary Vascular Disease Unit (176).

2.7 RESEARCH BASED METHODOLOGIES

2.7.1 Positron Emission Tomography (PET)

Fluorodeoxyglucose (FDG) is a glucose analogue, which is typically bound to 18-Fluorine, a positron emitter. 3D images of the uptake of FDG can be produced using a PET scanner (positron emission tomography), which allows for qualitative and quantitative assessment of tissue glucose uptake and therefore, an assessment of metabolic activity. As the spatial resolution of PET scanning is relatively low (typical voxel sizes are 5mm (92)), the scan is performed at the same time as CT, for anatomical location. In IPAH, there is heterogenous uptake within the lung parenchyma and significantly increased FDG uptake within the right ventricle, a prognostic marker (177–180). In a few centres the availability of PET-MRI scanners allows anatomical location of the uptake on cardiac MRI (181), providing clearer anatomical detail from the soft tissues and simultaneous assessment of cardiac function.

In addition, PET may be used in patients with proximal CTEPH, particularly when extending into the pulmonary trunk when conditions such as pulmonary sarcoma are suspected. Whereas, tumour would be expected to show increased uptake of FDG this would not be the case with chronic clot, Error! Reference source not found. (113,182). T his information can be used to inform discussions with patients prior to surgery.

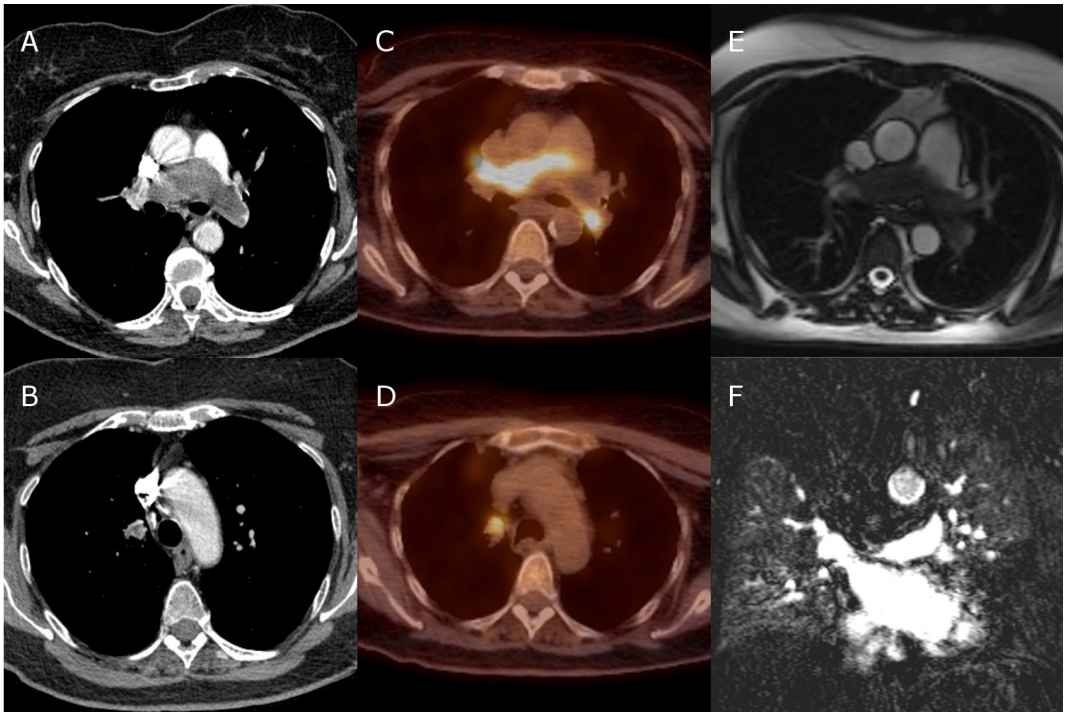

Figure 2.19: *A selection of images from a patient with a pulmonary artery angiosarcoma. There is a soft tissue density filling defect on the CTPA within the proximal pulmonary artery, extending into both left and right pulmonary arteries (A), and also extending into the right upper lobe (B). This is hot on the PET-CT scan (C+D). SSFP cine cardiac MRI demonstrates the mass as an isodense filling defect in the pulmonary arteries (E) and there is a perfusion defect in the right upper lobe (F).*

2.7.2 Optical Coherence Tomography (OCT)

CTPA and DSA are frequently used in the assessment of vascular defects in patients with CTEPH; however, they only provide information on the lumen, with limited information about the vessel wall. Optical coherence tomography is an invasive technique, performed at pulmonary angiography, which uses near infra-red light to image the vessel wall, with resolutions of 10-20μm (183). OCT can demonstrate the intimal thickening that is characteristic of PAH (184,185), subclinical pre-capillary remodelling in patients with borderline pulmonary arterial pressures (mPAP 21-24mmHg) (184) and reversal of remodelling after vasodilator therapy (184,186). In CTEPH, OCT can be used as an adjunct to balloon pulmonary angioplasty and allows for the assessment of the underlying morphology of vascular lesions (187). It has the potential to separate fresh 'red' thrombus from chronic 'white' thrombus (188), identifying suitable targets for balloon angioplasty. Due to the invasive nature of this test and requirement of specialist equipment and expertise, it is currently confined to a small number of centres.

2.8 CLINICAL APPLICATIONS OF IMAGING PH

The key steps for the investigation of patients with suspected pulmonary hypertension are: i) diagnose, ii) identify the cause, iii) identify at risk patients, and iv) assess response to treatment. The role of imaging in this regard is outlined below.

2.8.1 Making the Diagnosis of Pulmonary Hypertension

The possibility of pulmonary hypertension is usually first suggested by echocardiography although it may be made incidentally by an imaging investigation performed for unexplained breathlessness (e.g. demonstrating enlargement of the central pulmonary arteries on chest radiograph or CT). The diagnostic approach for patients with suspected PH was highlighted in the most recent ERS/ESC guideline (1), however, the approach is dependent in part on local availability of imaging and expertise.

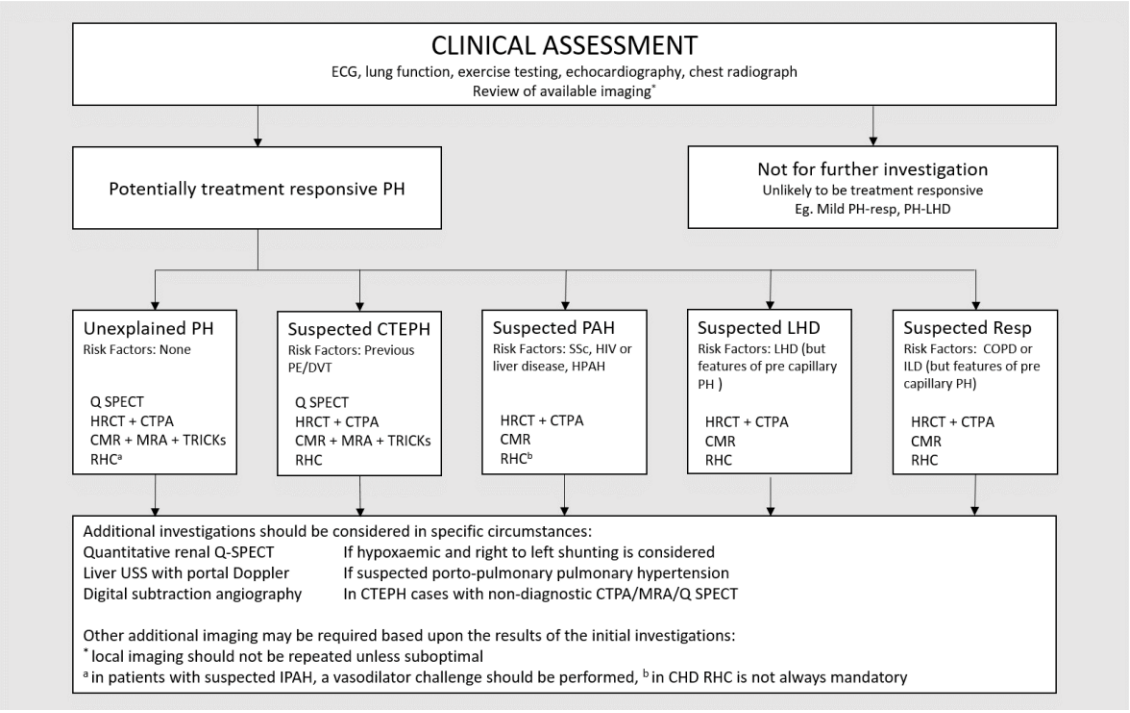

Figure 2.20: Investigation flow chart in the Sheffield Pulmonary Vascular Disease Unit.
ECG: Electrocardiogram, PH: Pulmonary Hypertension, PH-Resp: Pulmonary Hypertension Due To Respiratory Disease, PH-LHD: Pulmonary Hypertension Due To Left Heart Disease, CTEPH: Chronic Thrombo-Embolic Pulmonary Hypertension, PAH: Pulmonary Arterial Hypertension, Q SPECT: Perfusion Single Positron Emission Computed Tomography, HRCT: High Resolution Computed Tomography, CTPA: Computed Tomography Pulmonary Angiography, CMR: Cardiac Magnetic Resonance Imaging, MRA: Magnetic Resonance Angiography, Tricks: Time Resolved Imaging Of Contrast Kinetics, RHC: Right Heart Catheter, USS: Ultrasound, IPAH: Idiopathic Pulmonary Arterial Hypertension, CHD: Congenital Heart Disease.

Diagnostic strategies to confirm or refute the diagnosis of pulmonary hypertension, including deciding on the need for cardiac catheterisation and the approach to imaging is dependent on the physician ensuring that further investigation is in the best interests of the patient. An appreciation of factors that increase the pre-test probability of forms of PH likely to benefit from therapy is crucial in this respect. In the Sheffield Pulmonary Vascular Unit, a tertiary PH referral centre for pulmonary hypertension, patients are initially assessed in an out-patient clinic with an electrocardiogram, exercise and lung function testing and echocardiography. For appropriately identified patients, a multimodality approach is used combining radionuclide imaging, CT, MRI and cardiac catheterisation as shown in Figure 2.20. As many patients travel long distances for their investigations, this multimodality approach is taken to reduce the requirement for repeat visits and recognises the complementary information provided by different imaging investigations. In other centres, a step-wise approach may negate the need for some of the diagnostic tests, as advocated by current ESC/ERS guidelines.

2.8.2 Identifying the Cause of Pulmonary Hypertension

One of the major values in using a multimodality approach is the provision of detailed information to aid phenotyping pulmonary hypertension. The identification of the cause of PH is key in defining treatment: patients with PAH benefit from drug therapy and patients with CTEPH can be potentially cured by pulmonary endarterectomy. Whilst invasive haemodynamics are the gold standard for the measurement of pressure, imaging features can also give an indication as to the likelihood and severity of PH in addition to providing detailed information on the likely underlying cause. Information from imaging is integrated with other investigations including blood testing and lung function testing.

Group 1: The typical imaging findings in patients with idiopathic pulmonary arterial hypertension (IPAH) are pulmonary artery enlargement, right ventricular and atrial dilatation, right ventricular hypertrophy (usually most apparent in the outflow tract) and septal bowing, as shown in Figure 2.22. In addition, the left atrium and left ventricle are often reduced in volume due to poor filling. On CT, patients with PAH often have centrilobular ground glass nodules (**Figure 2.6**), and if this is seen centrally may suggest systemic sclerosis-PAH, especially if the oesophagus is dilated.

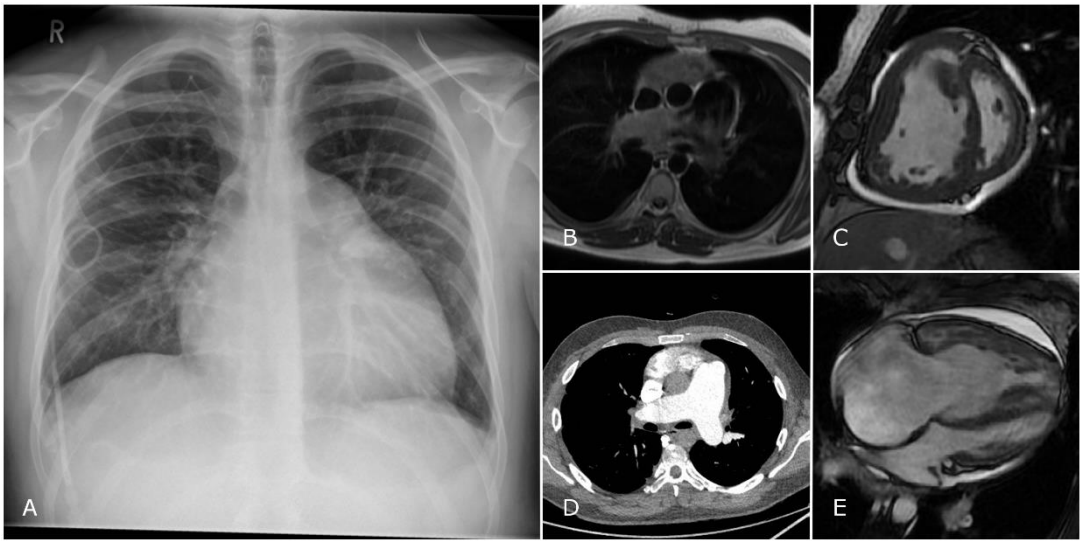

Figure 2.21: Typical imaging features in a patient with idiopathic pulmonary arterial hypertension.
The chest radiograph shows cardiomegaly with dilatation of the pulmonary artery, the patient has a PICC for intravenous delivery of iloprost. Black blood imaging (B) and CTPA (D) confirm the dilated pulmonary artery. Further features of pulmonary hypertension are shown with slow flow artefact on black blood (B), flattening of the interventricular septum (C) and dilatation of the right sided chambers (C and D). Note is also made of poor filling of the left sided chambers and a moderate pericardial effusion.

A diagnoses of IPAH requires and exclusion of other causes. Time resolved contrast imaging such as TRICKs might be of use in the identification of right to left shunts, as shown in Figure 2.16, which demonstrates a right to left shunt in a patient with IPAH and a patent foramen ovale.

Group 2: Patients with PH due to left heart disease often have biatrial dilation and a varying amount of left ventricular, right ventricular and right atrial enlargement (figure 3). Features of pulmonary hypertension seen in IPAH, such as septal flattening may be masked due to high left ventricular filling pressures, and the presence of a flattened septum in addition to features of left heart disease suggests a pre-capillary

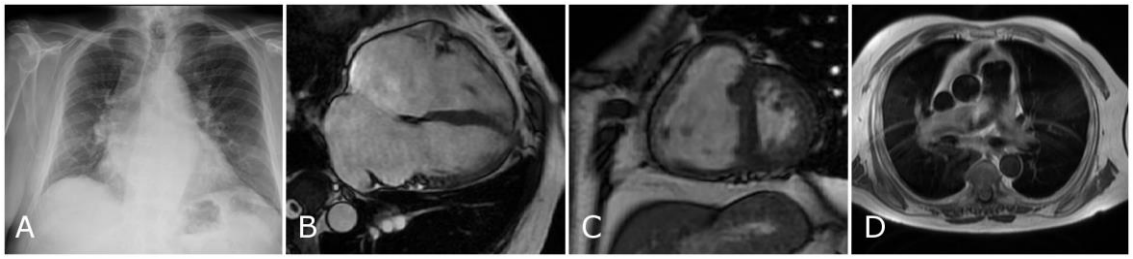

Figure 2.22: Typical features of pulmonary hypertension due to left heart disease.
A chest radiograph (A) showing moderate cardiomegaly and upper lobe venous distension. Subsequent magnetic resonance imaging (MRI) shows bi-atrial dilatation (B), flattening of the interventricular septum (C) and slow flow black blood artefact (D). The flattening of the interventricular septum suggests that there is a pre-capillary component to the pulmonary hypertension.

component to the PH. There may be features of previous cardiac surgery or valvular replacement. Patients with left heart disease may also have features of cardiac decompensation such as pleural effusions, septal lines, ascites and reflux of contrast into the IVC/hepatic veins.

Group 3: Imaging evidence of lung disease is helpful in ensuring that patients with PH-Lung are not misclassified as IPAH and characteristic features of the form of parenchymal lung disease are easily appreciated. It is important to recognize that patients with severe emphysema may have normal spirometry (although these patients usually have a severe reduction in gas transfer) and in patients with interstitial lung disease (particularly in the setting of connective tissue disease) the spirometry may be normal.

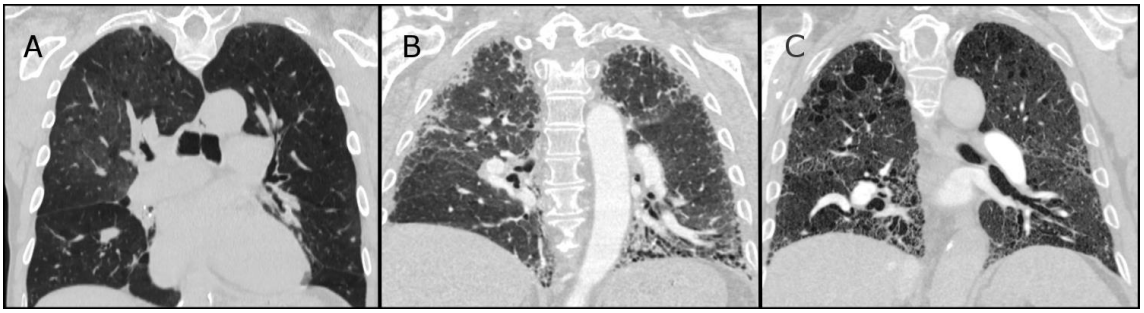

Figure 2.23: Coronal reconstruction of CTPAs from patients with pulmonary hypertension due to respiratory disease.
A – Emphysema, B – idiopathic pulmonary fibrosis (IPF), C – combined pulmonary fibrosis and emphysema (CPFE)

Group 4: The diagnosis of CTEPH may be suggested by a mosaic attenuation pattern on CT, due to underlying perfusion abnormalities and sub-pleural scarring due to pulmonary infarction. These features should trigger a thorough assessment of the pulmonary arteries for features of chronic thrombo-embolic disease, shown in Figure 2.5. It should also be appreciated that patients may have overlapping features of different forms of pulmonary hypertension.

Group 5: Conditions such as sarcoidosis, lymphangioleiomyomatosis and Langerhans histiocytosis have classical radiological features and haematological conditions may also have typical changes on CT, such as expansion of the medullary cortex of bones in patients with thalassemia.

Table 2.2: *Specific imaging features present in each World Health Organization classification of PH*

	1. PAH	2. Left Heart Disease	3. Lung Disease	4. CTEPH	5. Misc
RHC	mPAP: ↑↑ PAWP: ↔ CO: ↔, ↓ or ↓↓ RA: ↔ or ↑	mPAP: ↑ PAWP:↑ CO: ↔ or ↓ RA: ↑ or ↑↑	mPAP: ↑ PAWP:↔ CO: ↔ or ↓ RA: ↔ or ↑	mPAP: ↑↑ PAWP:↔ or mild↑ CO: ↔, ↓ or ↓↓ RA: ↔ or ↑	mPAP: ↑ or ↑↑ PAWP:↔ CO: ↔, ↓, ↓↓ or ↑ RA: ↔, ↑ or ↑↑
CT	PA: ↑ or ↑↑ RV: ↑ or ↑↑ LV and LA:↓↓ Flattened IVS Centrilobular nodules Neovascularity	PA: ↔ or ↑ RV: ↔ or ↑ LA:↑↑ Pleural or pericardial effusions	PA: ↑ or ↑↑ RV: ↑ or ↑↑ Parenchymal lung disease e.g. Emphysema or fibrosis	PA: ↑ or ↑↑ RV: ↑ or ↑↑ Chronic emboli: webs, stenoses, mural thrombus Mosaic perfusion	PA: ↑ or ↑↑ RV: ↑ or ↑↑ CT evidence of disease e.g. sarcoidosis
CMRI	PA: ↑ or ↑↑ RV: ↑ or ↑↑ LV and LA:↓↓ Flattened IVS	PA: ↔ or ↑ RV: ↔ or ↑ LV: ↔ or ↑, LA:↑↑ Septum only flattened in Cpc-PH Pleural/Pericardial Effusions	PA: ↑ or ↑↑ RV: ↑ or ↑↑	PA: ↑ or ↑↑ RV: ↑ or ↑↑ Flattened IVS Chronic emboli on MRA	PA: ↑ or ↑↑ RV: ↑ or ↑↑
V/Q SPECT	No segmental defects Renal uptake in R-L shunt	No segmental defects	No segmental defects Abnormal due to lung disease	Segmental perfusion defects	No segmental defects

PAH: Pulmonary arterial hypertension, CTEPH: Chronic thrombo-embolic pulmonary hypertension, mPAP: Mean pulmonary arterial pressure, PAWP: Pulmonary arterial wedge pressure, CO: Cardiac output, RA: Right atrium, LV: Left ventricle, LA: Left atrium, IVS: Interventricular septal angle, MRA: Magnetic resonance angiography, V/Q SPECT: ventilation/perfusion single photon emission computed tomography.

2.8.3 **Prognostic evaluation of patients with pulmonary hypertension**

The assessment of prognosis is important when counselling patients and planning treatment, in particular when considering interventions such as initiation of parenteral prostanoid therapy and triggering referral for transplantation. This assessment is usually based on an assessment of clinical status, exercise capacity and right ventricular function. Increasingly imaging has been used to aid assessment of ventricular function and aid the classification of PH, which also influences prognosis. An important question surrounds the benefit of increasingly complex tests in the prognostic assessment of PH.

Helpful prognostic information can be gained from a simple assessment of the clinical status of the patient, and World Health Organization (WHO) functional class is a useful tool in this regard. A historical study showed that patients with WHO functional class IV had median survival of 6 months, class III had a median survival of 2.5 years and class I and II had a median survival of 6 years without treatment(2). In the modern age, pulmonary vascular therapies have improved median survival in PAH to 4 years and 100 days (189,190). Older age, male sex are associated with a worse prognosis and the cause of pulmonary hypertension also impacts on outcome. Exercise capacity, which was traditionally used as end-point for many of the pivotal drug trials, has also been shown to be an important prognostic indicator. (191–196).

Right ventricular function may be measured in different ways. Traditionally a right heart catheter has been used to provide prognostic information on right ventricular function, including right atrial pressure, cardiac output/index, stroke volume index and mixed venous oxygen saturation. A number of echocardiographic measures have prognostic value including, tricuspid annular plane systolic excursion (TAPSE) (197), RV Doppler index (198,199), interventricular septal displacement (200) and right atrial area index (200). Serum levels of NT-proBNP are also linked to right ventricular dysfunction, and have been shown to have prognostic value in PAH (201). Cardiac MRI is also a useful tool in the assessment of prognosis, and **Table 2.3** provides the evidence for assessment of prognosis using cardiac MRI parameters. Multiple studies have identified that stroke volume, RVEF, LV and RV end diastolic volumes are associated with outcome (202,203), particularly when adjusted for age and sex (204).

The strength of RVEF as a predictor of outcome in PAH was highlighted in a recently published systematic review (205). More recently, a larger study of 576 patients from Sheffield showed that right ventricular end systolic volume (indexed for age and sex) and pulmonary arterial relative area change were independent predictors of mortality, providing added prognostic value to patient age, sex, subgroup diagnosis and WHO functional class (124). The presence of a pericardial effusion on echocardiography, CT or cardiac MRI is also associated with a poor prognosis (200), and other features of cardiac decompensation such as pleural effusions and ascites are predictive of a poor outcome.

A number of parameters have been identified as important for assessing disease severity, stability and importance and have produced the "traffic light" approach to prognosis in patients with PH, as outlined in **Figure 2.24** below. The number of "low risk" features has been shown to predict survival in a large cohort of patients (206).

Determinants of prognosis[a] (estimated 1-year mortality)	Low risk <5%	Intermediate risk 5–10%	High risk >10%
Clinical signs of right heart failure	Absent	Absent	Present
Progression of symptoms	No	Slow	Rapid
Syncope	No	Occasional syncope[b]	Repeated syncope[c]
WHO functional class	I, II	III	IV
6MWD	>440 m	165–440 m	<165 m
Cardiopulmonary exercise testing	Peak VO_2 >15 ml/min/kg (>65% pred.) VE/VCO_2 slope <36	Peak VO_2 11–15 ml/min/kg (35–65% pred.) VE/VCO_2 slope 36–44.9	Peak VO_2 <11 ml/min/kg (<35% pred.) VE/VCO_2 slope ≥45
NT-proBNP plasma levels	BNP <50 ng/l NT-proBNP <300 ng/l	BNP 50–300 ng/l NT-proBNP 300–1400 ng/l	BNP >300 ng/l NT-proBNP >1400 ng/l
Imaging (echocardiography, CMR imaging)	RA area <18 cm^2 No pericardial effusion	RA area 18–26 cm^2 No or minimal, pericardial effusion	RA area >26 cm^2 Pericardial effusion
Haemodynamics	RAP <8 mmHg CI ≥2.5 l/min/m^2 SvO_2 >65%	RAP 8–14 mmHg CI 2.0–2.4 l/min/m^2 SvO_2 60–65%	RAP >14 mmHg CI <2.0 l/min/m^2 SvO_2 <60%

Figure 2.24: Parameters that have been established for the assessment of prognosis, severity and prognosis in PAH.

Reproduced with permission from Galiè N, Humbert M, Vachiery J-L, Gibbs S, Lang I, Torbicki A, et al. 2015 ESC/ERS Guidelines for the diagnosis and treatment of pulmonary hypertension: The Joint Task Force for the Diagnosis and Treatment of Pulmonary Hypertension of the European Society of Cardiology (ESC) and the European Respiratory Society (ERS): Endor. Eur Heart J. 2016 Jan 1;37(1):67–119 (1).

Table 2.3: *Cardiopulmonary MRI predictors of outcome in PH*

Author	Number of patients	Follow up	CMR metric	Hazard Ratio (confidence interval)
Van de Veerdonk (130)	110 PAH	1 year	Baseline RVEF	0.938 (0.902–0.975)**
			One year ΔRVEF	0.929 (0.875–0.985)*
			RVESVI (ml/m2)	1.014 (1.001-1.027)*
			LVEDVI (ml/m2)	0.962 (0.931–0.994)**
			LVESVI (ml/m2)	0.942 (0.888-0.998)*
Van Wolferen (129)	64 IPAH	1 year	SVI (Phase contrast at pulmonary artery) (ml/m2)	0.32 (0.13-0.84)*
			LVEDVI (ml/m2)	0.31 (0.13-0.81)*
			RVEDVI (ml/m2)	4.2 (1.31-8.30).*
Gan (207)	70	4 years	RAC (%) right main PA	0.87(0.76-0.96)**
Swift (208)	134	20 months	RAC (%) main PA	0.85 (0.74-0.98)*
Hagger (209)	40 PAH-SSc		VMI	N/A – Kaplan Meier analysis
Rajaram (210)	81		RVEDV	1.02 (1.01-1.03)**
			VMI	5.56 (1.50-35.5)*
Freed (211)	58	10 months	RVIP-LGE	10.0 (1.3 to 77.1)*
Swift (212)	79	2 years	FWHM lung perfusion MRI	1.08 (1.01 to 1.16)*
			PTT	1.10 (1.03 to 1.18)*
Dawes (213)	256	4 years	3D RV motion	2.75 (1.73 to 4.35)**
Swift (124)	576	30 months	RVESVI (%pred)	1.217 (1.06 to 1.54)**
			RAC	0.76 (0.623 to 0.93)**

*RVEF: right ventricular ejection fraction, RVESVI: right ventricular end systolic volume index, LVEDVI: left ventricular end diastolic volume index, LVESVI: left ventricular end systolic volume index, SVI: stroke volume index, RAC: relative area change, VMI: ventricular mass index, RVIP-LGE: right ventricular insertion point late gadolinium enhancement, FWHM: full width half maximum, PTT: pulmonary transit time, RV: right ventricle, * p <0.05, ** p <0.001*

The challenge facing clinicians is how to incorporate large amounts of data from various imaging modalities and how best to integrate these with other data from the clinic to aid treatment decisions in a way that is meaningful and beneficial to patients and is cost effective. The lack of a current consensus reflects a paucity of head-to-head comparisons of different prognostic approaches and the recent emergence of new tools such as MRI.

One area of growing interest is in modelling methods to streamline the decision making pathway, with the increasing implementation of automated methodologies (214–216). There is interest in the use of empirical linear regression models (125,217) and more physiologically linked models, such as the Windkessel model (218,219), which are likely to aid the diagnosis of pulmonary hypertension and refine assessment of progression or response to therapy. As computing processing power and research datasets increase, it is likely that we will see machine learning approaches, either from large volumes of prior measurements (220) or directly from images themselves (213). There is great interest in precision medicine and tailored drug therapy (221), the integration of imaging metrics and the study of "omics" are likely to be driving factors (222).

2.8.4 **Follow-up of patients with pulmonary hypertension**

Currently, several parameters are used to assess patients, including WHO functional class (195), exercise tests (223–225) and widely available blood test such as N-terminal BNP (226,227). There has been some concern regarding the ability of the 6MWT to reflect changes in pulmonary vascular status and this has led to a drive to explore other markers that are more likely to be sensitive to change. Consequently, there has been a lot of recent interest in cardiac MRI as a highly reproducible, non-invasive, non-ionizing tool to assess right ventricular function. Van de Veerdonk and colleagues, showed that cardiac MRI is sensitive to change, with right ventricular volume changes preceding clinical deterioration in apparently clinically stable patients with idiopathic pulmonary arterial hypertension (228). The same group also showed that changes in stroke volume were a marker of clinical improvement in patients after 1 year of treatment (202). Furthermore, measures of right ventricular function on cardiac MRI have been shown to be highly reproducible (124).

In SPVDU, a multi-modality approach is used to assess response to treatment based on clinical assessment, exercise testing and MRI to assess right ventricular function, given its excellent reproducibility and sensitivity to change. Cardio-pulmonary vascular MRI is not readily available in all centres, so the choice of follow up modality is based on real life local availability of tests. Echocardiography is an alternative for follow up, able to objectively quantify right ventricular function using TAPSE, right

ventricular tissue Doppler and right ventricular free wall strain, although there are concerns regarding the reproducibility of this technique and how it performs as a follow-up tool in routine clinical practice (229–231). Recently a study has shown that using a simple assessment of symptoms (WHO FC), exercise capacity (6 minute walk test distance) and BNP at follow-up, could be used to risk stratify patients, with no additional benefit provided by performing cardiac catheterisation (176), although in this study MRI was not evaluated.

Quality of life has consistently been identified by patients as an important goal of therapy, so assessment of follow up should also take into account patient reported symptoms, such as emPHAsis-10 (232). This is a 10 point questionnaire that has been shown to be sensitive to changes in clinical parameters such as WHO functional class.

In summary, a number of approaches are used in the follow-up of patients that should include a measurement of symptoms, exercise capacity, right ventricular function and also patient reported outcome measures such as emPHAsis-10.

2.9 The Choice of Imaging Modality

As outlined above, there a number of imaging modalities available for the investigation of patients with pulmonary hypertension. Each of these investigations has their pros and cons and the choice of the correct modality can be challenging.

The chest radiograph is widely available and easily interpreted by many practitioners. It is however limited by low sensitivity and specificity for pulmonary hypertension but can often be useful in the assessment of underlying lung disease.

Echocardiography has the advantage of being cheap and readily available and provides useful information regarding pulmonary arterial pressures and is therefore a useful tool to screen patients for the presence of PH.

Computed Tomography can give useful information regarding the pulmonary artery and the right ventricle along with parenchymal lung disease as outlined above. It is easily performed in centres across the world and is therefore a useful test in the identification of patient with PH. It is also useful in the assessment of surgical options in patients with CTEPH. Whilst MRI also provides useful structural and functional information, it is currently limited to specialist centres due to limited availability and expertise.

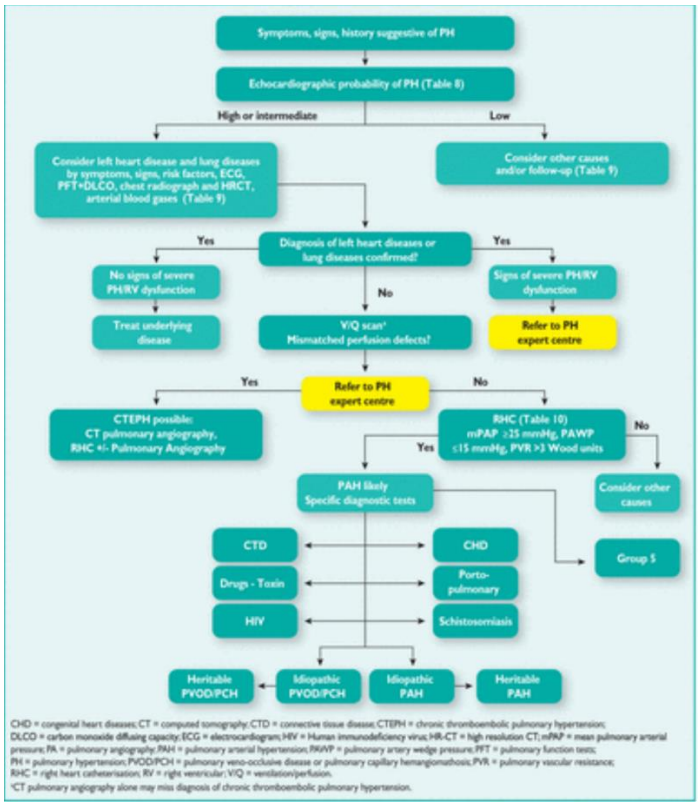

Figure 2.25: *Diagnostic algorithm for PH recommended by the ERS/ESC guidelines.*
Reproduced with permission from Galiè N, Humbert M, Vachiery J-L, Gibbs S, Lang I, Torbicki A, et al. 2015 ESC/ERS Guidelines for the diagnosis and treatment of pulmonary hypertension: The Joint Task Force for the Diagnosis and Treatment of Pulmonary Hypertension of the European Society of Cardiology (ESC) and the European Respiratory Society (ERS): Endor. Eur Heart J. 2016 Jan 1;37(1):67–119 (1).

3 RESEARCH QUESTIONS, AIMS AND METHODOLOGY

Whilst cardiac MRI is considered the gold standard for the assessment of left ventricular function (233), there remains heavy reliance upon invasive measures of pressure for the diagnosis, phenotyping and prognostic assessment of pulmonary hypertension (1). The overall aim of this PhD thesis is to evaluate the role of cardiac MRI in the non-invasive investigation of pulmonary hypertension, ultimately aiming to reduce the requirement for right heart catheterisation. The assessment of patients with suspected PH can be split into three distinct themes, as outlined in the previous chapter: diagnosis, phenotyping and risk assessment, which follows the pathway of clinical decision making in patients with suspected pulmonary hypertension. The structure of chapters in this thesis follow these key themes and allocated as below:

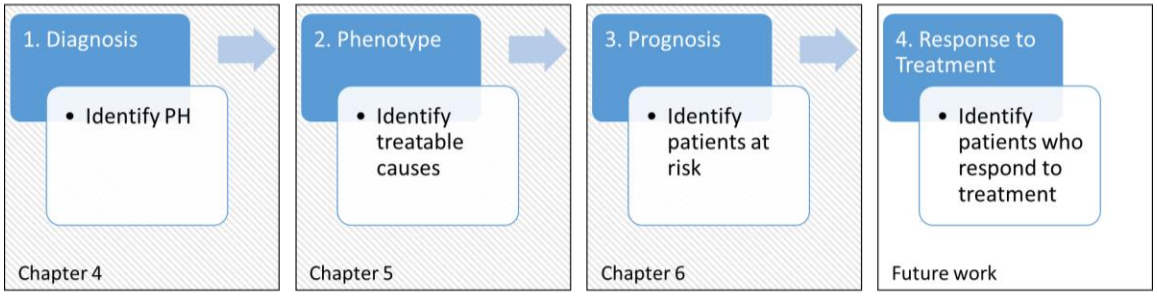

Figure 3.1: *The clinical decision pathway in suspected pulmonary hypertension.*

3.1 HYPOTHESES

1. Quantifiable cardiac MRI metrics can be used to assess pulmonary arterial pressure and therefore identify patients with pulmonary hypertension.
2. Dynamic contrast enhanced pulmonary perfusion MRI (DCE-MRI) can be used to screen for patients with CTEPH in patients with unexplained PH.
3. Cardio-pulmonary vascular MRI can be used to phenotype patients with pulmonary hypertension due to left heart disease.
4. Cardio-pulmonary vascular MRI is a useful tool for the assessment of prognosis in patients with PH due to respiratory disease, and PH due to left heart disease.

3.2 AIMS

3.2.1 Diagnosis (Chapter 4)

The first aim of this body of work is to improve the non-invasive assessment of mean pulmonary arterial pressure using cardio-pulmonary vascular MRI, and assess its role in the diagnosis of pulmonary hypertension. This is clearly key to the initiation of treatment. Improvements in non-invasive methodologies have the potential to reduce the burden of late diagnosis in pulmonary hypertension.

3.2.2 Phenotyping (Chapter 5)

The second aim of this PhD is to improve the non-invasive phenotyping of pulmonary hypertension patients using cardiac MRI. The correct identification of the WHO group of pulmonary hypertension is essential to initiate the correct therapy for each patient.

The key patients to identify are those who have "pre-capillary" pulmonary arterial remodelling. In current clinical practise, this patient group mainly comprises patients with group 1: pulmonary arterial hypertension. There is, however, increasing evidence that patients with other forms of PH also have a degree of pre-capillary pulmonary vascular remodelling, in a model that is similar to that seen in PAH. Whilst treatment with pulmonary vasodilators is currently only recommended in patients with PAH and non-surgical CTEPH, there is significant interest in the potential for pulmonary vascular therapy in specific patients with PH due to left heart disease and lung disease.

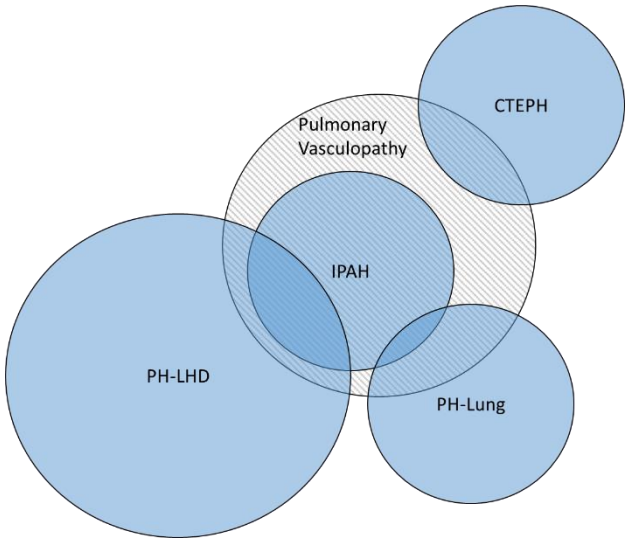

Figure 3.2: *Multiple causes of PH share pre-capillary pulmonary vascular remodelling. Chapter 5 explores the role of MRI in the identification of each of these causes of PH.*

3.2.3 **Prognostic Assessment (Chapter 6)**

The third aim of this PhD thesis is to identify the role of cardiac MRI in the prognostic evaluation of patients with pulmonary hypertension. The role of cardio-pulmonary vascular MRI in the risk assessment of patients with idiopathic pulmonary arterial hypertension has been examined in previous work from Sheffield (124) and other centres (124,129,130,207–213).

3.3 MATERIALS & METHODS

This chapter describes the methods that are used throughout this thesis. In order to allow for chapters to be read in isolation, the relevant methods are repeated in the chapter specific methods section. The data that is analysed in this thesis was acquired as part of the routine clinical pathway of patients in the Sheffield Pulmonary vascular disease unit. The MRI and clinical metrics were all measured at the time of the scan by the clinical team. I collected all of the relevant databases and joined them together, analysed the data and wrote all of the text for this thesis.

3.3.1 The ASPIRE PH MRI Sub-Database

Sheffield is one of seven UK tertiary referral centres for adult pulmonary hypertension. In 2016, there were 1,675 active patients at the Sheffield Pulmonary Vascular Disease Unit (SPVDU), representing 24% of 7,035 active patients in the United Kingdom (234).

All patients who underwent cardiac MRI at the Sheffield Pulmonary Vascular Disease Unit from April 2012 to October 2017 were entered into an anonymised database. Each patient was given a unique identifier, with a document linking the patient to the identifier stored on a password protected departmental computer.

All patient data was downloaded from the clinical database (Infoflex). Matlab scripting was used to create a table of each investigation for each patient. These were then joined to create database of the incident cardiac MRI data with closest right heart catheter, exercise test, pulmonary function test data allowing with diagnostic, demographic and treatment data. A similar methodology was implemented to identify the scan closest to 1-year follow up.

Ethical approval was granted from a local ethics committee for this retrospective study, written consent was waived (ref c06/Q2308/8).

3.3.1.1 Inclusion and Exclusion Criteria

All patients studied in this thesis were referred to the Sheffield Pulmonary Vascular Disease Unit with suspected pulmonary hypertension. In order to be included, the patients were required to have had both MRI and right heart catheter. Any MRI that was not of diagnostic quality was excluded from analysis. Study specific inclusion and exclusion criteria will be explained, as relevant, in each chapter.

3.3.1.2 Incident Cases

The ASPIRE MRI sub-registry contains 2437 MRI scans for patients with suspected or confirmed pulmonary hypertension. Within this database, there are 1272 incident cases with suspected pulmonary hypertension, of which 957 (75%) had RHC and MRI within 14 days.

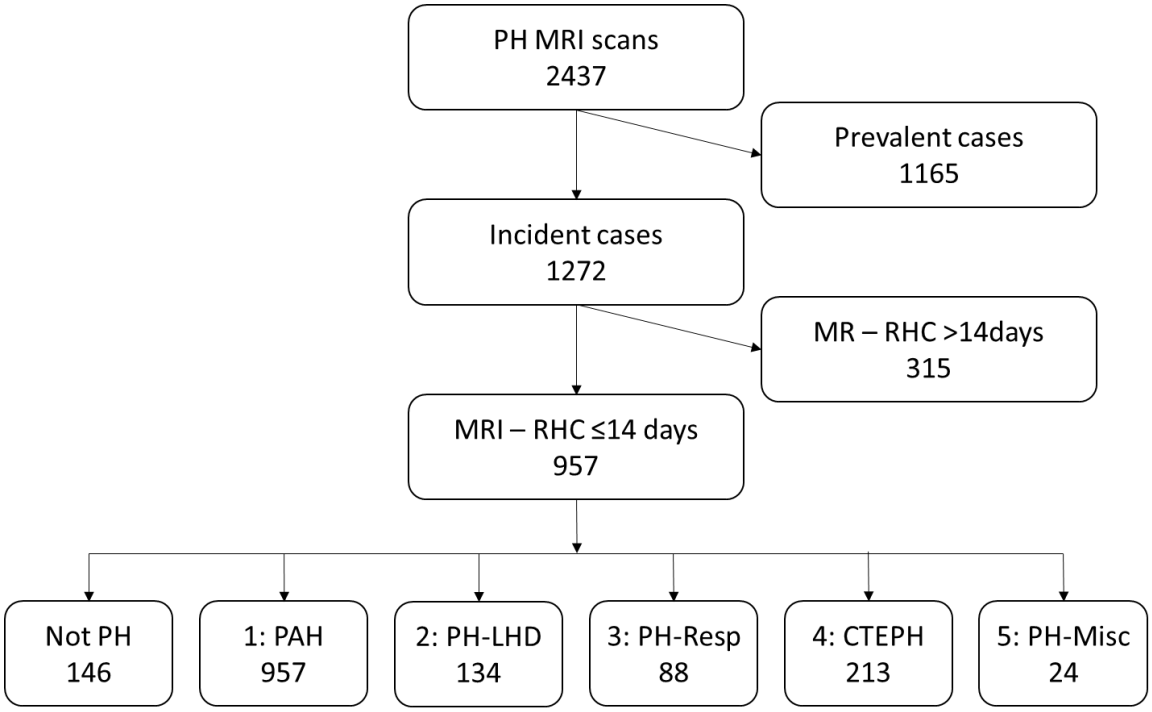

Figure 3.3: *Flow chart demonstrating the split of incident cases within the ASPIRE MRI sub-registry*

There was no difference in survival (log rank chi-squared = 2.8, p=0.097) or in length of follow up (p=0.661) between the cases who were included and those who were excluded due to the catheter being more than 2 weeks from the MRI.

Table 3.1: *Baseline demographics of the incident patients within the MRI ASPIRE sub-registry, mean with standard deviation*

	All patients	Not PH	1: PAH	2: PH-LHD	3: PH-Resp	4: CTEPH	5: PH Multi
Number	957	146	347	134	88	213	24
Age (years)	65 (13)	60 (16)	62 (14)	72 (8)	67 (10)	66 (12)	66 (10)
Sex (F/M)	591/366	105/41	242/105	88/46	42/46	98/116	13/11
WHO functional class (I,II,III,IV)	3,106,740,87	1,52,78,3	0,10,289,44	1,14,113,6	0,8,61,19	1,22,175,14	0,0,22,1
ISWT (m)	207 (182)	293 (222)	189 (173)	145 (116)	143 (109)	248 (199)	164 (147)
mPAP (mmHg)	41.0 (14.6)	19.7 (3.1)	47.2 (13.0)	40.0 (10.0)	40.0 (10.8)	45.8 (12.2)	46.5 (11.1)
mRAP (mmHg)	10.4 (5.8)	5.8 (3.3)	10.9 (6.2)	14.6 (5.3)	9.4 (4.5)	10.6 (5.0)	10.2 (5.7)
PAWP (mmHg)	13.3 (5.8)	10.5 (3.6)	11.6 (4.0)	22.6 (5.7)	12.7 (4.2)	12.2 (3.7)	12.7 (3.8)
CI	2.7 (2.6)	3.1 (0.9)	2.6 (0.8)	2.7 (0.7)	2.8 (0.8)	2.4 (0.7)	2.8 (1.0)
PVRI (dyne.s/cm5)	294 (242)	80 (43)	415 (268)	169 (131)	256 (145)	342 (221)	369 (214)
SvO2 (%)	64.9 (9.0)	71.5 (7.4)	63.7 (9.6)	65.2 (9.0)	66.1 (6.9)	61.9 (7.6)	63.7 (8.5)
FEV1 (% predicted)	0.78 (0.23)	0.88 (0.22)	0.77 (0.23)	0.72 (0.19)	0.62 (0.27)	0.84 (0.21)	0.68 (0.20)
FVC (% predicted)	0.80 (0.23)	0.83 (0.19)	0.77 (0.22)	0.71 (0.16)	0.74 (0.29)	0.91 (0.22)	0.71 (0.24)
FEV1/FVC	0.69 (0.12)	0.73 (0.11)	0.70 (0.12)	0.68 (0.10)	0.61 (0.18)	0.67 (0.1)	0.68 (0.14)
TLCO	3.71 (2.04)	5.0 (1.7)	3.0 (2.0)	3.7 (1.3)	2.2 (1.0)	4.7 (1.9)	2.3 (0.9)
Days between RHC & MR	0 (2)	0 (2)	1 (2)	1 (2)	0 (1)	0 (1)	1 (3)

WHO: World Health Organisation, RHC: right heart catheter, mPAP: right heart catheter measured mean pulmonary artery pressure, mRAP: mean right atrial pressure, PAWP: pulmonary artery wedge pressure, CI: cardiac index, PVRI: pulmonary vascular resistance index, SvO_2: mixed venous oxygen saturation, FEV1: Forced expiratory volume in 1 second, FVC: Forced vital capacity, TLCO: transfer for carbon monoxide, 4 cases had no diagnosis of PH group.

3.3.2 Standard Cardiac and Pulmonary Vascular MRI Protocol

3.3.2.1 MRI Sequences

MRI was performed as part of the routine clinical care on a GE HDx 1.5-T whole body scanner (GE Healthcare, Milwaukee, Wisconsin), using an 8-channel cardiac coil, with the patient supine.

Table 3.2: *Standard MRI sequences used in the Sheffield Academic Radiology Department for patients in the Sheffield Pulmonary Vascular Disease Unit.*

Cardiac Cine	Black Blood	Q Flow	+/-
4 Chamber	Pulmonary artery	Pulmonary Artery	Contrast enhancement
Short axis		Aorta	Pulmonary Perfusion
LIFOF			Pulmonary Angiography
LVLA			Late Gadolinium
RIFOF			Enhancement
RVOT			

LIFOF: Left ventricle inflow outflow, LVLA: Left ventricle long axis, RIFOF: right ventricle inflow outflow, RVOT: Right ventricle outflow tract.

3.3.2.1.1 FIESTA (Fast Imaging Employing Steady State Acquisition)

Proton anatomical imaging was performed as a coronal stack of 2D bSSFP images in inspiration with a single breath hold of 12 seconds. The following parameters were used: TR 2.8 ms, TE 0.79ms, flip angle 50°, FOV 48 x 43 cm, 256 x 256 Matrix, 125 kHz bandwidth and slice thickness 10mm.

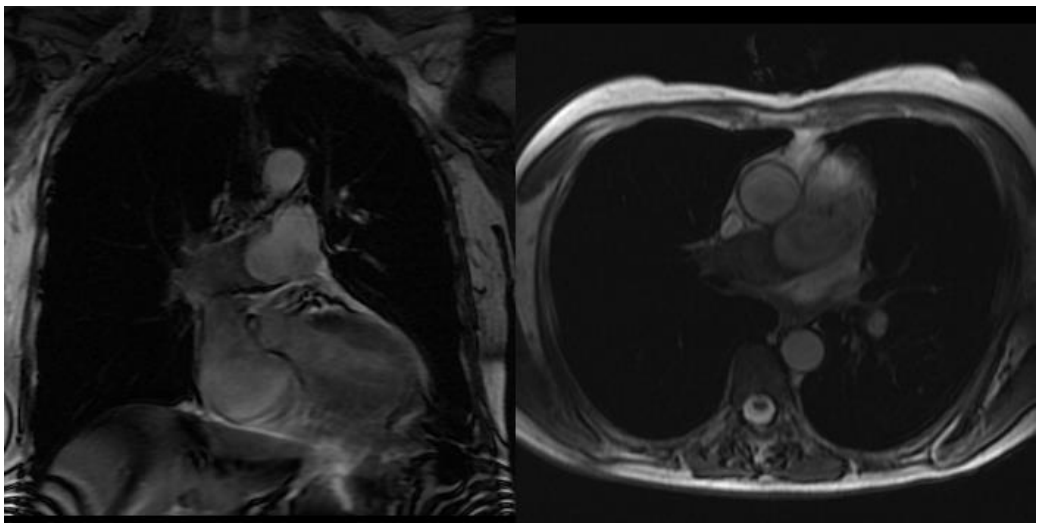

Figure 3.4: *coronal and axial FIESTA images from a patient with CTEPH.*
Note the change in signal in the right main pulmonary artery due to mural thrombus.

3.3.2.1.2 Cardiac Cine

4 chamber, short axis, left ventricle long axis (LVLA), left ventricle inflow outflow (LIFOF), right ventricle inflow outflow (RIFOF) and right ventricle outflow tract (RVOT) cardiac cine imaging was acquired using a retrospectively cardiac gated multi-slice steady-state free precession (SSFP) sequence (FIESTA).

A stack of axial images in the short axis (SA) plane with slice thickness of 8 mm with a 2 mm inter-slice gap or 10 mm with no inter-slice gap were acquired, covering both ventricles from base to apex. The SSFP sequence parameters were: TR 2.8 ms, TE 1.0ms, flip angle 50°, field of view 48x43.2, 256x256 matrix, 125 kHz bandwidth, and slice thickness 8 to 10 mm.

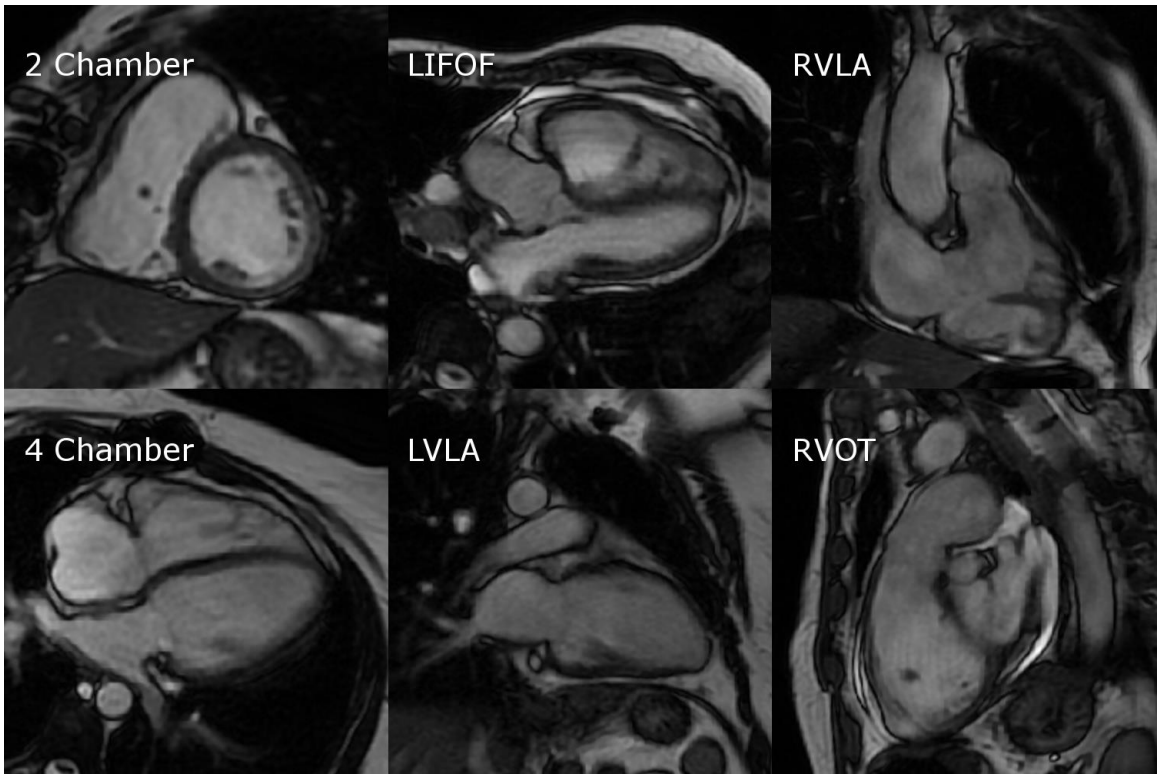

Figure 3.5: *Cardiac MRI SSFP cine views.*
LIFOF: left ventricle inflow outflow, LVLA: left ventricle long axis, RIFOF: right ventricle inflow outflow, RVOT: right ventricle outflow tract

3.3.2.1.3 Black Blood Imaging

Axial black blood imaging of the pulmonary arteries was performed using a double inversion recovery fast spin echo sequence (DIR-FSE), with a stack of 8mm slices with 10mm spacing taken through the long axis plane of the pulmonary artery acquired using an 8 channel cardiac coil during a breath-hold. There is a 180˚ non-selective inversion pulse, immediately followed by a slice-selective 180˚ de-inversion pulse. The TI is then calculated based on the R-R interval on the ECG, it is 650ms at 60bpm. The other sequence parameters were: TR around 1000ms (dependent upon R-R interval), TE 40ms, FSE flip angle 90˚, echo train length 32 with approximately 2.5ms between echoes, field of view 4cm, 256x256 matrix, 31.2 kHz bandwidth, ASSET parallel imaging factor 2.

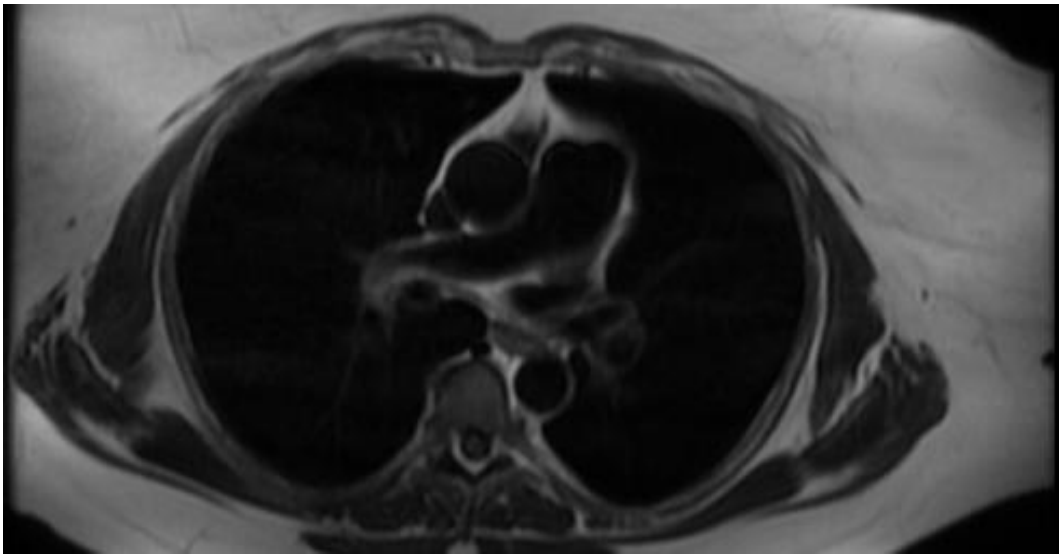

Figure 3.6: *Black blood imaging.*
Due to flow there is no signal returned from the pulmonary artery or aorta in health.

3.3.2.1.4 Phase Contrast Flow Sensitized Imaging

Phase contrast imaging was performed perpendicular to the pulmonary trunk and ascending aorta. The phase contrast imaging was performed using a 2D gradient echo sequence, the imaging parameters were: TR 5.6 ms, TE 2.7 ms, slice thickness 10 mm, FOV 48x28.8, bandwidth 62.5 kHz, matrix 256x128 and velocity encoding (Venc) 150 cm/s. The images were retrospectively ECG gated with 40 phases.

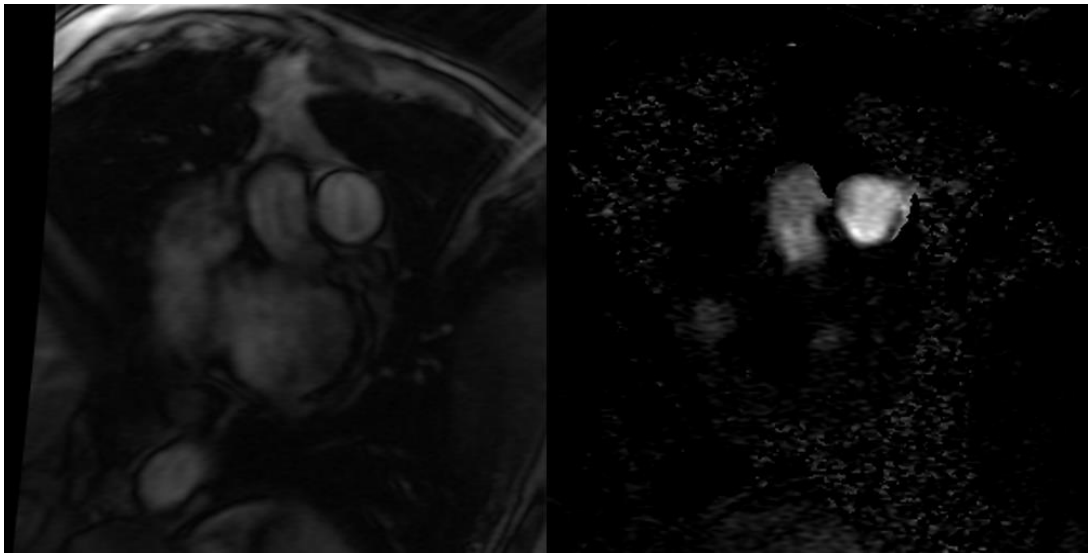

Figure 3.7: *Phase contrast imaging of the pulmonary artery.* Magnitude (left) and flow (right) images of the PA.

3.3.2.1.5 Dynamic Contrast Enhanced MRI and MR Angiography

Dynamic contrast enhanced MRI and MRA was undertaken when there was a clinical suspicion of CTEPH. DCE-MRI was performed using a contrast injection of a 0.05ml per kg patient weight dose of Gd-BT-D30A (Gadovist, Schering, Berlin, Germany) was injected at a rate of 4 ml per second with the injection rate controlled using an activated pump injector (Spectris, MedRad, Warrendale, Pennsylvania) typically via a vein in the antecubital fossa using an 18G cannula, followed by a 20ml saline flush. Subsequently serial 3D gradient echo images of the chest were acquired. The sequence parameters were: TE=1.1 ms, TR=2.5 ms, Flip angle 30°, FOV 48 cm x 48 cm, parallel imaging in plane x 2, in plane resolution 200x80, bandwidth 250 kHz, slice thickness 10 mm, approximately 32 slices, 48 time points with an overall effective 3D frame rate of ~ 0.5 s. Images were acquired in a coronal orientation.

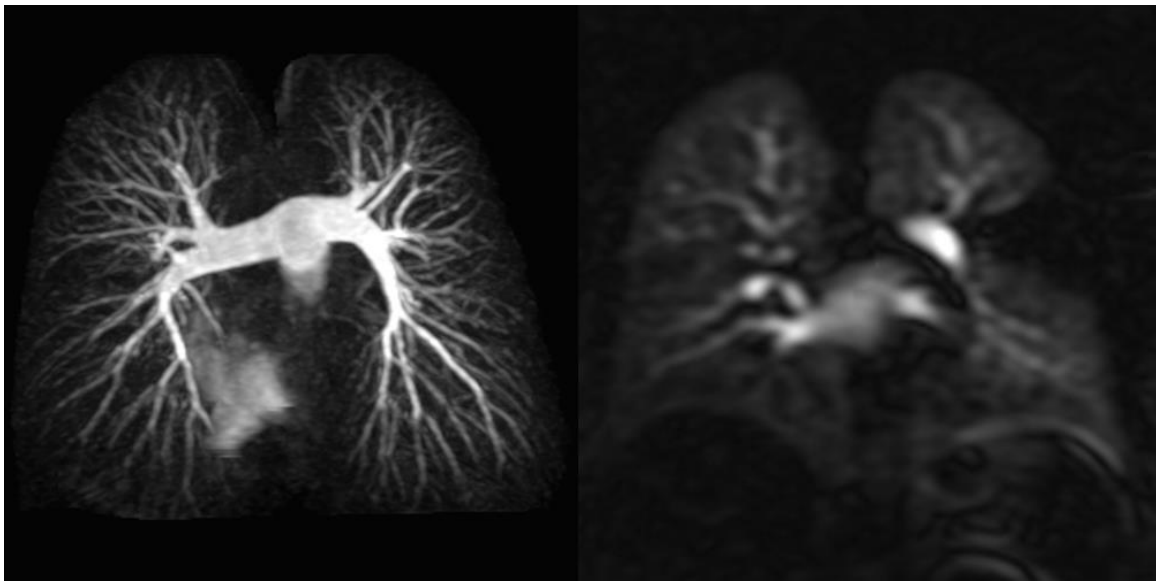

Figure 3.8: *Contrast enhanced MRA and dynamic contrast enhanced MRI.*
Note the wedge shaped perfusion defect in the DCE perfusion imaging in this patient with chronic pulmonary emboli.

3.3.2.2 Image Analysis

MR images were analysed manually analysed by DC (a cardiac MRI radiographer of 9 years cardiac MRI experience) on a GE Advantage Workstation 4.4 using GE Advantage Workstation ReportCard software, blinded to all clinical information and other investigations. The MRI was considered non-diagnostic if the volumetric analysis could not be adequately performed. Reproducibility metrics for these cardiac MRI metrics in our centre have been previously published (124). Where appropriate, these metrics were indexed to body surface area. In the future, increasingly automated methods for the segmentation of cardiac contours are likely to be implemented (235).

3.3.2.2.1 Biventricular Volumes

The endocardial surfaces of the left and right ventricles were traced on the short axis images to give the left and right ventricular end-diastolic volume, end-systolic volumes. The smallest volume was considered end systole and the largest end-diastole. Right and left ventricular stroke volume and mass were calculated as the difference of end diastolic and end systolic volume. Right and left ventricular ejection fraction were calculated as $RVEF = \frac{RVEDV - RVESV}{RVEDV}$.

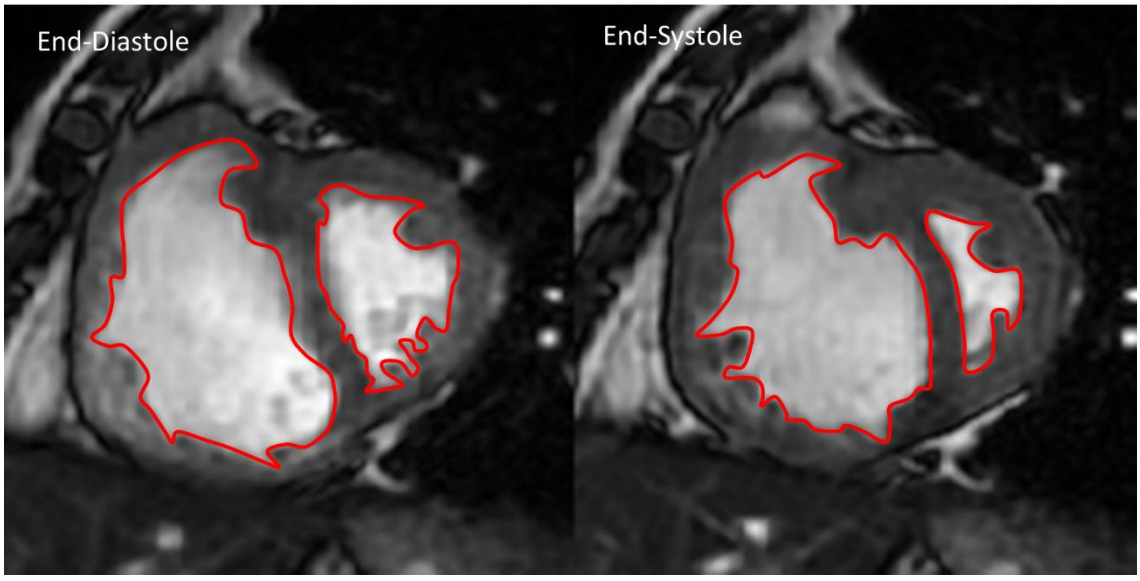

Figure 3.9: The endocardial contour on short axis images.

The right ventricle is the chamber on the left, and in this patient with IPAH is markedly dilated.

3.3.2.2.2 Ventricular Mass

On the short axis images, the endocardial and epicardial contours were traced for the left and right ventricles. The interventricular septum was considered part of the left ventricle. The myocardial volume was calculated as the sum of the myocardial area multiplied by slice thickness. When multiplied by the assumed myocardial density (1.05g/cm^3) this gave the myocardial mass. Ventricular mass index was calculated as RV mass divided by LV mass (133).

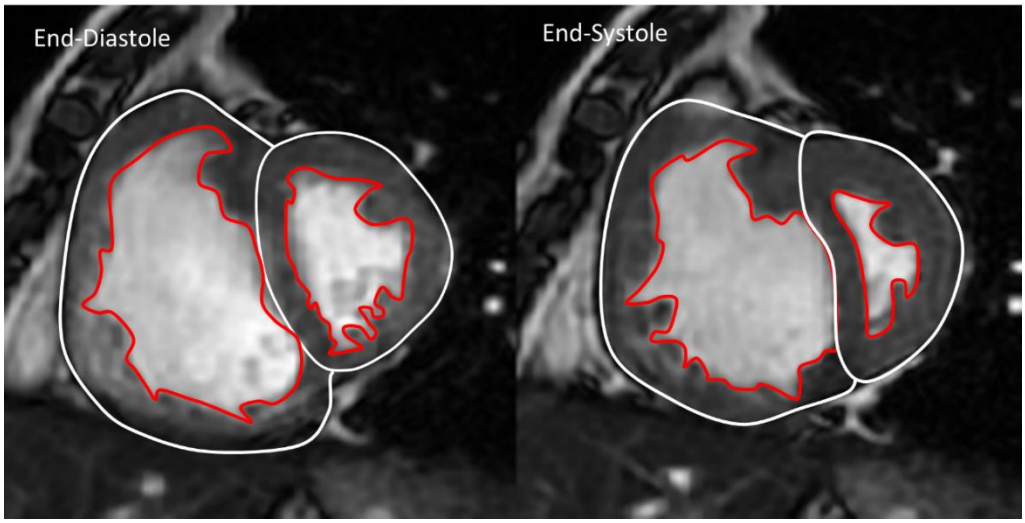

Figure 3.10: *Ventricular Mass.*
The ventricular mass of the left and right ventricle can be calculated as the difference between the endocardial and epicardial contours. This is often expressed as ventricular mass index (VMI), the ratio of right to left ventricular mass, elevated in this case with IPAH.

3.3.2.2.3 Interventricular Septal Angle

The interventricular septal angle was measured as the angle formed between the insertion points of the ventricles to the mid-point of the septum, measured on a mid-chamber slice at end-systole (125,134,236). Page 123 shows this has a high reproducibility.

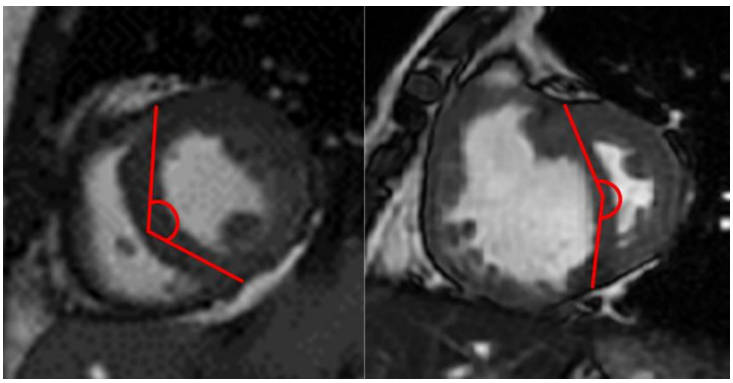

Figure 3.11: *Measurement of the interventricular septal angle.*
The measurement is taken from the short axis SSFP cardiac cine, from a mid-chamber slice. The angle between the RV insertion point and the mid septum is quantified. The patient on the left has a normal septal angle and the patient on the right has a flattened septum.

3.3.2.2.4 Pulmonary Arterial Area

On the magnitude phase contrast images of the pulmonary artery, the maximal and minimal PA areas were manually traced. Pulmonary artery relative area change was defined by the following equation: $PA\ RAC = \frac{Max\ PA\ area - Min\ PA\ area}{Min\ PA\ area}$ (208). It is also possible to perform this measurement on ECG gated CT (112).

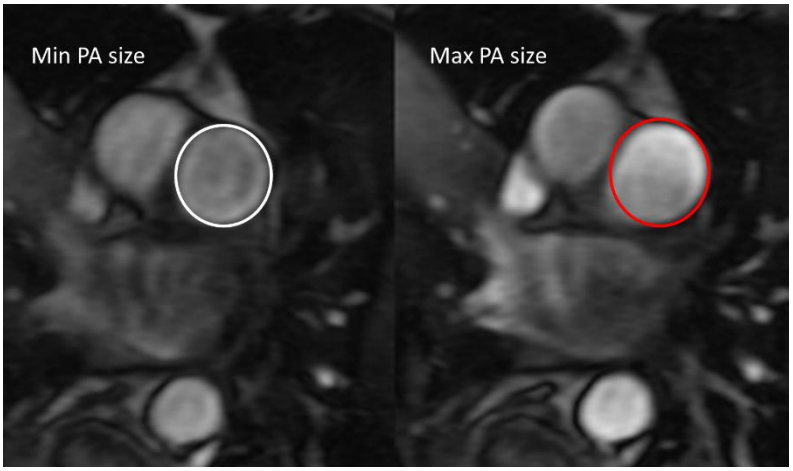

Figure 3.12: Images from the magnitude images of phase contrast imaging *The images are taken perpendicular to the main pulmonary artery. The left image is taken at minimum PA size, the right is taken at maximum PA size.*

3.3.2.2.5 Black Blood Flow Artefact

From the dual inversion recovery fast spin echo pulmonary arterial black blood images, black blood slow flow artefact was scored. A semi-quantitative scale from 0 to 5 was used (0 = absent, 1 = segmental, 2 = lobar, 3 = distal main, 4 = proximal main and 5 = trunk) (135).

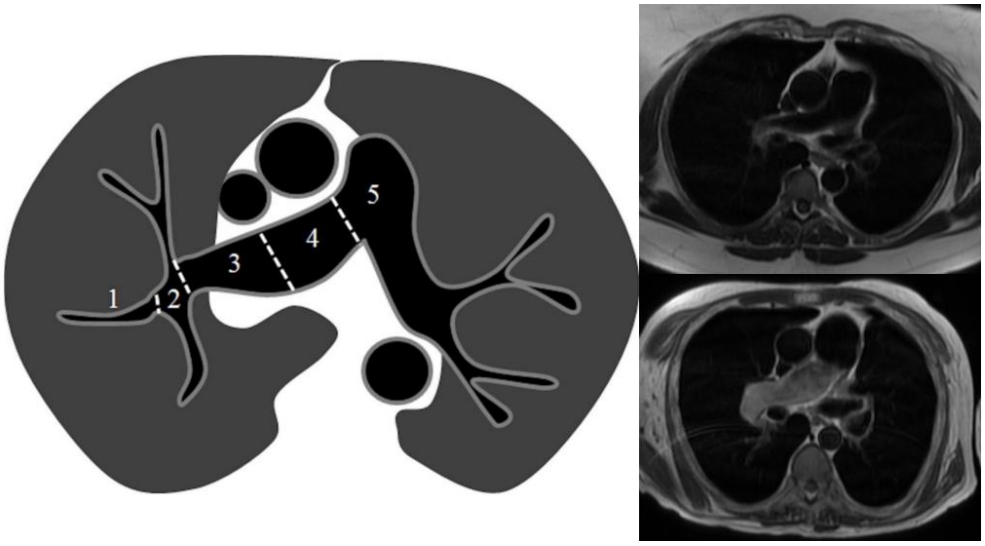

Figure 3.13: Scoring of black blood slow flow artefact.
Adapted by permission from European Springer European Radiology, Black blood MRI has diagnostic and prognostic value in the assessment of patients with pulmonary hypertension, Swift et al, copyright 2012.

3.3.2.2.6 Left Atrial Volume

Left atrial volume was calculated using the bi-plane area length method, using the LVLA and 4-chamber cardiac cine. $LA\ volume = \frac{(0.85 \times A1 \times A2)}{L1 \times L2/2}$ where A1 is the area on the 4Ch, L1 is length on the 4 chamber, A2 is the area on LVLA and L2 is length on LVLA (237). Thresholds of ≥41ml/m2 and ≥43ml/m2 have been proposed for the

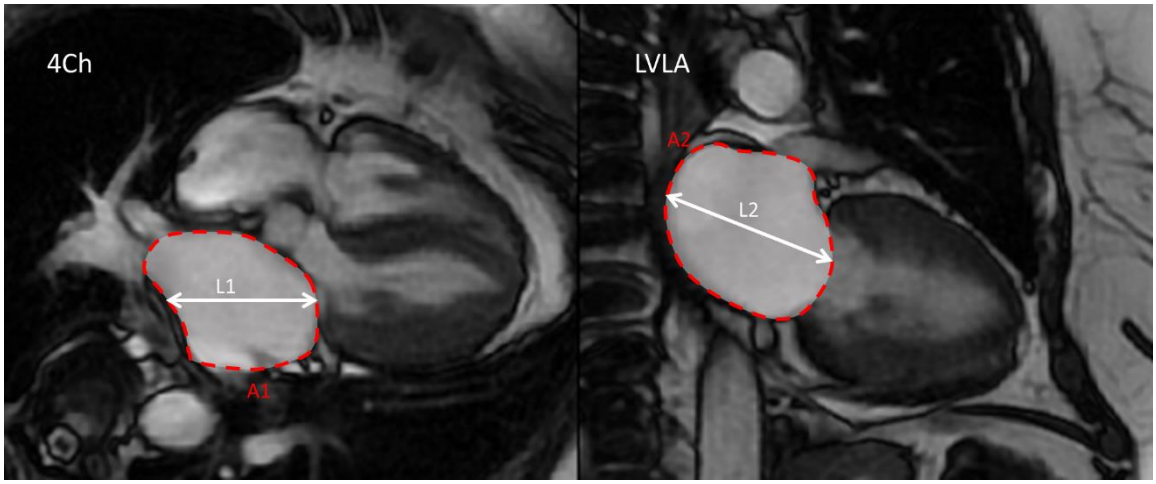

Figure 3.14: Calculation of left atrial volume using the bi-plane area length method.
Area (dotted outline) and length (arrows) derived from the four chamber and left ventricle long axis views.

diagnosis of PH-left heart disease (238,239).

3.3.2.2.7 Phase Contrast Flow Imaging

The contours of the vessel were automatically traced, with manual correction when required. The software then calculated the velocity of all the pixels included within the region of interest (ROI). Pulmonary artery average velocity was calculated as QFlow forward PA velocity/diastolic PA size.

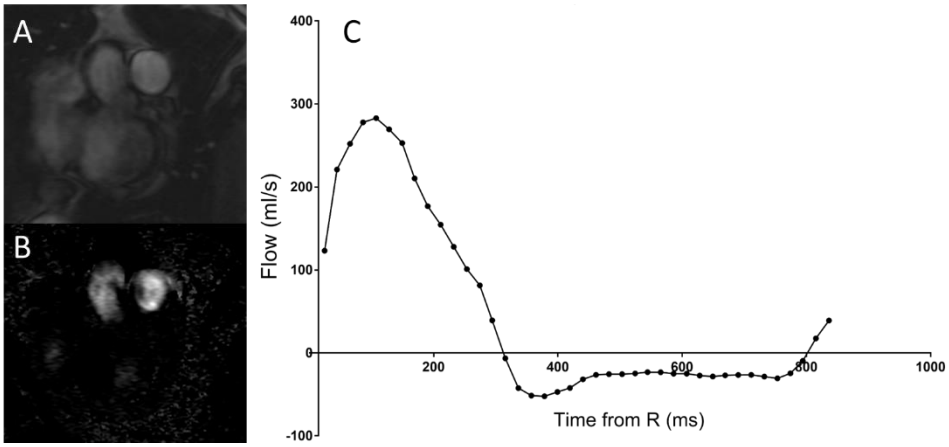

Figure 3.15: Phase contrast imaging of the pulmonary artery.
A: the magnitude image, B- The phase contrast image, C: the flow time curve derived from the Q-flow data.

3.3.2.2.8 Dynamic Contrast Enhanced MRI Transit Times

Signal enhancement time curves were generated from the dynamic contrast enhanced MRI images, for a region of interest within the pulmonary artery and the left atrium. **Figure 3.16** shows the typical time signal curves for a healthy volunteer. The pulmonary transit time (PTT) was calculated as the time delay from peak signal in the pulmonary artery and peak signal in the left atrium. The full-width-half-maximum (FWHM) of the contrast bolus passage was calculated as the time between half the maximum signal intensity on the up and down-slopes of the pulmonary artery time-enhancement curve as previously described (212)(240).

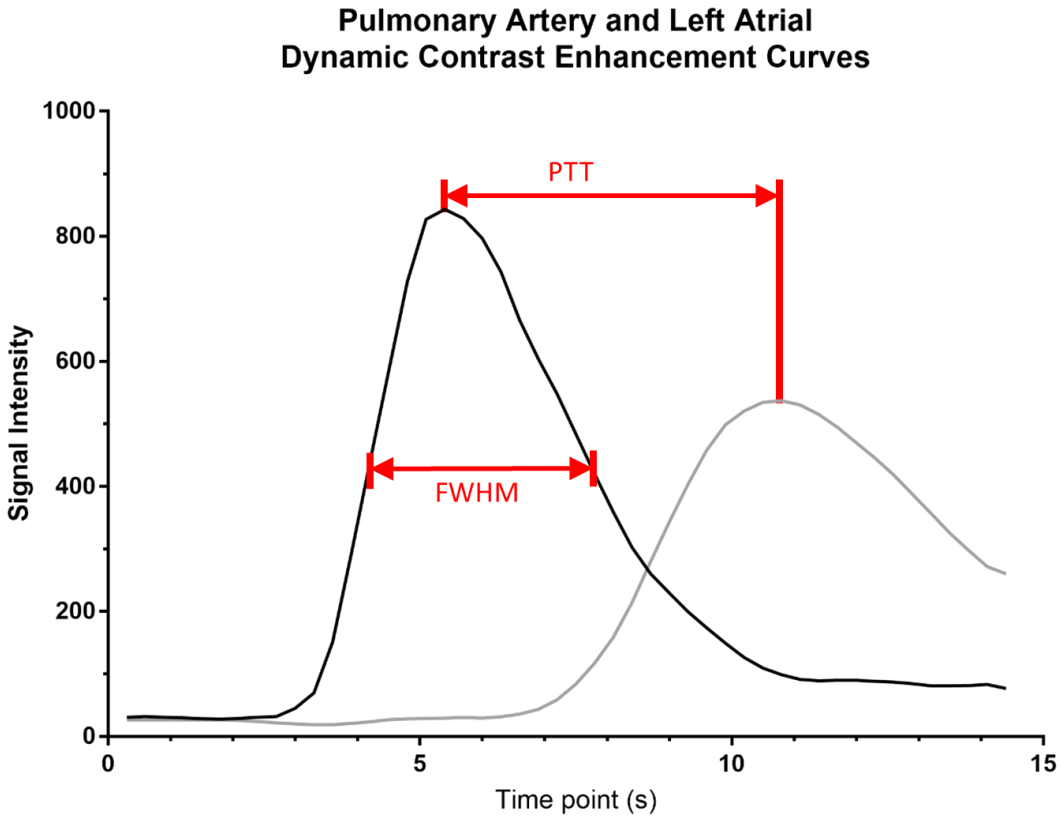

***Figure 3.16*:** Signal-time curves for dynamic contrast enhanced imaging.

The black line shows the contrast enhancement curve of the pulmonary artery and the grey line the left atrium in a healthy volunteer. The calculations of PTT and FWHM are shown.

3.3.3 Single Photon Emission Computed Tomography

Single photon emission computed tomography (SPECT) imaging was performed on a General Electric Infinia SPECT system using a low energy general-purpose collimator. 100MBq 99mTc MAA was administered through a direct intravenous injection with a needle of 21G or larger. The image acquisition parameters were: acquisition matrix 128x128, 60 projections per detector and 7 seconds per projection. Images were acquired prone, and where possible, with the patient's arms extended above their heads.

3.3.4 Computed Tomography

In the chapter assessing phenotypes of pulmonary hypertension due to lung disease, the CTPA was analysed to confirm the underlying cause of pulmonary hypertension. This was used to classify the patients as chronic obstructive lung disease (COPD), interstitial lung disease (ILD) or combined fibrosis and emphysema syndrome (CPFE).

When performed at the local centre, CTPA images were acquired on a 64-slice MDCT (Light-Speed General Electric Medical) during a single breath-hold. Typical acquisition parameters were: 100 mA with automated dose reduction, 120 kV, pitch of 1, rotation time 0.5 s and 0.625-mm collimation, field of view = 400×400 mm, acquisition matrix 512× 512. 100 mL of intravenous contrast agent (Ultravist 300; Bayer Schering, Berlin, Germany) was administered at a rate of 5 mL/s, typically through an 18G cannula in the antecubital fossa. CT images from other centres were also used when no local imaging was available, as long as they were considered to be of diagnostic quality.

3.3.5 Statistical Analysis

Statistical analysis was performed using SPSS version 22 (IBM, Chicago) and figures were created using GraphPad Prism (GraphPad Software, San Diego). When required mathematical scripting was performed using Matlab R2017a (MathWorks, MA). A p value of <0.05 was considered statistically significant, except when multiple hypotheses were tested in which case Bonferroni correction was applied to reduce the risk of type 1 error. The following sections detail the main statistical methodologies used in this thesis.

3.3.5.1 Group comparisons

Comparison of metrics between groups was performed using independent t-test for continuous data and chi-squared test for categorical data. When multiple groups were analysed, ANOVA testing with Bonferroni correction was used.

3.3.5.2 Relationship between MRI and RHC metrics

Correlations between continuous data were calculated using Person's correlation coefficient and for discrete data, Spearman's rank was used.

3.3.5.3 Linear Regression Fitting

To calculate predictive non-invasive equations for right heart catheter measurements, multivariable linear regression curve fitting was used. This uses multiple independent variables (MRI metrics) to predict a single dependent variable (RHC measured mPAP). A least squares approach was used, which builds a model which serially reduces the sum of the squares of the residuals with each new equation produced. The analysis was performed using SPSS in a forward direction. Any metrics that significantly correlated with mPAP at univariate analysis after Bonferroni correction were entered into the linear regression analysis. As the linear regression modelling requires/infers a linear relationship, a scatter plot between all independent metrics and mPAP was examined to ensure linearity and where appropriate the $\log_{10}$ was taken for inclusion in the regression analysis.

3.3.5.4 Diagnostic performance

Diagnostic performance was assessed using receiver operator characteristics (ROC) curve analysis. ROC curve analysis was first developed during World War 2 to analyse radar signals after the attack on Pearl Harbour, but has now been widely adopted in

medicine as a method to assess the diagnostic accuracy of a test. The curve is created by plotting the sensitivity (true positive rate) against 1-specificity (false positive rate) at each value of the variable that is being examined, as a predictor of a dichotomous outcome/diagnosis. A metric that does not predict the outcome will have a straight line at 45˚ from 0 to 1 (ie. at each threshold true positive rate = false positive rate, so it is not discriminatory). A perfect test will have a single point at X=0 and Y=1. Diagnostic accuracy is often quantified by the area under the ROC curve.

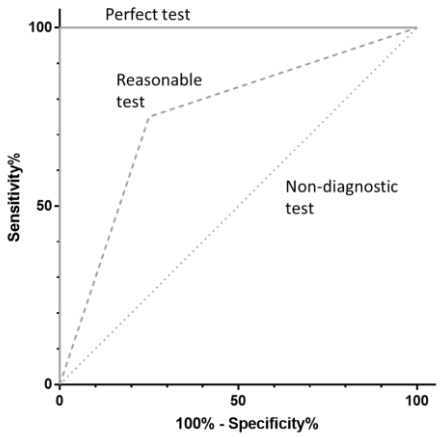

***Figure 3.17*:** An example of a ROC curves.
This diagram gives an example of a non-diagnostic test, a reasonably diagnostic test and a perfect test.

When a threshold was derived this was first derived from the Youden index of the ROC curve in a derivation cohort (Youden's J = sensitivity + specificity - 1) unless otherwise specified. An example of the Youden index is shown in **Figure 3.18**. This was then tested in a separate validation cohort.

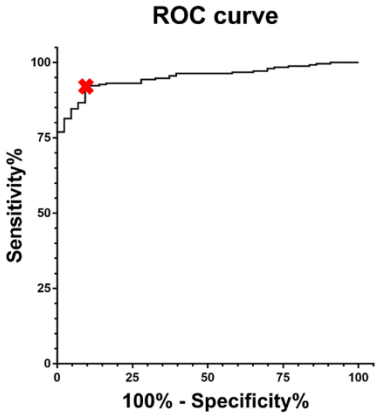

***Figure 3.18*:** ROC curve showing the Youden index.
An example of ROC analysis, the red cross shows the point which balances the sensitivity and specificity (as per Youden's index).

Sensitivity, specificity, negative and positive predictive values were calculated from a 2x2 contingency table and Fisher's exact test was used to determine the statistical significance.

3.3.5.5 Prognosis

For prognosis, the interval between the MRI or right heart catheter to all cause of death or census was considered the follow up period. Cox proportional hazards regressions analysis was used to generate hazard ratios for death for demographic, MRI and right heart catheter data. In order to account for the scale of the variable, all metrics were first standardised to the z score for the population studied, $z = \frac{x-\mu}{\sigma}$, where μ is the mean for the population and σ is the standard deviation of the population.

Kaplan-Meier plots were generated using published thresholds, where available. Where no threshold was available, patients were dichotomised by the median value. Log rank χ^2 was calculated for the Kaplan Meier data. ROC curve analysis was also performed for the prediction at death at a time point that balanced patient numbers and number of deaths.

4 CARDIAC MRI CAN DIAGNOSE PULMONARY HYPERTENSION

The first step in the management of patients with suspected pulmonary hypertension is to identify the presence of a raised pulmonary arterial pressure (mPAP ≥25mmHg). The first body of original research in this thesis centres on improving the non-invasive diagnosis of pulmonary hypertension using magnetic resonance imaging[ii].

4.1 RATIONALE

Pulmonary hypertension (PH) is a condition with a poor morbidity and mortality. It has a varied aetiology, but is defined invasively at right heart catheterisation by a mean pulmonary artery pressure (mPAP) ≥25mmHg at rest (1). Right heart catheterisation is the gold standard for the diagnosis of pulmonary hypertension, although this is an invasive test with 1% serious complication rate (8).

Current guidelines recommend echocardiography to screen patients with suspected pulmonary hypertension: using an assessment of the risk of the presence of PH, as either low, medium or high (1). Doppler echocardiographic measurement of systolic pulmonary arterial pressure requires an estimation of right atrial pressure, and the current estimation from IVC size doesn't accurately predict the true right atrial pressure on right heart catheterization (81). Assessment of pulmonary arterial pressures on echocardiography also requires the patient to have tricuspid regurgitation. Whilst commonly seen in pulmonary hypertension it is not always present, and severe tricuspid regurgitation causes erroneously low or high echocardiographic predictions of mean pulmonary arterial pressures (241). As such, estimation of pulmonary arterial pressures shows only moderate agreement with right heart catheter measured mean pulmonary arterial pressure (242), with 95% limits of agreement on Bland Altman analysis ranging from +38.8 to -40.0 mm Hg (81). A large meta-analysis showed only modest diagnostic accuracy for the presence of pulmonary hypertension with sensitivity and specificity of 83% and 72% respectively (243). Furthermore, echocardiography is not possible in the context of severe lung

[ii] The work presented in this chapter has been submitted to *Radiology* and is currently under review.

disease, due to loss of acoustic windows, and when it is measurable it is often erroneous (244).

A number of cardiac MRI metrics have been identified as predictors of raised pulmonary arterial pressures, and a number of models (both empirical and physiological), have been proposed. These are summarised in **Table 4.6**. These previously identified markers have been tested in single centres in relatively small numbers, and often have modest diagnostic accuracy.

A specific test to identify raised mean pulmonary arterial pressures in patients with suspected pulmonary hypertension would have the potential to reduce the number of invasive right heart catheters that are performed and also allow for simultaneous assessment of prognosis, such as right ventricular function (124).

4.1.1 **Hypotheses**

1. Quantifiable cardiac MRI metrics can predict right heart catheter measured mean pulmonary arterial pressure in patients with suspected PH.
2. The prediction of mean pulmonary arterial pressure and diagnostic accuracy of cardiac MRI can be improved by using a linear regression modelling.

4.1.2 **Aims**

The aim of this chapter was to derive and assess a new regression model for estimation of mPAP using MRI measurements, and assess the diagnostic accuracy of this model in a different patient cohort. A secondary outcome was to assess the accuracy of previously published MRI based metrics.

4.2 MATERIALS AND METHODS

4.2.1 Patients

Consecutive incident patients with suspected pulmonary hypertension who were referred to a tertiary PH centre from April 2012 to October 2016 were identified from the ASPIRE database (Assessing the Spectrum of Pulmonary hypertension Identified at a REferral centre) (245). The first half were used as a derivation cohort and the second half were used as a validation cohort. Only incident patients with MRI and RHC within 14 days were included. Any patient with a left atrial volume index of ≥41 was excluded as this is a potential MRI marker of PH due to left heart disease (PH-LHD) (239). The 2015 ESC/ERS guidelines recommend that these patients are not referred to tertiary referral centres, unless there are features of severe PH or RV dysfunction. Furthermore, as septal angle and VMI are highly correlated with mPAP and previous work has used these as a model for mPAP estimation, it was expected that patients with left heart disease would potentially require a different model. Ethical approval was granted from a local ethics committee for this retrospective study and written consent was waived (ref c06/Q2308/8).

4.2.2 Image Acquisition

Cardiac MRI was performed on a GE HDx 1.5-T whole body scanner (GE Healthcare, Milwaukee, Wisconsin), with the patient supine, using an 8-channel cardiac coil. Four-chamber (4Ch) and short axis (SA) cine images were acquired using a retrospectively cardiac gated multi-slice steady-state free precession (SSFP) sequence, as previously published (217). A stack of axial images in the SA plane with slice thickness of 8 mm with a 2 mm inter-slice gap or 10 mm with no inter-slice gap were acquired, covering both ventricles from base to apex. The SSFP sequence parameters were: TR 2.8 ms, TE 1.0ms, flip angle 50°, field of view 48x43.2, 256x256 matrix, 125 kHz bandwidth, and slice thickness 8 to 10 mm.

Phase contrast imaging was performed perpendicular to the pulmonary trunk. The phase contrast imaging parameters were: TR 5.6 ms, TE 2.7 ms, slice thickness 10 mm, FOV 48x28.8, bandwidth 62.5 kHz, matrix 256x128 and velocity encoding 150 cm/s. The images were retrospectively ECG gated with 40 phases.

Black blood imaging of the pulmonary arteries was performed using a double inversion recovery fast spin echo sequence (DIR-FSE), with a stack of 8mm slices with 10mm spacing taken through the long axis plane of the pulmonary artery acquired using an 8 channel cardiac coil during a breath-hold. There is a 180˚ non-selective inversion pulse, immediately followed by a slice-selective 180˚ de-inversion pulse. The TI is then calculated based on the R-R interval on the ECG, it is 650ms at 60bpm. The other sequence parameters were: TR around 1000ms (dependent upon R-R interval), TE 40ms, FSE flip angle 90˚, echo train length 32 with approximately 2.5ms between echoes, field of view 4cm, 256x256 matrix, 31.2 kHz bandwidth, ASSET parallel imaging factor 2.

4.2.3 **Image Analysis**

MR images were manually analysed by DC (a cardiac MRI radiographer of 9 years cardiac MRI experience) on a GE Advantage Workstation 4.4 and GE Advantage Workstation ReportCard software, blinded to all clinical information and other investigations. Left and right ventricular end-diastolic volume, end-systolic volumes, right and left ventricular stroke volume and mass were calculated (all indexed to body surface area), right and left ventricular ejection fractions, ventricular mass index (RV mass divided by LV mass) (133) and interventricular septal angle were measured as previously described (125). Maximal and minimal PA areas were manually traced, and relative area change was defined by the following equation: RAC= (maximum area-minimum area)/minimum area (208). Pulmonary artery average velocity was calculated as QFlow forward PA velocity/diastolic PA size. Reproducibility metrics for these cardiac MRI metrics for DC and AJS have been previously published (124). Black blood slow flow artefact was scored using a semi-quantitative scale from 0 to 5 (0 = absent, 1 = segmental, 2 = lobar, 3 = distal main, 4 = proximal main and 5 = trunk), and has been shown to have good inter-observer reproducibility (135). A diagram of the key imaging metrics that were measured is shown in **Figure 4.1**. Multiple previously published parametric models, developed for diagnostic assessment of pulmonary hypertension, were derived from Cardiac MRI. These are summarised in **Table 4.6:** Previously published models and their diagnostic accuracy..

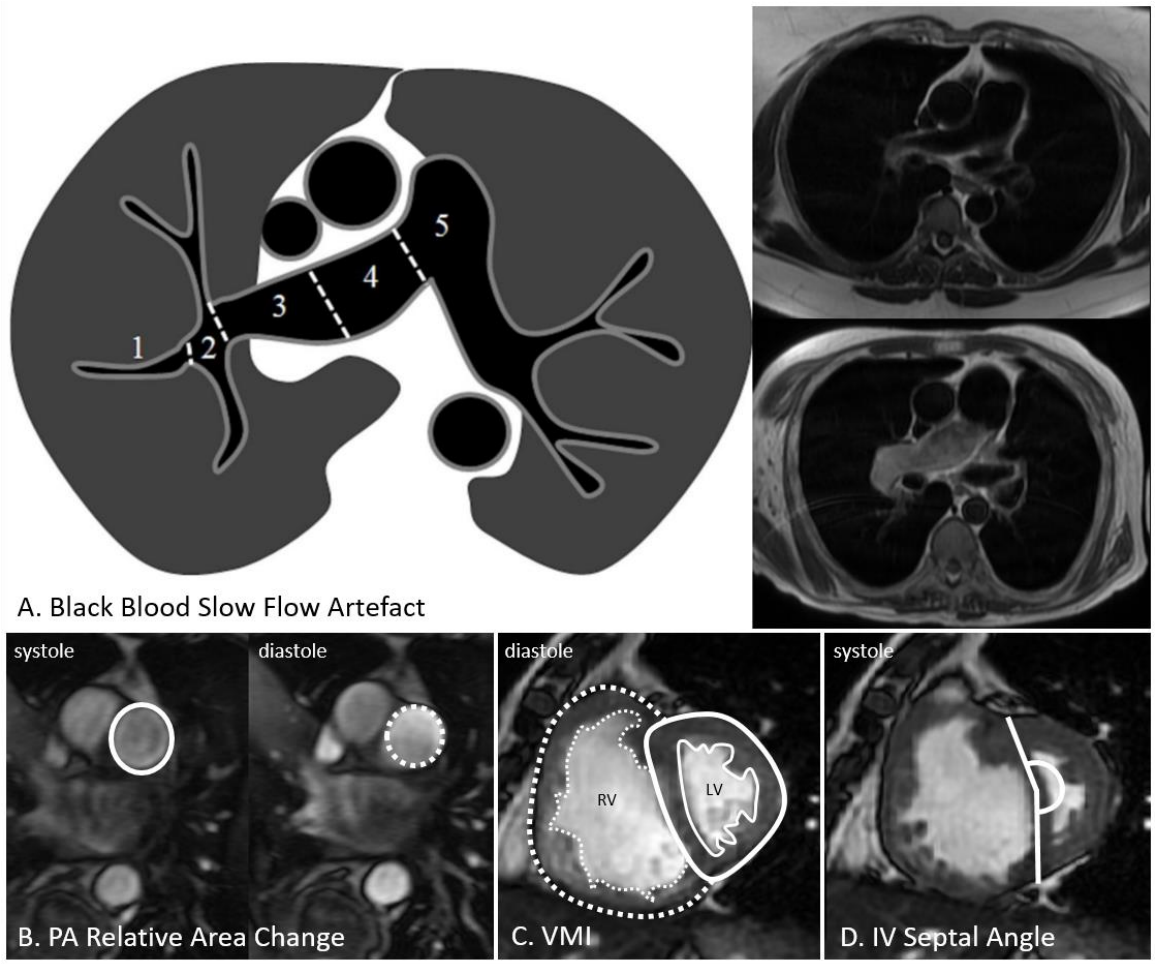

Figure 4.1: *Multi-figure showing the MRI metrics used in this chapter.*
A, a diagrammatic representation of the semi-quantitative scoring of black blood slow flow artefact from the dual inversion recovery fast spin echo black blood images, and inset an example of a case with a score of 1 and a score of 4. B, calculation of pulmonary arterial relative area change (PA RAC) from the systolic and diastolic steady state free procession (SSFP) images of the pulmonary artery. C, the ventricular mass index (VMI), which is the ratio of muscle mass of the right and left ventricular myocardium taken from the 2 chamber SSFP cardiac cine. And D, the interventricular septal angle, taken from the 2 chamber SSFP images at end-systole. Black blood slow flow scoring reprinted with permission from Springer Nature: Black blood MRI has diagnostic and prognostic value in the assessment of patients with pulmonary hypertension. Swift, A.J., Rajaram, S., Marshall, H. et al. Eur Radiol (2012) (135).

4.2.4 Right Heart Catheterisation

Right heart catheterisation was performed using a balloon tipped 7.5Fr thermodilution catheter (Becton-Dickinson, Franklin Lakes, New Jersey). Pulmonary hypertension was defined as a resting mPAP ≥25mmHg, as per recognised guidelines (1). Cardiac output was measured using thermodilution.

4.2.5 Statistical Analysis

Statistical analysis was performed using SPSS 22 (IBM, Chicago) and graphs were produced using GraphPad Prism. Unless otherwise stated, a p value of <0.05 was considered statistically significant.

4.2.5.1 Derivation cohort

The first half of the patients were used as a derivation cohort to derive a new model of mean pulmonary artery pressure estimation. The Pearson correlation coefficient between quantifiable cardiac MRI characteristics and RHC-mPAP were calculated. As multiple correlations were assessed, the risk of type 1 error was reduced using Bonferroni correction and therefore a p-value of <0.002 was considered statistically significant (30 different correlations were assessed). Scatter plots were constructed to ensure linearity between the cardiac MRI metric and mPAP. Any statistically significant correlations were used to calculate a linear regression equation for estimation of mPAP. An ROC curve was constructed to assess a suitable diagnostic threshold for the new model, one that was highly specific and one that had a balance of specificity and sensitivity (the Youden index). ROC curves were also constructed for the CMR-PARV model to identify a threshold with high specificity, for assessment in the validation cohort.

4.2.5.2 Validation cohort

The second half of the patients were used as a validation cohort. The correlation of the new regression equation for mPAP prediction against RHC measured mPAP was calculated and diagnostic performance was assessed using ROC curve analysis,

sensitivity and specificity, negative and positive predictive values. The accuracy of the model was assessed using Bland-Altman plot.

The accuracy of the other previously published models was also assessed. The Pearson correlation coefficient for each model with mPAP or PVR was calculated. ROC curve analysis, sensitivity and specificity, negative and positive predictive values were also calculated for each of these models to assess their diagnostic performance. **Table 4.1** provides the equations for the calculation of the new and previously published models.

Table 4.1: Models referred to in this chapter.

Name	Equation
α index	Minimum PA area/RVEF
RV_{CMR}	–4.6 + (inter- ventricular septal angle x 0.23) + (ventricular mass index x 16.3)
$PAWP_{CMR}$	6.43 + (LA Volume Index * 0.22)
PVR_{CMR}	$(RV_{CMR} – PAWP_{CMR})/CO_{CMR}$
$PARV_{CMR}$[iii]	-21.806 + (IVS angle x 0.31) + (VMI x 11.5) + (diastolic PA area x 0.01) – (PA RAC x 0.22)
$RVBB_{CMR}$	-178.7 + (42.730 * log10 IVS angle) + (7.569 * log10 VMI) + (3.393 * BB)

*PA: Pulmonary artery, RVEF: Right ventricle ejection fraction, LA: Left atrium, CO_{CMR}: Cardiac output calculated from CMR = stroke volume * heart rate, IVS: Interventricular septal angle, VMI: Ventricular mass index, BB: Black blood slow flow artefact score.*

[iii] The $PARV_{CMR}$ model is discussed in Chapter 6, but in this chapter is tested in a separate cohort of all patients with suspected PH.

4.3 RESULTS

4.3.1 Patients

The ASPIRE MRI sub-registry contains 2437 MRI scans for patients with suspected or confirmed pulmonary hypertension. Within this, there are 1272 incident cases with suspected pulmonary hypertension, of which 957 had RHC and MRI within 14 days. 603 of these cases had a left atrial volume index of <41, so were included in this study. The first 300 patients were used as the derivation cohort and the second 303 were used as a validation cohort. **Figure 4.2** shows the process of patient selection. The baseline clinical and RHC characteristics of the patients are provided in **Table 4.2**. Aside from cardiac index, there were no significant differences in the clinical demographics of patients between the derivation and validation cohorts as shown in **Table 4.3**. The difference in cardiac index between the two groups was very small and unlikely to be of clinical significance. There were 93 cases with no pulmonary hypertension, 264 cases with PAH, 11 with PH-LHD (even after exclusion of the dilated left atria), 60 with PH due to respiratory disease, 157 with CTEPH and 18 with PH due to unclear or multifactorial mechanisms.

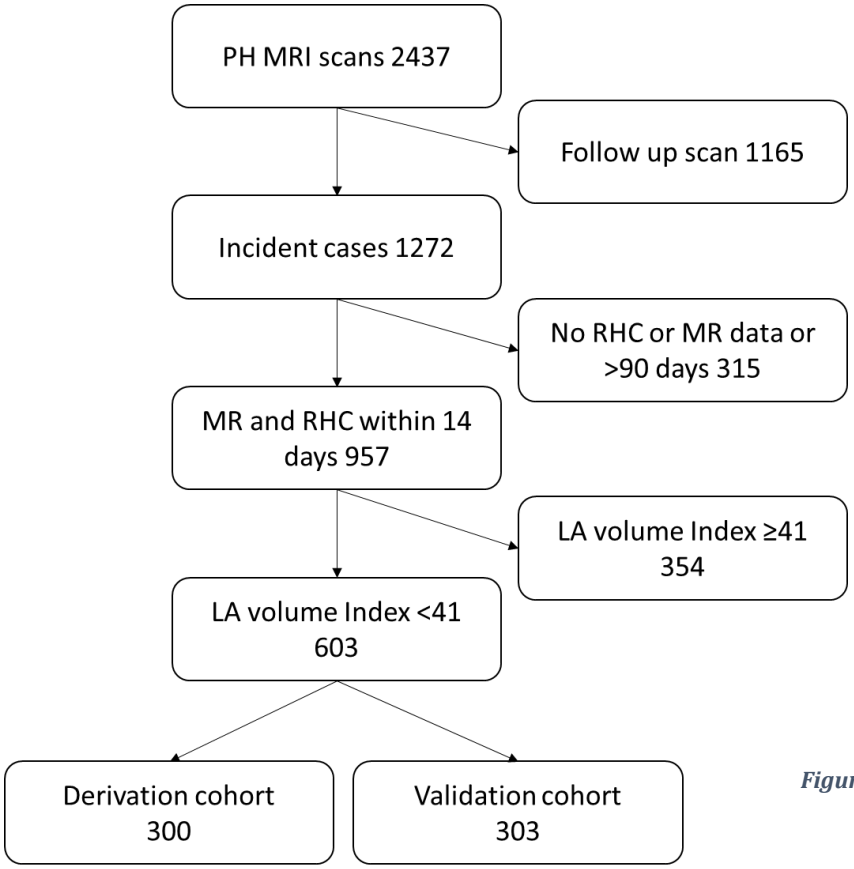

Figure 4.2: *Patient flow*

Table 4.2: *Baseline demographics for all cases, mean with standard deviation, p-value between each PH group, calculated using ANOVA*

	All patients	Not PH	PAH	PH-LHD	PH-Resp	CTEPH	PH Multi	P-value
Number	603	93	264	11	60	157	18	<0.0001
Age (years)	61 (14)	56 (16)	60 (14)	62 (12)	66 (10)	64 (12)	62 (9)	<0.0001
Sex (F/M)	365/238	63/30	188/76	10/1	25/35	70/87	9/9	<0.0001
WHO functional class (I,II,III,IV)	1,64,459,63	0,33,48,3	0,7,216,37	1,2,8,0	0,5,42,13	0,17,130,9	0,0,15,1	<0.0001
ISWT (m)	225 (191)	296 (218)	200 (182)	180 (157)	150 (115)	263 (199)	191 (181)	<0.0001
mPAP (mmHg)	42 (16)	20 (3)	49 (13)	34 (9)	40 (11)	47 (12)	47 (13)	<0.0001
mRAP (mmHg)	10 (6)	6 (3)	11 (6)	12 (3)	9 (4)	11 (5)	10 (7)	<0.0001
PAWP (mmHg)	11 (4)	10 (4)	11 (3)	20 (7)	12 (4)	11 (3)	11 (4)	<0.0001
CI	2.6 (0.8)	3.1 (0.7)	2.5 (0.8)	2.7 (0.5)	2.8 (0.7)	2.4 (0.7)	2.6 (0.9)	<0.0001
PVRI (dyn.s/cm^5)	336 (260)	75 (40)	438 (268)	152 (114)	260 (157)	362 (234)	397 (251)	<0.0001
SvO_2	64 (9)	71 (7)	63 (9)	71 (9)	66 (6)	62 (8)	64 (8)	<0.0001
FEV1 (% predicted)	78 (24)	87 (21)	76 (23)	66 (24)	60 (29)	84 (22)	64 (22)	<0.0001
FVC (% predicted)	81 (24)	84 (19)	76 (22)	65 (15)	72 (31)	92 (22)	76 (28)	<0.0001
FEV1/FVC	69 (13)	74 (12)	71 (12)	68 (15)	62 (18)	67 (11)	65 (14)	<0.0001
TLCO (% predicted)	46 (23)	62 (18)	37 (21)	44 (15)	29 (14)	58 (18)	34 (19)	<0.0001
Days between RHC & MR	1 (2)	1 (2)	1 (2)	1 (4)	1 (0)	1 (1)	1 (4)	0.076

Table 4.3: *Demographics of the training and validation cohorts*

	Derivation	Validation	P-value
Number	300	303	
Age (years)	60 (14)	61 (14)	0.279
Sex (F/M)	189/111	176/127	0.243
WHO functional class (I,II,III,IV)	0,34,223,33	1,30,236,30	0.084
ISWT (m)	228 (184)	223 (198)	0.776
mPAP (mmHg)	42 (16)	42 (15)	0.943
mRAP (mmHg)	10 (6)	10 (6)	0.317
PAWP (mmHg)	11 (4)	11 (4)	0.248
CI (L/min/m2)	2.8 (0.8)	2.5 (0.8)	<0.0001
PVRI (dyns)	326 (241)	345 (277)	0.389
SvO_2 (%)	64 (9)	64 (9)	0.934
FEV1 (% predicted)	78 (24)	78 (25)	0.885
FVC (% predicted)	82 (23)	80 (24)	0.864
FEV1/FVC (ratio)	68 (13)	70 (12)	0.240
TLCO (% predicted)	46 (23)	46 (21)	0.978
Days between RHC & MR	1 (2)	1 (2)	0.591

WHO: World Health Organisation, RHC: right heart catheter, mPAP: right heart catheter measured mean pulmonary artery pressure, mRAP: mean right atrial pressure, PAWP: pulmonary artery wedge pressure, CI: cardiac index, PVRI: pulmonary vascular resistance index, SvO_2: mixed venous oxygen saturation, FEV1: Forced expiratory volume in 1 second, FVC: Forced vital capacity, TLCO: transfer for carbon monoxide

4.3.2 Derivation cohort

Table 4.4 shows the Pearson's correlation coefficient for each cardiac MRI metric with right heart catheter measured mPAP and PVR. The strongest correlations with mPAP were for systolic interventricular septal angle, black blood artefact score, RV ejection fraction, right ventricular end systolic volume index and ventricular mass index (R=0.740, 0.694, -0.602, 0.585 and 0.529, respectively all p values <0.0001). Increasing RV volumes (RV end diastolic and end systolic volumes), reducing LA volume index and LV end diastolic volume, increasing PA size and reducing PA relative area change and velocity all showed statistically significant correlations with increasing mean pulmonary arterial pressure. Visual inspection of the scatter plots of interventricular septal angle and ventricular mass index revealed an exponential relationship, so the $\log_{10}$ of these metrics was used in further calculations.

Regression analysis, performed in a forwards direction for any metric that showed a statistically significant correlation with mPAP ($p<0.05$) produced the following equation:

$$RVBB_{CMR} = -178.7 + 42.730 \times \mathrm{IVS}_{angle} + 7.569 \times log_{10}(VMI) + 3.393 \times BB$$

where, $\mathrm{IVS}_{\mathrm{angle}}$ is the interventricular septal angle, VMI is the ventricular mass index and BB is the black blood slow flow artefact. ROC curve analysis in the derivation cohort identified 41mmHg as a threshold that was highly specific (98%), with reasonable sensitivity (72%). A separate threshold of 25mmHg was identified that was a balance of sensitivity and specificity (Youden index), with sensitivity of 96% and specificity of 73%. The $\mathrm{RV}_{\mathrm{CMR}}$ model has a previously published threshold for diagnosis set at 25mmHg to mimic the threshold for mPAP. 36mmHg was identified as a highly specific threshold (100% specific) within the derivation cohort.

	mPAP	PVR	AUC
RVEDVI	0.480*	0.480*	0.782
RVESVI	0.585*	0.611*	0.854
RVEF	-0.602*	-0.623*	0.835
RVSVI	-0.101	-0.159*	0.573
LVEDVI	-0.396*	-0.502*	0.738
LVESVI	-0.091	-0.107	0.531
LVEF	-0.302*	-0.368*	0.703
LVSVI	-0.491*	-0.597*	0.805
RV mass	0.535*	0.138*	0.862
LV diastolic mass	-0.031	-0.227*	0.512
LV systolic mass	-0.145	-0.336*	0.598
IV Septal angle (systole)	0.740*	0.704*	0.908
IV Septal angle (diastole)	0.548*	0.530*	0.794
4Ch LA area	-0.254*	-0.380*	0.643
4Ch LA length	-0.038	-0.115	0.535
2Ch LA area	0.04	-0.123	0.566
2Ch LA length	0.102	-0.032	0.608
LA volume index	-0.183*	-0.277*	0.552
Aortic flow	-0.290*	-0.470*	0.653
PA flow	-0.138	-0.330*	0.586
Systolic PA area	0.411*	0.234*	0.817
Diastolic PA area	0.504*	0.342*	0.878
PA RAC	-0.357*	-0.382*	0.664
Black blood score	0.694*	0.654	0.909
Diastolic VMI	0.529*	0.533*	0.872
Systolic VMI	0.553*	0.563*	0.897
Av PA velocity	-0.505*	-0.548*	0.828

Table 4.4: *Training cohort correlations with mPAP and PVR and area under the ROC curve for the diagnosis of PH.*
*RVEDV: right ventricular end-diastolic volume, RVESV: right ventricular end-systolic volume, RVEF: right ventricular ejection fraction, RV: right ventricle, LVEDV: left ventricular end-diastolic volume, LVESV: left ventricular end-systolic volume, LVEF: left ventricular ejection fraction, PA RAC: pulmonary artery relative area change, VMI: ventricular mass index, IVS: interventricular septum, *p<0.001*

Threshold (mmHg)	Sensitivity (%)	Specificity (%)
20	100	32
25	96	73
30	92	87
35	85	98
40	75	98
45	59	100
50	41	100

Table 4.5: *Sensitivity and specificity data from the ROC curve in the training cohort for the $RVBB_{CMR}$ model.*
A threshold of 25 was identified as the Youden index to balance sensitivity and specificity and 41 was identified as a highly specific threshold.

4.3.3 **Validation cohort**

The newly derived model for mPAP prediction correlated strongly with right heart catheter measured mPAP (R= 0.798, p<0.001). It showed high diagnostic accuracy (AUC = 0.951, p<0.001), and the more specific threshold (41mmHg) had 62% (56-68%) sensitivity, 100% (92-100%) specificity, 100% (98-100%) positive predictive value and 32% (24-40%) negative predictive value. The threshold that balanced sensitivity and specificity (25mmHg) had 93% sensitivity, 79% specificity, 96% positive predictive value and 67% negative predictive value. Bland-Altman analysis showed a small bias (3.9%), with reasonable 95% agreement (-42 to 50%).

The next best model was the $PARV_{CMR}$ model, which strongly correlated with mPAP (R=0.753, p<0.0001), and showed good diagnostic accuracy (AUC 0.914, p<0.001). The highly specific threshold of 36mmHg identified in the derivation cohort had 57% sensitivity, 100% specificity, 100% positive predictive value and 29% negative predictive value. The threshold that was previously published as a balance of sensitivity and specificity (25mmHg) had 91% sensitivity, 62% specificity, 93% positive predictive value and 55% negative predictive value. Bland Altman analysis showed a reasonable bias (14%) with reasonable 95% agreement (-35 to 64%). **Figure 4.3** shows the scatter and Bland-Altman plots for the $RVBB_{CMR}$ and $PARV_{CMR}$ models.

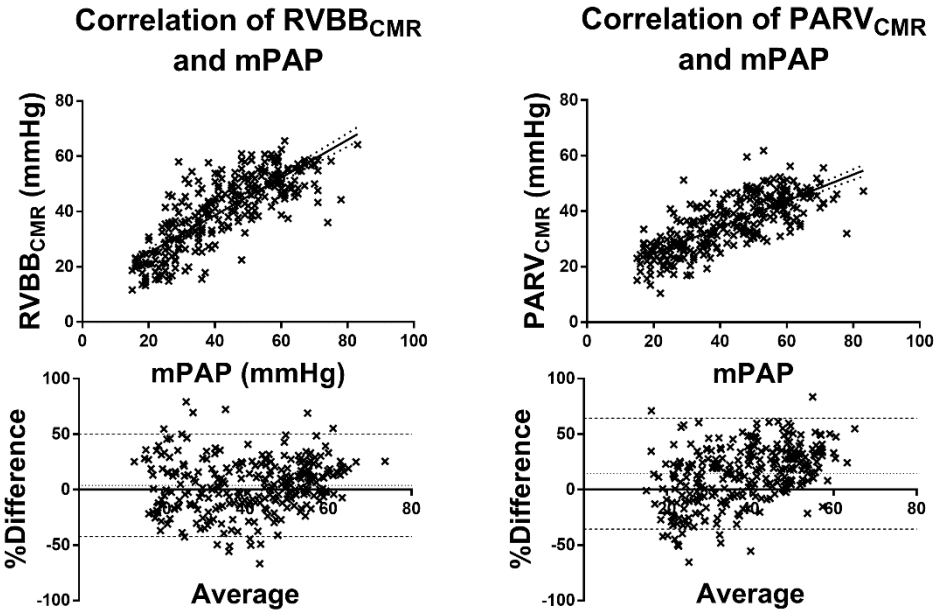

Figure 4.3: *Correlation of the $RVBB_{CMR}$ and $PARV_{CMR}$ models with right heart catheter measured mPAP (top row) and the corresponding Bland-Altman plot (bottom row) in the validation cohort.*
The dotted line shows the bias and the dashed line the 95% levels of agreement.

Table 4.6 shows how the previously published metrics and models perform as diagnostic tools in pulmonary hypertension. The remaining models all had reasonable diagnostic accuracy for the presence of pulmonary hypertension, **figure 4** shows the diagnostic performance of each of the models and the incremental benefit provided by the newly derived $RVBB_{CMR}$ model.

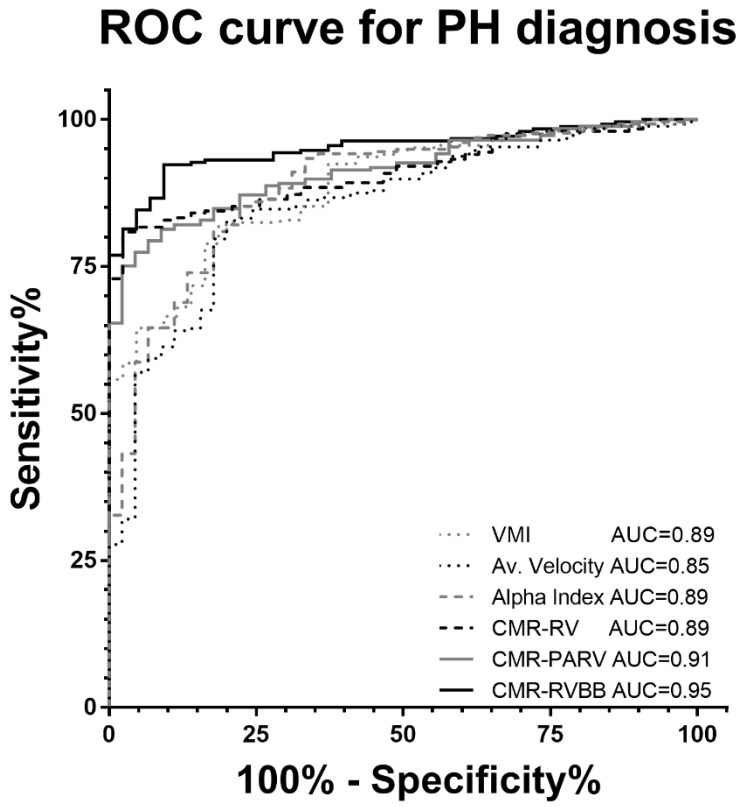

Figure 4.4: *ROC curve for each of the models.* All p-values are statistically significant.

Table 4.6: *Previously published models and their diagnostic accuracy.*

Author	Year	Cases	RHC metric	CMR marker	Initial publication			Validation cohort		Diagnostic accuracy for PH				
					Correlation	AUC	Threshold	Correlation	AUC	Sensitivity	Specificity	PPV	NPV	p-value
Roeleveld (246)	2005	44/0	mPAP	VMI	0.56*		0.6	0.705**	0.887	25 (20-30)	100 (92-100)	100 (94-100)	19 (14-24)	<0.0001
Sanz (247)	2007	42/17	mPAP	Average PA velocity	-0.73**	0.9	11.7cm/s	-0.538**	0.858	4 (2-7)	73 (59-84)	45 (27-65)	12 (9-16)	<0.0001
				Diastolic PA area	0.67**	0.95	6.6cm2	0.445**	0.871	81 (76-86)	80 (66-89)	96 (91-98)	43 (33-54)	<0.0001
			PVRI	Average PA velocity	-0.86**	0.92	11.7cm/s	-0.521**	0.802	4 (2-7)	73 (59-84)	45 (27-65)	12 (9-16)	<0.0001
				Diastolic PA area	0.64**	0.93	6.0cm2	0.235**	0.756	92 (86-95)	40 (31-48)	66 (59-72)	79 (59-72)	<0.0001
Gan (207)	2007	70/16	mPAP	PA RAC	0.47*			-0.352**	0.607	77 (72-82)	36 (23-50)	87 (82-91)	21 (14-32)	<0.0001
Garcia-Alvarez (248)	2011	100/0	PVR	PVR_{CMR}	0.84**	0.97	4.2WU	0.631**	0.878	96 (93-98)	38 (25-52)	90 (86-93)	65 (46-81)	<0.0001
Swift (208)	2012	194/39	mPAP	VMI	0.78**	0.91	0.4	0.705**	0.887	55 (49-61)	100 (92-100)	100 (97-100)	28 (21-35)	<0.0001
				Diastolic PA area	0.35*	0.82	6.0cm2	0.445**	0.871	88 (83-91)	69 (51-80)	94 (90-96)	50 (38-62)	<0.0001
				PA RAC	-0.54**	0.87	≤15%	-0.352**	0.607	77 (72-82)	36 (23-50)	87 (82-91)	21 (14-32)	<0.0001
Moral (249)	2012	152/33	mPAP	α index	0.61**	0.97	7.2	0.528**	0.885	99 (97-100)	13 (6-26)	87 (82-90)	75 (41-96)	0.0002
Swift (125)	2013	64+64/12+10	mPAP	RV_{CMR} model	0.82**	0.96	≥32mmHg	0.787**	0.911	88 (84-92)	60 (46-74)	93 (89-96)	47 (35-60)	<0.0001
			PVR	PVR_{CMR} model	0.87**	0.94	≥3WU	0.805	0.860	90 (85-93)	45 (32-60)	91 (86-94)	43 (30-58)	<0.0001
Johns (217)	2017	87/15 (COPD)	mPAP	$PARV_{CMR}$ model	0.732**	0.93	25mmHg	0.753**	0.914	91 (87-94)	62 (48-75)	93 (89-96)	55 (41-68)	<0.0001
Johns	2017	300/302	mPAP	$RVBB_{CMR}$	N/A	N/A	25mmHg	0.798	0.951	93 (89-96)	79 (65-89)	96 (93-98)	67 (53-78)	<0.0001

*mPAP: mean pulmonary arterial pressure, VMI: ventricular mass index, PVR(I): pulmonary vascular resistance (index), PA: pulmonary artery PA RAC: Pulmonary arterial relative area change, LGE: late gadolinium enhancement, * p <0.05, ** p <0.001. CMR PVR = 19.38 - (4.62*Ln average Pa velocity) - (0.08 * RVEF), α=minimum PA area/RVEF, RV_{CMR} model = –4.6 + (inter- ventricular septal angle x 0.23) + (ventricular mass index x 16.3), PVR_{CMR} model = $(mPAP_{CMR} – PAWP_{CMR})/CO$, $PARV_{CMR}$ model = -21.806 + (inter- ventricular septal angle x 0.31) + (ventricular mass index x 11.5) + (diastolic pulmonary artery area x 0.01) – (PA relative area change x 0.22), $RVBB_{CMR}$ = -178.7 + 42.730 * log10 IVS angle + 7.569 * log10 VMI + 3.393 * BB.*

4.4 DISCUSSION

This chapter shows that multiple cardiac MRI metrics have high diagnostic accuracy for the presence of pulmonary hypertension, which can be improved when combined as regression model. We have derived a new linear regression model (in 300 cases) and shown high diagnostic accuracy in a large validation cohort of cases (a further 303). We have also validated previously published models for the prediction of PH, and shown high diagnostic accuracy. Whilst echocardiography is currently the mainstay of non-invasive estimation of pulmonary arterial pressures, it has only modest diagnostic accuracy and is limited in certain aetiologies (244,250). Cardiac MRI is well established as a highly reproducible method for non-invasive assessment of right ventricular function (251,252), which is sensitive to change (130,253,254) and does not require exposure to ionising radiation and is therefore potentially suitable as a screening tool for PH.

Currently, whilst echocardiography is recommended for screening patients with suspected pulmonary hypertension, the diagnosis is made invasively using mean pulmonary arterial pressure, measured on right heart catheter (1). We have shown that a model based upon easily measured cardiac MRI metrics (that have been previously shown to be of high reproducibility) can be used to predict pulmonary arterial pressure with reasonable accuracy. More importantly, for a diagnostic test, we have shown that this model has very high diagnostic accuracy, and a threshold of 41mmHg on the model can identify patients with pulmonary hypertension with 98-100% specificity. Whilst this data requires validation in a different cohort of patients with suspected pulmonary hypertension, identifying patients who have PH using a threshold of 41 on this model would have the potential to reduce the number of diagnostic right heart catheters performed in our centre by 333 over the 4.5 years studied. Although clearly, further work is required in the assessment of cardiac and pulmonary vascular MRI in this regard, as patients with PAH will still require vasoreactivity testing and identification of patients with PH due to left heart disease (who do not respond to treatment) requires pulmonary arterial wedge pressure measurement. Increasing the use of non-invasive methodologies with “off the shelf” cardiac MRI sequences, will also help with screening for patients with PH in the clinical context of unexplained breathlessness, where a more sensitive threshold

(such as the 25mmHg threshold proposed in this paper) may be useful in identifying patients before referral to specialist centres. The newly defined model was derived in a training cohort and tested in a validation cohort. There was a statistically significant difference in the cardiac index between the 2 cohorts, although this was unlikely to be of clinical significance (both had significantly reduced cardiac index) and is likely to represent type 1 error.

Whilst not assessed in this thesis, the ability to non-invasively predict pulmonary arterial pressure would be useful at follow up and to assess response to treatment. RHC is advocated for assessment of treatment response when clinical assessment, exercise testing and echocardiography are equivocal (1). Some physicians follow an approach combining both right heart catheter and cardiac MRI to identify when falls in pulmonary vascular resistance (PVR) measured at RHC are actually due to failure of the right ventricle, rather than response to treatment. Furthermore, a number of cardio-pulmonary vascular MRI metrics which reflect right ventricular structure/function and pulmonary arterial stiffness have been identified as strong markers of prognosis in patients with PH, and can be assessed in the same sitting (124). These markers are reproducible (251,252) and sensitive to change (130,253,254), making them perfect candidates for assessment at follow up.

We recommend the use of the $RVBB_{CMR}$ model proposed from linear regression in this paper as it is the most accurate predictor of right heart catheter measured mPAP. It comprises measurement of displacement of the interventricular septum (a marker of the pressure and volume differential between the left and right ventricle), remodelling of the right ventricle (ventricular mass index - VMI) and slow or turbulent flow artefact in the pulmonary artery on black blood imaging. These measurements are easily acquired from standard MRI sequences, require little post-processing time and are reproducible (124). Black blood pulmonary arterial flow artefact is a reproducible marker of outcome in PAH (135). It is likely to be a composite of slow flow and vortical or turbulent flow within the pulmonary artery. The increasing use of 4D phase contrast flow imaging will likely allow this metric within the model to be improved upon (140–142). The parameters of black blood imaging that are susceptible to flow artefacts (slice thickness, TI, TE, echo train length, cardiac triggering point) were kept the same between subjects, and could be easily

adopted for standardized use in different centres. In centres where black blood imaging is not available or adopted, a previously published model ($PARV_{CMR}$) using the interventricular septal angle, ventricular mass index, diastolic pulmonary arterial size and pulmonary arterial relative area change can be implemented with a threshold (36mmHg) that has similarly high specificity of 100%.

In patients with pulmonary hypertension due to left heart disease, treatment is aimed at the underlying cause (often left ventricular diastolic dysfunction) and not at the pulmonary vasculature. As such, current guidelines recommend that patients with suspected pulmonary hypertension, who have left heart disease and no features of severe PH are not referred to specialist pulmonary hypertension centres (1). We have considered this recommendation in our patient selection, using CMRI derived left atrial volume index (255) ($\geq 41 ml/m^2$) as a cardiac MRI marker for the presence of left heart disease (239). Further work is required to improve the identification of patients with PH due to left heart disease using cardiac MRI such as trans-mitral flow and left atrial and ventricular filling parameters.

This work presents data from a large cohort of incident patients with suspected pulmonary hypertension. It is however, limited by its single centre, retrospective design. In order to further assess the validity of the newly derived model it would be useful to assess the diagnostic accuracy in a cohort of suspected pulmonary hypertension in a different centre. The tertiary referral centre population potentially limits it's applicability in the wider clinical setting.

4.5 CONCLUSION

Cardiac MRI has high diagnostic accuracy in a cohort of incident patients referred to a tertiary referral centre with suspected pulmonary hypertension. A model comprising simple, reproducible and easy to obtain metrics (interventricular septal angle, ventricular mass index and black blood score) is able to identify patients with pulmonary hypertension with 100% specificity, potentially reducing the current reliance upon invasive right heart catheterisation.

5 CARDIAC MRI CAN PHENOTYPE PULMONARY HYPERTENSION

Once the diagnosis of pulmonary hypertension has been made, identification of the underlying cause of pulmonary hypertension is key to initiating the correct treatment. The following chapter explores the use of cardiac MRI in the phenotyping of patients with pulmonary hypertension.

Patients with group 1: PAH and group 4: CTEPH can be successfully treated with pulmonary vasodilators, and in the case of CTEPH, cured with pulmonary end-arterectomy. It is therefore vital that these patients are correctly identified from the other groups of pulmonary hypertension. There are two key clinical questions in this regard. The first challenge is to identify those patients with chronic thrombo-embolic pulmonary hypertension, to correctly identify those patients who should be considered for curative therapy with pulmonary end-arterectomy. The second big challenge is the identification of patients with group 1: pulmonary arterial hypertension from those patients with pulmonary hypertension due to left heart disease. This is particularly hindered by a phenotype of patients with pulmonary hypertension with combined pre and post pulmonary hypertension, due to additional pre-capillary pulmonary arteriolar remodelling.

The following chapter is split into three parts[iv]: i) identifying patients with pulmonary hypertension due to left heart disease (group 2), who have a pre-capillary component to their pulmonary hypertension, ii) assessing the differences and similarities in cardiac phenotype between PH-lung patients (group 3), and iii) identifying patients with chronic thrombo-embolic pulmonary hypertension (group 4).

[iv] Each section of this chapter makes up work in separate papers.
Cardiac MRI Can Identify and Phenotype PH in Left Heart Disease is based upon a manuscript currently under second review with *Radiology.*
Cardio-Pulmonary MRI Can Screen For CTEPH has been published in in the *Journal of Magnetic Resonance imaging* entitled "Lung Perfusion: MRI vs. SPECT for Screening in Suspected Chronic Thromboembolic Pulmonary Hypertension" (89)

5.1 CARDIAC MRI CAN IDENTIFY AND PHENOTYPE PH IN LEFT HEART DISEASE

5.1.1 Rationale

Patients with left heart disease commonly develop pulmonary hypertension (PH) (28). This initially results from passive backward transmission of high left ventricular filling pressures through the pulmonary circulation. Current guidelines define this post-capillary disease by a pulmonary arterial wedge pressure (PAWP) >15mmHg (22). Some patients with post-capillary disease may subsequently develop a degree of pre-capillary vascular remodelling due to prolonged elevation of pulmonary arterial pressures (22,30–37). Previously, the difference between mean pulmonary arterial pressure (mPAP) and PAWP (the trans-pulmonary gradient, TPG) was used to identify patients with PH "out of proportion" to left heart disease. Subsequently a study by Gerges et al identified the diastolic pulmonary pressure gradient (DPG = diastolic pulmonary artery pressure - mean PAWP) as a superior prognostic parameter in patients with post-capillary disease (30). The 5th world PH symposium therefore introduced the classification of combined pre and post capillary pulmonary hypertension (Cpc-PH), defined as mPAP ≥ 25mmHg, PAWP >15 mmHg, DPG of ≥7 and/or pulmonary vascular resistance (PVR) >3 WU (22). Patients with Cpc-PH are at greater risk of deterioration than those with isolated post-capillary PH (Ipc-PH), but may benefit from PAH-specific therapy, especially in the context of randomized controlled trials (37,40,41) (and ClinicalTrials.gov identifier: NCT02070991).

Previous non-invasive techniques using MRI measured left atrial volume index (255), echocardiographic parameters (256) or a combination of clinical, electrocardiographic and echocardiographic features (33) have been shown to distinguish between pre- and post-capillary disease. However, there currently is no non-invasive method for identifying patients likely to have Cpc-PH. As the interventricular septal angle is likely to represent a maker of the pressure differential between the right and left ventricles we anticipated that the interventricular septal angle was a marker of the diastolic pulmonary gradient, and therefore the presence of combined pre and post capillary pulmonary hypertension. We also aimed to assess other cardiac MRI metrics as markers of the diastolic pulmonary gradient.

5.1.1.1 Hypotheses

1. The interventricular septal angle is a marker of the pressure differential between the left and right ventricle
2. Patients with combined pre and post capillary pulmonary hypertension have flattening of the interventricular septum.
3. Left atrial volume index has limited diagnostic utility in the assessment of the pulmonary arterial wedge pressure.

5.1.1.2 Aims

The aim of this chapter is to assess the interventricular septal angle, measured by MRI as a diagnostic tool to differentiate isolated post capillary pulmonary hypertension from combined pre and post capillary pulmonary hypertension in pulmonary hypertension due to left hear disease.

5.1.2 **Methods**

All consecutive, incident patients with suspected pulmonary hypertension, who underwent cardiopulmonary MRI at a pulmonary hypertension referral centre (245) from April 2012 to April 2017 were identified. Patients who had MRI and right heart catheter performed on the same day were included in the study. Ethical approval was granted from a local ethics committee for this retrospective study, written consent was waived (ref c06/Q2308/8).

5.1.2.1 Image acquisition and analysis

All patients underwent cardiac MRI at a pulmonary hypertension referral centre as part of the routine clinical pathway. MRI was performed on a GE HDx 1.5-T whole body scanner (GE Healthcare, Milwaukee, Wisconsin), with the patient supine, using an 8-channel cardiac coil. Short axis (SA) cine images were acquired using a retrospectively cardiac gated multi-slice steady-state free precession (SSFP) sequence during a breath-hold, with 20 phases per cardiac cycle. A stack of axial images with slice thickness of 8 mm with a 2 mm inter-slice gap or 10 mm with no inter-slice gap was acquired, covering both ventricles from base to apex. The SSFP sequence parameters were: TR 2.8 ms, TE 1.0ms, flip angle 50°, field of view 48x43.2, 256x256 matrix and 125 kHz bandwidth.

MR images were analysed on a GE Advantage Workstation 4.4 using GE Advantage Workstation ReportCard software by DC (a cardiac radiographer with 9 years experience), blinded to all clinical information and other investigations. Right and Left ventricular mass, volumes and ejection fraction were measured as previously described (257). The interventricular septal angle was measured as the angle formed between the insertion points of the ventricles to the mid-point of the septum, measured at end-systole (125,134,236). Figure 6 shows the measurement of septal angle in a patient with a high DPG and in a patient with low DPG. Left atrial volume was measured using the 2 and 4 chamber views and was calculated using the bi-plane area-length method (258).

To assess the reproducibility of the interventricular septal angle measurement, I (a radiologist with 6 years' experience) analyzed the interventricular septal angle in the first consecutive 20 patients with a raised pulmonary arterial wedge pressure. In a separate sitting, the same 20 patients were re-analysed.

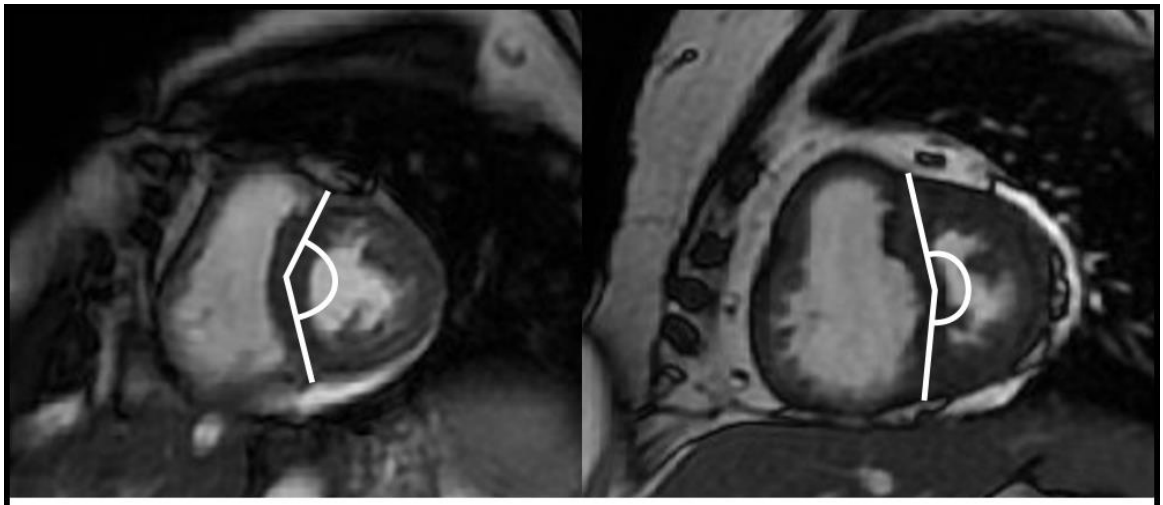

Systolic septal angle	127°	Systolic septal angle	192°
DPG	-3.0 mmHg	DPG	30 mmHg
mPAP	33 mmHg	mPAP	69 mmHg
PAWP	20 mmHg	PAWP	18 mmHg
CI	2.9 L/min/m^2	CI	3.4 L/min/m^2
PVRI	153 dyne.s	PVRI	364 dyne.s
TPG	13 mmHg	TPG	51 mmHg
SPG	37 mmHg	SPG	52 mmHg

DPG: Diastolic pressure gradient, mPAP: mean pulmonary artery pressure, PAWP: pulmonary artery wedge pressure, CI: cardiac index, PVRI: pulmonary vascular resistance index, TPG: trans-pulmonary gradient, SPG: systolic pressure gradient

Figure 5.1: *Representative images from a patient with a negative DPG and normal septal angle (left) and a patient with an elevated DPG with a high septal angle (right).*

5.1.2.2 Right heart catheterisation

Right heart catheterisation was performed at a pulmonary hypertension referral centre using a balloon-tipped 7.5 Fr thermodilution catheter (Becton-Dickinson, Franklin Lakes, NJ), introduced using a Swann-Ganz catheter, usually with vascular access via the internal jugular vein. Left heart disease was defined as a pulmonary arterial wedge pressure (PAWP) of >15mmHg (1). The diastolic pressure gradient (DPG) was calculated as diastolic pulmonary arterial pressure – mean pulmonary artery wedge pressure (22), and a threshold of ≥7mmHg was considered diagnostic for combined pre and post capillary pulmonary hypertension, as per recognized guidelines (1,259). Cardiac output was measured by thermodilution. Pulmonary vascular resistance was defined as (mPAP –PAWP)/cardiac output. Further analysis was performed using pulmonary vascular resistance, with a threshold of >3 Woods units (or 240 dyne.s), in order to assess the interventricular septal angle as a marker for Cpc-PH using both potential methods.

5.1.2.3 Statistical analysis

To test the accuracy of cardiac MRI measured structural and functional quantitative parameters in the assessment of diastolic pressure gradient, the correlation coefficient was calculated to assess for the strength of correlation between each variable with the diastolic pulmonary gradient, trans-pulmonary gradient and pulmonary vascular resistance. Scatter plots of the metrics with strongest correlation with diastolic pulmonary gradient, trans-pulmonary gradient and pulmonary vascular resistance were interrogated to ensure linearity. Receiver operating characteristic (ROC) curve analysis was performed to assess the diagnostic accuracy of each MRI parameter as a potential diagnostic tool and to assess a suitable diagnostic threshold. Analysis was also performed in the after exclusion of patients with normal pulmonary arterial wedge pressure, to ensure that the results were valid in the patients who had pulmonary hypertension due to left heart disease (PAWP >15mmHg and mPAP ≥25mmHg).

To assess the hemodynamic basis of the interventricular septal angle as a predictor of the diastolic pulmonary gradient all incident patients were assessed. The correlation of interventricular septal angle and diastolic pulmonary gradient with the mean, systolic and diastolic pulmonary arterial to systemic pressure ratios were analysed. In order to assess the underlying mechanism for the interventricular septal angle as a marker of the trans pulmonary gradient linear regression analysis of significant candidate correlates, including inter ventricular septal angle with other significant cardiac MRI volumetric data was assessed. In addition right and left ventricular end diastolic and end systolic volumes and the ratio of right to left end diastolic and end systolic volumes was calculated and were included in the regression if significant at univariate analysis. The Z score from the left heart disease population was calculated ($z = \frac{x-\mu}{\sigma}$, where μ is the mean and σ is the standard deviation), to allow comparison of the independent associations of MRI metrics with trans-pulmonary gradient.

Census was performed on 16/06/17 and all-cause mortality was used as the outcome. The study period was defined as MRI to census or all-cause mortality. Survival analysis was performed using Cox proportional hazards regression analysis and the log rank test at Kaplan-Meier curve analysis. For ready comparison between the measurements on Cox proportional hazards regression analysis, the measurements

were standardized by the z-score. Kaplan-Meier plots were constructed using recognized diagnostic thresholds, where available. For interventricular septal angle, the newly identified diagnostic threshold was used. ROC curve analysis was also used to assess for each variable's strength of prediction of death. ROC curve analysis for prediction of death was chosen at 2 years, as this had a balance of patient numbers (n=122) and number of deaths (n=36). Analysis of the 2x2 contingency table and chi-square test were used to determine sensitivity, specificity, positive and negative predictive (PPV, NPV) values.

The intra and inter-observer reproducibility using intra class coefficient (using two-way mixed absolute agreement) and construction of Bland-Altman graphs.

In order to assess cardiac MRI as a non-invasive tool to identify patients with left heart disease, the diagnostic accuracy of left atrial volume index was assessed in the entire cohort of incident cases. This has previously been shown to identify patients with left heart disease, with a threshold of ≥43ml/m^2 being identified to have 97% sensitivity and 100% specificity (255). A scatter plot of left atrial volume index against PAWP and ROC curve for the diagnosis of left heart disease were interrogated.

Statistical analysis was performed using SPSS 22 (IBM, Chicago) and GraphPad Prism 7 (GraphPad Software, San Diego). A p-value of <0.05 was considered statistically significant. The data is presented as mean (standard deviation), unless otherwise stated.

5.1.3 **Results**

In the period studied, 2643 patients underwent cardio-pulmonary MRI in pulmonary hypertension service. 1315 were incident patients, of which 758 had their MRI and right heart catheter on the same day. In 50 cases, the PAWP was not recorded. 171 patients had a PAWP >15 and 537 had PAWP ≤15mmHg. **Figure 5.2** shows the algorithm for selection of patients.

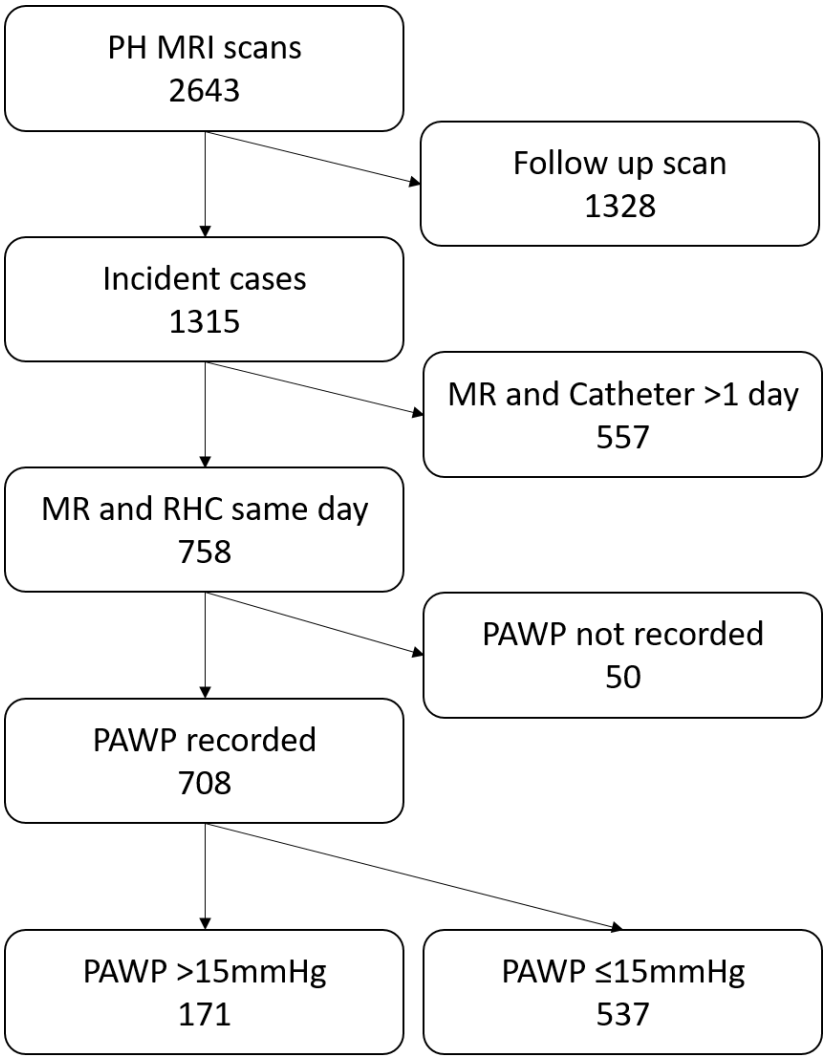

Figure 5.2: *Patient flow*

5.1.3.1 Prediction of a high diastolic pulmonary gradient

In the left heart disease cohort (PAWP >15mmHG), the average age was 70 (±10) years, 61% were female. Fifty-six (32%) had a diastolic pulmonary gradient (DPG) ≥7mmHg, 57 (33%) a DPG 0-7mmHg and 58 (33%) a negative DPG. **Table 5.1** presents the demographic and right heart catheter data. Five patients had a wedge pressure >15mmHg but did not have pulmonary hypertension (these all had a

Table 5.1: *Baseline patient demographics, haemodynamics and cardiac MRI metrics for the whole cohort split by PAWP of 15mmHg.*

	PAWP<15	PAWP >15	p-value
Number	537	171	
Demographics			
Age (years)	63 (13)	70 (10)	<0.001
Sex (F/M)	346/191	105/66	0.473
WHO functional class (I,II,III,IV)	3,75,404,46	0,18,144,9	0.166
ISWT (m)	224 (195)	158 (126)	<0.001
Survival (years)	1.3 (1)	2.1 (1.3)	0.945
RHC			
mPAP (mmHg)	39 (15)	43 (12)	<0.001
mRAP (mmHg)	9 (5)	15 (5)	<0.001
PAWP (mmHg)	11 (3)	21 (5)	<0.001
CI (L/m^2)	2.7 (0.9)	2.6 (0.7)	0.514
PVRI ($dyne.s.m^2$)	997 (764)	720 (483)	<0.001
SvO_2 (%)	66 (9)	64 (9)	0.027
DPG (mmHg)	12 (10)	4 (9)	<0.001
TPG (mmHg)	28 (15)	21 (11)	<0.001
SPG (mmHg)	53 (26)	47 (21)	0.002
CMRI			
RV EDV index ($ml.m^{-2}$)	80 (30)	89 (31)	0.001
RV ESV index ($ml.m^{-2}$)	48 (26)	48 (23)	0.44
RVEF (%)	43 (14)	46 (13)	0.006
RV mass index ($ml.m^{-2}$)	19 (11)	19 (10)	0.623
LV EDV index ($ml.m^{-2}$)	54 (16)	68 (21)	<0.001
LV ESV index ($ml.m^{-2}$)	18 (10)	24 (14)	<0.001
LVEF (%)	68 (10)	65 (12)	0.014
LV mass index ($ml.m^{-2}$)	48 (11)	56 (20)	<0.001
PA RAC (%)	12 (9)	12 (9)	0.691
VMI (ratio)	0.42 (0.24)	0.36 (0.19)	0.003
IV septal angle (˚)	161 (24)	154 (20)	<0.001
LA vol index ($ml.m^{-2}$)	34 (16)	62 (28)	<0.001
Stroke volume (ml)	67 (23)	82 (25)	<0.001
Black blood score	3 (2)	3 (1)	0.853

WHO-FC: World Health Organization-Functional Class, ISWT: incremental shuttle walk test, mPAP: mean pulmonary artery pressure, mRAP: mean right atrial pressure, PAWP: pulmonary arterial wedge pressure, CI: cardiac index, PVRI: pulmonary vascular resistance index, SvO_2: Mixed venous oxygen saturations, TPG: trans pulmonary pressure gradient (mPAP-PAWP), SPG: systolic pressure gradient (sPAP-PAWP), RVEDV: right ventricular end-diastolic volume, RVESV: right ventricular end-systolic volume, RVEF: right ventricular ejection fraction, RV: right ventricle, LVEDV: left ventricular end-diastolic volume, LVESV: left ventricular end-systolic volume, LVEF: left ventricular ejection fraction, PA RAC: pulmonary artery relative area change, VMI: ventricular mass index, IVS: interventricular septum

diastolic pulmonary gradient <7). 103 patients had pulmonary hypertension due to left heart disease alone, 32 patients had combined pre and post capillary pulmonary hypertension, 17 had coexistent lung disease and 19 had co-existent chronic thrombo-embolic disease, as defined by the multidisciplinary team meeting upon review of all imaging and clinical details. Left heart disease was due to left ventricular diastolic dysfunction in 149 cases, left ventricular systolic dysfunction in 9 and valve disease in 13 (mitral regurgitation – 5, aortic stenosis – 5, aortic regurgitation – 1, mixed mitral and aortic disease – 1, unknown - 1). 127 of the patients with left heart disease did not receive vasodilator therapy. 31 of the cases were treated with sildenafil alone and 13 were treated with dual therapy (sildenafil with macitentan - 8, bosentan - 4 or ambrisentan - 1).

Systolic interventricular septal angle correlated with diastolic pulmonary pressure gradient (r=0.739, p-value <0.001) and pulmonary vascular resistance (r=0.626, p-value <0.001). **Figure 5.3** presents scatter plots of interventricular septal angle against diastolic pulmonary gradient and pulmonary vascular resistance. Systolic interventricular septal angle correlated with TPG, PAWP and mPAP (r= 0.772, p<0.001, r=-0.203, p=0.008 and r= 0.637, p<0.001 respectively). Other MRI predictors had weak or modest correlations with diastolic pulmonary gradient (r=0.033, p=0.668 to r=0.550, p=<0.001). **Table 5.2** shows the correlations and p-values for each metric with diastolic pulmonary gradient, trans-pulmonary gradient and pulmonary vascular resistance.

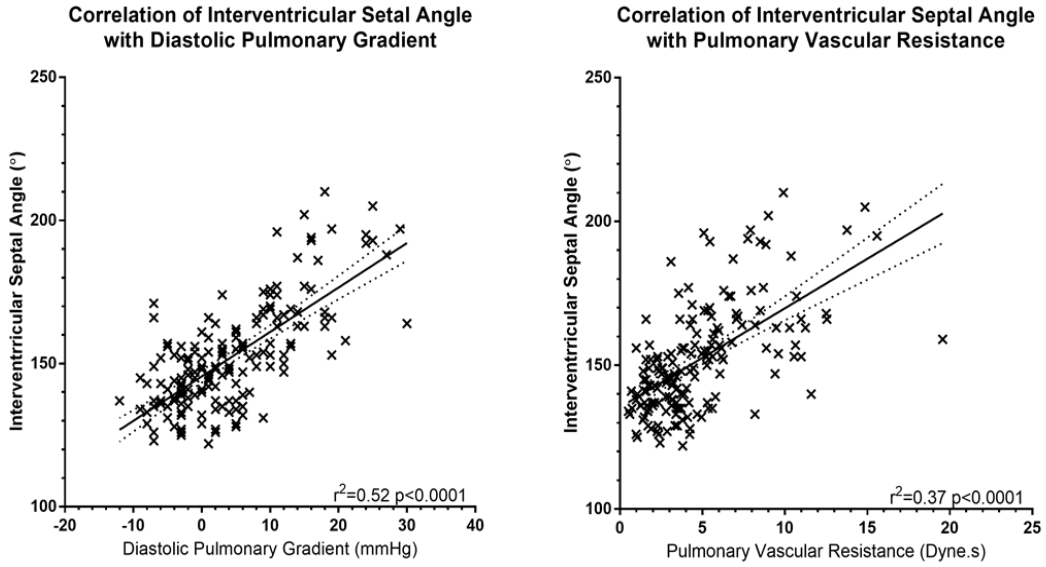

Figure 5.3: *Scatter plot showing the relationship between systolic interventricular septal angle with diastolic pulmonary pressure gradient and pulmonary vascular resistance.*

Table 5.2: *Cardiac MRI metrics linear correlations with DPG, TPG and PVR, for the patients with pulmonary arterial wedge pressure (PAWP) >15mmHg.*

	DPG		TPG		PVR	
	r	p-value	r	p-value	r	p-value
Systolic IVS angle	0.739	<0.001	0.772	<0.001	0.626	<0.001
Diastolic IVS angle	0.534	<0.001	0.534	<0.001	0.575	<0.001
RVEDVI	0.118	0.124	0.095	0.219	0.079	0.304
RVESVI	0.356	<0.001	0.219	0.004	0.279	<0.001
RVEF	-0.550	<0.001	-0.516	<0.001	-0.469	<0.001
RVSVI	-0.297	<0.001	-0.28	<0.001	-0.262	0.001
LVEDVI	-0.398	<0.001	-0.296	<0.001	-0.287	<0.001
LVESVI	-0.205	0.007	-0.194	<0.001	-0.162	0.034
LVEF	-0.033	0.668	0.046	0.546	0.000	1.000
LVSVI	-0.441	<0.001	-0.283	<0.001	-0.304	<0.001
RV mass index	0.323	<0.001	0.333	<0.001	0.293	<0.001
LV mass index	-0.249	0.001	0.127	0.098	-0.247	0.001
LA volume index	-0.326	<0.001	-0.257	0.001	-0.206	0.007
Systolic PA area	0.301	<0.001	0.348	<0.001	0.254	0.001
Diastolic PA area	0.364	<0.001	0.422	<0.001	0.329	<0.001
PA RAC	-0.230	0.003	-0.288	<0.001	-0.285	<0.001
Black Blood Score	0.432	<0.001	0.405	<0.001	0.455	<0.001
VMI	0.500	<0.001	0.465	<0.001	0.463	<0.001

RVEDVI: right ventricular end-diastolic volume index, RVESVI: right ventricular end-systolic volume index, RVEF: right ventricular ejection fraction, RV: right ventricle, LVEDVI: left ventricular end-diastolic volume index, LVESVI: left ventricular end-systolic volume index, LVEF: left ventricular ejection fraction, PA RAC: pulmonary artery relative area change, VMI: ventricular mass index, IVS: interventricular septum, DPG: diastolic pulmonary gradient, TPG: trans pulmonary gradient, PVR: pulmonary vascular resistance

Receiver operating characteristics (ROC) curve analysis (**Figure 5.4**) showed that septal angle was predictive of the presence of an elevated diastolic pulmonary gradient (defined by a DPG ≥7) with an area under the curve of 0.911 (p <0.001). Interventricular septal angle was also predictive of the presence of an elevated pulmonary vascular resistance (defined by a PVR >3 Woods units, or >240 Dyne.s) with an area under the curve of 0.783 (p <0.001). Analysis of the ROC data showed that a septal angle of 160˚ represented a reasonable diagnostic threshold to predict a DPG of ≥7mmHg, with 70% sensitivity, 93% specificity, 83% positive predictive value and 86% negative predictive value (p <0.0001).

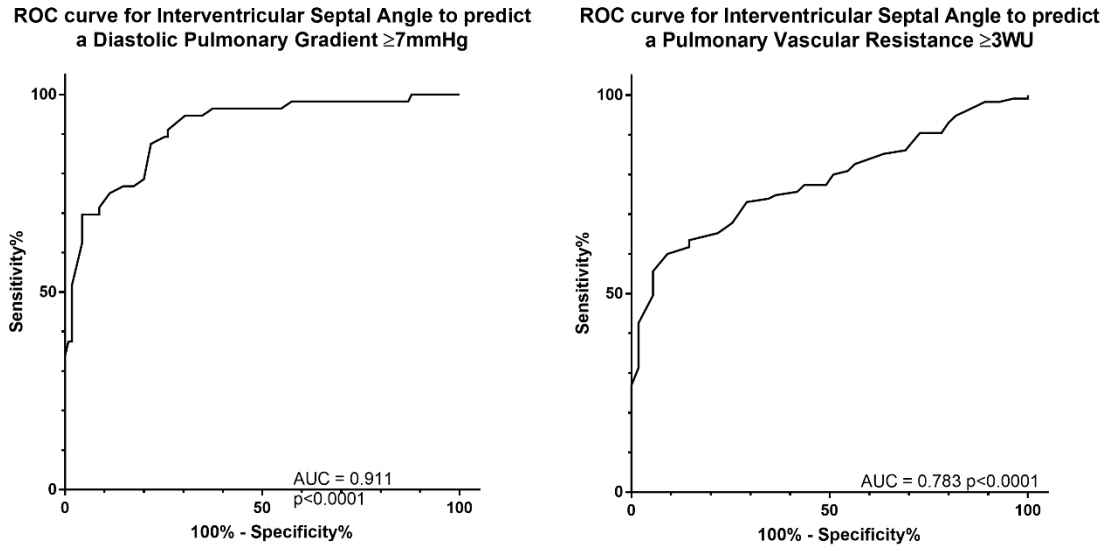

Figure 5.4: *ROC analysis for Septal angle to assess for an elevated DPG or PVR*

After exclusion of the patients without pulmonary hypertension (n=5) there was still a significant correlation between the interventricular septal angle and DPG (r=0.716, p<0.001), PVR (r=0.596, p<0.001). The area under the ROC curve for the diagnosis of a raised DPG was 0.907 (p<0.001). A septal angle of 160˚ gave sensitivity of 70%, specificity of 93%, positive predictive value 86% and negative predictive value 86%.

5.1.3.2 Haemodynamic Basis of Interventricular Septal Angle

Table 5.3 shows the correlation between interventricular septal angle and diastolic pulmonary gradient with the ratio of mean, diastolic and systolic pulmonary artery to systemic pressure ratio. This is provided in **Table 5.3** for the whole cohort of incident cases and the cases with left heart disease (PAWP >15mmHg). Whilst interventricular septal angle and diastolic pulmonary gradient correlated with all three ratios, the strongest was with systolic pulmonary arterial pressure and systolic systemic pressure ratio (for septal angle: 0.728 for all cases and 0.674 for the raised PAWP cases, and for the DPG 0.759 for all cases and 0.702 for the raised PAWP cases).

Systolic interventricular septal angle had modest correlations with right ventricular end diastolic volume (R=0.257, p=0.001), right ventricular end systolic volume (R=0.302, p <0.001), left ventricular end diastolic volume (R=-0.231, p=0.002), left

ventricular end systolic volume (R=-0.140, p=0.067) and the ratio of right:left end diastolic volume (R=0.420, p<0.001) and end systolic volume (R=0.462, p<0.001). On multivariate analysis, DPG was independently associated with the interventricular septal angle (hazard ratio 11.807, 95% CI 9.7-13.9), right:left end-systolic volume ratio (HR 3.400, 95% CI 1.3-5.5).

Table 5.3: *Correlations between haemodynamic measures in the whole cohort of patients and in the left heart disease cohort alone.*

	mPAP:MAP		sPAP:SAP		dPAP:DAP	
	All	Raised PAWP	All	Raised PAWP	All	Raised PAWP
IVS angle	0.570	0.557	0.728	0.674	0.646	0.514
DPG	0.626	0.637	0.759	0.702	0.761	0.662

IVS: interventricular septum, DPG: diastolic pulmonary gradient, TPG: trans pulmonary gradient, PVR: pulmonary vascular resistance, mPAP: mean pulmonary arterial pressure, MAP: mean systemic arterial pressure, sPAP: systolic pulmonary arterial pressure, SAP: systemic systolic blood pressure, dPAP: diastolic pulmonary arterial pressure, DAP: diastolic systemic blood pressure, PAWP: Pulmonary arterial wedge pressure. All correlations were significant (p<0.05).

5.1.3.3 Reproducibility of the interventricular septal angle measurement

There was excellent inter-observer agreement with intra class correlation (ICC) of 0.902 (p<0.001), Bland-Altman plot showed a tiny bias of -2% and close 95% limits of agreement of -12 to 8%. There was also excellent intra-observer agreement, with ICC of 0.979 (p<0.001), Bland-Altman showed a tiny bias of 2% and 95% limits of agreement of -4 to 8%. **Figure 5.5** provides the Bland-Altman plots for intra and inter-observer reproducibility.

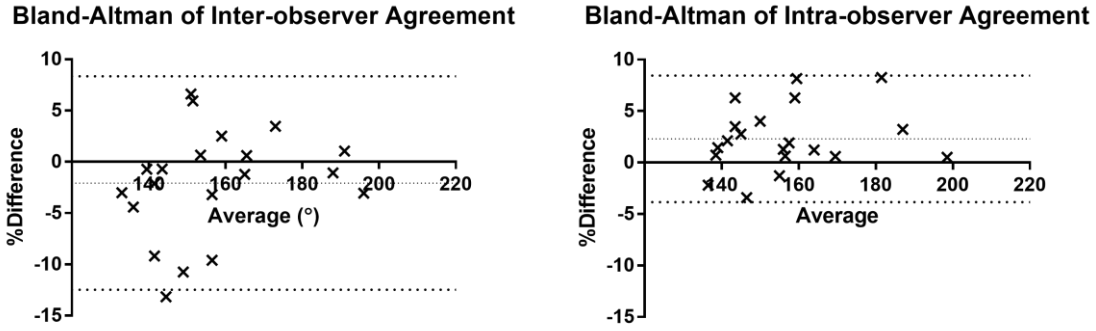

Figure 5.5: *Bland-Altman plots of inter and intra-observer agreement for systolic interventricular septal angle.*

5.1.3.4 Prediction of outcome

Median follow up was 2.4 years (SD 1.3), during which time there were 48 deaths. Systolic interventricular septal angle was predictive of outcome on univariate analysis, with a Cox proportional hazards ratio of 1.615 (95% confidence interval 1.253-2.082, p-value <0.001), when standardized to the z score for the left heart disease population. Kaplan-Meier curve analysis, dichotomized by the threshold of 160˚, showed a significant difference in outcome (**Figure 5.6**) with Log-Rank chi-square 11.02 (p-value=0.0009).

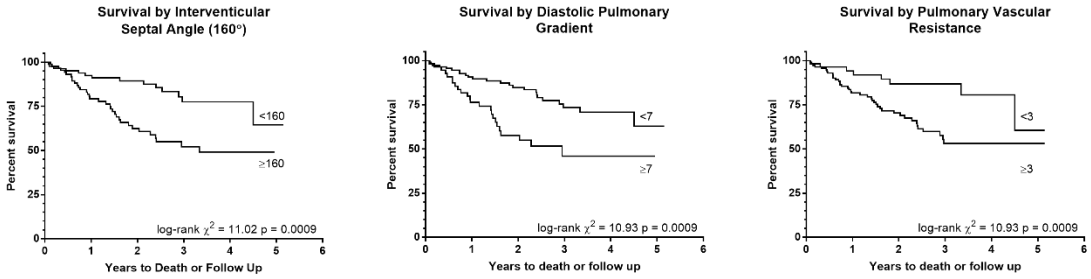

Figure 5.6: *Kaplan Meier analysis*
Patients with elevated PAWP dichotomized by interventricular septal angle, diastolic pulmonary gradient and pulmonary vascular resistance. The interventricular septal angle does not have a published threshold so the diagnostic threshold identified in this chapter is used.

DPG, PVR and TPG were predictive of death with standardized Cox proportional hazards ratio of 1.708, 1.667 and 1.609 respectively (all p values <0.05). The interventricular septal angle, DPG and PVR all predicted death at 2 years (AUC 0.71, 0.71 and 0.71, and p-values 0.0003, 0.0002 and 0.0001 respectively), see **Figure 5.7.**

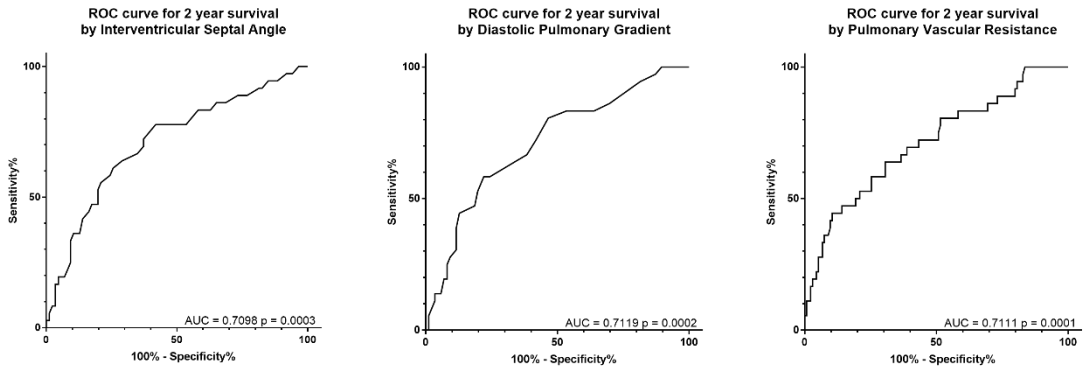

Figure 5.7: *ROC curve analysis for the prediction of death at 2 years*

On univariate analysis, treatment with PAH vasodilator therapy was associated with death, with Cox univariate hazard ratio 1.83 (95% CI 1.026-3.266, P = 0.041) and log-rank chi-square 4.316 (p = 0.038). However, when treatment was entered as a dummy variable into a multi-variate Cox proportional hazards assessment individually with septal angle or the hemodynamic parameters, it did not reach statistical significance (p=0.257).

5.1.3.5 Prediction of a raised PAWP

Left atrial volume index showed reasonable correlation with pulmonary arterial wedge pressure measurement (r2=0.30) and reasonable diagnostic accuracy with area under the receiver operating curve of 0.825 (p<0.0001). The previously published threshold of ≥43ml/m2 had 74% sensitivity, 79% specificity, 53% positive predictive value and 91% negative predictive value for the presence of a PAWP >15. **Figure 5.8** shows a scatter plot of left atrial volume index against PAWP and the ROC curve for the diagnosis of left heart disease.

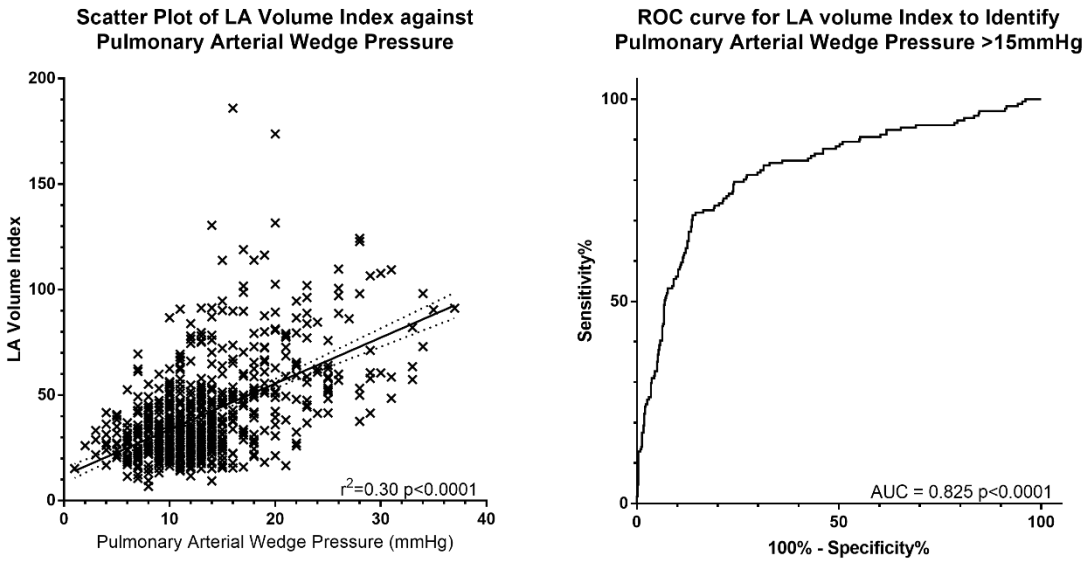

Figure 5.8: *Diagnostic accuracy of left atrial volume index.*
A scatter plot of LA volume index against pulmonary arterial wedge pressure, and an ROC curve for left atrial volume index to identify the presence of PAWP>15mmHg.

5.1.4 **Discussion**

The data presented in this section of the thesis shows that interventricular septal angle can be used to predict the presence of Cpc-PH in a cohort of incident patients referred to a pulmonary hypertension referral centre with a pulmonary arterial wedge pressure (PAWP) >15mmHg. In our cohort of pulmonary hypertension patients with raised PAWP, a systolic interventricular septal angle of 160˚ accurately identified patients with a raised diastolic pulmonary gradient, with 70% sensitivity and 93% specificity. The interventricular septal angle threshold of 160˚ also dichotomised patients into higher and lower risk categories for death.

We postulate that the interventricular septal angle represents a good quantitative marker that reflects the trans-pulmonary gradient as it is responsive to the pressure difference between the left and right ventricle (260). Although, it should be noted that this is different from the diastolic pressure gradient, which is a measure of the pressure differential between the pulmonary artery and the mean pulmonary arterial wedge pressure (used as a surrogate marker for left atrial pressure). In the absence of invasive measures of left ventricular pressure, we have shown that the ratio of pressures between the pulmonary arterial and the systemic circulations, particularly at systole are accurately reflected by the interventricular septal angle. We have also demonstrated a strong relationship between the pulmonary arterial to systemic pressure ratio and the diastolic pulmonary gradient. We have shown that the association of flattening of the interventricular septal angle and trans pulmonary gradient is independent of other cardiac volumetric and functional measurements. However, the relative volumes of the right and left ventricle also contribute, though to a lesser extent when compared to septal flattening. We have shown that whilst there is a modest correlation between right ventricular and left ventricular volumes, and the ratio of these, the strongest correlation is with DPG, suggesting that the flattening is most associated with the pressure gradient between the right and left ventricles.

Patients with combined pre and post capillary pulmonary hypertension had features of precapillary pulmonary hypertension on cardiac MRI. The patients with Cpc-PH had significantly increased right ventricular end systolic volumes and mass (and therefore ventricular mass index), reduced stroke volume and right ventricular

ejection fraction, due to increased right ventricular afterload. In the Cpc-PH cohort the left ventricular end diastolic volume and the left atrial volume index were reduced due to reduced filling. Supporting the model that pre-capillary pulmonary vascular remodelling causing reduced precapillary arterial compliance in the patients with Cpc-PH, pulmonary arterial relative area change was significantly reduced. These findings may suggest the presence of the pre-capillary PH in patients with left heart disease, but the strongest predictor was the systolic interventricular septal angle, as discussed above. The systolic interventricular septal angle is easily measured on commercially available PACS stations and we have shown that it has excellent inter and intra-observer reproducibility, it is likely that the small variability that has been demonstrated (around ±10% intra and inter-observer 95% agreement) explains the slightly reduced sensitivity. As the analysed images are cardiac cine SSFP sequences, the time-point of measurement of the interventricular septal angle measurement is important. In the data that we present, we show that the systolic interventricular septal angle is the most predictive of the diastolic pulmonary gradient, likely as this is the time in the cardiac cycle when the pressure difference in the right and left ventricle is most marked.

Left heart disease is an increasingly prevalent disease (23), and whilst the prevalence of PH in left heart disease is not fully known (27,261), it is associated with a poor outcome (24,25). The differentiation of left heart disease from idiopathic pulmonary arterial hypertension is often hard to make (9), and this is further compounded by the fact that a subgroup of patients have combined pre and post capillary pulmonary hypertension, thought to be due to pre-capillary vascular remodelling (30). Previously published non-invasive techniques which utilize left atrial volume index measured at MRI have had a high diagnostic accuracy in the assessment of left heart disease (255). Further centres have also studied the echocardiographic parameters (256) or a combination of clinical, electrocardiographic and echocardiographic features (33) as non-invasive methods to distinguish between pre- and post-capillary disease. The work presented in this chapter furthers these tools, allowing the non-invasive identification of patients who have elevated trans pulmonary gradient in patients with pulmonary hypertension owing to left heart disease.

There is ongoing debate regarding the best way to assess for combined pre and post capillary pulmonary hypertension. Initially, the trans-pulmonary gradient (TPG, mean pulmonary arterial pressure minus mean pulmonary arterial wedge pressure) was used to identify patients who had a precapillary component to their pulmonary hypertension, with 12mmHg being used as a cut-off (22). As the trans-pulmonary gradient is affected by cardiac output, pulmonary vascular resistance and pulmonary arterial wedge pressure, it is now recommended that a diastolic pressure gradient of ≥7mmHg and/or pulmonary vascular resistance of >3 Woods units, should be used to define the presence of combined pre and post capillary pulmonary hypertension (259,262). This is felt to represent a physiologically more reliable measure of the pressure drop across the pulmonary vasculature. The interventricular septal angle correlated more strongly with the DPG than the PVR, likely because it changes in response to the pressure differences rather than the vascular resistance, which is also related to cardiac output. There have been multiple discussions over the significance of a negative diastolic pressure gradient, with reports of a negative diastolic pulmonary gradient being associated with a favourable outcome, rather than a representation of the inaccuracies of pulmonary arterial wedge pressure measurement (263). The underlying mechanisms are not entirely clear, but it is plausible that the reason for a negative diastolic pulmonary gradient is due to the use of mean pulmonary artery wedge pressure in the DPG calculation, rather than the diastolic pulmonary artery wedge pressure. Further work is warranted to identify the most robust hemodynamic marker for Cpc-PH.

It would be useful to identify a non-invasive methodology for the accurate identification of patients with left heart disease in the population of patients with suspected pulmonary hypertension. In a comparison between idiopathic pulmonary arterial hypertension and PH owing to left heart disease, it was shown that a left atrial volume index of ≥43ml/m^2 was highly predictive of the presence of left heart disease (255). The results from our population of 708 incident cases showed that the left atrial index is diagnostic, but not to the same high accuracy (AUC 0.825, $p<0.001$). Part of this may be related to the population studied: In this section, we assess the left atrial volume index in all incident patients with suspected pulmonary hypertension, rather than in the selected idiopathic pulmonary arterial hypertension vs left heart disease cases. Furthermore, the pulmonary arterial wedge pressure reading has inherent

inaccuracies as a measurement of left ventricular end-diastolic pressure, potentially adding error (264,265). Further work is required to identify more robust non-invasive measures of left ventricular dysfunction as a cause for pulmonary hypertension.

Current recommendations for pulmonary hypertension due to left heart disease centre on treatment of the underlying left heart disease, for example correcting valvular heart disease and optimizing volume status or heart failure therapy. There is currently no body of evidence to support the use of targeted pulmonary vascular therapies in patients with left heart disease as a whole, nor in combined pre and post capillary pulmonary hypertension (Cpc-PH). Although there is increasing interest in potential treatment options in these patients as they have worse outcome and pre-capillary remodelling, similar to pulmonary arterial hypertension (PAH) patients. It would be useful to have a non-invasive and simple measurement from imaging, such as interventricular septal angle to differentiate Cpc-PH from Ipc-PH for inclusion in potential clinical trials (10–13).

This study is limited by its retrospective design, conducted in a pulmonary hypertension referral centre, where the incidence of pulmonary hypertension is significantly higher than in the general population of left heart disease patients. As such, the results are only valid in patients in this setting, and not necessarily applicable to the wider population of left heart disease. Furthermore, we have assessed a potential threshold of interventricular septal angle to identify patients with high diastolic pressure gradients, but this requires validation in a separate cohort. Future work is required to evaluate the threshold we have defined, to assess the role of septal measurement in a more general cohort of left heart disease patients, and to assess the similarities with idiopathic pulmonary arterial hypertension. Furthermore, as discussed above, further work is required to assess the non-invasive estimation of left ventricular filling pressures and their role in diagnosis and prognosis.

5.1.5 **Conclusion**

Cardiac MRI derived interventricular septal angle can be used to non-invasively predict the presence of an elevated diastolic pressure gradient in suspected pulmonary hypertension patients with elevated pulmonary arterial wedge pressures.

The interventricular septal angle can predict left heart disease patients with a poor outcome and in the future, may offer the potential to identify patients for targeted therapy.

5.2 CARDIAC MRI PHENOTYPES OF PH - LUNG DISEASE

5.2.1 Rationale

Pulmonary hypertension is a common complication of chronic lung disease and is defined on right heart catheter (RHC) by a mean pulmonary arterial pressure (mPAP) ≥25mmHg. Reportedly as many as 90% of patients with COPD Gold stage IV have a mean pulmonary artery pressure of 20-35mmHg but only 5% have a mean pulmonary artery pressure ≥35mmHg, which defines a cohort of lung disease patients as severe pulmonary hypertension (44,49,50). In lung disease, the presence of pulmonary hypertension is associated with a universally poor prognosis (42–46,53). Pulmonary hypertension is likely to represent the end-stage of pulmonary disease: for example COPD patients are more likely to die or be hospitalised due to cardiovascular rather than respiratory complications (48).

The development of pulmonary hypertension in COPD is thought to result from multiple different mechanisms: hypoxic pulmonary vasoconstriction, polycythaemia from chronic hypoxia, destruction of the pulmonary vascular bed by emphysema, hyperinflation causing intrathoracic pressures that are greater than pulmonary venous pressure and endothelial dysfunction and remodelling (43,51,52). The mechanisms by which pulmonary hypertension develops in ILD and CPFE appears to be much less understood. A potential difference in the development of pulmonary hypertension in lung disease is highlighted by the high incidence of severe pulmonary hypertension in combined pulmonary fibrosis and emphysema (CPFE), in contrast to patients with chronic obstructive pulmonary disease (COPD) and interstitial lung disease (ILD), in whom severe pulmonary hypertension is rare (50,267).

5.2.1.1 Hypothesis

1. The difference in prevalence and severity of PH and outcome in patients with PH due to COPD, ILD and CPFE are due to an underlying difference in the cardiac phenotype.

5.2.1.2 Aims

The aim of this study was to identify any differences in the cardiac phenotype of patients with pulmonary hypertension due to lung disease, through assessment of the

baseline demographic, haemodynamic and cardiac MRI characteristics of patients with pulmonary hypertension at a tertiary referral centre.

5.2.2 **Methods**

All consecutive patients who underwent MRI at a pulmonary hypertension referral centre (245) from April 2012 to October 2016 with suspected pulmonary hypertension were assessed for inclusion. All patients with PH due to lung disease were identified, as defined at the weekly PH multi-disciplinary team meeting. Any patients without a thoracic CT for analysis were excluded and any patients with more than 30 days between MRI and right heart catheterisation were excluded. A further cohort of patients with idiopathic pulmonary arterial hypertension who were scanned over the same time was also included for comparison. Ethical approval was granted from a local ethics committee for this retrospective study, written consent was waived (ref c06/Q2308/8).

5.2.2.1 Right Heart Catheterisation

Right heart catheterisation was performed using a balloon tipped 7.5Fr thermodilution catheter (Becton-Dickinson, Franklin Lakes, New Jersey). Pulmonary hypertension was defined as a resting mPAP ≥25mmHg and severe pulmonary hypertension as a resting mPAP ≥35mmHg. Cardiac output was calculated using thermodilution.

5.2.2.2 Pulmonary Function Testing

All patients underwent lung function testing as part of routine care. All spirometry is presented as percentage of predicted value.

5.2.2.3 Image Acquisition

Cardiac MRI was performed supine on a GE HDx 1.5-T whole body scanner (GE Healthcare, Milwaukee, Wisconsin), using an 8-channel cardiac coil. Four-chamber (4Ch) and short axis (SA) cine images were acquired using a retrospectively cardiac gated multi-slice steady-state free precession (SSFP) sequence. A stack of axial images in the SA plane with slice thickness of 8 mm with a 2 mm inter-slice gap or 10 mm with no inter-slice gap were acquired, covering both ventricles from base to apex. The

SSFP sequence parameters were: TR 2.8ms, TE 1.0ms, flip angle 50°, field of view 48x43.2, 256x256 matrix, 125 kHz bandwidth, and slice thickness 8 to 10 mm.

Axial black blood imaging was performed using a dual inversion recovery fast spin echo sequence, with a stack of 8mm slices with 10mm spacing taken through the long axis plane of the pulmonary artery. The sequence parameters were: TR 984ms, TE 40ms, flip angle 90˚, echo train length 32, field of view 4cm, 256x256 matrix, 31.2 kHz bandwidth on an 8 channel cardiac coil.

Phase contrast imaging was performed perpendicular to the pulmonary trunk and ascending aorta. The phase contrast imaging parameters were: TR 5.6 ms, TE 2.7 ms, slice thickness 10 mm, FOV 48x28.8, bandwidth 62.5 kHz, matrix 256x128 and velocity encoding (Venc) 150 cm/s. The images were retrospectively ECG gated with 40 phases.

DCE-MRI was performed using a contrast injection of 0.05ml per kg dose of Gd-BT-D30A (Gadovist, Schering, Berlin, Germany), injected at a rate of 4 ml per second with the using an activated pump injector (Spectris, MedRad). Typically administered via a vein in the antecubital fossa using an 18G cannula. This was followed by a 20ml saline flush. Serial 3D gradient echo images of the chest were acquired with the following sequence parameters: TE=1.1 ms, TR=2.5 ms, Flip angle 30°, FOV 48 cm x 48 cm, parallel imaging in plane x 2, in plane resolution 200x80, bandwidth 250 kHz, slice thickness 10 mm, approximately 32 slices, 48 time points with an overall effective 3D frame rate of ~ 0.5 s. Images were acquired in a coronal orientation.

When performed at the local centre, CTPA images were acquired on a 64-slice MDCT (Light-Speed General Electric Medical) during a single breath-hold. The acquisition parameters were: 100 mA with automated dose reduction, 120 kV, pitch of 1, rotation time 0.5 s and 0.625-mm collimation, field of view = 400×400 mm, acquisition matrix 512× 512. 100 mL of intravenous contrast agent (Ultravist 300; Bayer Schering, Berlin, Germany) was administered at a rate of 5 mL/s, typically through an 18G cannula in the antecubital fossa. CT images from other centres were also used when no local imaging was available, as long as they were considered to be of diagnostic quality.

5.2.2.4 Image Analysis

MR images were analysed on a GE Advantage Workstation 4.4 with GE Advantage Workstation ReportCard software, the observer was blinded to all clinical information and other investigations. Left and right ventricular end-diastolic volume, end-systolic volumes, right and left ventricular stroke volume and mass were calculated (all indexed to body surface area), right and left ventricular ejection fractions, ventricular mass index (RV mass divided by LV mass) (133) and interventricular septal angle were measured as previously described (125). Maximal and minimal PA areas were manually traced, and relative area change was defined by the following equation: RAC= (maximum area-minimum area)/minimum area (14, 28).

From the dual inversion recovery fast spin echo pulmonary arterial black blood images black blood slow flow artefact was scored. A semi-quantitative scale from 0 to 5 was used (0 = absent, 1 = segmental, 2 = lobar, 3 = distal main, 4 = proximal main and 5 = trunk) (135). From the phase contrast imaging data, the contours of the vessel were automatically traced, with manual correction when required. The software then calculated the velocity of all the pixels included within the region of interest (ROI). Pulmonary artery average velocity was calculated as QFlow forward PA velocity/diastolic PA size.

Signal enhancement versus time curves were generated from the dynamic contrast enhanced MRI images, for regions of interest in the pulmonary artery and the left atrium. Pulmonary transit time (PTT) was calculated as the time delay between peak pulmonary arterial signal and peak left atrial signal. The full-width-half-maximum (FWHM) of the contrast bolus passage was calculate as the time delay between half maximum signal intensity on the up and down-slopes of signal in the pulmonary artery enhancement curve.

The closest CT to the date of the MRI was chosen to identify the cause of the pulmonary disease. The cases were reviewed by 2 radiologists, a general radiologist (CSJ, 5 years' experience) and a chest radiologist (AJS, 11 years' experience), who were blinded to all other clinical and imaging information. Images were reviewed on a clinical workstation in the clinical radiology department, on diagnostic quality Barco screens (Barco, UK). CT images were reviewed using lung windows. Cases were split

into interstitial lung disease, chronic obstructive pulmonary disease (emphysema and bronchitis) or combined pulmonary fibrosis and emphysema based on agreed qualitative CT evidence of each of the diseases (268). Any cases without CT evidence of lung disease were classified as "other". Any disagreements were corrected by consensus between the two radiologists, again blinded to other clinical and imaging data. The severity of lung disease was given a score of 0-3 for each case.

5.2.2.5 Statistical Analysis

Statistical differences between each group of PH-lung disease were calculated for all demographic, right heart catheter and cardiac MRI indices using ANOVA.

Statistical analysis was performed using SPSS (IBM, Chicago), and all graphs were produced using GraphPad prism 7 (GraphPad Software, San Diego). A p-value of <0.05 was considered statistically significant.

In order to correct for the discrepancy in severity of PH between the different groups, sub-analysis was performed in the patients with severe pulmonary hypertension (mPAP ≥35 mmHg).

5.2.3 **Results**

Over the period studied, 2437 patients in the pulmonary hypertension referral centre underwent a cardio-pulmonary MRI; of these 1272 were incident cases. 190 patients had PH due to lung disease and right heart catheter within 30 days of MRI. Two were excluded as there was no thoracic CT available to review and two were excluded as the CT was non-diagnostic due to artefact. Over the same time, 111 patients with idiopathic pulmonary arterial hypertension (IPAH) had right heart catheter within 30 days of MRI and were used as a comparison group. **Figure 5.9** shows the flow of patients.

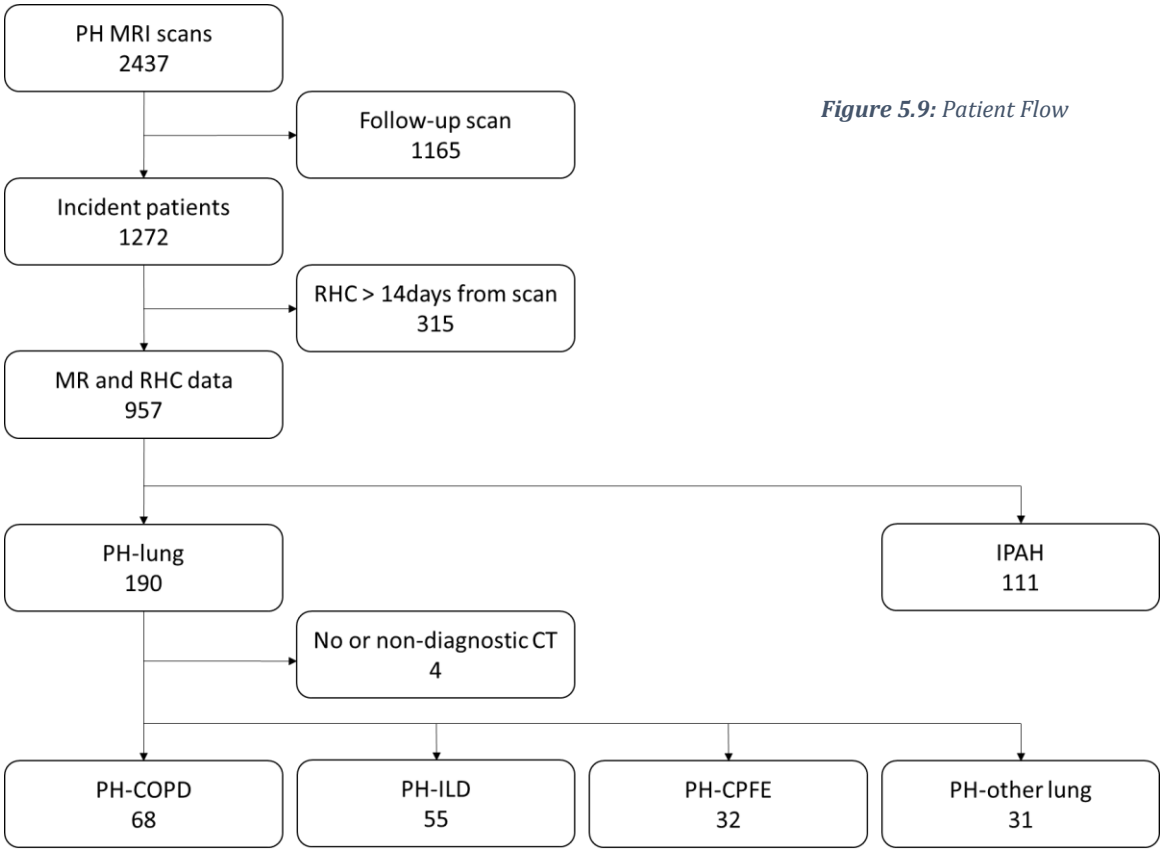

Figure 5.9: *Patient Flow*

Of the cases with PH lung (190), 68 had chronic obstructive pulmonary disease (COPD), 55 interstitial lung disease (ILD), 32 combined pulmonary fibrosis and emphysema (CPFE) and 31 had other respiratory disease. Baseline demographic data is provided in **Table 5.4** and **Table 5.5**. Analysis of the baseline characteristics and outcome in other lung diseases group has not been performed due to the heterogeneous nature of this group of patients, which is made up of small numbers of sleep disordered breathing and alveolar hypoventilation disorders.

Table 5.4: *Patient demographics, mean with standard deviation and ANOVA p-value between the subgroups. Significant differences are shown by the icon below.*

	All	COPD	ILD	CPFE	p-value
Number	190	68	55	32	
Demographics					
Age (years)	67 (10)	68 (9)	65 (11)	69 (9)	0.183
Sex (F/M)	103/87	34/34	33/22	12/20	0.126
WHO functional class (II,III,IV)	8,141,40	3,54,10	3,38,14	0,22,10	0.249
ISWT (m)	137 (145)	131 (102)	152 (225)	141 (90)	0.120
Days RHC to MR	0 (1)	0 (1)	0 (0)	0 (0)	0.106
Survival (years)	2.5 (0.1)	2.8 (0.2)	1.7 (0.2)	2.5 (0.3)	0.029
RHC					
mPAP (mmHg)	43 (11)	42 (10) †	41 (12) †	48 (10) ‡*	0.011
mRAP (mmHg)	10.1 (5.2)	10.1 (4.8)	8.7 (5.6)	10.6 (4.9)	0.190
PAWP (mmHg)	12.7 (0.8)	12.6 (3.8)	11.7 (5.5)	11.7 (3.4)	0.475
CI (L/m^2)	2.6 (0.8)	2.7 (0.8) †	2.7 (0.8) †	2.3 (0.6) ‡*	0.024
PVRI (dynes)	318 (199)	308 (190)	307 (239)	402 (168)	0.083
SvO_2 (%)	64 (8)	65 (8)	67 (7) †	62 (7) *	0.042
Spirometry					
FEV1 (% predicted)	67 (26)	56 (29) †*	70 (22) ‡	80 (21) ‡	<0.001
FVC (% predicted)	75 (27)	79 (31) *	64 (20) †‡	90 (24) ‡*	<0.001
FEV1/FVC	64 (17)	50 (13) †*	77 (12) †‡	65 (13) ‡*	<0.001
TLCO (% predicted)	27 (15)	25 (17)	26 (10)	24 (8)	0.726

**significant difference to ILD, †significant difference to CPFE, ‡significant difference to COPD*

Table 5.5: *Baseline cardiopulmonary MRI characteristics, mean with standard deviation and ANOVA p-value between the subgroups. Significant differences are shown by the icon below.*

	All	COPD	ILD	CPFE	p-value
RV EDV index (ml/m^2)	85.7 (34.6)	90.8 (37.9)	78.8 (31.9)	89.1 (6.3)	0.155
RV ESV index (ml/m^2)	55.1 (30.8)	57.6 (34.6)	49.8 (27.3)	33.2 (11.9)	0.203
RVEF (%)	38.4 (13.1)	40.6 (14.4) †	39.1 (12.8) †	33.2 (11.9) ‡*	0.038
RVSVI (ml/m^2)	30.9 (12.2)	33.2 (10.0) †	29.0 (11.1)	27.3 (10.9) ‡	0.015
RV mass index (g/m^2)	22.1 (13.9)	24.9 (17.7) *	18.5 (11.4) ‡	22.6 (9.7)	0.052
LV EDV index (ml/m^2)	52.9 (17.5)	56.1 (19.8)	50.3 (17.4)	48.6 (13.5)	0.078
LV ESV index (ml/m^2)	18.5 (9.9)	20.3 (12.6)	16.2 (8.7)	18.8 (8.0)	0.106
LVEF (%)	65.5 (11.6)	64.6 (12.4)	68.1 (11.9)	61.8 (11.6)	0.055
LVSVI (ml/m^2)	34.5 (11.9)	35.9 (12.4)	34.0 (12.5)	29.8 (9.1)	0.058
LV mass index (g/m^2)	51.0 (12.3)	52.7 (14.4)	49.2 (11.6)	48.4 (9.9)	0.199
LA volume index (ml/m^2)	35.4 (18.7)	39.0 (19.9) †	35.4 (19.6) †	26.2 (7.2) ‡*	0.005
PA RAC (cm^2)	9.5 (6.5)	9.6 (7.0)	9.8 (7.3)	8.2 (4.9)	0.579
Diastolic PA size	851 (233)	872 (273)	831 (203)	838 (189)	0.597
Systolic PA size	929 (254)	955 (298)	911 (216)	908 (215)	0.553
VMI	0.46 (0.28)	0.50 (0.34)	0.42 (0.25)	0.49 (0.23)	0.279
IVS angle (˚)	168 (21)	166 (20) †	166 (21)	179 (22) ‡	0.006
Average PA velocity (cm/s)	6.0 (2.2)	6.1 (2.0)	6.3 (2.5)	5.3 (1.6)	0.133
Distensibility	0.19 (0.18)	0.18 (0.16)	0.21 (0.22)	0.16 (0.11)	0.422
Compliance	1.6 (1.6)	1.6 (1.6)	1.7 (1.8)	1.4 (0.95)	0.629
Ees/Ea	0.84 (0.58)	0.92 (0.66) †	0.90 (0.56) †	0.60(0.34) ‡*	0.026

**significant difference to ILD, †significant difference to CPFE, ‡significant difference to COPD*

Table 5.6: *Patient demographics for the patients with severe PH. An IPAH cohort is provided for reference.*

	All lung	COPD	ILD	CPFE	p-value	IPAH
Number	134	48	33	28		92
Demographics						
Age (years)	68 (9)	68 (9)	67 (10)	69 (8)	0.885	58 (17)
Sex (F/M)	73/65	22/26	20/13	10/18	0.144	63/30
WHO functional class (II,III,IV)	2,102,33	1,36,10	0,23,10	0,19,9	0.643	1,76,14
ISWT (m)	130 (157)	119 (96)	153 (288)	146 (94)	0.700	218 (190)
Days RHC to MR	0 (2)	1 (1)	0 (0)	0 (0)	0.106	2 (5)
Survival (years)	1.4 (1.0)	1.6 (1.1) *	1.0 (0.8) ‡	1.3 (1.0)	0.022	3.3 (0.2)
RHC						
mPAP (mmHg)	48 (9)	47 (8)	49 (9)	50 (8)	0.228	56 (11)
mRAP (mmHg)	11 (5)	11 (5)	11 (6)	11 (5)	0.996	12 (6)
PAWP (mmHg)	13 (4.9)	13 (4)	12 (6)	12 (3)	0.577	12 (4)
CI (L/m^2)	2.5 (0.8)	2.5 (0.8)	2.5 (0.1)	2.3 (0.7)	0.335	2.3 (0.7)
PVRI (dynes)	377 (202)	368 (197)	414 (254)	424 (167)	0.460	536 (291)
SvO_2 (%)	63 (8)	63 (9)	64 (8)	62 (7)	0.450	59 (8)
Spirometry						
FEV1 (%)	71 (24)	59 (24) †*	74 (23) ‡	82 (20) ‡	<0.001	79 (21)
FVC (%)	80 (24)	83 (25) *	67 (21) ‡†	94 (21) *	<0.001	81 (18)
FEV1/FVC	63 (17)	50 (14) †*	77 (12) ‡†	64 (13) ‡*	<0.001	69 (13)
TLCO (%)	27 (13)	24 (10)	24 (7)	24 (8)	0.998	44 (21)

**significant difference to ILD, †significant difference to CPFE, ‡significant difference to COPD*

Table 5.7: *Baseline cardiac MRI characteristics for the patients with severe PH lung.*

	All	COPD	ILD	CPFE	p-value	IPAH
RV EDV index (ml/m^2)	91 (31)	101 (36)	91 (33)	86 (22)	0.141	101 (36)
RV ESV index (ml/m^2)	60 (28)	66 (34)	60 (29)	59 (21)	0.481	63 (27)
RVEF (%)	36 (12)	37 (14)	36 (12)	34 (12)	0.541	35 (10)
RVSVI (ml/m^2)	31 (11)	34 (10) †	30 (11)s	28 (11) ‡	0.027	32 (12)
RV mass index (g/m^2)	25 (15)	29 (19)	22 (13)	22 (9)	0.092	26 (11)
LV EDV index (ml/m^2)	51 (18)	54 (21)	47 (18)	47 (13)	0.184	46 (14)
LV ESV index (ml/m^2)	18 (10)	21 (14)	16 (9)	18 (7)	0.223	16 (8)
LVEF (%)	65 (12)	63 (14)	66 (12)	62 (12)	0.367	66 (10)
LVSVI (ml/m^2)	33 (12)	34 (12)	31 (12)	30 (9)	0.315	30 (10)
LV mass index (g/m^2)	51 (12)	52 (15)	49 (12)	49 (10)	0.458	47 (11)
LA volume index (ml/m^2)	37 (20)	40 (22) †	39 (23) †	26 (7) *‡	0.008	32 (20)
PA RAC (cm^2)	8.5 (5.6)	8.5 (6.3)	7.6 (5.3)	8.6 (5.0)	0.742	8.1 (5.1)
Diastolic PA size	894 (229)	907 (263)	882 (216)	848 (190)	0.574	892 (223)
Systolic PA size	968 (250)	985 (291)	947 (227)	922 (218)	0.565	966 (251)
VMI	0.52 (0.29)	0.58 (0.36)	0.52 (0.28)	0.49 (0.22)	0.414	0.60 (0.25)
IVS angle (˚)	173 (20)	172 (19)	173 (19)	180 (23)	0.208	181 (21)
Black blood score						5.0 (1.8)
PA to LA TTP (s)	7.3 (2.6)	7.2 (2.4)	5.2 (0.9)	8.2 (0.9)	0.016	0.14 (0.10)
Average PA velocity (cm/s)	5.8 (2.1)	5.7 (1.9)	5.9 (2.5)	5.4 (1.5)	0.683	1.4 (1.0)
Distensibility	0.17 (0.13)	0.19 (0.17)	0.15 (0.13)	0.17 (0.10)	0.605	58 (11)
Compliance	1.5 (1.3)	1.7 (1.8)	1.3 (1.2)	1.5 (1.0)	0.395	8.1 (8.4)
Ees/Ea	0.69 (0.45)	0.69 (0.52)	0.65 (0.42)	0.59 (0.32)	0.651	0.57 (0.33)

5.2.3.1 Baseline characteristics of PH lung disease

The patients with PH-lung disease had significant differences in all cardio-pulmonary MRI characteristics at baseline, but there was also a significant difference in mean pulmonary artery pressure. In order to compensate for this, baseline analysis was performed in the patients with severe pulmonary hypertension (mPAP ≥35mmHg). There were 138 patients with mPAP ≥35mmHg: 48 severe PH-COPD, 33 severe PH-ILD, 28 severe PH-CPFE and 29 severe PH-other respiratory disease. In the ILD group radiological patterns of fibrosis included six patients with usual interstitial pneumonitis (UIP), 18 with Non-Specific Pneumonitis (NSIP), 5 with a chronic hypersensitivity pneumonitis (HP) pattern and 4 with an unknown radiological pattern of fibrosis.

5.2.3.1.1 Demographic differences

Baseline demographic data for the severe PH-lung patients is provided in **Table 5.6**. There was no significant difference in age or sex between the lung disease groups, although the severe PH-COPD and CPFE groups had a higher proportion of male patients, whereas the ILD group had a predominance of female patients. WHO functional class and walk distance were also not significantly different, although the walk distance was significantly lower for all PH-respiratory groups compared to IPAH.

5.2.3.1.2 Haemodynamic differences

When comparing all patients there was a significantly higher mean mPAP in the CPFE group with correspondingly low cardiac index. A higher proportion of patients with CPFE had severe PH (28/32) than COPD (48/68) and ILD (33/55).

When comparing the severe PH-lung disease patients, although the COPD patients had the lowest (42mmHg) and the CPFE patients the highest mPAP (48mmHg), there was no significant difference in haemodynamics, although the numbers have significantly reduced. The PH lung and severe PH lung patients had significantly lower mPAP than the IPAH comparison group. Pulmonary arterial wedge pressure (PAWP) was not elevated in any group.

There was no correlation between the visual severity on CT in the COPD or the ILD cohorts (r=0.028, p=0.818 and r=-0.39, p=0.775 respectively).

5.2.3.1.3 Spirometric differences

Spirometry showed the expected differences between the severe PH-lung groups: COPD patients had significantly reduced forced expiratory volume in one second (FEV1) percent predicted (59%, sd 24) and low forced expiratory volume in second to forced vital capacity (FEV1/FVC) (50, sd 14), whereas ILD patients had reduced FVC (67%, sd 21) p-values for all spirometry were <0.0001. Transfer capacity for carbon monoxide (TLCO) percent predicted was similarly low in COPD, ILD and CPFE (24% in all, p-value 0.998). Mixed venous oxygen saturation (SvO2) was not different across the groups but was significantly lower in the severe PH lung patients than in the IPAH patients.

5.2.3.2 Cardiac MRI phenotypes of severe PH-lung

In all patients with severe PH-lung disease right ventricular volumes (end-diastolic and end-systolic) were moderately elevated (91ml/m^2 and 60 ml/m^2) with no significant difference between the groups (p-value 0.141 and 0.481 respectively). Right ventricular ejection fraction was low in all severe PH-lung groups, but with no significant differences between them (36% for the severe PH-lung cohort as a whole, p-value 0.541). **Table 5.6** and **Table 5.7** provide the baseline cardiac MRI metrics for patients with severe PH.

Left ventricular end diastolic volume was low in all of the groups but not significantly different between the groups (51ml/m^2). Left ventricular end systolic volume and ejection fraction were normal and similar across the groups (18ml/m^2 and 65%, p-values 0.481 and 0.541 respectively). Left ventricular stroke volume index was low in all groups, but again, not different between the groups (33ml/m^2, p-value 0.315).

Left atrial volume index was low in all of the PH-lung cases, but was significantly lower in the CPFE cases (mean 26 ml/m^2, p-value 0.008). The interventricular septal angle was increased (flattened septum) in all cases but with no significant differences between groups (173, p-value 0.208).

The time to peak perfusion from the pulmonary artery to the left atrium was significantly longer in the COPD and CPFE patients (7.9 and 8.2 secs) than in the ILD patients (5.1 secs, ANOVA p-value 0.016), and although the inverse of this relationship

was shown in pulmonary arterial average velocity, it was not found to be statistically significant.

5.2.4 **Discussion**

The work presented in this section, discusses the baseline cardiac MRI characteristics in a cohort of severe PH-lung disease cohort in a tertiary referral centre (245). Patients with PH due to CPFE were significantly more likely to have severe PH than those with COPD or ILD.

On first glance there appear to be significant differences in the baseline characteristics of the patients with COPD and ILD in comparison to CPFE. The most striking difference is with right heart catheter measured mean pulmonary artery pressure, the mean mPAP of COPD and ILD was 42 and 41mmHg respectively and in the CPFE patients was 48mmHg (p-value 0.011). A higher proportion of CPFE patients had severe pulmonary hypertension at baseline. In order to correct for this, comparison was performed in the cases who had lung disease with severe pulmonary hypertension (mPAP ≥35mmHg). When corrected in this way, the only significant differences between the groups was stroke volume and left ventricular volume index, both of which were lower in CPFE. It is expected that this result would be due to an increased PVR in the CPFE patients, but right heart catheter measured PVRI was not significantly different across the groups.

It would be interesting to identify the relationship between lung disease severity on CT and the severity of pulmonary hypertension. Unfortunately, as the CT cans were performed as part of the clinical workflow, they were performed as CTPAs, to assess the pulmonary artery and the right ventricle. This meant that quantitative assessment of the pulmonary parenchyma was not possible. It is also difficult to account for the severity of disease between COPD, ILD and CPFE using either clinical, lung function or imaging criteria. In this patient cohort we found no correlation between visual score of CT severity and severity of PH elevation in the COPD and ILD patients, however this is limited by small patient numbers and differs from published literature in much larger numbers, but with a lower incidence of PH (103,269,270). Studies assessing the relationship between PH and severity of lung disease in COPD and ILD and a comparison of the two will require large datasets to account for the heterogeneity of lung disease (270).

This work is limited by its retrospective single centre design, although all quantification was performed at the time of the scan, blinded to the diagnosis. As a result of the study taking place in a PH referral centre, the population has a trend towards the presence of pulmonary hypertension. The proportion of PH and the severity of PH is probably more than expected for the general COPD, ILD and CPFE population as only patients with significant symptoms would be referred for further investigation (a large number of patients with COPD and ILD would be managed in the community or in local secondary care clinics). This also leads to a potential problem in the definition of baseline, as the baseline is the point at which the patient is referred to the PH service, rather than the point at which they develop PH.

5.2.5 **Conclusion**

At baseline cardiac MRI, there were no significant differences between the pulmonary hypertension lung groups when allowing for differences in mean pulmonary arterial pressure. A higher proportion of PH-CPFE patients have mean pulmonary arterial pressure ≥35mmHg than the ILD and COPD groups. Future work will be required to assess the role of lung disease severity in the development of PH in larger numbers.

5.3 CARDIO-PULMONARY MRI CAN SCREEN FOR CTEPH

5.3.1 Rationale

Chronic thromboembolic pulmonary hypertension (CTEPH) is a potentially curable form of pulmonary hypertension (61). The diagnosis requires a mean pulmonary artery pressure (mPAP) ≥25 mmHg at right heart catheterization (RHC), in the presence of at least one segmental defect on perfusion imaging or filling defects on computed tomography pulmonary angiography (CTPA), after at least 3 months of effective anticoagulation (62). The true incidence and prevalence of CTEPH is not known, but the cumulative incidence of CTEPH after survival from an acute pulmonary embolus is reported as 3.8% at 2 years (63). The pathological process is thought to be due to incomplete lysis of the acute pulmonary embolus; the subsequent organization of the obstructing thrombus leading to obstruction of pulmonary vascular bed (64). This ultimately leads to increased pulmonary arterial pressure, right ventricular dysfunction and if untreated the prognosis is poor (65).

Patients with CTEPH usually have a history of either pulmonary embolism or deep venous thrombosis, although a significant proportion may present with unexplained breathlessness or pulmonary hypertension of unknown cause (66,67). It is important that the diagnosis of CTEPH is made as pulmonary endarterectomy is associated with increased survival and a favourable functional outcome in CTEPH (61). The 2013 World Symposium on Pulmonary Hypertension recommended single photon emission computed tomography (SPECT) V/Q scintigraphy as the preferred screening test for CTEPH (271), this entails injection of 100MBq of 99mTc labelled macroaggregated human albumin, resulting in exposure to ionizing radiation with an effective dose of 0.017mSv/MBq (87).

Cardio-pulmonary MR imaging is emerging as an important tool for assessing the structure and function of the right ventricle in patients with PH (155), and it has already been shown that 3D dynamic contrast enhanced (DCE) lung perfusion MRI has a similar sensitivity for diagnosing CTEPH when compared with planar perfusion scintigraphy (91). Planar scintigraphy is increasingly being replaced by SPECT in clinical practice, due to the higher spatial resolution and improved sensitivity in the detection of smaller perfusion defects (272).

5.3.1.1 Hypotheses

1. Dynamic contrast enhanced perfusion MRI has high diagnostic accuracy in the identification of patients with chronic thrombo-emboli disease.
2. DCE-MRI has non-inferior diagnostic accuracy to perfusion SPECT in the identification of chronic thrombo-embolic disease.

5.3.1.2 Aims

The aim of this study was to assess the diagnostic accuracy of perfusion MRI against perfusion SPECT in screening for CTEPH.

5.3.2 Patients and Methods

Consecutive patients with suspected CTEPH or unexplained pulmonary hypertension attending a pulmonary hypertension referral centre (245) underwent contrast enhanced lung perfusion MRI, perfusion SPECT and CTPA within 14 days of right heart catheterization, from April 2013 to April 2014 were identified. A diagnosis of CTEPH was based upon a review of multimodality imaging, clinical correlates and right heart catheterisation as per standard clinical criteria (62), this was decided at a multi-disciplinary team meeting and was used as the reference standard. Patients with chronic thrombo-embolic disease, but without pulmonary hypertension were considered a true positive. This was decided as the current method of diagnosis of pulmonary hypertension is not made on imaging, but instead relies on pressure measurements in the pulmonary artery on right heart catheterization. The local research ethics committee granted ethical approval for this retrospective study, written consent was waived.

5.3.2.1 Image acquisition

MR imaging was performed on a 1.5T whole body system (HDx, GE Healthcare, Milwaukee, USA) using a time-resolved 3D spoiled gradient echo sequence with view-sharing (273). An 8-channel cardiac receiver array coil was used. The sequence parameters were: TE=1.1 ms, TR=2.5 ms, Flip angle 30°, FOV 48 cm x 48 cm, parallel imaging in plane x 2, in plane resolution 200x80, bandwidth 250 kHz, slice thickness 10 mm, approximately 32 slices, 48 time points with an overall effective 3D frame rate of ~ 0.5 s. Images were acquired in a coronal orientation during a single breath-hold. The acquired voxel size was 1.875 x 1.875 x 10 mm. Contrast injection of a 0.05ml per kg patient weight dose of Gd-BT-D30A (Gadovist, Schering, Berlin, Germany) was injected at a rate of 4 ml per second with the injection rate controlled using an activated pump injector (Spectris, MedRad) typically via a vein in the antecubital fossa using an 18G cannula, followed by a 20ml saline flush.

SPECT imaging was performed on a General Electric Infinia SPECT system using a low energy general-purpose collimator. 100 MBq 99mTc MAA was administered through a direct intravenous injection with a needle of 21G or larger. The image acquisition parameters were: acquisition matrix 128x128, 60 projections per detector and 7 seconds per projection. Images were acquired prone with the patient's arms extended

above their heads, where possible. Figure 5.10 shows an example of SPECT and MRI perfusion imaging I a patient with and without CTEPH.

5.3.2.2 Image analysis

DCE perfusion images were analysed on a slice-by-slice basis by subtraction of the baseline pre-contrast image, this was performed on a GE Advantage workstation (General Electric Healthcare). The peak enhancement image in the contrast passage time series was independently analysed by a general radiologist (CSJ, 5 years of experience) and a consultant chest radiologist (AJS, 11 years of experience) blinded to all other imaging and clinical information. The images were reviewed on a general reporting workstation in the general radiology department on diagnostic quality Barco screens (Barco, UK). The images were qualitatively assessed as either positive or negative for chronic thromboembolic disease. On both DCE perfusion MRI and perfusion SPECT, the presence of one or more segmental or subsegmental perfusion defects was considered positive for pulmonary embolic disease, as per recognized clinical guidelines (1). The dynamic contrast enhanced perfusion images were typically viewed with a window of 40 and a level of 19, although this was manipulated if required. Subsequently the SPECT imaging was reviewed by the same radiologists, at a separate sitting, separated from the time of the MRI analysis by at least one week, blinded to all other imaging and clinical information. Any disagreements were resolved by consensus. The multidisciplinary decision of the presence or absence of chronic thrombo-embolic disease, as outlined above, was considered the reference standard.

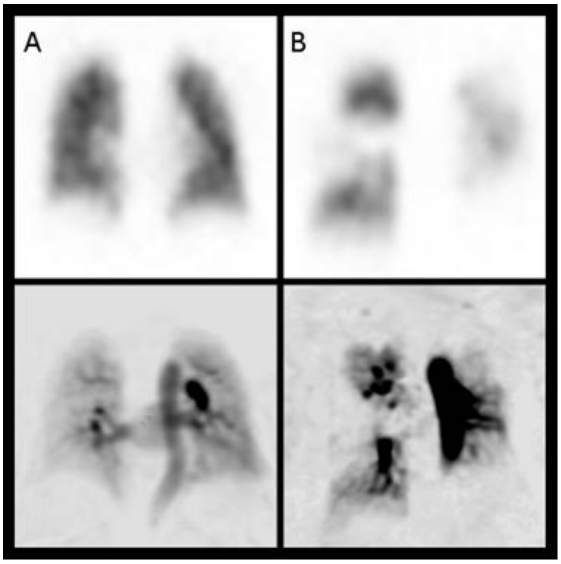

Figure 5.10: SPECT and DCE MRI perfusion images.
Matched slices from 3D coronal SPECT perfusion images (top row) and DCE MR perfusion images (bottom) in a patient with normal lung perfusion (A) and with CTEPH (B). This shows the typical wedge-shaped perfusion defects (arrows) in the right mid, left lower, and left upper zones on the MR and the SPECT imaging of patient B. Note the images are presented on an inverse grey scale as reviewed clinically for SPECT.

5.3.2.3 Statistical analysis

Diagnostic accuracy was assessed for SPECT and DCE perfusion MRI using a 2x2 predictive table to calculate sensitivity, specificity, negative and positive predictive value. Inter-observer and inter-test agreement was assessed using kappa, with 0.60-0.79 considered moderate agreement, 0.80-0.89 strong and above 0.90 excellent agreement (274). Statistical analysis was performed using SPSS 22 (IBM, Chicago) and GraphPad Prism 7 (GraphPad Software, San Diego). A p-value of <0.05 was considered statistically significant.

5.3.2.4 Patient Demographics

Over the 1-year period of the study, 74 patients with suspected CTEPH attended for perfusion MRI, SPECT and CTPA. 36 patients were diagnosed with CTEPH and 10 patients with CTED (chronic thromboembolic disease without pulmonary hypertension) according to standard criteria. In the CTEPH and CTED group there were 20 female and 26 male patients. The mean age of both groups was 62 years (standard deviation 14 years).

5.3.3 **Results**

DCE perfusion MRI correctly identified all CTEPH and CTED patients (sensitivity of 100%), compared to 97% sensitivity for SPECT, p-values for all data were <0.0001 (see table 1 for more details). The specificity of MR was 81% and SPECT 81%. The patient not identified by SPECT had mild, inoperable CTEPH, and was correctly identified on CTPA and perfusion MRI. There was one indeterminate SPECT case and two indeterminate MRI cases. The kappa value between SPECT and MRI was 0.88, indicating strong agreement. Inter-observer kappa was 0.80 and 0.88 for SPECT and MRI respectively indicating strong inter-observer agreement.

Table 5.8: *Summary of diagnostic performance of SPECT and MR perfusion with 95% confidence interval (CI), the p-values for all data were <0.0001.*

	SPECT Perfusion	Perfusion MRI
Sensitivity	97% (95% CI 88-99%)	100% (95% CI 92-100%)
Specificity	81% (95% CI 62-94%)	81% (95% CI 62-94%)
Positive predictive value	90% (95% CI 78-97%)	90% (95% CI 78-97%)
Negative predictive value	96% (95% CI 78-100%)	100% (95% CI 85-100%)
Inter-observer agreement (kappa)	0.80	0.88

5.3.4 **Discussion**

DCE lung perfusion MRI has increased sensitivity when compared to SPECT perfusion scintigraphy in the detection of CTEPH. In the patients studied, a combination of perfusion MR and CTPA identified all patients with CTEPH and CTED. This reflects and updates the findings of a previous study by Rajaram et al. which compared DCE perfusion MRI with planar scintigraphy (91). There were two indeterminate sets of MRI scans, it was felt that low signal to noise ratios in these images was the underlying reason for an indeterminate study. Perfusion MRI can be performed in the same sitting as high-resolution pulmonary MR angiography and cardiac MRI scan, and has the potential for a "one-stop-shop" analysis of pulmonary perfusion and assessment of right heart and pulmonary vascular characteristics. Cardiac MR assessment of baseline and progression of right ventricular characteristics over time in idiopathic pulmonary artery hypertension (IPAH) has been previously shown to be a predictor of outcome (130,204).

These results differ somewhat from the literature regarding MR in the diagnosis of acute pulmonary emboli (PE). The PIOPED III study assessed the efficacy of MR angiography, and showed a sensitivity of 78% for acute PE detection in technically adequate scans, 25% of patients had technically inadequate scans (275). However, there have been more recent reports of improving diagnostic rates, particularly when performed in dedicated centres (276–278). Although it should be noted that whilst contrast enhanced MRA and DCE perfusion images are different methods for assessment of the pulmonary vasculature, in that MRA focuses on structural form of the major vessels whilst DCE perfusion MR highlights downstream perfusion of the small vessels, it is likely that the main difference in the sensitivity of MR in the assessment of acute and chronic PE could be due to the size of thrombus detected. Due to improvements in technologies, modern day CTPA is able to pick up very small subsegmental acute PEs, which (in our opinion), are likely to be smaller than those that can be currently detected on MR angiography or MR perfusion imaging. These peripheral acute emboli are very unlikely to cause CTEPH, so the lower spatial resolution of MR angiography and perfusion imaging when compared to CTPA should not miss clinically significant chronic thrombo-embolic disease. In the present study, DCE-MRI had the highest sensitivity for detecting CTEPH although SPECT Q only failed to identify a single patient with distal thromboembolic disease. Importantly, however,

no modality missed surgical accessible CTEPH. The case that was missed by SPECT was in a patient with coexistent lung pathology which caused a defect that was not typical of embolic disease on the SPECT image, the anatomical information available on the non-subtracted MRI database meant that was less of an issue for the MR perfusion scan. Whilst CTPA is widely available and may give clues to other differential diagnoses, it should be noted that CTEPH and CTED may be missed on CTPA by radiologists not experienced in the assessment of pulmonary vascular disease leading to the recommendation in the latest international guidelines that SPECT Q is preferred to CTPA when screening for CTEPH (1). Given the similarities between the images obtained by DCE-MRI and SPECT Q, it is anticipated that DCE-MRI would have similar diagnostic performance in the hands of a general radiologist. In this study, perfusion imaging had a modest specificity of 81% (for both SPECT and DCE-MRI), in keeping with the known false positive rate of SPECT perfusion imaging (238).

Although SPECT imaging and DCE perfusion MRI both demonstrate pulmonary perfusion of the small (sub-voxel size) vessels, there are fundamental differences in the method of acquisition and contrast enhancement. SPECT imaging represents deposition of radio-isotope particles in the capillaries and small arterioles in the lung (87), with acquisition times around ten minutes in a pseudo steady state of lung perfusion. DCE MR perfusion images are, however, dynamically acquired in the first pass of gadolinium; and a 3D dataset is acquired (here approximately every 0.5 secs) during a breath-hold. The initial "unenhanced" pre-bolus arrival dataset is subtracted from the peak enhancement dataset to give the perfusion images. As such, the MR images are interpreted as a snapshot of the 'peak' first pass perfusion signal and also the enhanced signal from blood in the conducting major vessels is not explicitly segmented from the signals from the rest of the pulmonary blood pool.

An alternative method of analysis which might closer represent the cumulative signal of a SPECT scan would be to integrate the dynamic perfusion signal with time to create maps of regional perfused blood volume (279). An example of the quantitative parametric maps of pulmonary perfusion is provided on page 54 (Figure 2.18). Using the arterial input function and unenhanced lung T1 maps, time-contrast curves can be calculated for each voxel and peak contrast, mean transit time and pulmonary

perfusion can be calculated, as previously described (146,280). These are calculated for each voxel over the time-course of the perfusion dataset and can be presented in a parametric map. Techniques to segment out the major vessels could also be employed to mask the signal from the perfused capillary bed (281), although background signal from the major vessels was however not felt to affect the radiological interpretation of the images in this study.

This study has a number of limitations. As our study was conducted in a pulmonary hypertension referral centre (245) the negative and positive predictive value will only be valid for a population where the probability of CTEPH and CTED is high, although given the high sensitivity and specificity of MRI it would be expected to perform well in symptomatic patients following PE where the prevalence of CTEPH is increased. The retrospective nature of the study has the potential to introduce bias, however, both reviewers were blinded to each other's observations and clinical information. A prospective study examining the value of MRI and SPECT VQ as a screening test for CTEPH will be required to address the clinical utility and diagnostic performance of these investigations in populations at risk.

5.3.5 **Conclusion**

Dynamic contrast enhanced perfusion MRI has high sensitivity for CTEPH and does not use ionising radiation making it an ideal imaging screening test for patients with suspected CTEPH.

6 CARDIAC MRI CAN PROGNOSTICATE IN PULMONARY HYPERTENSION

Once patients have been assessed for potential therapeutic options, it is important to identify those who are at risk of a poor outcome. The final chapter of results in this thesis aims to assess the role of cardiac MRI in the evaluation of mortality risk in patients with pulmonary hypertension.

Previous work has shown that cardiac MRI markers of right ventricular structure and function can provide incremental prognostic information in patients with pulmonary arterial hypertension (124). In both patients with left heart and respiratory disease, the presence of pulmonary hypertension is known to be a marker of a poor outcome. There is little data available in these patient groups to identify which of the patients within these groups are at risk of death after the development of pulmonary hypertension. Work from our group, which is ongoing, has identified that the largest risk factor for a poor outcome in patients with CTEPH is whether the patient has pulmonary end-arterectomy, either due to patient choice or technical factors (282). Future work is concentrating on the risk factors for death in the group of patients who decline surgery.

The following sections in this chapter explore the prognostic information that can be gained from cardiac magnetic resonance imaging in the context of respiratory disease (specifically COPD) and left heart disease[v].

[v] Each section of this chapter makes up work in separate papers.
Cardiac MRI has Prognostic Value in PH-LHD is based upon a manuscript currently under review with *the Journal of the American College of Cardiology: Heart Failure.*
Cardiac MRI can Identify Patients with PH-COPD Who Are At Risk Of Death is based upon a manuscript that has been published in *European Radiology*, entitled "Non-invasive methods for estimating mPAP in COPD using cardiovascular magnetic resonance imaging" (217).

6.1 CARDIAC MRI HAS PROGNOSTIC VALUE IN PH-LHD

6.1.1 Rationale

Pulmonary hypertension is most commonly seen in patients with left heart disease (1,9,20,21). It is increasingly recognised (23), and is associated with a poor prognosis (24–27) and high levels of health care utilization. It is seen in the setting of both reduced and preserved left ventricular systolic function (283,284). Heart failure with preserved ejection fraction (HFpEF) accounts for approximately half of all patients with heart failure (285). In contrast to improvements in outcome following pharmaceutical and mechanical interventions in patients with heart failure and reduced left ventricular systolic function (HFrEF) there has been very limited progress in patients with HFpEF (23). The development of pulmonary hypertension and right ventricular dysfunction in these patients is associated with a worse outcome regardless of aetiology (286–289) Interestingly, approaches to reduce pulmonary artery pressure guided by implantable pulmonary artery pressure monitors (using primarily diuretic therapy) can improve outcomes in these patients (285,290).

In most patients with HFpEF who develop pulmonary hypertension, elevated pulmonary artery pressures are thought to reflect a "passive" transmission of high left ventricular filling pressures through the pulmonary circulation (29). However, a proportion of patients develop a pre-capillary component to their pulmonary hypertension (combined pre-and-post capillary pulmonary hypertension, Cpc-PH), defined at right heart catheterization by a diastolic pulmonary gradient (>7mmHg) or pulmonary a vascular resistance (>3WU) (1,30,291). It has been shown that these patients have a worse prognosis than patients with isolated post capillary pulmonary hypertension (Ipc-PH) and some of these patients share histological changes with patients with pulmonary arterial hypertension (22,30,31). This has focussed attention on the potential role of pulmonary arterial vasodilator therapy (29,259). Although small studies have suggested benefit (266,292,293), large randomised controlled studies have been negative and there is concern that patients most likely to benefit from pulmonary vasodilator therapy were not included in these studies.

Whilst cardiac catheterisation is considered the gold standard to define the presence of pulmonary hypertension, MRI is considered the gold standard technique to assess right ventricular function.

6.1.1.1 Hypotheses

1. Cardiac MRI can provide a non-invasive assessment of prognosis in patients with PH due to left heart disease.

6.1.1.2 Aims

Given the emerging evidence that impairment of right ventricular function is an important determinant of outcome in HFpEF (289), the aim of this chapter was to examine the prognostic value of MRI metrics, haemodynamics, demographics and other routinely performed investigations in a comprehensively phenotyped cohort of patients with HFpEF using gold standard techniques to identify the presence of pulmonary hypertension and assess right ventricular function.

6.1.2 **Methods**

Consecutive, treatment naive patients with suspected pulmonary hypertension who underwent cardiac MRI at the Sheffield Pulmonary Vascular Disease Unit from April 2012 to April 2017 were assessed for inclusion in the study. Patients underwent systematic evaluation including multimodality imaging and cardiac catheterisation as previously described in the ASPIRE Registry (4). Patients were required to have undergone right heart catheterisation and MRI within 30 days and inclusion criteria required a mean pulmonary arterial pressure ≥25mmHg, a pulmonary artery wedge pressure >15 mmHg, a left ventricular ejection fraction >50% and a left atrial volume index >41ml/m^2 (255) and no other potential cause for pulmonary hypertension, **Figure 6.1**.

6.1.2.1 Right Heart Catheter

Right heart catheterisation was performed using a balloon tipped 7.5Fr thermodilution catheter (Becton-Dickinson, Franklin Lakes, New Jersey). Pulmonary hypertension was defined as a resting mPAP ≥25mmHg and left heart disease was defined as pulmonary arterial wedge pressure >15mmHg. Cardiac output was calculated using the thermodilution technique. The following calculations were made:

$$Diastolic\ Pulmonary\ Gradient\ (DPG) = dPAP - PAWP$$

Where dPAP is the diastolic pulmonary arterial pressure and PAWP is the mean pulmonary arterial wedge pressure.

$$Systolic\ Pulmonary\ Gradient\ (SPG) = sPAP - PAWP$$

Where sPAP is the systolic pulmonary arterial pressure and PAWP is the mean pulmonary arterial wedge pressure.

$$Pulmonary\ Vascular\ Resistance\ Index\ (PVR) = \frac{mPAP - PAWP}{CI}$$

Where mPAP is the mean pulmonary arterial pressure, PAWP is the mean pulmonary arterial wedge pressure and CI is the cardiac index (CI = Cardiac Output/Body Surface Area).

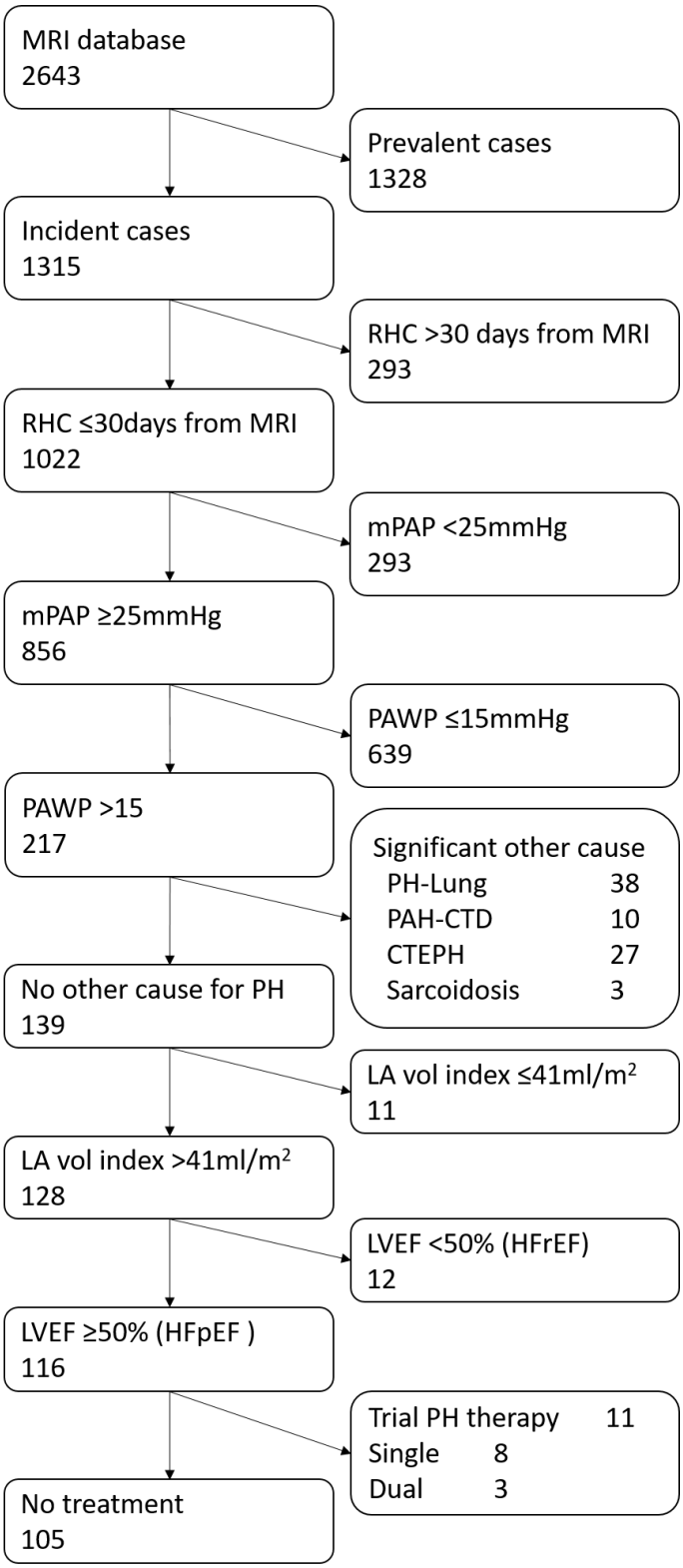

Figure 6.1: *Patient flow.*

RHC: right heart catheter, mPAP: mean pulmonary arterial pressure, PAWP: pulmonary arterial wedge pressure, PH: pulmonary hypertension, LA: left atrium, LVEF: left ventricular ejection fraction

6.1.2.2 MR Image Acquisition and analysis

Cardiac MRI was performed in a pulmonary hypertension tertiary referral centre (245), on a GE HDx 1.5-T whole body scanner (GE Healthcare, Milwaukee, Wisconsin), using an 8-channel cardiac coil, with the patient supine. Four-chamber (4Ch) and short axis (SA) cine images were acquired, using a retrospectively cardiac gated multi-slice steady-state free precession (SSFP) sequence. We acquired a stack of axial images in the SA plane, with slice thickness of 10 mm with no inter-slice gap or 8 mm with a 2 mm inter-slice gap, from the base to apex of both ventricles. Time resolved images of the pulmonary artery were performed using a retrospectively cardiac gated SSFP sequence with a single slice of 10mm taken perpendicular to the long axis of the pulmonary artery. The SSFP sequence parameters were: TR 2.8ms, TE 1.0ms, flip angle 50°, field of view 48x48, 256x256 matrix, 125 kHz bandwidth, and slice thickness 8 to 10 mm.

Axial black blood imaging was performed using a dual inversion recovery fast spin echo sequence, with a stack of 8mm slices with 10mm spacing taken through the long axis plane of the pulmonary artery. The sequence parameters were: TR 984ms, TE 40ms, flip angle 90˚, echo train length 32, field of view 4cm, 256x256 matrix, 31.2 kHz bandwidth on an 8 channel cardiac coil.

MR images were manually analysed by DC (a cardiac MRI radiographer of 9 years cardiac MRI experience) on a GE Advantage Workstation 4.4 and GE Advantage Workstation ReportCard software, blinded to all clinical information. Left and right ventricular end-diastolic volume, end-systolic volumes, right and left ventricular stroke volume and mass were calculated (and indexed to body surface area), right and left ventricular ejection fractions, ventricular mass index (RV mass divided by LV mass) (257) and interventricular septal angle were measured as previously described (125,134). Right and left ventricular ejection fractions were calculated as end diastolic volume minus end-systolic volume divided by end diastolic volume. Maximal and minimal pulmonary arterial areas were manually traced, and relative area change was defined by the following equation: PA RAC= (maximum area-minimum area)/minimum area (208). Reproducibility metrics for these cardiac MRI metrics for DC and AJS have been previously published (124). Pulmonary arterial compliance was calculated as a composite metric of right heart catheter and cardiac MRI:

$$PCa = \frac{sPAP - dPAP}{PA\ RAC}$$

Where, PCa is the pulmonary arterial compliance, sPAP is the systolic pulmonary arterial pressure, dPAP is the diastolic pulmonary arterial pressure and PA RAC is the pulmonary arterial relative area change.

6.1.2.3 Statistics

Statistical analysis was performed using SPSS statistics 22 (IBM, Chicago) and all graphs were produced using GraphPad Prism (GraphPad, San Diego). A p-value of 0.05 was considered statistically significant. All continuous, normally distributed variables are presented as mean (standard deviation).

The interval from cardiac MRI until all cause of death or census was regarded as the follow-up period. The census was performed on 22nd May 2017. Log-log plots were inspected to ensure linearity with outcome data. Univariate and multivariate Cox proportional hazards regression was performed `with each variable standardised as the z score for the population studied, in order to allow for comparison between variables. Multivariate analysis was performed in a forward direction, for all variables with a statistically significant association with mortality on univariate analysis.

Kaplan-Meier plots were generated using published thresholds, where available. Where no threshold was available, patients were dichotomised by mean value. Log rank χ^2 was calculated for the Kaplan Meier data. ROC curve analysis was also performed for the prediction at death at 2 and 3 years, to balance patient numbers and number of deaths.

6.1.3 **Results**

6.1.3.1 Study Population

Between April 2012 and April 2017, 2643 patients underwent cardiac MRI, **Figure 6.1** shows the flow of patients in this study. Of these 1315 were incident, treatment naïve and 1022 of these had RHC and MRI within 30 days of each other. 856 patients had pulmonary hypertension and 217 had a raised PAWP (>15mmHg). 78 cases were excluded due to other causes of pulmonary hypertension (38 co-existing lung disease, 10 connective tissue disease, 27 CTEPH and 3 sarcoidosis), 12 patients were excluded with a LVEF <50% and 11 were excluded as they had a normal LA volume index on MRI (≤41ml/m^2), leaving 116 patients meeting the study criteria as having HFpEF.

Table 6.1 provides the baseline demographics of 116 patients with HFpEF. The average age was 73±7 years and 57% of patients were female. Ninety-three patients had isolated pre capillary pulmonary hypertension (defined by DPG <7mmHg) and 24 had combined pre and post capillary pulmonary hypertension (defined by DPG ≥7mmHg). 105 received no PH specific treatment and 11 patients received pulmonary vasodilator therapy (8 sildenafil alone, 3 sildenafil in combination with bosentan, macitentan or ambrisentan).

6.1.3.2 Prognostic markers

Median follow up was 23 months, during which time there were 37 deaths. **Table 6.2** provides the univariate Cox proportional hazards analysis data for each metric, and **Figure 6.2** provides a Forest plot of the outcome data. Male sex, hazard ratio (HR) of 0.328 (95% CI 0.328-0.167, p=0.001) and TL_{CO} percent predicted were strongly predictive of outcome, HR 0.792 (95% CI 0.314-0.770 p=0.002).

6.1.3.2.1 Right heart catheter metrics and prognosis

Diastolic pulmonary gradient (HR 2.862, 95% CI 1.775-4.615 p<0.001), mPAP (HR 1.726 p=0.006), PVR (HR 1.709 p <0.001), SPG (HR 2.096 p <0.001) and TPG (HR 2.656 p <0.001) predicted death, whilst mean right atrial pressure (HR 1.262 p 0.157), mean PAWP (HR 0.715 p 0.080) and cardiac index (HR 0.791 p 0.191) were not statistically significant predictors of death.

Table 6.1: *Baseline patient demographics.*

	HFpEF		Ipc-PH		Cpc-PH		
	Mean	sd	Mean	sd	Mean	sd	p-value
Number	116		93		23		
Demographics							
Age (years)	73	7	73	8	73	7	0.877
Sex (F/M)	66/50		55/38		11/12		0.227
FEV1 % predicted	71	18	72	18	69	21	0.634
FVC % predicted	71	17	72	17	67	19	0.314
FEV1/FVC	0.7	0.1	0.67	0.1	69	21	0.327
TLCO %Predicted	50	18	53	17	34	13	<0.001
ISWT (m)	149	121.0	155	123	122	123	0.306
Days MR to RHC	1	4	1	3	2	6	0.169
RHC							
mPAP (mmHg)	42	10	39	9	52	7	<0.001
PAWP (mmHg)	23	5	23	5	21	4	0.06
PVR (dyne.s)	334	236	273	187	580	253	<0.001
mRAP (mmHg)	15	5	15	5	18	6	0.024
Cardiac Index (ml/min/m^2)	2.8	1	2.9	1	2.5	0.7	0.037
DPG (mmHg)	1	7	-2	5	11	4	<0.001
SPG (mmHg)	45	18	40	15	65	12	<0.001
TPG (mmHg)	19	9	16	7	31	6	<0.001
CMR							
RV EDV index (ml/m^2)	93	34	93	37	95	23	0.847
RV ESV index (ml/m^2)	49	20	47	21	55	15	0.09
RVEF	48	10	50	10	42	8	<0.001
RV mass index (g/m^2)	20	10	18	9	25	11	0.006
LV EDV index (ml/m^2)	71	20	74	21	59	12	0.001
LV ESV index (ml/m^2)	24	11	25	12	19	7	0.019
LVEF	67	8	67	8	68	8	0.589
PA RAC	12	7	13	7	8	5	0.002
VMI	0.35	0.16	0.31	0.13	0.48	0.21	<0.001
IV septal angle (˚)	150	16	145	12	168	15	<0.001
LA vol index (ml/m^2)	74	27	75	28	68	22	0.226
LV Stroke volume (ml)	88	25	91	25	77	23	0.014

WHO-FC: World Health Organization-Functional Class, ISWT: incremental shuttle walk test, mPAP: mean pulmonary artery pressure, mRAP: mean right atrial pressure, PAWP: pulmonary arterial wedge pressure, CI: cardiac index, PVRI: pulmonary vascular resistance index, SvO_2: Mixed venous oxygen saturations, TPG: trans pulmonary pressure gradient (mPAP-PAWP), SPG: systolic pressure gradient (sPAP-PAWP), MAP: mean systemic arterial pressure, RVEDV: right ventricular end-diastolic volume, RVESV: right ventricular end-systolic volume, RVEF: right ventricular ejection fraction, RV: right ventricle, LVEDV: left ventricular end-diastolic volume, LVESV: left ventricular end-systolic volume, LVEF: left ventricular ejection fraction, PA RAC: pulmonary artery relative area change, VMI: ventricular mass index, IV septum: interventricular septum

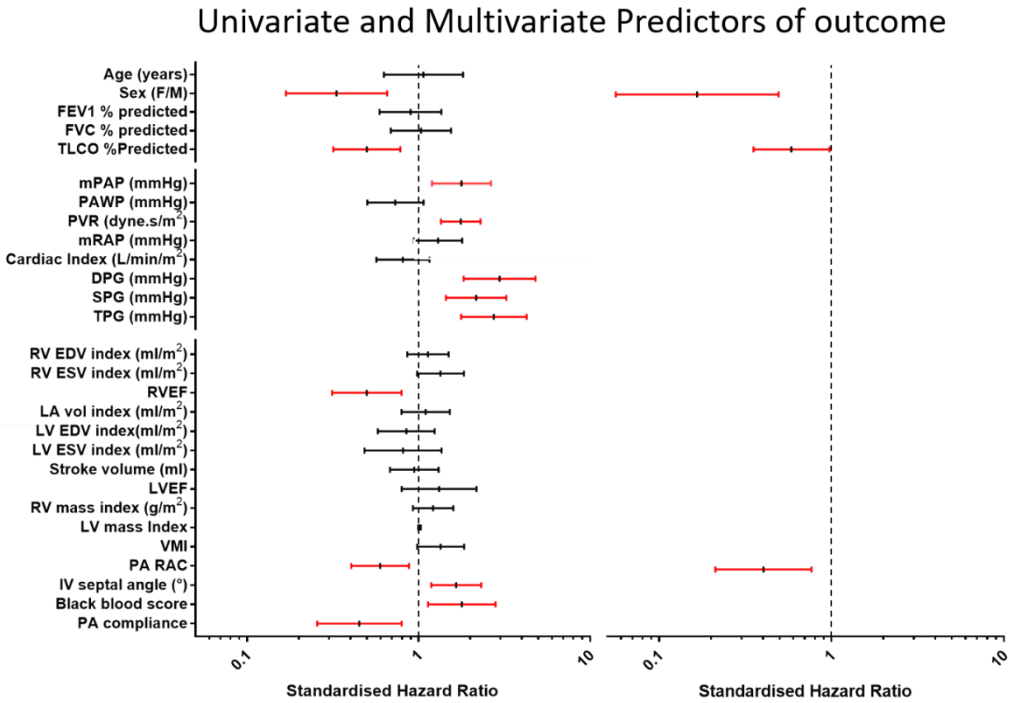

Figure 6.2: *Forrest plot analysis of survival.*

Standardized uni and multivariate hazard ratios for the prediction of all-cause mortality in patients with PH-HFpEF. Any statistically significant correlation is shown in red.

6.1.3.2.2 MRI metrics and prognosis

Right ventricular ejection fraction, PA relative area change, interventricular septal angle and black blood artefact score were all statistically significant predictors of outcome on Cox proportional hazards linear regression (HR 0.499 p 0.004, HR 0.597 p 0.009, HR 1.658 p 0.003 and HR 1.788 p 0.012 respectively) and on ROC analysis for death at 1, 2 and 3 years (**Table 6.3**). **Figure 6.5** provides the Kaplan Meier analysis for MR metrics as predictors of survival. Pulmonary arterial compliance, based on a composite of cardiac MRI and right heart catheter measures, was also predictive of outcome (HR 0.451, p 0.006).

6.1.3.2.3 Multivariate analysis

Pulmonary artery RAC, TLCO percent predicted and male sex were independent predictors of outcome. This did not change when the right ventricular volumes and ejection fractions were corrected for age and sex. **Figure 6.2** and **Table 6.2** give the data from the multivariate analysis.

Table 6.2: *Cox proportional hazards predictors of mortality from variables normalised to the z-score, HFpEF excluding treated patients*

	Univariate				Multivariate			
	HR	95%	CI	p-value	HR	95%	CI	p-value
Demographics								
Age (years)	1.047	0.618	1.774	0.865				
Sex (F/M)	0.328	0.167	0.645	0.001	0.166	0.056	0.492	0.001
WHO FC	1.37	0.952	1.971	0.090				
FEV1 % predicted	0.881	0.583	1.33	0.546				
FVC % predicted	1.013	0.677	1.515	0.950				
FEV1/FVC	1.479	0.039	55.714	0.832				
TLCO %Predicted	0.492	0.314	0.77	0.002	0.584	0.352	0.972	0.038
ISWT (m)	0.919	0.614	1.374	0.679				
RHC								
mPAP (mmHg)	1.726	1.166	2.553	0.006				
PAWP (mmHg)	0.715	0.492	1.041	0.080				
PVR (dyne.s/m^2)	1.709	1.313	2.224	<0.001				
mRAP (mmHg)	1.262	0.915	1.742	0.157				
Cardiac Index (L/min/m^2)	0.791	0.556	1.125	0.191				
DPG (mmHg)	2.862	1.775	4.615	<0.001				
SPG (mmHg)	2.096	1.402	3.132	<0.001				
TPG (mmHg)	2.656	1.716	4.111	<0.001				
CMR								
RV EDV index (ml/m^2)	1.134	0.858	1.498	0.376				
RV ESV index (ml/m^2)	1.343	0.98	1.839	0.067				
RVEF	0.499	0.313	0.796	0.004				
LA vol index (ml/m^2)	1.100	0.796	1.522	0.563				
LV EDV index (ml/m^2)	0.848	0.579	1.241	0.395				
LV ESV index (ml/m^2)	0.812	0.484	1.362	0.430				
LV Stroke volume (ml)	0.944	0.681	1.31	0.731				
LVEF	1.318	0.798	2.176	0.281				
RV mass index (g/m^2)	1.216	0.927	1.594	0.157				
LV mass Index (g/m^2)	1.012	0.995	1.03	0.168				
VMI	1.346	0.982	1.844	0.065				
PA RAC (%)	0.597	0.405	0.88	0.009	0.403	0.212	0.765	0.005
IV septal angle (˚)	1.658	1.186	2.318	0.003				
Black blood score	1.788	1.136	2.812	0.012				
Other								
PA compliance	0.451	0.256	0.797	0.006				

WHO-FC: World Health Organization-Functional Class, ISWT: incremental shuttle walk test, mPAP: mean pulmonary artery pressure, mRAP: mean right atrial pressure, PAWP: pulmonary arterial wedge pressure, CI: cardiac index, PVRI: pulmonary vascular resistance index, SvO_2: Mixed venous oxygen saturations, TPG: trans pulmonary pressure gradient (mPAP-PAWP), SPG: systolic pressure gradient (sPAP-PAWP), MAP: mean systemic arterial pressure,

Table 6.3: *ROC curve analysis for survival at 1, 2 and 3 years, AUC and p-values.*

	1 Year		2 Years		3 Years	
	AUC	p-value	AUC	p-value	AUC	p-value
Survivors/Non survivors	84/16		57/27		31/35	
RHC						
mPAP (mmHg)	0.740	0.002	0.677	0.009	0.641	0.071
PVR (dyne.s/m^2)	0.761	0.001	0.698	0.004	0.708	0.004
mRAP (mmHg)	0.556	0.482	0.581	0.233	0.569	0.337
DPG (mmHg)	0.739	0.003	0.709	0.002	0.762	<0.001
SPG (mmHg)	0.745	0.002	0.711	0.002	0.695	0.007
TPG (mmHg)	0.755	0.001	0.704	0.003	0.738	0.001
PAWP (mmHg)	0.481	0.812	0.549	0.467	0.593	0.196
Cardiac Index (L/min/m^2)	0.636	0.087	0.622	0.067	0.616	0.070
Demographics						
Age (years)	0.574	0.436	0.526	0.759	0.543	0.649
FEV1 % predicted	0.575	0.431	0.539	0.342	0.547	0.619
FVC % predicted	0.605	0.272	0.553	0.648	0.505	0.956
TLCO %Predicted	0.744	0.014	0.744	0.004	0.815	0.001
FEV1/FVC	0.618	0.089	0.622	0.154	0.635	0.264
ISWT (m)	0.605	0.291	0.521	0.809	0.622	0.194
CMR						
RV EDV index (ml/m^2)	0.555	0.488	0.501	0.992	0.519	0.792
RV ESV index (ml/m^2)	0.578	0.328	0.572	0.296	0.593	0.197
RVEF	0.805	<0.001	0.685	0.007	0.65	0.037
RV mass index (g/m^2)	0.700	0.011	0.66	0.020	0.604	0.073
LV EDV index (ml/m^2)	0.611	0.159	0.593	0.176	0.607	0.134
LV ESV index (ml/m^2)	0.571	0.372	0.556	0.414	0.656	0.030
LVEF	0.523	0.776	0.515	0.824	0.625	0.082
PA RAC	0.759	0.001	0.717	0.002	0.684	0.039
VMI	0.683	0.021	0.703	0.003	0.614	0.113
IV septal angle (˚)	0.591	0.25	0.659	0.020	0.657	0.028
LA vol index (ml/m^2)	0.560	0.447	0.553	0.439	0.607	0.134
Stroke volume (ml)	0.554	0.497	0.558	0.400	0.502	0.974
Black blood score	0.748	0.002	0.641	0.039	0.684	0.001
LV mass Index						
Other						
PA compliance	0.788	<0.001	0.718	0.06	0.67	0.017

WHO-FC: World Health Organization-Functional Class, ISWT: incremental shuttle walk test, mPAP: mean pulmonary artery pressure, mRAP: mean right atrial pressure, PAWP: pulmonary arterial wedge pressure, CI: cardiac index, PVRI: pulmonary vascular resistance index, SvO2: Mixed venous oxygen saturations, TPG: trans pulmonary pressure gradient (mPAP-PAWP), SPG: systolic pressure gradient (sPAP-PAWP), MAP: mean systemic arterial pressure, RVEDV: right ventricular end-diastolic volume, RVESV: right ventricular end-systolic volume, RVEF: right ventricular ejection fraction, RV: right ventricle, LVEDV: left ventricular end-diastolic volume, LVESV: left ventricular end-systolic volume, LVEF: left ventricular ejection fraction, PA RAC: pulmonary artery relative area change, VMI: ventricular mass index, IV septum: interventricular septum

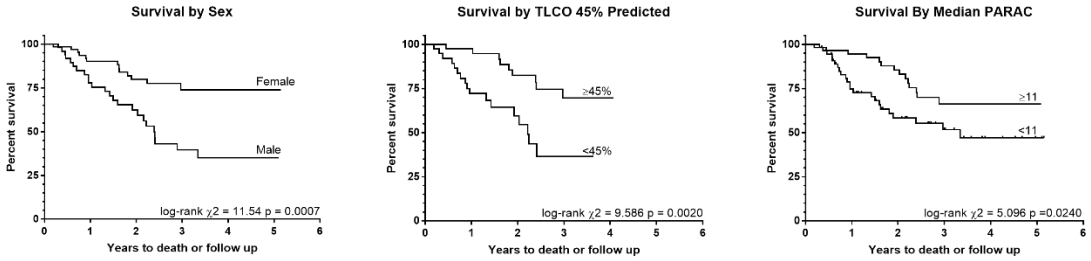

Figure 6.5: *A) Kaplan-Meier curves for the independent predictors of mortality in PH-HFpEF.*

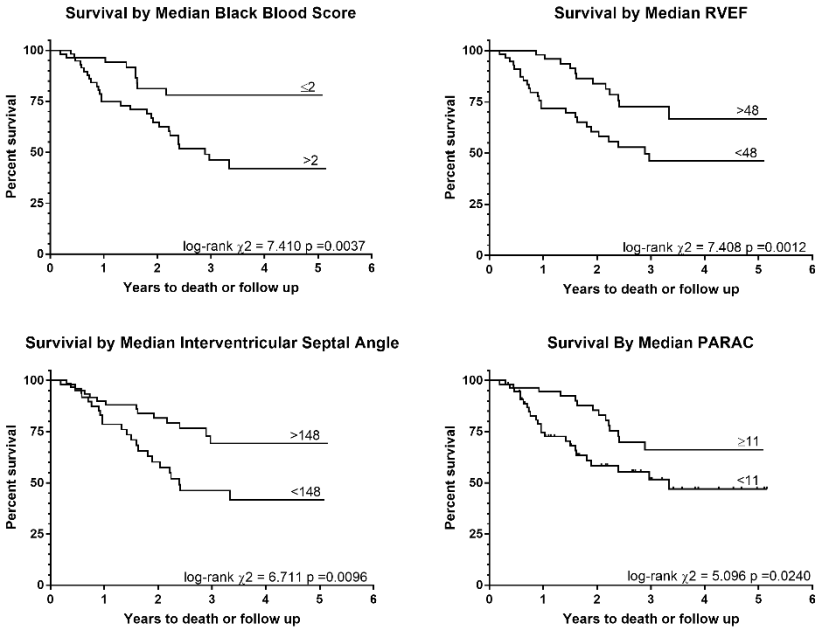

Figure 6.5: *B) Kaplan-Meier curves for the statistically significant MRI predictors of mortality in PH-HFpEF.*

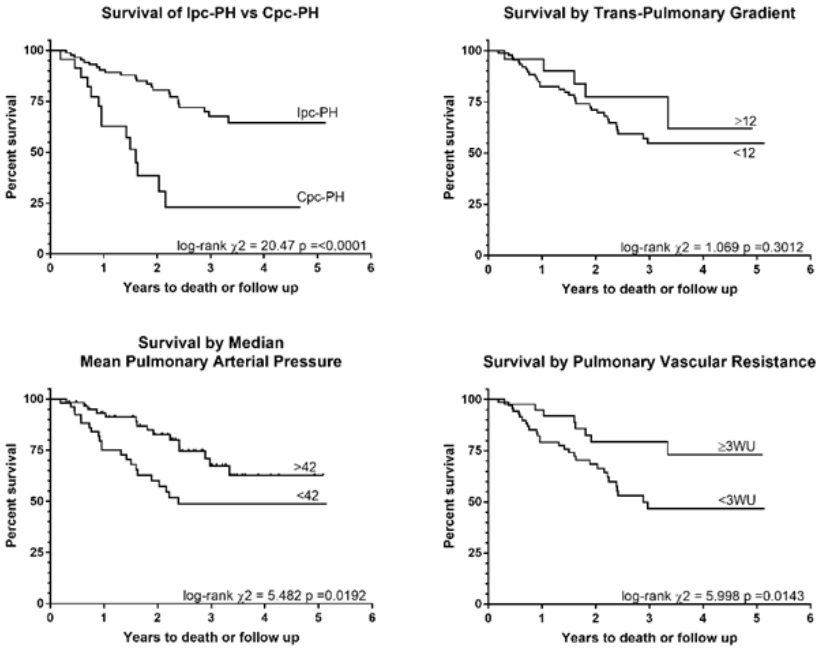

Figure 6.5: *C) Kaplan-Meier curves for the statistically significant right heart catheter predictors of mortality in PH-HFpEF.*

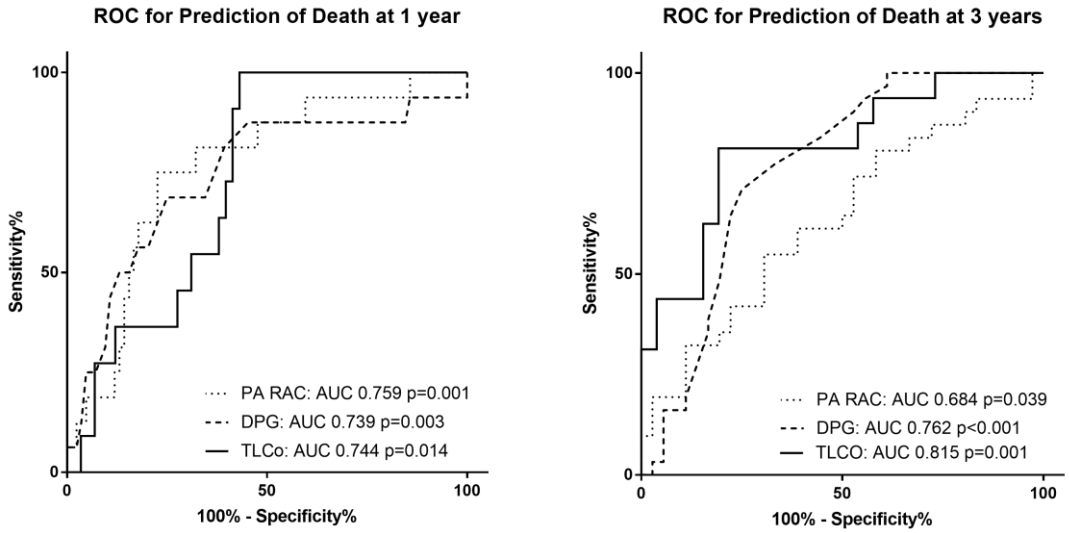

Figure 6.6: *ROC curve analysis for death at 1 and 3 years*

6.1.4 **Discussion**

In this chapter, assessing the predictors of mortality in 116 patients with pulmonary hypertension due to heart failure with preserved ejection fraction, we show that baseline demographics, invasive measurements of haemodynamics, pulmonary function testing and cardiac MRI are all useful in the prediction of outcome. On multivariate analysis, sex, TLCO percent predicted and PA relative area change were all predictive of outcome.

The results of this chapter fit with work presented in chapter 5.1 (Cardiac MRI can Identify and Phenotype Patients with PH in Left Heart Disease), in that the presence of combined pre and post capillary pulmonary hypertension is associated with increased risk of death. The diastolic pulmonary gradient (along with PVR, systolic and trans-pulmonary gradients to lesser degrees), interventricular septal angle and PA relative area change are all predictors of outcome, likely because they are predictive of the presence of pre-capillary portion to the pulmonary hypertension (Cpc-PH).

Male sex, and low TLCO percent predicted and pulmonary arterial relative area change were independent predictors of mortality on multivariate analysis. This is useful in the clinical setting, as a combination of demographic information (sex), routine pulmonary function tests (TLCO percent predicted) and cardiac MRI

sequences (PA RAC) can be used to assess prognosis, potentially reducing reliance on invasive tests, such as right heart catheterisation. This strengthens the previously presented data that identified interventricular septal angle as a potential marker for the presence of combined pre and post capillary pulmonary hypertension in patients with PH due to left heart disease. Pulmonary arterial relative area change is likely to be predictive of outcome as it is a marker of pulmonary arterial remodelling in pulmonary hypertension, and correlates with diastolic pulmonary gradient. It is possible to measure PA relative area change using ECG gated CT (112). TLCO has previously been identified as a marker of prognosis in patients with PH-HFpEF, and potentially acts as a marker of capillary and post-capillary disease in PH patients (25,294). In our cohort of PH-HFpEF, the reduction in TLCO is not due to cardiac output/index (there was no correlation between TLCO percent predicted and cardiac output, $r=0.033$ and $p=0.765$, and neither cardiac output, nor cardiac index was predictive of outcome). It is also interesting that the black blood artefact score was predictive of outcome, whereas the cardiac output was not, supporting the idea that black blood score may be a marker of turbulent or vortical blood flow in the pulmonary artery (135).

In this section we have demonstrated that MRI markers of the structure and function of the right ventricle and pulmonary artery provide prognostic information in patients with pulmonary hypertension due to heart failure with preserved ejection fraction. Cardiac MRI is considered the gold standard for the assessment of left ventricular function (233) and markers of RV and PA have been shown to be reproducible (124) and sensitive to change in PH patients (130,253,254). Access to cardiac MRI may be limited in certain centres, in which echocardiographic indices, although not assessed in these results, could be used to assess right ventricular function.

This study is limited by its retrospective, single centre design. This also leads to a bias in the population, as it is more likely that the patients with severe pulmonary hypertension or those with features of pre-capillary pulmonary hypertension will be referred. Unfortunately due to the nature of the referral pathway, echocardiography was not performed at a similar time to the cardiac MRI, so comparison between the two was not possible in this study.

6.1.5 **Conclusion**

Low TLCO, male sex and low pulmonary arterial relative area change are the most significant measures of outcome in patients with pulmonary hypertension due to heart failure with preserved ejection fraction. The use of spirometry and cardiac MRI is useful for the identification of patients who are at risk, and may be helpful in assessment during trials for potential pulmonary arterial therapies.

6.2 CARDIAC MRI CAN IDENTIFY PATIENTS WITH PH DUE TO COPD WHO ARE AT RISK OF DEATH

6.2.1 Rationale

Pulmonary hypertension is a predictor of death and hospitalisation (42–46) in patients with chronic obstructive pulmonary disease (COPD). Patients with pulmonary hypertension in COPD, as defined by a mean pulmonary artery pressure (mPAP) of ≥25mmHg have a 5 year survival rate of 36% (47). A number of studies in patients with severe COPD have shown that mild pulmonary hypertension is common: a recent study in patients with severe COPD referred for lung volume reduction surgery demonstrating pulmonary hypertension at right heart catheter in 50% (295,296). More recently, with the advent of therapies for other forms of pulmonary hypertension there has been increasing interest in the subset of lung disease patients with severe (previously called "out of proportion") pulmonary hypertension, defined as an mPAP ≥35mmHg or mPAP ≥35mmHg with cardiac index ≤2.0 (50), where a cardiovascular limitation to exercise, rather than respiratory limitation exists (297). This raises the possibility that pulmonary vascular therapies may improve symptoms and outcome in this patient group (298).

The gold standard for diagnosis of pulmonary hypertension is right heart catheter (RHC), however, this is an invasive test (8). As such, patients are screened for pulmonary hypertension with echocardiography, but unfortunately, this is less accurate in COPD where pulmonary artery pressure, when able to be measured is often overestimated (244,250). A non-invasive method for estimating mPAP in COPD patients would therefore be useful to help diagnose PH, in prognostication and for possible assessment of treatment response or follow up in clinical trials.

Several predictive cardiac magnetic resonance (CMR) imaging models have been proposed for estimation of pulmonary artery pressure (125,235,249,299). The predictive value of these MR derived imaging models in a population of patients with suspected pulmonary hypertension in COPD remains unknown.

6.2.1.1 Hypotheses

1. Models of mean pulmonary arterial pressure prediction from cardiac MRI can be used to identify patients with PH due to COPD.
2. Cardiac MRI is able to assess the risk of death in patients with COPD and suspected PH.

6.2.1.2 Aims

The aim of this section was to assess the diagnostic accuracy and the prognostic value of these published models of non-invasive mPAP prediction using cardiovascular MRI.

6.2.2 Materials and Methods

All consecutive patients who underwent MRI at a pulmonary hypertension referral centre (245) from April 2012 to October 2015 with suspected pulmonary hypertension were assessed for inclusion. Inclusion criteria were a formal diagnosis of COPD (according to standard criteria), as per the ASPIRE (Assessing the Spectrum of Pulmonary hypertension Identified at a REferral centre) registry (245). Patients were assessed for either obstructive spirometry (defined as FEV1/FVC ratio of ≤0.70) or qualitative CT evidence of emphysema, as per standard radiological practice (268). Any patients without RHC and MRI within 90 days were excluded. Ethical approval was granted from a local ethics committee for this retrospective study, written consent was waived (ref c06/Q2308/8).

6.2.2.1 Image Acquisition

Cardiac MRI was performed in a pulmonary hypertension tertiary referral centre (245), on a GE HDx 1.5-T whole body scanner (GE Healthcare, Milwaukee, Wisconsin), using an 8-channel cardiac coil, with the patient supine. Four-chamber (4Ch) and short axis (SA) cine images were acquired using a retrospectively cardiac gated multi-slice steady-state free precession (SSFP) sequence. A stack of axial images in the SA plane with slice thickness of 8 mm with a 2 mm inter-slice gap or 10 mm with no inter-slice gap were acquired, covering both ventricles from base to apex. The SSFP sequence parameters were: TR 2.8ms, TE 1.0ms, flip angle 50°, field of view 48x43.2, 256x256 matrix, 125 kHz bandwidth, and slice thickness 8 to 10 mm. This cardiac MRI scan protocol takes approximately 40 minutes to perform.

6.2.2.2 Image Analysis and Metrics

MR images were manually analysed by DC (a cardiac MRI radiographer of 9 years cardiac MRI experience) on a GE Advantage Workstation 4.4 and GE Advantage Workstation ReportCard software, with the observer blinded to all clinical information and other investigations. Left and right ventricular end-diastolic volume, end-systolic volume, right and left ventricular stroke volume and mass were calculated (all indexed to body surface area), right and left ventricular ejection fraction, ventricular mass index (RV mass divided by LV mass) (133) and interventricular septal angle were measured as previously described (125). Right and left ventricular ejection fractions were calculated as (end diastolic volume minus end-

systolic volume) divided by end diastolic volume. Maximal and minimal PA areas were manually traced, and relative area change was defined by the following equation: RAC= (maximum area-minimum area)/minimum area (208). Reproducibility metrics for these cardiac MRI metrics for DC and AJS have been previously published (124). Please see **Figure 6.7** for a diagram of the key imaging metrics that were measured.

6.2.2.3 CMR image based models

Previously published parametric models, developed for diagnostic and prognostic assessment in PH, were derived from Cardiac MRI metrics:

1. The RV_{CMR} model; is based on ventricular mass index and interventricular septal angle: mPAP = –4.6 + (interventricular septal angle x 0.23) + (ventricular mass index x 16.3), see Figure 1 (A and B). This model was developed in a cohort of 64 treatment naïve patients with suspected pulmonary hypertension in a tertiary referral centre. In a derivation cohort of 64 patients with suspected pulmonary hypertension, this showed good correlation with right heart catheter measured mPAP and strong diagnostic accuracy. The published threshold of ≥32 mmHg had 87% sensitivity and 90% specificity for the presence of all causes of pulmonary hypertension (125).
2. The $PARV_{CMR}$ model; is similar to the CMR-RV model (above), with the addition of basic function metrics of the pulmonary artery: CMR-PA/RV = -21.806 + (inter-ventricular septal angle x 0.31) + (ventricular mass index x 11.5) + (Diastolic pulmonary artery area x 0.01) – (PA relative area change x 0.22), see Figure 1 (A, B, C and D). This model was derived in 247 patients with suspected pulmonary hypertension patients and was predictive of pulmonary hypertension in a separate prospective cohort of 115 patients, with an area under the receiver operator curve of 0.92 (299).
3. The alpha index; comprises both functional and structural information, utilising right ventricular function along with pulmonary artery size: Alpha index = minimum PA area/RV ejection fraction. This model was assessed in a cohort of 185 patients, with an area under ROC curve of 0.95 (249).

The diagnostic cut-off for pulmonary hypertension for RV_{CMR} was ≥32 and alpha index ≥7.2, as published in the literature (125,249,299). PA/RV_{CMR} does not have a

published threshold, so we used a threshold of ≥25, as this mirrors the threshold of invasively-measured mPAP at right heart catheterisation.

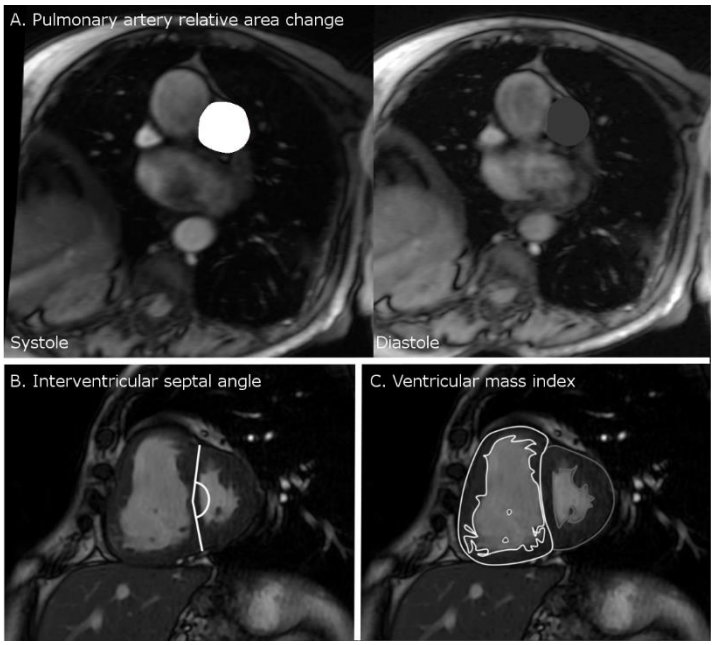

Figure 6.7: *Cardiac MRI metrics. Pulmonary artery relative area change (A) taken from cine images taken at the level of the pulmonary trunk, perpendicular to the main pulmonary artery; septal angle (B) taken as the angle made between the insertion points of the RV to the mid septum on the end-systolic image from the short axis stack; and (C) ventricular mass index taken by segmentation of the muscle mass of the left and right ventricle on the stack of images taken in the short axis plane.*

6.2.2.4 Right Heart Catheterisation

Right heart catheterisation was performed using a balloon tipped 7.5Fr thermodilution catheter (Becton-Dickinson, Franklin Lakes, New Jersey). Pulmonary hypertension was defined as a resting mPAP ≥25mmHg and severe pulmonary hypertension as a resting mPAP ≥35mmHg. Cardiac output was calculated using thermodilution.

6.2.2.5 Statistics

Pearson's correlation between CMR models and RHC-mPAP were calculated. The relative accuracy of the models was assessed using Bland-Altman plots. Diagnostic accuracy was calculated from the 2x2 contingency table to calculate sensitivity, specificity, negative predictive value and positive predictive value. Receiver operating characteristic (ROC) curves were constructed and the area under the ROC curve (AUC) recorded.

The interval from CMR until all cause death or census was regarded as the follow-up period. The census was performed on 25/02/2016. Log-log plots were visually inspected to ensure linearity with outcome data. Survival analysis was performed using univariate and multivariate Cox proportional hazards regression. In order to

allow for comparison between each metric, this was performed with each variable standardised as the z score for the population studied. Multivariate analysis was performed in a forward direction, for all variables with a statistically significant association with mortality on univariate analysis.

Kaplan-Meier plots were generated for each model and RHC measured mPAP, dichotomised by a value of 35, and Chi square values were calculated using the Log rank test, as this is the threshold value for severe pulmonary hypertension (50). Statistical analysis was made using SPSS 22 (IBM, Chicago) and graphs were created using GraphPad Prism 7 (GraphPad Software, San Diego). A p-value of <0.05 was considered statistically significant.

6.2.3 **Results**

A total of 1864 patients were referred to the pulmonary hypertension centre during the period studied and underwent right heart catheterisation: of these 145 had a documented diagnosis of COPD from a respiratory specialist. 102 had MRI and RHC within 90 days, so were included in the study. There were 87 patients with pulmonary hypertension (69 of these had severe pulmonary hypertension) and 15 patients without pulmonary hypertension (please see **Figure 6.8** for the patient selection pathway).

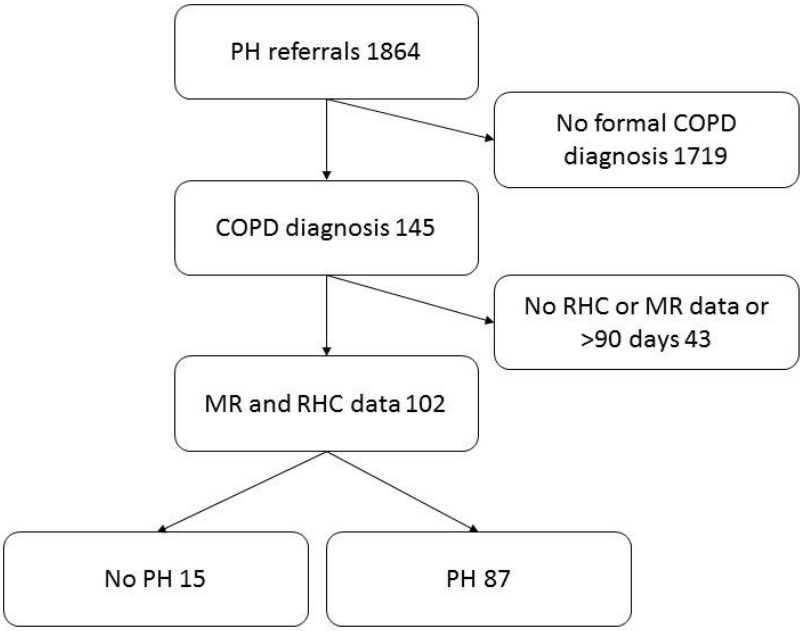

Figure 6.8: *Patient flow*

There were 24 with Gold severity 1, 40 with GOLD severity 2, 18 with GOLD severity 3 and 7 with GOLD severity 4, 13 patients did not have spirometry results available for analysis. Of the 102 cases of COPD included in the study, 75 had spirometric evidence of airflow limitation (FEV1/FVC ratio <0.7), and the remaining 17 had evidence of emphysema on CT.

Table 6.4 shows the patient demographics and clinical characteristics for the whole group and split into no PH (mPAP <25mmHg), PH (mPAP 25≥35mmHg) and severe PH (mPAP ≥35mmHg).

Table 6.4: *Patient demographics, mean with standard deviation with ANOVA p-value.*

	All patients	No PH	PH	Severe PH	P-value (ANOVA)
Number	102	15	18	69	
Clinical Demographics					
Age (years)	67 (12)	59 (17)	67 (12)	69 (9)	0.012
Sex (F/M)					
WHO functional class (II,III,IV)					
ISWT (m)	174 (169)	432 (264)	141 (101)	121 (87)	<0.001
Baseline catheter data					
mPAP (mmHg)	40 (12)	21 (3)	31 (3)	47 (8)	<0.001
mRAP (mmHg)	11 (6)	6 (2)	8 (3)	11 (7)	0.056
PAWP (mmHg)	12 (4)	10 (3)	12 (3)	13 (4)	0.013
CI (Litre/m^2)	2.8 (0.9)	3.1 (0.7)	3.2 (0.9)	2.6 (0.9)	0.005
PVRI (WU)	3.7 (2.7)	1.1 (0.6)	2.0 (0.5)	4.37 (2.7)	<0.001
SvO2 (%)	65 (9)	72 (8)	69 (5)	62 (9)	<0.001
Days RHC to MR	5 (15)	5 (19)	5 (13)	5 (14)	0.989
Spirometry	n=89	n=9	n=17	n=63	
FEV1 (% Pred)	66 (24)	76 (24)	58 (15)	66 (25)	0.165
FVC (% Pred)	85 (22)	92 (20)	77 (15)	87 (24)	0.155
FEV1/FVC	0.55 (0.15)	0.63 (0.20)	0.51 (0.10)	0.55 (0.15)	0.179
TLCO (% Pred)	30 (22)	80 (31)	33 (15)	21 (9)	<0.001
Cardiac MRI					
RV EDV index	89 (35)	72 (30)	70 (32)	97 (34)	0.002
RV ESV index	56 (31)	36 (18)	37 (26)	66 (30)	<0.001
RVEF	40 (14)	51 (8)	51 (11)	35 (12)	<0.001
RV mass index					
LV EDV index	55 (18)	62 (10)	63 (18)	52 (19)	0.026
LV ESV index	20 (18)	19 (6)	20 (10)	20 (12)	0.921
LVEF	64 (12)	69 (10)	69 (9)	61 (12)	0.014
PA RAC	10 (8)	16 (14)	12 (8)	8 (6)	0.008
VMI	0.43 (0.28)	0.28 (0.11)	0.28 (0.17)	0.51 (0.31)	0.001
IVS angle	165 (24)	134 (10)	152 (14)	174 (20)	<0.001
Black blood score	3 (1)	1 (1)	2 (1)	3 (1)	<0.001
Alpha-index	25 (14)	13 (6)	16 (6)	30 (14)	<0.001
RV_{CMR}	41 (9)	33 (4)	35 (5)	44 (9)	<0.001
$PARV_{CMR}$	35 (9)	23 (5)	30 (5)	39 (7)	<0.001

PH: pulmonary hypertension, WHO: World Health Organisation, ISWT: Incremental shuttle walk test, FEV1: Forced expiratory volume in 1 second, RVC-mPAP: right heart catheter measured mean pulmonary artery pressure, mRAP: mean right atrial pressure, PAWP: pulmonary arterial wedge pressure, CI: cardiac index, PVRI: pulmonary vascular resistance index, SvO_2: mixed venous oxygen saturation, FVC: forced vital capacity, TLCO: transfer factor for carbon monoxide, RHC: right heart catheter, MRI: magnetic resonance imaging.

6.2.3.1 Diagnostic accuracy

Table 6.5 shows the univariate correlations of CMR imaging metrics: RV end diastolic volume index, RV end systolic volume index, RV ejection fraction, RV mass, PA diastolic area and relative area change, ventricular mass index, interventricular septal angle septal angle, average velocity and black blood score all showed statistically significant correlations with mPAP. All of the models showed strong correlations with RHC measured mPAP, with p-values <0.0001. The $PARV_{CMR}$ model showed stronger correlation with mPAP than the individual quantitative measurements alone. A scatter plot of the MRI models against mPAP is given in **Figure 6.9**. The models all showed a stronger correlation with mPAP in the patients with mPAP <35mmHg (r and p-values for RV_{CMR} were 0.550 and 0.001, $PARV_{CMR}$ 0.653 and <0.001 and alpha 0.341 and 0.052) than in the patients with mPAP ≥35mmHg (r and p-value for RV_{CMR} were 0.431 and <0.001, $PARV_{CMR}$ 0.407 and 0.001 and alpha 0.210 and 0.083).

Table 6.5: *CMR imaging metrics and MRI model correlations with mPAP*

	Correlation with mPAP	
	R	p-value
RVEDV index	0.377	<0.0001
RVESV index	0.482	<0.0001
RVEF	-0.585	<0.0001
RV mass	0.372	<0.0001
LVEDV index	-0.304	0.002
LVESV index	-0.029	0.772
LVEF	-0.221	0.026
PA diastolic area	0.401	<0.0001
PA RAC	-0.344	<0.0001
VMI	0.470	<0.0001
IVS angle	0.710	<0.0001
Average PA velocity	-0.428	<0.0001
Black blood score	0.603	<0.0001
RV_{CMR}	0.689	<0.0001
$PARV_{CMR}$	0.732	<0.0001
Alpha index	0.527	<0.0001

RVEDV: right ventricular end-diastolic volume, RVESV: right ventricular end-systolic volume, RVEF: right ventricular ejection fraction, RV: right ventricle, LVEDV: left ventricular end-diastolic volume, LVESV: left ventricular end-systolic volume, LVEF: left ventricular ejection fraction, PA: pulmonary artery, PA RAC: pulmonary artery relative area change, VMI: ventricular mass index, IVS: interventricular septum

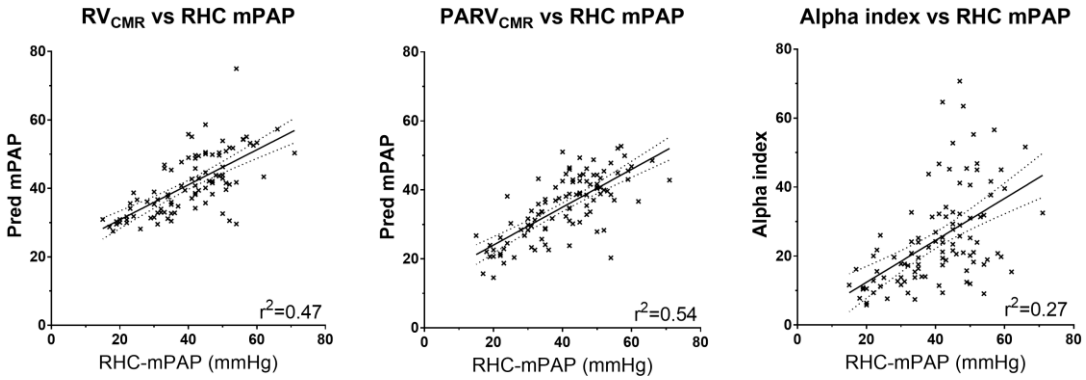

Figure 6.9: *Scatter plots showing correlations of each MRI model with right heart catheter measured mPAP.*

Bland-Altman plots were also created to assess the accuracy of the models against RHC-mPAP (**Figure 6.10**), this was not performed for alpha index as it was not designed to directly assess mPAP. Bland-Altman analysis showed modest accuracy for RV_{CMR} (bias -5.2%, limits of agreement -51.2 to 40.8%) and PA/RV_{CMR} models (bias 12.2% and limits of agreement -30.7 to 55.0%). **Table 6.5** shows the correlation of the CMR models against RHC mPAP. **Figure 6.11** shows the ROC curves for the three CMR models. $PARV_{CMR}$ and RV_{CMR} had the largest AUC values, 0.93 (95% confidence interval 0.86-1.0) and 0.91 (95% confidence interval 0.84-0.97) respectively, and alpha index also showed good diagnostic accuracy with AUC 0.837 (95% confidence interval 0.74-0.94). The sensitivity and specificity of the PA/RV_{CMR} model was 92% and 80%, CMR-RV model 90% and 79%, and the alpha index 100% and 13% respectively (as shown in **Table 6.6**).

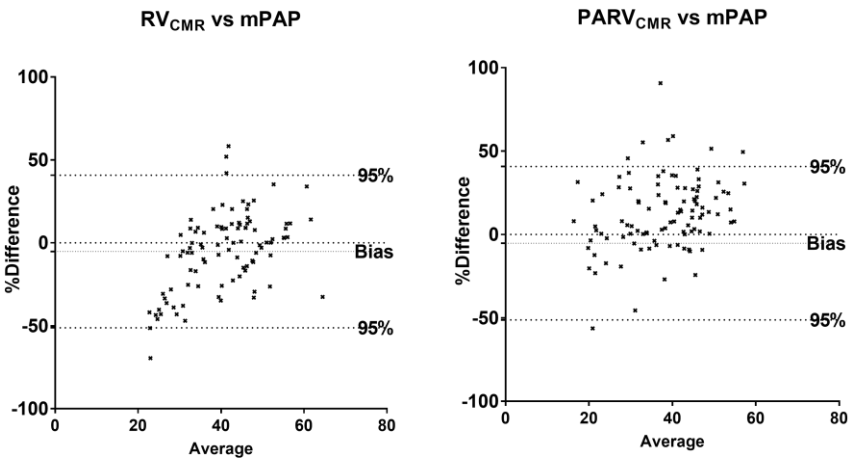

Figure 6.10: *Bland-Altman plots showing the accuracy of each model against RHC-mPAP.*

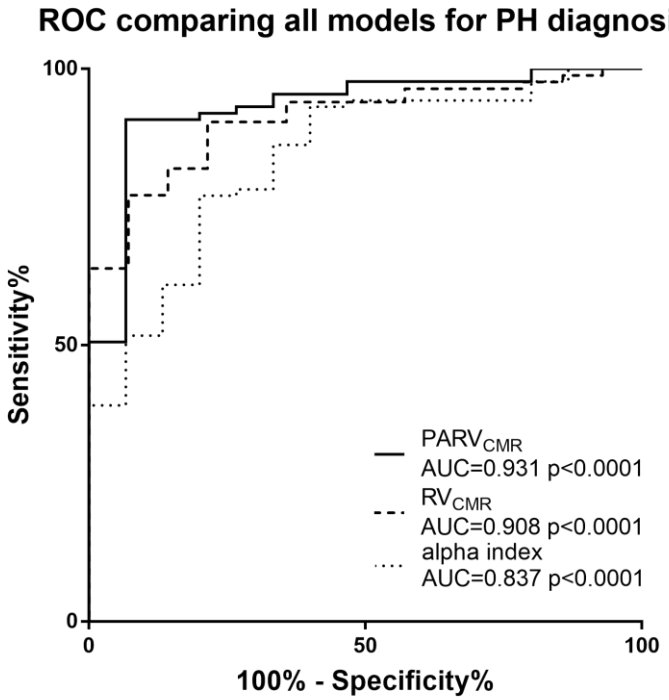

Figure 6.11: *ROC curve for the diagnosis of pulmonary hypertension.*

Table 6.6: *Diagnostic accuracy for pulmonary hypertension.*

	Sensitivity	Specificity	PPV	NPV	ROC AUC	P-value
RV_{CMR} (≥32)	90% (95% CI 82-95)	79% (95% CI 52-92)	96% (95% CI 89-99)	58% (95% CI 36-77%)	0.908 (95% CI 0.84-0.97)	<0.0001
$PARV_{CMR}$ (≥25)	92% (95% CI 84-96%)	80% (95% CI 55-93%)	96% (95% CI 90-93%)	63% (95% CI 41-81%)	0.931 (95% CI 0.86-1.00)	<0.0001
Alpha Index (≥7.2)	100% (95%CI 96-100)	13% (95% CI 0-38)	87% (95% CI 79-92%	100% (95% CI 18-100%)	0.837 (95% CI 0.73-0.94)	0.020

PPV: positive predictive value, NPV: negative predictive value.

6.2.3.2 Outcome

During a mean follow up period of 1.5 years (standard deviation 0.9) there were 33 deaths. **Table 6.7** gives the scaled univariate Cox proportional hazards regression results for patient demographics, RHC and CMR measurements. Age, sex, walk distance FEV1 percent predicted, FVC percent predicted and FEV1/FVC ratio were not univariate predictors of mortality. PA relative area change, right ventricular mass index, ventricular mass index, interventricular septal angle and RV end-diastolic volume index were univariate predictors of mortality (p=0.009, p=<0.001, p=0.002 and p=0.023 respectively). RHC measured mPAP was a strong predictor of mortality (p=0.004), as were the RV_{CMR} and $PARV_{CMR}$ models (p=0.002 and p=0.012 respectively). There was a statistically significant difference in survival when the population was split by a threshold of 35mmHg for RHC-mPAP, RV_{CMR} and $PARV_{CMR}$ models, with a log rank chi squared of 5.03, 5.47 and 7.10 respectively (see **figure 6**).

On multivariate analysis (performed on all univariate predictors of outcome for demographics, right heart catheter and cardiac MRI), right ventricular mass index and PA relative area change were statistically significant, with scaled Cox multivariate hazard ratios 1.549 (95% CI 1.172-2.047, p=0.002) and 0.561 (95% CI 0.333-0.946, p=0.030) respectively.

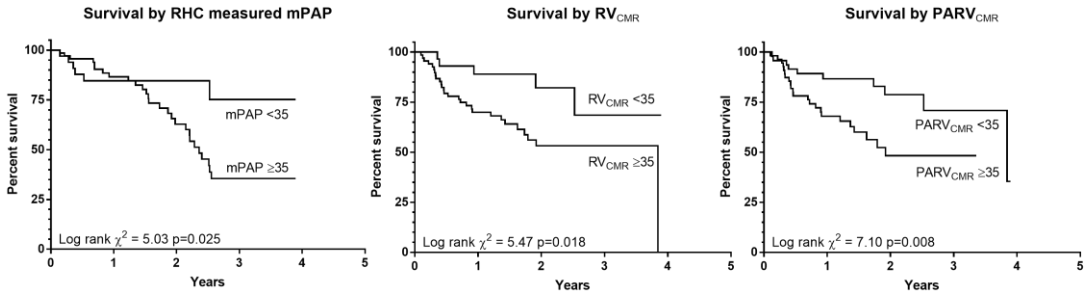

Figure 6.12: *Kaplan-Meier survival tables, all dichotomised by 35.*

Table 6.7: *Univariate Cox proportional hazards regression analysis for survival.*

	Hazard ratio	95% confidence interval		p-value
Demographics				
Age	1.424	0.936	2.166	0.098
Sex	0.781	0.388	1.57	0.487
WHO functional status	1.45	1.031	2.039	0.033
Walk distance	0.475	0.167	1.354	0.164
FVC % pred	1.221	0.835	1.785	0.304
FEV1 % pred	1.399	0.928	2.108	0.109
FEV1/FVC	1.244	0.85	1.82	0.262
TLCO % pred	0.593	0.19	1.852	0.369
Right heart catheter				
mPAP	1.74	1.198	2.526	0.004
mRAP	1.297	0.873	1.927	0.199
PAWP	0.933	0.651	1.338	0.707
CI	0.847	0.566	1.268	0.421
PVRI	1.384	1.034	1.853	0.029
SvO2	0.857	0.59	1.245	0.418
Cardiac MRI				
RV EDV index	1.381	1.013	1.882	0.041
RV ESV index	1.338	0.981	1.824	0.066
RVEF	0.784	0.548	1.122	0.183
RV mass index	1.673	1.303	2.148	<0.001
LV EDV index	0.759	0.494	1.166	0.209
LV ESV index	0.766	0.478	1.228	0.269
LVEF	1.077	0.756	1.535	0.681
PA RAC	0.543	0.343	0.859	0.009
VMI	1.417	1.135	1.768	0.002
IVS angle	1.48	1.055	2.075	0.023
Black blood score	1.377	0.925	2.05	0.115
Average PA velocity	1.018	0.697	1.484	0.928
Alpha-index	1.19	0.858	1.65	0.297
RV_{CMR}	1.565	1.175	2.083	0.002
$PARV_{CMR}$	1.59	1.108	2.282	0.012

WHO: World Health Organisation, FEV1: Forced expiratory volume in 1 second, FVC: Forced vital capacity, RHC: right heart catheter, mPAP: right heart catheter measured mean pulmonary artery pressure, mRAP: mean right atrial pressure, PAWP: pulmonary artery wedge pressure, CI: cardiac index, PVRI: pulmonary vascular resistance index, SvO_2: mixed venous oxygen saturation, CMR: cardiopulmonary magnetic resonance, RVEDV: right ventricular end-diastolic volume, RVESV: right ventricular end-systolic volume, RVEF: right ventricular ejection fraction, RV: right ventricle, LVEDV: left ventricular end-diastolic volume, LVESV: left ventricular end-systolic volume, LVEF: left ventricular ejection fraction, PA RAC: pulmonary artery relative area change, VMI: ventricular mass index, IVS: interventricular septum, RV_{CMR}: right ventricle based cardiopulmonary magnetic

6.2.4 **Discussion**

This study demonstrates that CMR models can be used to assess for the presence of pulmonary hypertension in COPD with good diagnostic accuracy, whilst also providing prognostic information similar to right heart catheterisation. This data supports the potential use of CMR in the non-invasive assessment of suspected pulmonary hypertension in patients with COPD. We have shown that single measurements from cardiac MRI (most notably septal angle) correlate strongly with right heart catheter measured mPAP. A model which includes measurements from the right ventricle, the diagnostic accuracy is slightly reduced, but inclusion of basic measurements of pulmonary arterial structure and function increases the accuracy of predicted mPAP and therefore the presence of pulmonary hypertension. Therefore, we recommend the use of $PARV_{CMR}$ model in the diagnosis of pulmonary hypertension in patients with COPD. In the presence of COPD, right ventricular mass index and PA relative area change are the strongest predictors of outcome, but further work to develop prognostic thresholds is required.

Studies performed primarily in patients with pulmonary arterial hypertension have shown that structural and functional indices of the right ventricle (RV end diastolic volume index, RV end-systolic volume index, RV ejection fraction, RV mass, interventricular septal angle) and pulmonary artery (PA area, PA relative area change and black blood score) correlate with RHC measured mPAP. Inter and intra-observer reproducibility data for these cardiac MRI metrics for DC and AJS have been previously published. RV end-diastolic and systolic measurements had excellent inter-observer reproducibility (ICC 0.959 and 0.991) and pulmonary artery relative area change had high inter-observer reproducibility (ICC 0.891). Right ventricular ejection fraction also had high inter-observer reproducibility (ICC 0.957) (124). We and others, have shown that we can further develop predictive equations using MR metrics to estimate measurements made at cardiac catheterisation. However, to date there is very little data on the use of MR imaging as a diagnostic and prognostic tool in patients with COPD and suspected pulmonary hypertension. In this study we have shown that these structural and functional indices of the right ventricle and pulmonary artery correlate with right heart catheter measured mean pulmonary arterial pressure: with pulmonary artery relative area change, ventricular mass index and interventricular septal angle having the strongest correlations. We have shown

that the use of $PARV_{CMR}$ and RV_{CMR} models, improve the prediction of mPAP and also the diagnostic accuracy of quantitative CMR measures.

The alpha model showed good correlation with mPAP, but had a low diagnostic accuracy: this model suffered from a diagnostic threshold that was too low for this cohort, significantly reducing its specificity. Changing the threshold of the alpha index to 16 increased the diagnostic accuracy of this model to 77% sensitivity and 80% specificity. This inaccuracy may be related to the measurement of right ventricular ejection fraction, particularly the reproducibility between different centres. In the original paper, it was not described how the right ventricular endocardial contours were measured, specifically, whether the papillary muscles and RV trabeculations were included, which may potentially add a bias into the calculation.

Pulmonary hypertension, confirmed by right heart catheter, has been recognised for many years as a marker of disease severity in COPD. In this study we have shown that cardiac MRI measured right ventricular mass and therefore ventricular mass index, along with pulmonary artery relative area change are significant predictors of mortality on univariate analysis. However, by using CMR derived parametric models, particularly the RV_{CMR} model which combine these CMRI derived measures, we can improve the prediction of outcome in COPD patients on multivariate analysis. These models may be further improved with novel imaging biomarkers in pulmonary hypertension assessment. One such marker is the 4D flow assessment of the life of vortices within the pulmonary artery, which has been shown to have a very high correlation with mPAP (r^2 0.95) (141).

A potential source of error arises from the use of MR models, which were developed for use in a cohort of all causes of pulmonary hypertension, and not validated in specific sub-groups, such as PH-COPD in this case. We feel that it is likely that the findings of a raised interventricular septal angle and ventricular mass index are likely to occur most subgroups of pulmonary hypertension (with the exception of left heart disease) as they are related to the pressure differential between the left and right ventricles. The measures of pulmonary arterial structure and function (size and relative area change) are likely to be transferable across subgroups, as they are markers of pulmonary vascular compliance and remodelling. We therefore feel that it reasonable to use these models in specific sub-groups of pulmonary hypertension,

although validation, such as in this chapter, would be useful. The models that are used in this chapter use parameters that are stated with a degree of precision (for example an offset of 21.806 for $PARV_{CMR}$), likely more than is required for this purpose. We have maintained the equations in the published form to reduce any bias in the calculations, but it is likely that less decimal places could be used for these parameters for the prediction of outcome and the presence of pulmonary hypertension in COPD.

Currently, RHC is the gold standard test for the assessment of pulmonary hypertension, and is used to assess prognosis in suspected COPD-PH cases. The ability to use non-invasive CMR models in this patient group may avoid the need for RHC, as we have shown CMR to be as good in the assessment of prognosis. The strong correlation of CMR imaging models with RHC mPAP suggest it may also have a role in follow up, and also in assessment of treatment response in possible future trials assessing vasodilator response in COPD-PH. The role of cardiac MRI in COPD is further strengthened as this is a cohort of patients in which echocardiography is challenging. In the presence of COPD echocardiography has a relatively high rate of non-diagnostic quality studies. It has a good negative predictive value but a poorer positive predictive value (244). In patients with a normal right ventricle and predicted systolic pulmonary artery pressure (estimated from the tricuspid regurgitant jet velocity using the Bernoulli equation) pulmonary hypertension is highly unlikely. The main role for cardiac MRI in patients with COPD, therefore, probably lies in the group of patients with high estimated systolic pulmonary artery pressures or non-diagnostic scans. This may be at diagnosis, as studied, or potentially at follow up.

The non-invasive estimation of mPAP has multiple other potential uses, beyond prognosis in COPD, although these have not been addressed in this thesis. In advanced COPD patients considered for lung volume reduction surgery (LVRS), severe pulmonary hypertension is considered a contraindication (300), so the non-invasive assessment of mPAP on MR would be a useful tool in patient selection. Furthermore, left or right ventricular dysfunction is considered a relative contraindication to LVRS (300), and can be assessed at the same CMR sitting. In COPD patients with pulmonary hypertension there is evidence that outcome may be improved if treated with lung transplantation over LVRS (301), assessment of mPAP could be performed in the same sitting as a ventilation study in the preoperative assessment of LVRS or

transplant candidates (162,302), allowing for the assessment of the best surgical option and the best target in the lung.

This study is limited by its single centre, retrospective design, at a tertiary pulmonary hypertension referral centre where the severity of pulmonary hypertension is more severe. The results, therefore represent a biased population as the patients have been screened by echocardiography and excessive symptoms for the presence of pulmonary hypertension before referral (the vast majority of patients with COPD are managed in primary care). This has resulted in a smaller proportion of non-pulmonary hypertension patients than would be present in a general population of COPD, however in the absence of a prospective trial, this is difficult to overcome. Furthermore, the assessment of the presence of COPD in the population relied upon the accurate documentation of a clinical diagnosis of COPD. This likely resulted in a lower proportion of patients being identified, but is likely to be more robust than using either spirometry or CT defined emphysema alone. Furthermore, the end-point was defined as all-cause mortality, which doesn't take into account other causes of death in patients with COPD, such as coronary heart disease (60) and COPD exacerbation (59).

Despite this, we feel that these tools are valid for the assessment of patients who are referred to a pulmonary hypertension centre regarding the presence of pulmonary hypertension and prognosis, as this is the population that was studied. It may be that more specific diagnostic thresholds would be suitable for use in the general COPD population.

6.2.5 **Conclusion**

The use of the $PARV_{CMR}$ model, derived from cardiovascular magnetic resonance imaging in the assessment of COPD allows for accurate, non-invasive estimation of pulmonary artery pressure and the presence of pulmonary hypertension. Right ventricular mass index and pulmonary artery relative area change are most predictive of outcome.

7 DISCUSSION AND FUTURE DIRECTIONS

Cardiac MRI is considered the gold standard for the assessment of left ventricular structure and function. It also provides similar information on the right ventricle and pulmonary artery, which are useful in the diagnosis and assessment of suspected pulmonary hypertension.

7.1 DIAGNOSIS

In a large cohort of incident patients referred to a tertiary referral centre with suspected pulmonary hypertension, the data presented in this thesis shows that cardio-pulmonary MRI has high diagnostic accuracy. A model comprising simple, reproducible and easy to obtain metrics (interventricular septal angle, ventricular mass index and black blood score) can identify patients with pulmonary hypertension with 100% specificity and 62% sensitivity. A more sensitive threshold has also been identified with 93% sensitivity and 79% specificity, which may be useful to screen for patients with pulmonary hypertension, although this would need to be validated in a screening population.

Whilst this highly specific measurement is useful in the identification of patients with pulmonary hypertension, there is still a requirement for assessment of response to nitric oxide in patients with suspected pulmonary arterial hypertension to assess for optimal therapeutic strategies. This work can be further improved with inclusion of an assessment of vasodilator response on cardiac MRI.

Patients with dilated left atria were excluded from the analysis, as it is expected that these patients will not be correctly identified using the proposed model (interventricular septal angle and ventricular mass index will be normalised due to high left ventricular filling pressures). Further work is required to identify a method of mPAP prediction in those patients with dilated left atria to accurately identify pulmonary hypertension. Although currently this is only performed to provide prognostic information and the use of septal angle can identify patients who may have a precapillary component to their PH-LHD and therefore should be assessed for the potential of PAH.

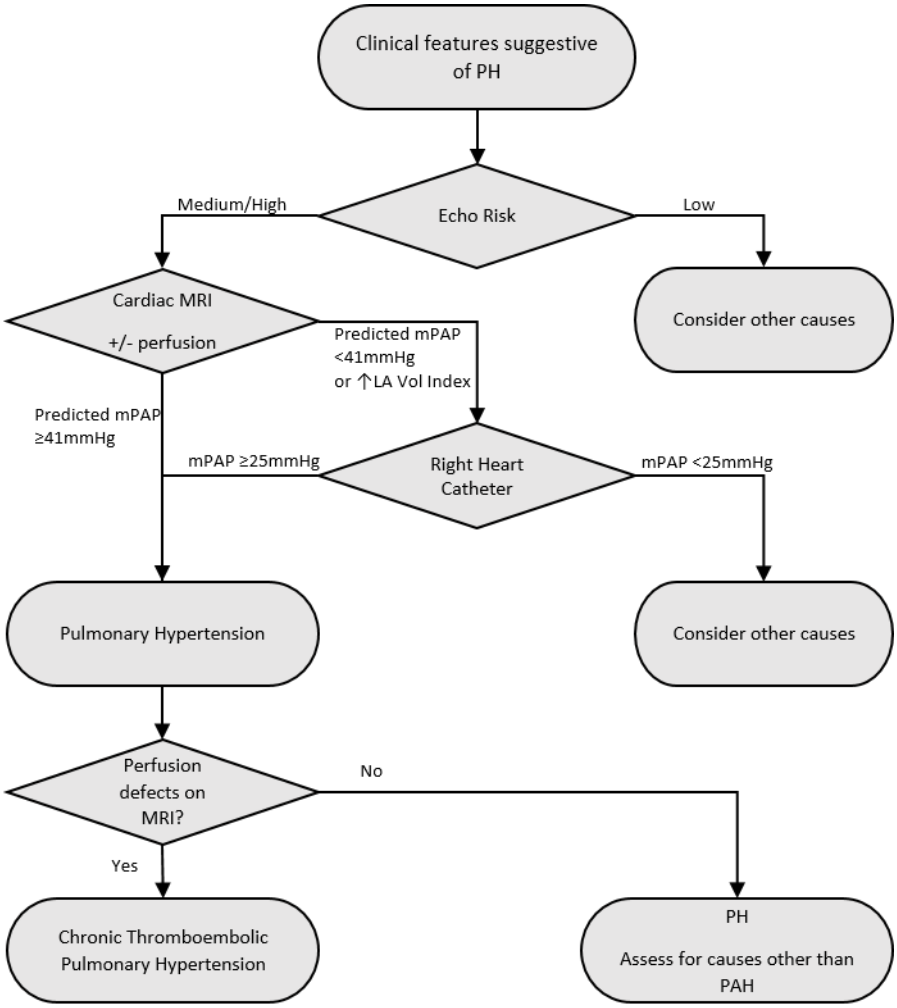

Figure 7.1: *A proposed flow chart for investigation of PH using cardiac MRI based upon the data presented in this thesis*

7.2 PHENOTYPING

Once the presence of pulmonary hypertension has been identified, it is important to assess the underlying cause to correctly initiate treatment. The most important groups to correctly identify are pulmonary arterial hypertension (which can be difficult to differentiate from left heart disease) and chronic thrombo-embolic pulmonary hypertension, as these are the groups of patients who respond to treatments directed at the pulmonary vasculature.

7.2.1 PH-Left Heart Disease

As previously discussed, further is work required in the differentiation of patients with pulmonary arterial hypertension from those with PH due to left heart disease. Left atrial volume index is considered the non-invasive assessment of choice for the presence of PH due to left heart disease, however in an unselected cohort of patients with suspected PH there is only a relatively modest prediction of raised pulmonary arterial wedge pressure using left atrial volume index alone. Cardiac MRI is able to assess structure of the cardiac chambers, as with left atrial volume index, but is also able to assess the function.

The left ventricle left atrium (LVLA) cine view provides a useful overview of left atrial area. When measured at each phase of the cardiac cycle, this gives a temporally resolved assessment of the function of the left atrium, and can be performed at the same time as an assessment of changes in left ventricular volume (Figure 7.3). In a similar methodology to atrial function on echocardiography, the relative proportions of reservoir, conduit and pump functions to the overall LA function can be calculated, in a similar methodology to with echocardiography.

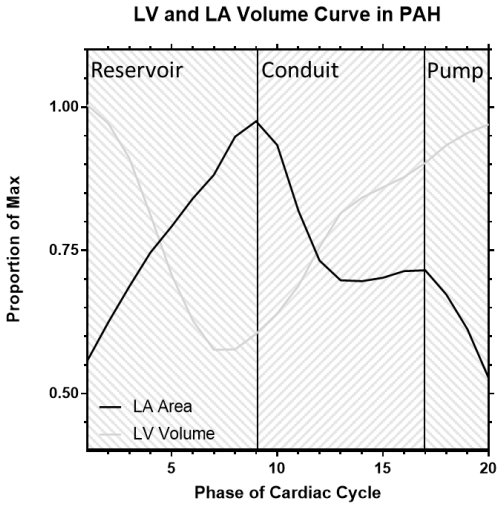

Figure 7.2: *Measurements of reservoir, conduit and pump function from the left atrial area curve.*

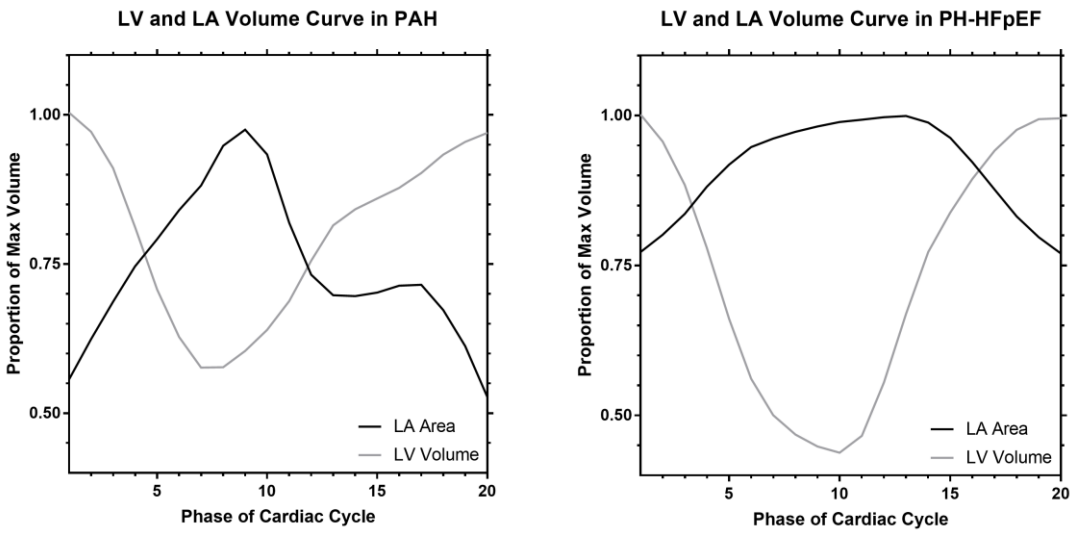

Figure 7.3: Example left atrial volume curves

A typical LA area and LV volume change in a patient with PAH and in a patient with PH-HFpEF.

Using phase contrast flow imaging, with the slice selected just below the level of the mitral and tricuspid valves, the flow through the tricuspid and mitral valves can be assessed, with a lower V_{enc}, the through plane motion (longitudinal) of the myocardium can also be calculated. This data can be analysed to provide the velocities of E, A and e' and a' velocities, in a similar methodology to echocardiography and likely to be useful in the assessment of the diastolic function of the left and right ventricles.

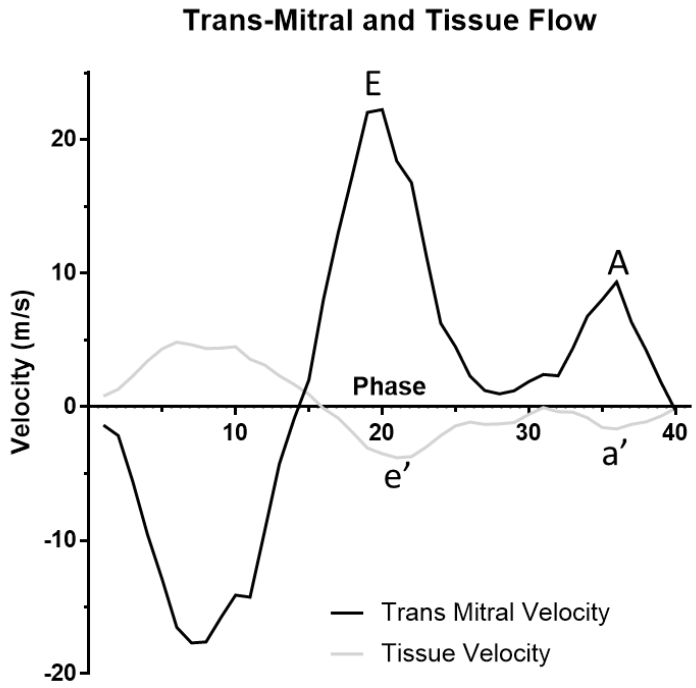

Figure 7.4: Trans-mitral and tissue flow.
The E and A waves can be identified from the trans mitral flow curve (black), along with the e' and a' waves from the tissue flow curve (grey). These represent passive filling and active filling of the left ventricle, respectively and are useful for the assessment of the left ventricular diastolic function.

A further group of patients who may benefit from selected therapy and have significant interest in the context of clinical trials are those patents with combined pre and post capillary pulmonary hypertension. Cardiac MRI derived interventricular septal angle can be used to non-invasively predict the presence of an elevated diastolic pressure gradient in suspected pulmonary hypertension patients with elevated pulmonary arterial wedge pressures with reasonable diagnostic accuracy (AUC 0.911). To date, trials assessing pulmonary hypertension specific therapies in patients with PH-LHD have assessed an unselected cohort of patients. The interventricular septal angle may offer the potential to identify patients for targeted therapy.

7.2.2 **CTEPH**

In a cohort of 74 patients referred to this centre with suspected CTEPH, DCE lung perfusion MRI has at least equivalent sensitivity when compared to SPECT perfusion scintigraphy in the detection of CTEPH. In the patients studied, a combination of perfusion MR and CTPA identified all patients with CTEPH and CTED. This reflects and updates the findings of a previous study by Smitha Rajaram, which compared DCE perfusion MRI with planar scintigraphy (91). Perfusion MRI can be performed in the same sitting as high-resolution pulmonary MR angiography and cardiac MRI scan, and has the potential for a "one-stop-shop" analysis of pulmonary perfusion and assessment of right heart and pulmonary vascular characteristics, as explored in the chapter on the diagnosis of pulmonary hypertension.

In the 1-year cohort of 74 patients studied for a comparison of DCE-MRI and SPECT, significant improvements in the diagnostic pathway could be made. DCE-MRI was able to correctly identify the presence of CTEPH, with only two indeterminate DCE-MRI scans, which would require screening with SPECT. In all of the other cases, we could replace nuclear medicine SPECT imaging with MRI. CTPA is also useful in this regard, however it has been shown to have reduced sensitivity in comparison to SPECT perfusion, particularly in non-specialist centres, so is not recommended as a screening tool for CTEPH (1,101). The increasing use of perfusion imaging and iodine mapping may help in this regard (108,109). Using a cut-off of MR-predicted mPAP ≥38 mmHg we would be able to avoid right heart catheterisation 39 patients of the 73 total, as MRI confirms that they have PH. This would represent a significant reduction

in the workload of the PH department, with its associated potential money saving. From a patient perspective a reduction in the need for multiple tests, one of which is invasive, and radiation exposure is valuable.

7.3 Assessment of Prognosis

The final theme of this thesis is the assessment of prognosis. Previous work has shown that cardiac MRI derived metrics are useful in the prognostic assessment of patients with pulmonary arterial hypertension (124) and surgery is the best predictor of survival in CTEPH (282). In a cohort of patients with pulmonary hypertension due to COPD, the use of the cardiac MRI multi-parametric models provides an accurate, non-invasive estimation of pulmonary artery pressure and the presence of pulmonary hypertension. In this group of patients, there is no PH specific therapy, so the diagnosis of PH is made for prognostic reasons. At the same sitting, the right ventricular mass index and pulmonary artery relative area change can be measured and are predictive of mortality, with no incremental benefit from the addition of right heart catheter based pressure measurements.

In patients with PH due to heart failure with preserved ejection fraction, low TLCO, male sex and low pulmonary arterial relative area change were the most significant measures of outcome. The use of pulmonary function testing and cardiac MRI can identify patients who are at risk, with no incremental benefit from right heart catheterisation.

7.4 Analysis of Vessel Abnormalities

Current methods of imaging in pulmonary hypertension concentrate on indirect consequences of raised pulmonary vascular resistance: the right ventricle and proximal pulmonary artery (cardiac MRI and CTPA) or the “end-organ” capillary level perfusion (perfusion SPECT and DCE-MRI). In pre-capillary pulmonary hypertension, the main pathophysiological drive is from pulmonary vascular remodelling. It seems logical, therefore, that there is an important role being played by the pulmonary vasculature causing increased pulmonary vascular resistance, driving the abnormalities of the right ventricle and main pulmonary artery, and leading to abnormal tissue perfusion. Although, the most important vessels in increased PVR are

likely to be too small to be visualised on CT. My future aim is to improve the methods of analysis of the pulmonary vascular tree from CTPA and assess its role in the development of pulmonary hypertension. Particularly in the assessment of the similarities between those patients with pre-capillary remodelling in PH-LHD and COPD and patients with PAH. Using third party software (VIDA Diagnostics, Coralville,, Iowa), it is possible to produce detailed maps of the pulmonary vascular tree, which can be interrogated to assess the underlying abnormalities (**Figure 7.5**).

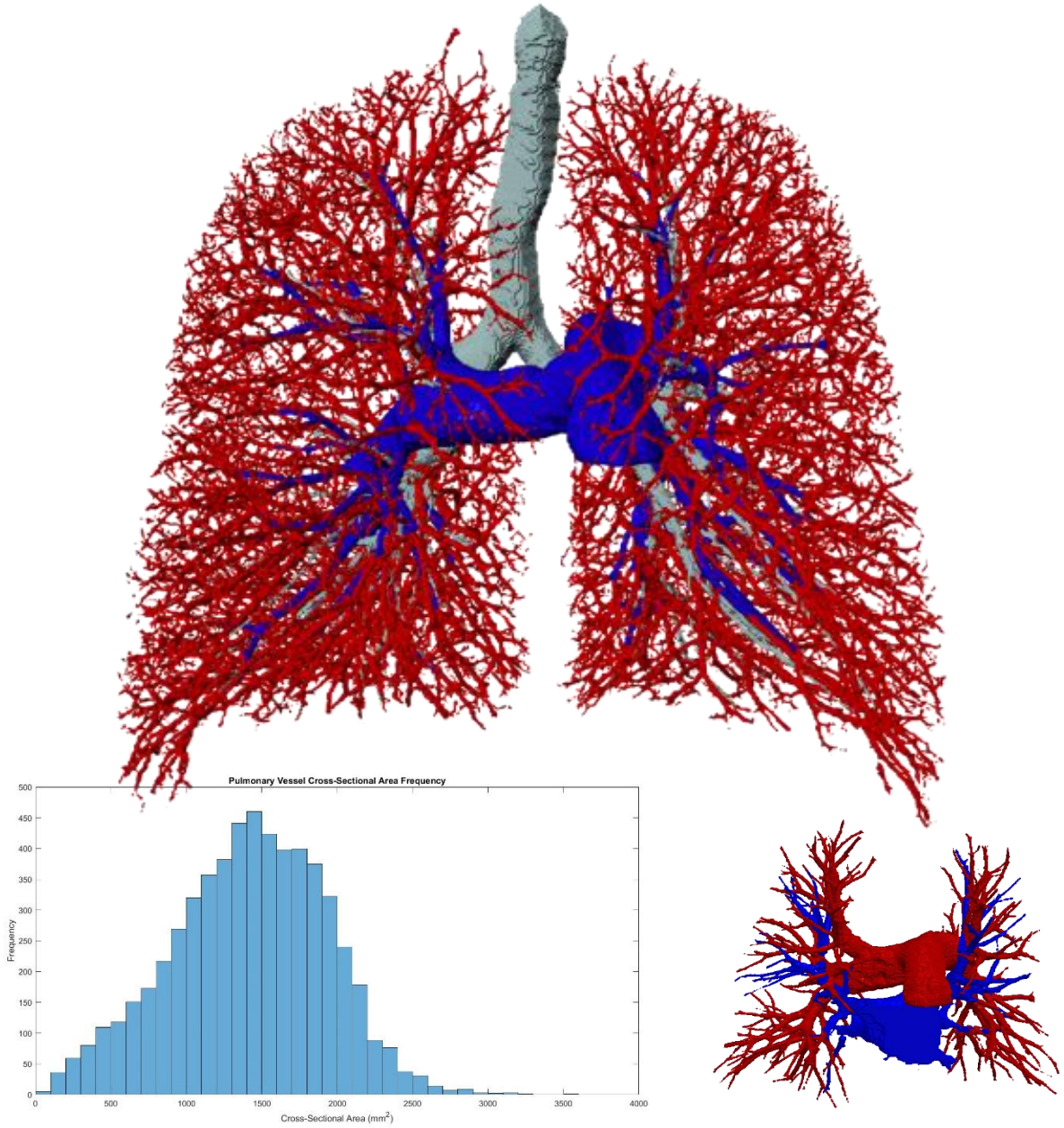

Figure 7.5: *A surface rendering of a model of the pulmonary vasculature taken from CTPA. The blue represents the proximal pulmonary vasculature and the red represents the distal vasculature, comprising arterial and venous structures. A semi-automated separation of the pulmonary arterial system from the pulmonary venous system is shown inlayed, as is the frequency distribution data for the cross*

Work from other centres has been published in the assessment of the pulmonary vasculature in patients with COPD and pulmonary hypertension, mainly using increasingly large unenhanced CT datasets (303,304). Initially, three slices were analysed for each patient at the level of the aortic arch, 1cm below the carina and 1cm below the right inferior pulmonary vein. A particle analysis segments any circular structures and assumes them to be vessels, then the cross-sectional areas are measured (305). Using this methodology, it has been shown that small vessel loss (measured as the percentage of vessels <5mm^2 cross-sectional area - %CSA<5) significantly correlates with CT densitometry measures of emphysema (percentage of lung volume with HU <-950 - %LAA$_{-950}$), r=−0.83, p<0.0001, and weak correlations with FEV_1 percent predicted and FEV_1/FVC (r=0.29, p<0.0001 and r=0.45, p<0.0001 respectively) in 191 cases in the National Lung Screening Trial (306). Further work in 79 patients with severe COPD on the National Emphysema Treatment Trial (NETT), showed that this loss of small vessels (%CSA<5) significantly correlates with mPAP (305) and in 81 cases with stable COPD small vessel loss was associated with an increased risk of acute exacerbation of COPD (307), which fits with data showing that main PA size is associated with exacerbation risk and therefore morbidity and mortality (59).

More recently, 3D analysis of the pulmonary vessels has been employed, confirming that with increasing emphysema on CT there is “pruning of the small blood vessels” (vessels with cross-sectional area of <5mm^2) (308), which in a small cohort of patients was shown to reverse with lung volume reduction surgery (309). The small vessel loss is associated with disease severity on CT (308), and also with reduced left ventricular filling in smokers without evidence of lung disease (310). More sophisticated methods of assessment of parenchymal disease also increase the ability to phenotype lung disease (311).

A study assessing the difference in quantitative pulmonary parenchymal abnormalities and vessel loss in patients with COPD-PH showed a significant difference between patients in the <35mmHg (non-severe PH) and ≥35mmHg (Severe PH). In severe PH, the strongest correlator with increasing mPAP was increasing small pulmonary vessel volumes (%CSA<5), whereas in the non-severe PH group the strongest correlator with increasing mPAP was bronchial wall thickness. Moreover,

in the non-severe PH patients an increase in mPAP was actually associated with a reduction in small vessel volumes (312). Hence, probing abnormalities in the small vessels in PH-lung disease has the potential to increase our understanding of the interaction between phenotypes of lung disease and pulmonary hypertension.

7.5 Assessment of Follow Up and Treatment Response

As discussed in the introductory sections of this thesis, the final part of clinical assessment in patients with PH is to identify those patients who respond and those patients who do not respond to therapy. MRI is sensitive to change and is reproducible and therefore represents a strong marker for the assessment of disease progression, non-invasively.

From the cohort of patients scanned in Sheffield there are a large number of patients with repeat scans, which would be interesting data to analyse for the best predictors of outcome and response to treatment.

APPENDIX 1: PUBLICATIONS, PRESENTATIONS AND AWARDS

PAPERS DIRECTLY RELATED TO THIS THESIS

Johns CS, Wild JM, Rajaram S, et al. Identifying at risk patients with combined pre and post capillary pulmonary hypertension using interventricular septal angle on Cardiac MRI. Radiology. 2018; In Press.

Johns CS, Wild JM, Rajaram S, Swift AJ, Kiely DG. Current and emerging imaging techniques in the diagnosis and assessment of pulmonary hypertension. Expert Rev Respir Med. 2017 Dec 20;17476348.2018.1420478.

Johns CS, Rajaram S, Capener DA, et al. Non-invasive methods for estimating mPAP in COPD using cardiovascular magnetic resonance imaging. Eur Radiol. 2017;

Christopher Johns, Andy Swift, Smitha Rajaram, Paul Hughes, Dave Capener, David Kiely, Jim M Wild. Lung Perfusion: DCE MRI vs SPECT for screening in suspected Chronic Thromboembolic Pulmonary Hypertension. J Magn Reson Imaging. 2017;

Johns CS, Swift AJ, Hughes PJC, Ohno Y, Schiebler M, Wild JM. Pulmonary MR angiography and perfusion imaging—A review of methods and applications. Eur J Radiol. Elsevier Ireland Ltd; 2017 Jan;86:361–70.

PAPERS NOT DIRECTLY RELATED TO THIS THESIS

Johns CS, M Schiebler, AJ Swift. Commentary on: Survey of UK imaging practice for the investigation of pulmonary embolism in pregnancy. Clinical Radiology. 2017.

Swift AJ, Capener D, Johns CS, Hamilton N, Rothman A, Elliot C, et al. Magnetic Resonance Imaging in the Prognostic Evaluation of Patients with Pulmonary Arterial Hypertension. Am J Respir Crit Care Med. 2017;

McGlashan NG, Johns CS, Connolly DJ. Imaging in paediatric stroke. Rad Mag. 2017;43(506):21–22.

Christopher Johns, S Kolla, A Hart, S Sinha, R Batty, DJA Connolly. A pictorial review of imaging in paediatric stroke. Postgrad Med J. 2016.

Currie BJ, Johns C, Chin M, Charalampopolous T, Elliot CA, Garg P, et al. CT derived left atrial size identifies left heart disease in suspected pulmonary hypertension: Derivation and validation of predictive thresholds. Int J Cardiol. 2018 Mar;

Smith LJ, West N, Hughes D, et al. Imaging Lung Function Abnormalities in Primary Ciliary Dyskinesia Using Hyperpolarised Gas Ventilation MRI. Ann Am Thorac Soc. 2018; Annals ATS. 2017.

CONFERENCE PROCEEDINGS

National/International Presentations

Johns C, Wild J, Rajaram S, et al. Septal Angle on MRI predicts Combined Pre and Post Capillary Pulmonary Hypertension. Br Thorac Soc Winter Meet 2017. London, UK; 2017.

Johns CS. A CMR approach to Phenotyping Pulmonary Hypertension due to left heart disease. Natl Pulm Hypertenstion Res Forum. London, UK; 2017.

Johns C, Kiely D, Capener D, et al. The use of cardiopulmonary MRI as a diagnostic tool in pulmonary hypertension. EuroCMR. Prague, Czech Republic; 2017.

Johns CS, Kiely DG, Capener DA, et al. Cardiopulmonary MRI as a diagnostic tool in Pulmonary Hypertension. ISMRM. Honolulu, Hawaii; 2017.

Johns CS, Swift AJ, Vogel-Claussen J, Kiely DG, Wild JM. The use of MRI in the diagnosis of Chronic Thromboembolic Pulmonary Hypertension. ISMRM. Honolulu, Hawaii; 2017.

C Johns, AJ Swift, S Rajaram, PJC Hughes, DJ Capener, DG Kiely JW. Lung Perfusion MRI: Screening for suspected CTEPH. Natl Pulm Hypertenstion Res Forum. London, UK; 2016.

Johns C, Capener D, Hammerton C, et al. Cardiopulmonary MR characteristics can estimate mPAP in COPD. ERS Int Congr. London, UK: European Respiratory Society; 2016. p. PA1884.

Johns C. Proton MR & CT Imaging in the assessment of Pulmonary Hypertension. Donald Heath Symp. Sheffield, UK; 2017.

Johns C. Cardiopulmonary MR characteristics can estimate MPAP in COPD patients. Insigneo Showc 2016. Sheffield, UK; 2016.

Other Conference Proceedings

Currie B, Johns C, Chin M, et al. Computed tomography in the diagnosis of left heart disease in patients with suspected pulmonary hypertension. Br Thorac Soc Winter Meet 2017. London, UK; 2017.

Quadery S, Swift A, Billings C, et al. Impact of patient choice on survival in patients with chronic thromboembolic pulmonary hypertension offered pulmonary endarterectomy. Br Thorac Soc Winter Meet 2017. London, UK; 2017.

Swift AJ, Capener D, Johns CS, et al. Independent prognostic value of changes in left atrial and ventricular volume in PAH – a cardiac MRI study. EuroCMR. Prague, Czech Republic; 2017.

Swift AJ, Capener D, Johns CS, et al. Magnetic resonance imaging in the prognostic evaluation of patients with pulmonary arterial hypertension. EuroCMR. Prague, Czech Republic; 2017.

Swift A, Swift AJ, Capener D, et al. High right ventricular mass is associated with poor outcome in pulmonary hypertension associated with congenital heart disease. EuroCMR. Prague, Czech Republic; 2017.

Johns C, Wild J, Rajaram S, et al. Septal Angle on MRI predicts Combined Pre and Post Capillary Pulmonary Hypertension. RCR2017. Liverpool, UK; 2017.

Johns C, Wild J, Solanki R, et al. Cardiopulmonary MRI as a diagnostic tool in Pulmonary Hypertension. RCR2017. Liverpool, UK; 2017.

Johns C, Biancardi A, Collier G, Capener C, Swift A, Wild J. 3D segmentation of the Pulmonary Arteries on Magnetic Resonance Angiography. ISMRM. Honolulu, Hawaii; 2017.

Johns C, Rajaram S, Capener D, Kiely D, Swift A, Wild J. Lung Perfusion: MRI Vs SPECT for Screening in Suspected Chronic Thromboembolic Pulmonary Hypertension. ISMRM. Singapore; 2016.

Johns CS, Kiely DG, Capener DA, et al. Cardiopulmonary MRI as a diagnostic tool in Pulmonary Hypertension. 16th Int PH. Vienna, Austria; 2016.

Shotton K, Walker H, Johns C, et al. Right ventricular MRI characteristics in patients with borderline pulmonary hypertension. ERS Int Congr. London, UK: European Respiratory Society; 2016. p. PA1874.

Johns C, Rajaram S, Capener D, Swift A, Wild J. Lung perfusion: MRI vs SPECT for screening in suspected chronic thromboembolic pulmonary hypertension. ERS Int Congr. London, UK: European Respiratory Society; 2016. p. PA2457.

Johns CS, Capener D, Hammerton C, et al. Non-invasive methods for the estimation of mPAP in COPD patients using cardiac MRI. Br Thorac Soc Winter Meet. London, UK: BMJ Publishing Group Ltd; 2016.

AWARDS RELATED TO THIS THESIS

A talk regarding the work in Chapter 4 ("Improving the Non-invasive Identification of Pulmonary Hypertension") was awarded "best oral presentation" at the 2016 *Insigneo Annual Scientific Meeting*.

Two talks generated from data in Chapters 4 and 5 ("Improving the Non-invasive Identification of Pulmonary Hypertension" and "Using Cardiac MRI to Differentiate Pre and Post Capillary PH in Left Heart Disease") were awarded Magna cum Laude awards at the 2017 *ISMRM* in Honolulu, Hawaii.

Two talks generated from data in Chapters 4 and 5 ("Improving the Non-invasive Identification of Pulmonary Hypertension" and "Using Cardiac MRI to Differentiate Pre and Post Capillary PH in Left Heart Disease") were awarded 1st place in the *Grainger Prize* in 2016 and 2017 respectively.

A poster generated from Chapter 4 ("Improving the Non-invasive Identification of Pulmonary Hypertension") was awarded 2nd place in the *Vera Ansell poster competition* at RCR2017 in Liverpool.

REFERENCES

1. Galiè N, Humbert M, Vachiery J-L, Gibbs S, Lang I, Torbicki A, et al. 2015 ESC/ERS Guidelines for the diagnosis and treatment of pulmonary hypertension: The Joint Task Force for the Diagnosis and Treatment of Pulmonary Hypertension of the European Society of Cardiology (ESC) and the European Respiratory Society (ERS): Endor. Eur Heart J. 2016 Jan 1;37(1):67–119.

2. D'Alonzo GE, Barst RJ, Ayres SM, Bergofsky EH, Brundage BH, Detre KM, et al. Survival in patients with primary pulmonary hypertension. Results from a national prospective registry. Ann Intern Med. 1991 Sep 1;115(5):343–9.

3. Heath D, Whitaker W, Brown JW. IDIOPATHIC PULMONARY HYPERTENSION. Br Heart J. 1957;19(1):83–92.

4. Gaine SP, Rubin LJ, Kmetzo JJ, Palevsky HI, Traill TA. Recreational use of aminorex and pulmonary hypertension. Chest. 2000 Nov;118(5):1496–7.

5. Kay JM, Smith P, Heath D. Aminorex and the pulmonary circulation. Thorax. BMJ Publishing Group Ltd; 1971 May 1;26(3):262–70.

6. Kovacs G, Berghold A, Scheidl S, Olschewski H. Pulmonary arterial pressure during rest and exercise in healthy subjects: A systematic review. Eur Respir J. Elsevier Inc; 2009 Oct;34(4):888–94.

7. Rosenkranz S, Preston IR. Right heart catheterisation: best practice and pitfalls in pulmonary hypertension. Eur Respir Rev. 2015 Dec;24(138):642–52.

8. Hoeper MM, Lee SH, Voswinckel R, Palazzini M, Jais X, Marinelli A, et al. Complications of right heart catheterization procedures in patients with pulmonary hypertension in experienced centers. J Am Coll Cardiol. 2006 Dec 19;48(12):2546–52.

9. Kiely DG, Elliot CA, Sabroe I, Condliffe R. Pulmonary hypertension: diagnosis and management. BMJ. 2013 Apr 16;346(apr16 1):f2028–f2028.

10. Rajaram S, Swift AJ, Wild JM, Kiely DG. Response to: 'CT assessment for

pulmonary hypertension requires systematic assessment of cardiac, vascular and parenchymal signs' by Marloes et al. Thorax. 2015 Jun 24;thoraxjnl-2015-207394.

11. Avouac J, Airò P, Meune C, Beretta L, Dieude P, Caramaschi P, et al. Prevalence of pulmonary hypertension in systemic sclerosis in European Caucasians and metaanalysis of 5 studies. J Rheumatol. 2010 Nov 1;37(11):2290–8.

12. Mandell MS, Groves BM. Pulmonary hypertension in chronic liver disease. Clin Chest Med. 1996 Mar;17(1):17–33.

13. Budhiraja R, Hassoun PM. Portopulmonary hypertension: a tale of two circulations. Chest. 2003 Feb;123(2):562–76.

14. Castro M, Krowka MJ, Schroeder DR, Beck KC, Plevak DJ, Rettke SR, et al. Frequency and clinical implications of increased pulmonary artery pressures in liver transplant patients. Mayo Clin Proc. 1996 Jun;71(6):543–51.

15. Sitbon O, Lascoux-Combe C, Delfraissy J-F, Yeni PG, Raffi F, De Zuttere D, et al. Prevalence of HIV-related pulmonary arterial hypertension in the current antiretroviral therapy era. Am J Respir Crit Care Med. 2008 Jan 1;177(1):108–13.

16. Simonneau G, Robbins IM, Beghetti M, Channick RN, Delcroix M, Denton CP, et al. Updated clinical classification of pulmonary hypertension. J Am Coll Cardiol. 2009 Jun 30;54(1 Suppl):S43-54.

17. Simonneau G, Galiè N, Rubin LJ, Langleben D, Seeger W, Domenighetti G, et al. Clinical classification of pulmonary hypertension. J Am Coll Cardiol. 2004 Jun 16;43(12 Suppl S):5S–12S.

18. Yuan JX-J, Rubin LJ. Pathogenesis of pulmonary arterial hypertension: the need for multiple hits. Circulation. 2005 Feb 8;111(5):534–8.

19. Rabinovitch M, Guignabert C, Humbert M, Nicolls MR. Inflammation and immunity in the pathogenesis of pulmonary arterial hypertension. Circ Res. 2014 Jun 20;115(1):165–75.

20. Hoeper MM, Barberà JA, Channick RN, Hassoun PM, Lang IM, Manes A, et al.

Diagnosis, assessment, and treatment of non-pulmonary arterial hypertension pulmonary hypertension. J Am Coll Cardiol. Elsevier Masson SAS; 2009 Jun 30;54(1 Suppl):S85-96.

21. Hussain N, Charalampopoulos A, Ramjug S, Condliffe R, Elliot CA, O'Toole L, et al. Pulmonary Hypertension in Patients with Heart Failure and Preserved Ejection Fraction: Differential Diagnosis and Management. Pulm Circ. 2016 Mar;6(1):3–14.

22. Naeije R, Vachiery J, Yerly P, Vanderpool R. The transpulmonary pressure gradient for the diagnosis of pulmonary vascular disease. Eur Respir J. 2012;41(1):217–23.

23. Redfield MM, Owan TE, Hodge DO, Herges RM, Jacobsen SJ, Roger VL, et al. Trends in prevalence and outcome of heart failure with preserved ejection fraction. N Engl J Med. 2006;355(3):251–9.

24. Damy T, Goode KM, Kallvikbacka-bennett A, Lewinter C, Hobkirk J, Nikitin NP, et al. Determinants and prognostic value of pulmonary arterial pressure in patients with chronic heart failure. Eur Heart J. 2010;31(18):2280–90.

25. Hoeper MM, Meyer K, Rademacher J, Fuge J, Welte T, Olsson KM. Diffusion Capacity and Mortality in Patients With Pulmonary Hypertension Due to Heart Failure With Preserved Ejection Fraction. JACC Hear Fail. Elsevier; 2016;4(6):441–9.

26. Bursi F, McNallan SM, Redfield MM, Nkomo VT, Lam CSP, Weston SA, et al. Pulmonary pressures and death in heart failure: a community study. J Am Coll Cardiol. Elsevier Inc.; 2012 Jan 17;59(3):222–31.

27. Lam CSPP, Roger VL, Rodeheffer RJ, Borlaug BA, Enders FT, Redfield MM. Pulmonary Hypertension in Heart Failure With Preserved Ejection Fraction. J Am Coll Cardiol. 2009 Mar;53(13):1119–26.

28. Guazzi M, Naeije R. Pulmonary Hypertension in Heart Failure. J Am Coll Cardiol. 2017 Apr;69(13):1718–34.

29. Drazner MH, Hamilton MA, Fonarow G, Creaser J, Flavell C, Stevenson LW.

Relationship between right and left-sided filling pressures in 1000 patients with advanced heart failure. J Heart Lung Transplant. 1999 Nov;18(11):1126–32.

30. Gerges C, Gerges M, Lang MB, Zhang Y, Jakowitsch J, Probst P, et al. Diastolic Pulmonary Vascular Pressure Gradient. Chest. 2013 Mar;143(3):758–66.

31. Naeije R. Measurement to predict survival: the case of diastolic pulmonary gradient. JACC Heart Fail. American College of Cardiology Foundation; 2015;3(5):425.

32. Pepke-zaba J, Coghlan JG, Scelsi L, Alto MD, Olsson KM, Ulrich S, et al. Pre-Capillary, Combined, and Post-Capillary Pulmonary Hypertension. 2016;68(4).

33. Jacobs W, Konings TC, Heymans MW, Boonstra A, Bogaard HJ, Van Rossum AC, et al. Noninvasive identification of left-sided heart failure in a population suspected of pulmonary arterial hypertension. Eur Respir J. 2015;46(2):422–30.

34. Leopold JA. Biological Phenotyping of Combined Post-Capillary and Pre-Capillary Pulmonary Hypertension: Focus on Pulmonary Vascular Remodeling∗. J Am Coll Cardiol. Elsevier; 2016;68(23):2537–9.

35. Opitz CF, Hoeper MM, Gibbs JSR, Kaemmerer H, Pepke-Zaba J, Coghlan JG, et al. Pre-Capillary, Combined, and Post-Capillary Pulmonary Hypertension: A Pathophysiological Continuum. J Am Coll Cardiol. 2016;68(4):368–78.

36. Hemnes AR, Larkin EK, Glazer AM, Xu M, Wells QS, Farber-eger EH, et al. Clinical and Biological Insights Into Combined Post- and Pre-Capillary Pulmonary Hypertension. J Am Coll Cardiol. 2016;68(23):2525–36.

37. Rosenkranz S, Gibbs JSR, Wachter R, De Marco T, Vonk-Noordegraaf A, Vachiéry J-LL. Left ventricular heart failure and pulmonary hypertension. Eur Heart J. 2016 Mar 21;37(12):942–54.

38. West JB, Mathieu-Costello O. Vulnerability of pulmonary capillaries in heart disease. Circulation. 1995 Aug 1;92(3):622–31.

39. Kurdak SS, Namba Y, Fu Z, Kennedy B, Mathieu-Costello O, West JB. Effect of

increased duration of high perfusion pressure on stress failure of pulmonary capillaries. Microvasc Res. 1995 Sep;50(2):235–48.

40. Bonderman D, Pretsch I, Steringer-Mascherbauer R, Jansa P, Rosenkranz S, Tufaro C, et al. Acute Hemodynamic Effects of Riociguat in Patients With Pulmonary Hypertension Associated With Diastolic Heart Failure (DILATE-1). Chest. 2014 Nov;146(5):1274–85.

41. Koller B, Steringer-Mascherbauer R, Ebner CH, Weber T, Ammer M, Eichinger J, et al. Pilot Study of Endothelin Receptor Blockade in Heart Failure with Diastolic Dysfunction and Pulmonary Hypertension (BADDHY-Trial). Hear Lung Circ. Australian and New Zealand Society of Cardiac and Thoracic Surgeons (ANZSCTS) and the Cardiac Society of Australia and New Zealand (CSANZ); 2017 May;26(5):433–41.

42. Chaouat A, Naeije R, Weitzenblum E. Pulmonary hypertension in COPD. Eur Respir J. 2008 Nov 1;32(5):1371–85.

43. Wright JL, Levy RD, Churg a. Pulmonary hypertension in chronic obstructive pulmonary disease: current theories of pathogenesis and their implications for treatment. Thorax. 2005 Jul 1;60(7):605–9.

44. Andersen KH, Iversen M, Kjaergaard J, Mortensen J, Nielsen-Kudsk JE, Bendstrup E, et al. Prevalence, predictors, and survival in pulmonary hypertension related to end-stage chronic obstructive pulmonary disease. J Hear Lung Transplant. Elsevier Inc.; 2012 Apr;31(4):373–80.

45. Burrows B, Kettel LJ, Niden AH, Rabinowitz M, Diener CF. Patterns of Cardiovascular Dysfunction in Chronic Obstructive Lung Disease. N Engl J Med. Massachusetts Medical Society; 1972 Apr 27;286(17):912–8.

46. Cooper R, Ghali J, Simmons BE, Castaner A. Elevated Pulmonary Artery Pressure. Chest. 1991 Jan;99(1):112–20.

47. Oswald-Mammosser M, Weitzenblum E, Quoix E, Moser G, Chaouat A, Charpentier C, et al. Prognostic Factors in COPD Patients Receiving Long-term Oxygen Therapy: Importance of Pulmonary Artery Pressure. Chest. 1995;107(5):1193–8.

48. Zvezdin B, Milutinov S, Kojicic M, Hadnadjev M, Hromis S, Markovic M, et al. A Postmortem Analysis of Major Causes of Early Death in Patients Hospitalized With COPD Exacerbation. Chest. 2009;136(2):376–80.

49. Chaouat A, Bugnet A-SS, Kadaoui N, Schott R, Enache I, Ducoloné A, et al. Severe pulmonary hypertension and chronic obstructive pulmonary disease. Am J Respir Crit Care Med. 2005;172(2):189–94.

50. Seeger W, Adir Y, Barber?? JA, Champion H, Coghlan JG, Cottin V, et al. Pulmonary hypertension in chronic lung diseases. J Am Coll Cardiol. 2013 Dec;62(25 SUPPL.):D109–16.

51. Shujaat A, Minkin R, Eden E. Pulmonary hypertension and chronic cor pulmonale in COPD. Int J Chron Obstruct Pulmon Dis. 2007;2(3):273–82.

52. Parker J. Right and left ventricular performance chronic obstructive lung disease. Am Heart J. 1971;82(3):319–27.

53. Kimura M, Taniguchi H, Kondoh Y, Kimura T, Kataoka K, Nishiyama O, et al. Pulmonary Hypertension as a Prognostic Indicator at the Initial Evaluation in Idiopathic Pulmonary Fibrosis. Respiration. 2013;85(6):456–63.

54. Nathan SD, Shlobin OA, Ahmad S, Koch J, Barnett SD, Ad N, et al. Serial development of pulmonary hypertension in patients with idiopathic pulmonary fibrosis. Respiration. 2008;76(3):288–94.

55. Brewis MJ, Church AC, Johnson MK, Peacock AJ. Severe pulmonary hypertension in lung disease: phenotypes and response to treatment. Eur Respir J. 2015 Nov;46(5):1247–50.

56. Boerrigter BG, Bogaard HJ, Trip P, Groepenhoff H, Rietema H, Holverda S, et al. Ventilatory and Cardiocirculatory Exercise Profiles in COPD: The Role of Pulmonary Hypertension. Chest. 2012;142(5):1166–74.

57. Wrobel JP, Thompson BR, Williams TJ. Mechanisms of pulmonary hypertension in chronic obstructive pulmonary disease: A pathophysiologic review. J Hear Lung Transplant. Elsevier Inc.; 2012;31(6):557–64.

58. Barberà JA, Blanco I, Barber?? JA, Blanco I. Gaining insights into pulmonary

hypertension in respiratory diseases. Eur Respir J. 2015;46(5):1247–50.

59. Wells JM, Washko GR, Han MK, Abbas N, Nath H, Mamary AJ, et al. Pulmonary Arterial Enlargement and Acute Exacerbations of COPD. N Engl J Med. 2012;367(10):913–21.

60. Williams MC, Murchison JT, Edwards LD, Agustí A, Bakke P, Calverley PMA, et al. Coronary artery calcification is increased in patients with COPD and associated with increased morbidity and mortality. Thorax. 2014 Aug;69(8):718–23.

61. Condliffe R, Kiely DG, Gibbs JSR, Corris PA, Peacock AJ, Jenkins DP, et al. Improved outcomes in medically and surgically treated chronic thromboembolic pulmonary hypertension. Am J Respir Crit Care Med. 2008;177(10):1122–7.

62. Wilkens H, Lang I, Behr J, Berghaus T, Grohe C, Guth S, et al. Chronic thromboembolic pulmonary hypertension (CTEPH): Updated Recommendations of the Cologne Consensus Conference 2011. Int J Cardiol. Elsevier Ireland Ltd; 2011;154(1):S54–60.

63. Pengo V, Lensing AWAA, Prins MH, Marchiori A, Davidson BL, Tiozzo F, et al. Incidence of chronic thromboembolic pulmonary hypertension after pulmonary embolism. N Engl J Med. 2004 May 27;350(22):2257–64.

64. Auger WR, Kim NH, Trow TK. Chronic thromboembolic pulmonary hypertension. Clin Chest Med. 2010 Dec;31(4):741–58.

65. Lewczuk J, Piszko P, Jagas J, Porada A, Sobkowicz B, Wrabec K, et al. Prognostic Factors in Medically Treated Patients With Chronic Pulmonary Embolism. Chest. 2001 Mar;119(3):818–23.

66. Auger W, Kim N, Kerr K, Fedullo P. Evaluation of patients with chronic thromboembolic pulmonary hypertension for pulmonary endarterectomy. Pulm Circ. 2012;2(2):155.

67. Condliffe R, Kiely DG, Gibbs JSR, Corris PA, Peacock AJ, Jenkins DP, et al. Prognostic and aetiological factors in chronic thromboembolic pulmonary

hypertension. Eur Respir J. 2008;33(2):332–8.

68. Galiè N, Humbert M, Vachiery J-L, Gibbs S, Lang I, Torbicki A, et al. 2015 ESC/ERS Guidelines for the diagnosis and treatment of pulmonary hypertension. Eur Heart J. 2016 Jan 1;37(1):67–119.

69. Humbert M, Ghofrani H-A. The molecular targets of approved treatments for pulmonary arterial hypertension. Thorax. 2016 Jan;71(1):73–83.

70. Medarov BI, Judson MA. The role of calcium channel blockers for the treatment of pulmonary arterial hypertension: How much do we actually know and how could they be positioned today? Respir Med. Elsevier Ltd; 2015 May;109(5):557–64.

71. Rich S, Kaufmann E, Levy PS. The effect of high doses of calcium-channel blockers on survival in primary pulmonary hypertension. N Engl J Med. 1992 Jul 9;327(2):76–81.

72. Rubin LJ, Badesch DB, Barst RJ, Galiè N, Black CM, Keogh A, et al. Bosentan Therapy for Pulmonary Arterial Hypertension. N Engl J Med. 2002;346(12):896–903.

73. Hoeper MM, Gall H, Seyfarth HJ, Halank M, Ghofrani HA, Winkler J, et al. Long-term outcome with intravenous iloprost in pulmonary arterial hypertension. Eur Respir J. 2009 Jul;34(1):132–7.

74. Olschewski H, Simonneau G, Galiè N, Higenbottam T, Naeije R, Rubin LJ, et al. Inhaled iloprost for severe pulmonary hypertension. N Engl J Med. 2002 Aug 1;347(5):322–9.

75. Galiè N, Ghofrani HA, Torbicki A, Barst RJ, Rubin LJ, Badesch D, et al. Sildenafil citrate therapy for pulmonary arterial hypertension. N Engl J Med. 2005 Nov 17;353(20):2148–57.

76. Rich S, Dantzker DR, Ayres SM, Bergofsky EH, Brundage BH, Detre KM, et al. Primary pulmonary hypertension. A national prospective study. Ann Intern Med. 1987 Aug;107(2):216–23.

77. Parasuraman S, Walker S, Loudon BL, Gollop ND, Wilson AM, Lowery C, et al.

Assessment of pulmonary artery pressure by echocardiography—A comprehensive review. IJC Hear Vasc. The Authors; 2016 Sep;12:45–51.

78. Galiè N, Hoeper MM, Humbert M, Torbicki A, Vachiery J-L, Barbera JA, et al. Guidelines for the diagnosis and treatment of pulmonary hypertension: the Task Force for the Diagnosis and Treatment of Pulmonary Hypertension of the European Society of Cardiology (ESC) and the European Respiratory Society (ERS), endorsed by the Internat. Eur Heart J. 2009 Oct 2;30(20):2493–537.

79. Currie PJ, Seward JB, Chan KL, Fyfe DA, Hagler DJ, Mair DD, et al. Continuous wave Doppler determination of right ventricular pressure: a simultaneous Doppler-catheterization study in 127 patients. J Am Coll Cardiol. United States; 1985 Oct;6(4):750–6.

80. Berger M, Haimowitz A, Van Tosh A, Berdoff RL, Goldberg E. Quantitative assessment of pulmonary hypertension in patients with tricuspid regurgitation using continuous wave Doppler ultrasound. J Am Coll Cardiol. United States; 1985 Aug;6(2):359–65.

81. Fisher MR, Forfia PR, Chamera E, Housten-Harris T, Champion HC, Girgis RE, et al. Accuracy of Doppler Echocardiography in the Hemodynamic Assessment of Pulmonary Hypertension. Am J Respir Crit Care Med. 2009 Apr 1;179(7):615–21.

82. Kiely DG, Cargill RI, Struthers AD, Lipworth BJ. Cardiopulmonary effects of endothelin-1 in man. Cardiovasc Res. 1997;33(2):378–86.

83. Ommen SR, Nishimura R a, Appleton CP, Miller F a, Oh JK, Redfield MM, et al. Clinical Utility of Doppler Echocardiography and Tissue Doppler Imaging in the Estimation of Left Ventricular Filling Pressures : A Comparative Simultaneous Doppler-Catheterization Study. Circulation. 2000 Oct 10;102(15):1788–94.

84. Nanthakumar K, Graham AT, Robinson TI, Grande P, Pugash RA, Clarke JA, et al. Contrast echocardiography for detection of pulmonary arteriovenous malformations. Am Heart J. 2001 Feb;141(2):243–6.

85. Attaran RR, Ata I, Kudithipudi V, Foster L, Sorrell VL. Protocol for optimal detection and exclusion of a patent foramen ovale using transthoracic

echocardiography with agitated saline microbubbles. Echocardiography. 2006 Aug;23(7):616–22.

86. Silvestry FE, Cohen MS, Armsby LB, Burkule NJ, Fleishman CE, Hijazi ZM, et al. Guidelines for the Echocardiographic Assessment of Atrial Septal Defect and Patent Foramen Ovale: From the American Society of Echocardiography and Society for Cardiac Angiography and Interventions. J Am Soc Echocardiogr. Elsevier Inc; 2015 Aug;28(8):910–58.

87. Bajc M, Neilly JB, Miniati M, Schuemichen C, Meignan M, Jonson B. EANM guidelines for ventilation/perfusion scintigraphy : PPPPart 1. Pulmonary imaging with ventilation/perfusion single photon emission tomography. Eur J Nucl Med Mol Imaging. 2009;36(8):1356–70.

88. Marshall H, Kiely DG, Parra-Robles J, Capener D, Deppe MH, van Beek EJR, et al. Magnetic resonance imaging of ventilation and perfusion changes in response to pulmonary endarterectomy in chronic thromboembolic pulmonary hypertension. Am J Respir Crit Care Med. American Thoracic Society; 2014 Sep 1;190(5):e18–9.

89. Johns CS, Swift AJ, Rajaram S, Hughes PJC, Capener DJ, Kiely DG, et al. Lung perfusion: MRI vs. SPECT for screening in suspected chronic thromboembolic pulmonary hypertension. J Magn Reson Imaging. 2017 Dec;46(6):1693–7.

90. Johns CS, Swift AJ, Hughes PJC, Ohno Y, Schiebler M, Wild JM. Pulmonary MR angiography and perfusion imaging—A review of methods and applications. Eur J Radiol. Elsevier Ireland Ltd; 2017 Jan;86:361–70.

91. Rajaram S, Swift AJ, Telfer A, Hurdman J, Marshall H, Lorenz E, et al. 3D contrast-enhanced lung perfusion MRI is an effective screening tool for chronic thromboembolic pulmonary hypertension: results from the ASPIRE Registry. Thorax. 2013 Jul;68(7):677–8.

92. Kapoor V, McCook BM, Torok FS. An introduction to PET-CT imaging. Radiographics. 2004;24(2):523–43.

93. Rajaram S, Swift a. J, Condliffe R, Johns C, Elliot C a., Hill C, et al. CT features of pulmonary arterial hypertension and its major subtypes: a systematic CT

evaluation of 292 patients from the ASPIRE Registry. Thorax. BMJ Group; 2015 Apr 1;70(4):382–7.

94. Tan RT, Kuzo R, Goodman LR, Siegel R, Haasler GR, Presberg KW. Utility of CT Scan Evaluation for Predicting Pulmonary Hypertension in Patients With Parenchymal Lung Disease. Chest. 1998 May;113(5):1250–6.

95. Edwards PD, Bull RK, Coulden R. CT measurement of main pulmonary artery diameter. Br J Radiol. 1998 Oct;71(850):1018–20.

96. Ramjug S, Hussain N, Hurdman J, Billings C, Charalampopoulos A, Elliot CA, et al. Idiopathic and Systemic Sclerosis-Associated Pulmonary Arterial Hypertension. Chest. 2017 Jul;152(1):92–102.

97. Condliffe R, Kiely DG, Peacock AJ, Corris PA, Gibbs JSR, Vrapi F, et al. Connective tissue disease-associated pulmonary arterial hypertension in the modern treatment era. Am J Respir Crit Care Med. 2009 Jan 15;179(2):151–7.

98. Sheehan R, Perloff JK, Fishbein MC, Gjertson D, Aberle DR. Pulmonary neovascularity: A distinctive radiographic finding in Eisenmenger syndrome. Circulation. 2005;112(18):2778–85.

99. Dong C, Zhou M, Liu D, Long X, Guo T, Kong X. Diagnostic accuracy of computed tomography for chronic thromboembolic pulmonary hypertension: a systematic review and meta-analysis. PLoS One. 2015;10(4):e0126985.

100. Reichelt A, Hoeper MM, Galanski M, Keberle M. Chronic thromboembolic pulmonary hypertension: Evaluation with 64-detector row CT versus digital substraction angiography. Eur J Radiol. 2009 Jul;71(1):49–54.

101. Tunariu N, Gibbs SJRR, Win Z, Gin-Sing W, Graham A, Gishen P, et al. Ventilation-perfusion scintigraphy is more sensitive than multidetector CTPA in detecting chronic thromboembolic pulmonary disease as a treatable cause of pulmonary hypertension. J Nucl Med. 2007 May;48(5):680–4.

102. Qanadli SD, El Hajjam M, Vieillard-Baron A, Joseph T, Mesurolle B, Oliva VL, et al. New CT index to quantify arterial obstruction in pulmonary embolism: comparison with angiographic index and echocardiography. AJR Am J

Roentgenol. 2001 Jun;176(6):1415–20.

103. Wong LF, Akram AR, McGurk S, Van Beek EJR, Reid JH, Murchison JT. Thrombus load and acute right ventricular failure in pulmonary embolism: correlation and demonstration of a 'tipping point' on CT pulmonary angiography. Br J Radiol. 2012 Nov;85(1019):1471–6.

104. Baque-Juston MC, Wells AU, Hansell DM. Pericardial thickening or effusion in patients with pulmonary artery hypertension: a CT study. Am J Roentgenol. 1999 Feb;172(2):361–4.

105. Groves A., Win T, Charman S., Wisbey C, Pepke-Zaba J, Coulden R. Semi-quantitative assessment of tricuspid regurgitation on contrast-enhanced multidetector CT. Clin Radiol. 2004 Aug;59(8):715–9.

106. Ohno Y, Koyama H, Matsumoto K, Onishi Y, Takenaka D, Fujisawa Y, et al. Differentiation of Malignant and Benign Pulmonary Nodules with Quantitative First-Pass 320–Detector Row Perfusion CT versus FDG PET/CT. Radiology. 2011 Feb;258(2):599–609.

107. Ohno Y, Fujisawa Y, Sugihara N, Kishida Y, Seki S, Koyama H, et al. Dynamic Contrast-Enhanced Perfusion Area-Detector CT: Preliminary Comparison of Diagnostic Performance for N Stage Assessment With FDG PET/CT in Non–Small Cell Lung Cancer. Am J Roentgenol. 2017 Nov;209(5):W253–62.

108. Mirsadraee S, Reid JH, Connell M, MacNee W, Hirani N, Murchison JT, et al. Dynamic (4D) CT perfusion offers simultaneous functional and anatomical insights into pulmonary embolism resolution. Eur J Radiol. Elsevier Ireland Ltd; 2016 Oct;85(10):1883–90.

109. Tamura M, Yamada Y, Kawakami T, Kataoka M, Iwabuchi Y, Sugiura H, et al. Diagnostic accuracy of lung subtraction iodine mapping CT for the evaluation of pulmonary perfusion in patients with chronic thromboembolic pulmonary hypertension: Correlation with perfusion SPECT/CT. Int J Cardiol. Elsevier Ireland Ltd; 2017 Sep 15;243:538–43.

110. Horton MR, Tuder RM. Primary pulmonary arterial hypertension presenting as diffuse micronodules on CT. Crit Rev Comput Tomogr. 2004;45(5–6):335–41.

111. Resten A, Maître S, Humbert M, Sitbon O, Capron F, Simoneau G, et al. Pulmonary Arterial Hypertension: Thin-Section CT Predictors of Epoprostenol Therapy Failure. Radiology. 2002 Mar;222(3):782–8.

112. Revel M-P, Faivre J-B, Remy-Jardin M, Delannoy-Deken V, Duhamel A, Remy J. Pulmonary hypertension: ECG-gated 64-section CT angiographic evaluation of new functional parameters as diagnostic criteria. Radiology. 2009 Feb;250(2):558–66.

113. David S, Hoeper MM, Vogel-Claussen J, Cebotari S. Pulmonary Arterial Sarcoma Presenting as Acute Pulmonary Embolism. Am J Respir Crit Care Med. 2017 Aug 15;196(4):523.

114. Thieme SF, Graute V, Nikolaou K, Maxien D, Reiser MF, Hacker M, et al. Dual Energy CT lung perfusion imaging--correlation with SPECT/CT. Eur J Radiol. Elsevier Ireland Ltd; 2012 Feb;81(2):360–5.

115. Johnson TRC, Krauss B, Sedlmair M, Grasruck M, Bruder H, Morhard D, et al. Material differentiation by dual energy CT: initial experience. Eur Radiol. 2007 Jun;17(6):1510–7.

116. Currie BJ, Johns C, Chin M, Charalampopolous T, Elliot CA, Garg P, et al. CT derived left atrial size identifies left heart disease in suspected pulmonary hypertension: Derivation and validation of predictive thresholds. Int J Cardiol. 2018 Mar;

117. Chandra N, Langan DA. Gemstone Detector: Dual Energy Imaging via Fast kVp Switching. In: Johnson T, Fink C, Schönberg SO, Reiser MF, editors. Dual Energy CT in Clinical Practice. Berlin, Heidelberg: Springer Berlin Heidelberg; 2011. p. 35–41.

118. Fornaro J, Leschka S, Hibbeln D, Butler A, Anderson N, Pache G, et al. Dual- and multi-energy CT: approach to functional imaging. Insights Imaging. 2011 Apr 19;2(2):149–59.

119. Ohana M, Jeung MY, Labani A, El Ghannudi S, Roy C. Thoracic dual energy CT: acquisition protocols, current applications and future developments. Diagn Interv Imaging. Elsevier Masson SAS; 2014 Nov;95(11):1017–26.

120. Ameli-Renani S, Rahman F, Nair A, Ramsay L, Bacon JL, Weller A, et al. Dual-Energy CT for Imaging of Pulmonary Hypertension: Challenges and Opportunities. Radiographics. 2013;34(7):1769–90.

121. Hoey ETD, Mirsadraee S, Pepke-Zaba J, Jenkins DP, Gopalan D, Screaton NJ. Dual-energy CT angiography for assessment of regional pulmonary perfusion in patients with chronic thromboembolic pulmonary hypertension: Initial experience. Am J Roentgenol. 2011;196(3):524–32.

122. Remy-Jardin M, Faivre J-B, Pontana F, Hachulla A-L, Tacelli N, Santangelo T, et al. Thoracic applications of dual energy. Radiol Clin North Am. 2010 Jan;48(1):193–205.

123. Ruzsics B, Lee H, Zwerner PL, Gebregziabher M, Costello P, Schoepf UJ. Dual-energy CT of the heart for diagnosing coronary artery stenosis and myocardial ischemia-initial experience. Eur Radiol. 2008 Nov;18(11):2414–24.

124. Swift AJ, Capener D, Johns CS, Hamilton N, Rothman A, Elliot C, et al. Magnetic resonance imaging in the prognostic evaluation of patients with pulmonary arterial hypertension. In: EuroCMR. Prague, Czech Republic; 2017.

125. Swift AJ, Rajaram S, Hurdman J, Hill C, Davies C, Sproson TW, et al. Noninvasive Estimation of PA Pressure, Flow, and Resistance With CMR Imaging. JACC Cardiovasc Imaging. 2013 Oct;6(10):1036–47.

126. Currie S, Hoggard N, Craven IJ, Hadjivassiliou M, Wilkinson ID. Understanding MRI: basic MR physics for physicians. Postgrad Med J. 2013 Apr;89(1050):209–23.

127. McRobbie D. MRI from Picture to Proton. Second Edi. Cambridge University Press; 2007.

128. Swift AJ, Rajaram S, Capener D, Elliot C, Condliffe R, Wild JM, et al. Longitudinal and transverse right ventricular function in pulmonary hypertension: cardiovascular magnetic resonance imaging study from the ASPIRE registry. Pulm Circ. 2015 Jul 24;5(3):000–000.

129. van Wolferen SA, Marcus JT, Boonstra A, Marques KMJJ, Bronzwaer JGFF,

Spreeuwenberg MD, et al. Prognostic value of right ventricular mass, volume, and function in idiopathic pulmonary arterial hypertension. Eur Heart J. 2007 May 29;28(10):1250–7.

130. van de Veerdonk MC, Kind T, Marcus JT, Mauritz G-J, Heymans MW, Bogaard H-J, et al. Progressive Right Ventricular Dysfunction in Patients With Pulmonary Arterial Hypertension Responding to Therapy. J Am Coll Cardiol. Elsevier Inc.; 2011 Dec 6;58(24):2511–9.

131. Mauritz G-J, Marcus JT, Boonstra A, Postmus PE, Westerhof N, Vonk-Noordegraaf A. Non-invasive stroke volume assessment in patients with pulmonary arterial hypertension: left-sided data mandatory. J Cardiovasc Magn Reson. 2008;10(1):51.

132. Jaspers K, Freling HG, van Wijk K, Romijn EI, Greuter MJW, Willems TP. Improving the reproducibility of MR-derived left ventricular volume and function measurements with a semi-automatic threshold-based segmentation algorithm. Int J Cardiovasc Imaging. 2013 Mar;29(3):617–23.

133. Saba TS, Foster J, Cockburn M, Cowan M, Peacock AJ. Ventricular mass index using magnetic resonance imaging accurately estimates pulmonary artery pressure. Eur Respir J. 2002 Dec;20(6):1519–24.

134. Roeleveld RJ, Marcus JT, Faes TJC, Gan T-J, Boonstra A, Postmus PE, et al. Interventricular Septal Configuration at MR Imaging and Pulmonary Arterial Pressure in Pulmonary Hypertension. Radiology. 2005 Mar;234(3):710–7.

135. Swift AJ, Rajaram S, Marshall H, Condliffe R, Capener D, Hill C, et al. Black blood MRI has diagnostic and prognostic value in the assessment of patients with pulmonary hypertension. Eur Radiol. 2012 Mar;22(3):695–702.

136. Hopkins SR, Wielpütz MO, Kauczor H-U. Imaging lung perfusion. J Appl Physiol. 2012;113(2):328–39.

137. Miyazaki M, Lee VS. Nonenhanced MR angiography. Radiology. 2008;248(1):20–43.

138. Barker AJ, Roldán-Alzate A, Entezari P, Shah SJ, Chesler NC, Wieben O, et al.

Four-dimensional flow assessment of pulmonary artery flow and wall shear stress in adult pulmonary arterial hypertension: Results from two institutions. Magn Reson Med. 2015 May;73(5):1904–13.

139. Markl M, Frydrychowicz A, Kozerke S, Hope M, Wieben O. 4D flow MRI. J Magn Reson Imaging. 2012;36(5):1015–36.

140. Reiter G, Reiter U, Kovacs G, Adelsmayr G, Greiser A, Stalder AF, et al. Counter-clockwise vortical blood flow in the main pulmonary artery in a patient with patent ductus arteriosus with pulmonary arterial hypertension : a cardiac magnetic resonance imaging case report. BMC Med Imaging. BMC Medical Imaging; 2016;16(1):45.

141. Reiter G, Reiter U, Kovacs G, Olschewski H, Fuchsjäger M. Blood flow vortices along the main pulmonary artery measured with MR imaging for diagnosis of pulmonary hypertension. Radiology. 2015;275(1):71–9.

142. Reiter G, Reiter U, Kovacs G, Kainz B, Schmidt K, Maier R, et al. Magnetic Resonance-Derived 3-Dimensional Blood Flow Patterns in the Main Pulmonary Artery as a Marker of Pulmonary Hypertension and a Measure of Elevated Mean Pulmonary Arterial Pressure. Circ Cardiovasc Imaging. 2008 Jul 1;1(1):23–30.

143. Wild JM, Marshall H, Bock M, Schad LR, Jakob PM, Puderbach M, et al. MRI of the lung (1/3): Methods. Insights Imaging. 2012;3:345–53.

144. Du J, Bydder M. High-resolution time-resolved contrast-enhanced MR abdominal and pulmonary angiography using a spiral-TRICKS sequence. Magn Reson Med. 2007 Sep;58(3):631–5.

145. Abolmaali ND, Hietschold V, Appold S, Ebert W, Vogl TJ. Gadomer-17-enhanced 3D navigator-echo MR angiography of the pulmonary arteries in pigs. Eur Radiol. 2002;12(3):692–7.

146. Ohno Y, Hatabu H, Murase K, Higashino T, Kawamitsu H, Watanabe H, et al. Quantitative assessment of regional pulmonary perfusion in the entire lung using three-dimensional ultrafast dynamic contrast-enhanced magnetic resonance imaging: Preliminary experience in 40 subjects. J Magn Reson Imaging. 2004;20(3):353–65.

147. Risse F. MR Perfusion of the Lung. Kauczor H-U, editor. MRI of the Lung. Berlin, Heidelberg: Springer Berlin Heidelberg; 2009. 25-34 p. (Medical Radiology).

148. Köstler H, Ritter C, Lipp M, Beer M, Hahn D, Sandstede J. Prebolus quantitative MR heart perfusion imaging. Magn Reson Med. 2004 Aug;52(2):296–9.

149. Li KL, Zhu XP, Waterton J, Jackson A. Improved 3D quantitative mapping of blood volume and endothelial permeability in brain tumors. J Magn Reson Imaging. 2000;12(2):347–57.

150. Meier P, Zierler KL. On the theory of the indicator-dilution method for measurement of blood flow and volume. J Appl Physiol. 1954 Jun;6(12):731–44.

151. Ley S, Ley-Zaporozhan J. Pulmonary perfusion imaging using MRI: clinical application. Insights Imaging. 2012;3(1):61–71.

152. Risse F, Semmler W, Kauczor H-U, Fink C. Dual-bolus approach to quantitative measurement of pulmonary perfusion by contrast-enhanced MRI. J Magn Reson Imaging. 2006;24(6):1284–90.

153. Agarwal R, Brunelli SM, Williams K, Mitchell MD, Feldman HI, Umscheid CA. Gadolinium-based contrast agents and nephrogenic systemic fibrosis: A systematic review and meta-analysis. Nephrol Dial Transplant. 2009;24(3):856–63.

154. Bitar R, Leung G, Perng R, Tadros S, Moody AR, Sarrazin J, et al. MR Pulse Sequences: What Every Radiologist Wants to Know but Is Afraid to Ask. RadioGraphics. 2006 Mar;26(2):513–37.

155. Rajaram S, Swift AJ, Capener D, Telfer A, Davies C, Hill C, et al. Diagnostic accuracy of contrast-enhanced MR angiography and unenhanced proton MR imaging compared with CT pulmonary angiography in chronic thromboembolic pulmonary hypertension. Eur Radiol. 2012;22(2):310–7.

156. Bieri O. Ultra-Fast Steady State Free Precession and Its Application to In Vivo 1H Morphological and Functional Lung Imaging at 1.5 Tesla. Magn Reson Med. 2013;70:657–63.

157. Martirosian P, Boss A, Schraml C, Schwenzer NF, Graf H, Claussen CD, et al. Magnetic resonance perfusion imaging without contrast media. Eur J Nucl Med Mol Imaging. 2010;37(SUPPL. 1):52–64.

158. Gao Y, Goodnough CL, Erokwu BO, Farr GW, Darrah R, Lu L, et al. Arterial Spin Labeling - Fast Imaging with Steady-State Free Precession (ASL-FISP): A Rapid and Quantitative Perfusion Technique for High Field MRI. NMR Biomed. 2014;27(8):996–1004.

159. Fischer A, Pracht ED, Arnold JFT, Kotas M, Flentje M, Jakob PM. Assessment of pulmonary perfusion in a single shot using SEEPAGE. J Magn Reson Imaging. 2008 Jan;27(1):63–70.

160. Van Beek EJR, Wild JM, Fink C, Moody AR, Kauczor HU, Oudkerk M. MRI for the Diagnosis of Pulmonary Embolism. J Magn Reson Imaging. 2003;18(6):627–40.

161. Bauman G, Scholz A, Rivoire J, Terekhov M, Friedrich J, De Oliveira A, et al. Lung ventilation- and perfusion-weighted Fourier decomposition magnetic resonance imaging: In vivo validation with hyperpolarized 3He and dynamic contrast-enhanced MRI. Magn Reson Med. 2013;69(1):229–37.

162. Bauman G, Puderbach M, Deimling M, Jellus V, Chefd'hotel C, Dinkel J, et al. Non-contrast-enhanced perfusion and ventilation assessment of the human lung by means of Fourier decomposition in proton MRI. Magn Reson Med. 2009;62(3):656–64.

163. Kjørstad Å, Corteville DMR, Fischer A, Henzler T, Schmid-Bindert G, Zöllner FG, et al. Quantitative lung perfusion evaluation using fourier decomposition perfusion MRI. Magn Reson Med. 2014;72(2):558–62.

164. Alexandre J, Saloux E, Dugué AE, Lebon A, Lemaitre A, Roule V, et al. Scar extent evaluated by late gadolinium enhancement CMR: a powerful predictor of long term appropriate ICD therapy in patients with coronary artery disease. J Cardiovasc Magn Reson. 2013;15(1):12.

165. Doltra A, Amundsen BH, Gebker R, Fleck E, Kelle S. Emerging concepts for myocardial late gadolinium enhancement MRI. Curr Cardiol Rev. 2013 Aug 1;9(3):185–90.

166. Swift AJ, Rajaram S, Capener D, Elliot C, Condliffe R, Wild JM, et al. LGE patterns in pulmonary hypertension do not impact overall mortality. JACC Cardiovasc Imaging. 2014 Dec;7(12):1209–17.

167. Blyth KG, Groenning BA, Martin TN, Foster JE, Mark PB, Dargie HJ, et al. Contrast enhanced-cardiovascular magnetic resonance imaging in patients with pulmonary hypertension. Eur Heart J. 2005 Oct 17;26(19):1993–9.

168. Spruijt OA, Vissers L, Bogaard H-J, Hofman MBM, Vonk-Noordegraaf A, Marcus JT. Increased native T1-values at the interventricular insertion regions in precapillary pulmonary hypertension. Int J Cardiovasc Imaging. Springer Netherlands; 2016 Mar 16;32(3):451–9.

169. Jellis CL, Yingchoncharoen T, Gai N, Kusunose K, Popović ZB, Flamm S, et al. Correlation between right ventricular T1 mapping and right ventricular dysfunction in non-ischemic cardiomyopathy. Int J Cardiovasc Imaging. Springer Netherlands; 2017 Mar 29;0(0):0.

170. Swift AJ. Developing the Role of Magnetic Resonance Imaging in Pulmonary Hypertension. University of Sheffield; 2012.

171. Auger WR, Peter Fedullo, Peterson K. Chronic Major-Vessel Thomboembolic Pulmonary Artery Obstruction: Appearance at Anglography. Radiology. 1992;182:393–8.

172. Ogo T. Balloon pulmonary angioplasty for inoperable chronic thromboembolic pulmonary hypertension. Curr Opin Pulm Med. 2015;21(5):p425–31.

173. Andreassen AK, Ragnarsson A, Gude E, Geiran O, Andersen R. Balloon pulmonary angioplasty in patients with inoperable chronic thromboembolic pulmonary hypertension. Heart. 2013;99(19):1415–20.

174. Kataoka M, Inami T, Hayashida K, Shimura N, Ishiguro H, Abe T, et al. Percutaneous transluminal pulmonary angioplasty for the treatment of chronic thromboembolic pulmonary hypertension. Circ Cardiovasc Interv. 2012;5(6):756–62.

175. Fukui S, Ogo T, Morita Y, Tsuji A, Tateishi E, Ozaki K, et al. Right ventricular

reverse remodelling after balloon pulmonary angioplasty. Eur Respir J. 2014;43(5):1394–402.

176. Quadery S, Billings C, Wild J, Swift A, Rajaram S, Davies C, et al. Chronic thrombo-embolic pulmonary hypertension: Long-term outcomes in operated and non-operated patients. Eur Respir J. 2016 Nov 8;48(suppl 60).

177. Hagan G, Southwood M, Treacy C, Ross RM, Soon E, Coulson J, et al. (18)FDG PET imaging can quantify increased cellular metabolism in pulmonary arterial hypertension: A proof-of-principle study. Pulm Circ. 2011;1(4):448–55.

178. Fang W, Zhao L, Xiong C-M, Ni X-H, He Z-X, He J-G, et al. Comparison of 18F-FDG uptake by right ventricular myocardium in idiopathic pulmonary arterial hypertension and pulmonary arterial hypertension associated with congenital heart disease. Pulm Circ. 2012;2(3):365–72.

179. Zhao L, Ashek A, Wang L, Fang W, Dabral S, Dubois O, et al. Heterogeneity in Lung 18FDG Uptake in pulmonary arterial hypertension: Potential of dynamic 18FDG Positron emission tomography with kinetic analysis as a bridging biomarker for pulmonary vascular remodeling targeted treatments. Circulation. 2013;128(11):1214–24.

180. Tatebe S, Fukumoto Y, Oikawa-Wakayama M, Sugimura K, Satoh K, Miura Y, et al. Enhanced [18F]fluorodeoxyglucose accumulation in the right ventricular free wall predicts long-term prognosis of patients with pulmonary hypertension: a preliminary observational study. Eur Heart J Cardiovasc Imaging. 2014 Jun;15(6):666–72.

181. Schlosser T, Nensa F, Mahabadi A a, Poeppel TD. Hybrid MRI/PET of the heart: a new complementary imaging technique for simultaneous acquisition of MRI and PET data. Heart. 2013 Mar 1;99(5):351–2.

182. Rajaram S, Swift AJ, Davies C, Hill C, Jenkins D, Goddard M, et al. Primary pulmonary artery sarcoma and coexisting chronic thromboembolic pulmonary hypertension. Am J Respir Crit Care Med. American Thoracic Society; 2013 Sep 1;188(5):e7-8.

183. Jorge E, Baptista R, Calisto J, Faria H, Monteiro P, Pan M, et al. Optical coherence

tomography of the pulmonary arteries: A systematic review. J Cardiol. 2016;67(1):6–14.

184. Dai Z, Fukumoto Y, Tatebe S, Sugimura K, Miura Y, Nochioka K, et al. OCT Imaging for the Management of Pulmonary Hypertension. JACC Cardiovasc Imaging. 2014 Aug;7(8):843–5.

185. Hou J, Qi H, Zhang M, Meng L, Han Z, Yu B, et al. Pulmonary vascular changes in pulmonary hypertension: optical coherence tomography findings. Circ Cardiovasc Imaging. 2010 May;3(3):344–5.

186. Dai Z, Sugimura K, Fukumoto Y, Tatebe S, Miura Y, Nochioka K, et al. Visualization of Complete Regression of Pulmonary Arterial Remodeling on Optical Coherence Tomography in a Patient With Pulmonary Arterial Hypertension. Circ J. 2014;78(11):2771–3.

187. Tatebe S, Fukumoto Y, Sugimura K, Nakano M, Miyamichi S, Satoh K, et al. Optical Coherence Tomography as a Novel Diagnostic Tool for Distal Type Chronic Thromboembolic Pulmonary Hypertension. Circ J. 2010;74(8):1742–4.

188. Hong C, Wang W, Zhong N, Zeng G, Zhang N. Visualization of Peripheral Pulmonary Artery Red Thrombi Utilizing Optical Coherence Tomography. Korean J Radiol. 2013;14(5):854.

189. Ling Y, Johnson MK, Kiely DG, Condliffe R, Elliot CA, Gibbs JSR, et al. Changing Demographics, Epidemiology, and Survival of Incident Pulmonary Arterial Hypertension. Am J Respir Crit Care Med. 2012 Oct 15;186(8):790–6.

190. Health and Social Care Information Centre NA of PH. National Audit of Pulmonary Hypertension. 2015;(April 2014).

191. McLaughlin V V., Presberg KW, Doyle RL, Abman SH, McCrory DC, Fortin T, et al. Prognosis of Pulmonary Arterial Hypertension*. Chest. 2004 Jul;126(1):78S–92S.

192. Miyamoto S, Nagaya N, Satoh T, Kyotani S, Sakamaki F, Fujita M, et al. Clinical correlates and prognostic significance of six-minute walk test in patients with primary pulmonary hypertension. Comparison with cardiopulmonary exercise

testing. Am J Respir Crit Care Med. 2000 Feb;161(2 Pt 1):487–92.

193. Sitbon O, Humbert M, Nunes H, Parent F, Garcia G, Hervé P, et al. Long-term intravenous epoprostenol infusion in primary pulmonary hypertension. J Am Coll Cardiol. 2002 Aug;40(4):780–8.

194. Billings CG, Hurdman JA, Condliffe R, Elliot CA, Smith IA, Austin M, et al. Incremental shuttle walk test distance and autonomic dysfunction predict survival in pulmonary arterial hypertension. J Heart Lung Transplant. 2017 Aug;36(8):871–9.

195. Rubin LJ. The 6-minute walk test in pulmonary arterial hypertension: how far is enough? Am J Respir Crit Care Med. 2012 Sep 1;186(5):396–7.

196. Demir R, Küçükoğlu MS. Six-minute walk test in pulmonary arterial hypertension. Anatol J Cardiol. 2015 Mar;15(3):249–54.

197. Forfia PR, Fisher MR, Mathai SC, Housten-Harris T, Hemnes AR, Borlaug BA, et al. Tricuspid Annular Displacement Predicts Survival in Pulmonary Hypertension. Am J Respir Crit Care Med. 2006 Nov 1;174(9):1034–41.

198. Tei C, Dujardin KS, Hodge DO, Bailey KR, McGoon MD, Tajik AJ, et al. Doppler echocardiographic index for assessment of global right ventricular function. J Am Soc Echocardiogr. 1996;9(6):838–47.

199. Yeo TC, Dujardin KS, Tei C, Mahoney DW, McGoon MD, Seward JB. Value of a Doppler-Derived index combining systolic and diastolic time intervals in predicting outcome in primary pulmonary hypertension. Am J Cardiol. 1998;81(9):1157–61.

200. Raymond RJ, Hinderliter AL, Willis PW, Ralph D, Caldwell EJ, Williams W, et al. Echocardiographic predictors of adverse outcomes in primary pulmonary hypertension. J Am Coll Cardiol. 2002 Apr;39(7):1214–9.

201. Nagaya N, Nishikimi T, Uematsu M, Satoh T, Kyotani S, Sakamaki F, et al. Plasma brain natriuretic peptide as a prognostic indicator in patients with primary pulmonary hypertension. Circulation. 2000;102:865–70.

202. van Wolferen SA, van de Veerdonk MC, Mauritz G-J, Jacobs W, Marcus JT,

Marques KMJ, et al. Clinically Significant Change in Stroke Volume in Pulmonary Hypertension. Chest. 2011 May;139(5):1003–9.

203. Peacock AJ, Vonk Noordegraaf A. Cardiac magnetic resonance imaging in pulmonary arterial hypertension. Eur Respir Rev. 2013;22(130):526–34.

204. Swift AJ, Rajaram S, Campbell MJ, Hurdman J, Thomas S, Capener D, et al. Prognostic value of cardiovascular magnetic resonance imaging measurements corrected for age and sex in idiopathic pulmonary arterial hypertension. Circ Cardiovasc Imaging. 2014 Jan 1;7(1):100–6.

205. Baggen VJM, Leiner T, Post MC, van Dijk AP, Roos-Hesselink JW, Boersma E, et al. Cardiac magnetic resonance findings predicting mortality in patients with pulmonary arterial hypertension: a systematic review and meta-analysis. Eur Radiol. European Radiology; 2016 Nov 4;26(11):3771–80.

206. Boucly A, Weatherald J, Savale L, Jaïs X, Cottin V, Prevot G, et al. Risk assessment, prognosis and guideline implementation in pulmonary arterial hypertension. Eur Respir J. 2017 Aug 3;50(2):1700889.

207. Gan CT-J, Lankhaar J-W, Westerhof N, Marcus JT, Becker A, Twisk JWR, et al. Noninvasively assessed pulmonary artery stiffness predicts mortality in pulmonary arterial hypertension. Chest. 2007 Dec;132(6):1906–12.

208. Swift AJ, Rajaram S, Condliffe R, Capener D, Hurdman J, Elliot C, et al. Pulmonary artery relative area change detects mild elevations in pulmonary vascular resistance and predicts adverse outcome in pulmonary hypertension. Invest Radiol. 2012 Oct;47(10):571–7.

209. Hagger D, Condliffe R, Woodhouse N, Elliot CA, Armstrong IJ, Davies C, et al. Ventricular mass index correlates with pulmonary artery pressure and predicts survival in suspected systemic sclerosis-associated pulmonary arterial hypertension. Rheumatology (Oxford). 2009 Sep;48(9):1137–42.

210. RAJARAM S, SWIFT AJ, CAPENER D, ELLIOT CA, CONDLIFFE R, DAVIES C, et al. Comparison of the Diagnostic Utility of Cardiac Magnetic Resonance Imaging, Computed Tomography, and Echocardiography in Assessment of Suspected Pulmonary Arterial Hypertension in Patients with Connective Tissue Disease. J

Rheumatol. 2012 Jun 1;39(6):1265–74.

211. Freed BH, Gomberg-Maitland M, Chandra S, Mor-Avi V, Rich S, Archer SL, et al. Late gadolinium enhancement cardiovascular magnetic resonance predicts clinical worsening in patients with pulmonary hypertension. J Cardiovasc Magn Reson. 2012 Feb 1;14:11.

212. Swift AJ, Telfer A, Rajaram S, Condliffe R, Marshall H, Capener D, et al. Dynamic Contrast–Enhanced Magnetic Resonance Imaging in Patients with Pulmonary Arterial Hypertension. Pulm Circ. 2014 Mar;4(1):61–70.

213. Dawes TJW, de Marvao A, Shi W, Fletcher T, Watson GMJ, Wharton J, et al. Machine Learning of Three-dimensional Right Ventricular Motion Enables Outcome Prediction in Pulmonary Hypertension: A Cardiac MR Imaging Study. Radiology. 2017 May;283(2):381–90.

214. Poor HD, Kawut SM, Liu C-Y, Smith BM, Hoffman EA, Lima JA, et al. Pulmonary hyperinflation due to gas trapping and pulmonary artery size: The MESA COPD Study. PLoS One. 2017;12(5):e0176812.

215. Maruoka Y, Nagao M, Baba S, Isoda T, Kitamura Y, Yamazaki Y, et al. Three-dimensional fractal analysis of 99mTc-MAA SPECT images in chronic thromboembolic pulmonary hypertension for evaluation of response to balloon pulmonary angioplasty: association with pulmonary arterial pressure. Nucl Med Commun. 2017 Jun;38(6):480–6.

216. Jacob J, Bartholmai BJ, Rajagopalan S, Karwoski R, Nair A, Walsh SLF, et al. Likelihood of pulmonary hypertension in patients with idiopathic pulmonary fibrosis and emphysema. Respirology. 2017 Dec 13;2017(November).

217. Johns CS, Rajaram S, Capener DA, Oram C, Elliot C, Condliffe R, et al. Non-invasive methods for estimating mPAP in COPD using cardiovascular magnetic resonance imaging. Eur Radiol. 2017 Nov 16;

218. Lungu A, Wild JM, Capener D, Kiely DG, Swift AJ, Hose DR. MRI model-based non-invasive differential diagnosis in pulmonary hypertension. J Biomech. 2014 Sep 22;47(12):2941–7.

219. Spazzapan M, Sastry P, Dunning J, Nordsletten D, de Vecchi A. The Use of Biophysical Flow Models in the Surgical Management of Patients Affected by Chronic Thromboembolic Pulmonary Hypertension. Front Physiol. 2018 Mar 13;9(MAR):1–13.

220. Swift AJ, Capener D, Johns C, Hamilton N, Rothman A, Elliot C, et al. Magnetic Resonance Imaging in the Prognostic Evaluation of Patients with Pulmonary Arterial Hypertension. Am J Respir Crit Care Med. 2017 Jul 15;196(2):228–39.

221. Mathai SC. Precision medicine in pulmonary hypertension: Start with the end (point). Int J Cardiol. Elsevier B.V.; 2018;257:339–40.

222. Hadinnapola C, Bleda M, Haimel M, Screaton N, Swift A, Dorfmüller P, et al. Phenotypic Characterization ofEIF2AK4Mutation Carriers in a Large Cohort of Patients Diagnosed Clinically With Pulmonary Arterial Hypertension. Circulation. 2017;136(21):2022–33.

223. Simonneau G, Rubin LJ, Galiè N, Barst RJ, Fleming TR, Frost AE, et al. Addition of sildenafil to long-term intravenous epoprostenol therapy in patients with pulmonary arterial hypertension: a randomized trial. Ann Intern Med. 2008 Oct 21;149(8):521–30.

224. Barst RJ, Rubin LJ, Long WA, McGoon MD, Rich S, Badesch DB, et al. A comparison of continuous intravenous epoprostenol (prostacyclin) with conventional therapy for primary pulmonary hypertension. N Engl J Med. 1996 Feb 1;334(5):296–301.

225. Billings C, Hurdman J, Condliffe R, Armstrong I, Smith I, Elliot C, et al. S121 The Utility Of The Incremental Shuttle Walking Test In Pulmonary Hypertension: Results From The Aspire Registry. Thorax. 2014 Dec 1;69(Suppl 2):A65–A65.

226. Leuchte HH, Holzapfel M, Baumgartner RA, Neurohr C, Vogeser M, Behr J. Characterization of Brain Natriuretic Peptide in Long-term Follow-up of Pulmonary Arterial Hypertension. Chest. 2005 Oct;128(4):2368–74.

227. Casserly B, Klinger JR. Brain natriuretic peptide in pulmonary arterial hypertension: biomarker and potential therapeutic agent. Drug Des Devel Ther. 2009 Dec 29;3:269–87.

228. van de Veerdonk MC, Marcus JT, Westerhof N, de Man FS, Boonstra A, Heymans MW, et al. Signs of Right Ventricular Deterioration in Clinically Stable Patients With Pulmonary Arterial Hypertension. Chest. 2015 Apr;147(4):1063–71.

229. Mazurek JA, Vaidya A, Mathai SC, Roberts JD, Forfia PR. Follow-up tricuspid annular plane systolic excursion predicts survival in pulmonary arterial hypertension. Pulm Circ. 2017;7(2):361–71.

230. Wright LM, Dwyer N, Celermajer D, Kritharides L, Marwick TH. Follow-Up of Pulmonary Hypertension With Echocardiography. JACC Cardiovasc Imaging. 2016;9(6):733–46.

231. Bossone E, D'Andrea A, D'Alto M, Citro R, Argiento P, Ferrara F, et al. Echocardiography in Pulmonary Arterial Hypertension: from Diagnosis to Prognosis. J Am Soc Echocardiogr. Elsevier Inc; 2013 Jan;26(1):1–14.

232. Yorke J, Corris P, Gaine S, Gibbs JSR, Kiely DG, Harries C, et al. emPHasis-10: development of a health-related quality of life measure in pulmonary hypertension. Eur Respir J. 2014 Apr 1;43(4):1106–13.

233. Hundley WG, Bluemke DA, Finn JP, Flamm SD, Fogel MA, Friedrich MG, et al. ACCF/ACR/AHA/NASCI/SCMR 2010 Expert Consensus Document on Cardiovascular Magnetic Resonance. J Am Coll Cardiol. 2010 Jun;55(23):2614–62.

234. NHS Digital. National Audit of Pulmonary Hypertension - 7th Annual Report, April 2015 to March 2016. Clinical Audits and Registries Management Service. 2017. 44 p.

235. Bluemke DA, Kronmal RA, Lima JAC, Liu K, Olson J, Burke GL, et al. The relationship of left ventricular mass and geometry to incident cardiovascular events: the MESA (Multi-Ethnic Study of Atherosclerosis) study. J Am Coll Cardiol. American College of Cardiology Foundation; 2008 Dec 16;52(25):2148–55.

236. Gan CT, Lankhaar J, Marcus JT, Westerhof N, Marques KM, Bronzwaer JGF, et al. Impaired left ventricular filling due to right-to-left ventricular interaction in patients with pulmonary arterial hypertension. 2006;1528–33.

237. Jiamsripong P, Honda T, Reuss CS, Hurst RT, Chaliki HP, Grill DE, et al. Three methods for evaluation of left atrial volume. Eur J Echocardiogr. 2008 May;9(3):351–5.

238. van Beek EJR, Tiel-van Buul MMC, Büller HR, van Royen EA, ten Cate JW, Buller HR, et al. The value of lung scintigraphy in the diagnosis of pulmonary embolism. Eur J Nucl Med. 1993 Feb;20(2):173–81.

239. Aune E, Baekkevar M, Roislien J, Rodevand O, Otterstad JE. Normal reference ranges for left and right atrial volume indexes and ejection fractions obtained with real-time three-dimensional echocardiography. Eur J Echocardiogr. 2009;10(6):738–44.

240. Skrok J, Shehata ML, Mathai S, Girgis RE, Zaiman A, Mudd JO, et al. Pulmonary arterial hypertension: MR imaging-derived first-pass bolus kinetic parameters are biomarkers for pulmonary hemodynamics, cardiac function, and ventricular remodeling. Radiology. 2012 Jun;263(3):678–87.

241. Lang RM, Badano LP, Mor-Avi V, Afilalo J, Armstrong A, Ernande L, et al. Recommendations for cardiac chamber quantification by echocardiography in adults: an update from the American Society of Echocardiography and the European Association of Cardiovascular Imaging. Eur Heart J Cardiovasc Imaging. Elsevier Inc; 2015 Mar;16(3):233–70.

242. D'Alto M, Romeo E, Argiento P, D'Andrea A, Vanderpool R, Correra A, et al. Accuracy and precision of echocardiography versus right heart catheterization for the assessment of pulmonary hypertension. Int J Cardiol. Elsevier Ireland Ltd; 2013 Oct 9;168(4):4058–62.

243. Janda S, Shahidi N, Gin K, Swiston J. Diagnostic accuracy of echocardiography for pulmonary hypertension: a systematic review and meta-analysis. Heart. 2011 Apr 15;97(8):612–22.

244. Arcasoy SM, Christie JD, Ferrari VA, Sutton MSJ, Zisman DA, Blumenthal NP, et al. Echocardiographic Assessment of Pulmonary Hypertension in Patients with Advanced Lung Disease. Am J Respir Crit Care Med. American Thoracic Society; 2003 Mar 1;167(5):735–40.

245. Hurdman J, Condliffe R, Elliot CA, Davies C, Hill C, Wild JM, et al. ASPIRE registry: Assessing the Spectrum of Pulmonary hypertension Identified at a REferral centre. Eur Respir J. 2012 Apr;39(4):945–55.

246. Roeleveld RJ, Marcus JT, Boonstra A, Postmus PE, Marques KM, Bronzwaer JGF, et al. A comparison of noninvasive MRI-based methods of estimating pulmonary artery pressure in pulmonary hypertension. J Magn Reson Imaging. 2005 Jul;22(1):67–72.

247. Sanz J, Kuschnir P, Rius T, Salguero R, Sulica R, Einstein AJ, et al. Pulmonary Arterial Hypertension: Noninvasive Detectio nwith Phase-Contrast MR Imaging. Radiology. 2007 Apr;243(1):70–9.

248. García-Alvarez A, Fernández-Friera L, Mirelis JG, Sawit S, Nair A, Kallman J, et al. Non-invasive estimation of pulmonary vascular resistance with cardiac magnetic resonance. Eur Heart J. 2011 Oct;32(19):2438–45.

249. Moral S, Fernández-Friera L, Stevens G, Guzman G, García-Alvarez A, Nair A, et al. New index alpha improves detection of pulmonary hypertension in comparison with other cardiac magnetic resonance indices. Int J Cardiol. Elsevier Ireland Ltd; 2012 Nov;161(1):25–30.

250. Fisher MR, Criner GJ, Fishman AP, Hassoun PM, Minai OA, Scharf SM, et al. Estimating pulmonary artery pressures by echocardiography in patients with emphysema. Eur Respir J. 2007 Nov 1;30(5):914–21.

251. Mooij CF, de Wit CJ, Graham DA, Powell AJ, Geva T. Reproducibility of MRI measurements of right ventricular size and function in patients with normal and dilated ventricles. J Magn Reson Imaging. 2008 Jul;28(1):67–73.

252. Bradlow WM, Hughes ML, Keenan NG, Bucciarelli-Ducci C, Assomull R, Gibbs JSR, et al. Measuring the heart in pulmonary arterial hypertension (PAH): implications for trial study size. J Magn Reson Imaging. 2010 Jan;31(1):117–24.

253. Gan CT-J, Holverda S, Marcus JT, Paulus WJ, Marques KM, Bronzwaer JGF, et al. Right Ventricular Diastolic Dysfunction and the Acute Effects of Sildenafil in Pulmonary Hypertension Patients. Chest. 2007 Jul;132(1):11–7.

254. Roeleveld RJ, Vonk-Noordegraaf A, Marcus JT, Bronzwaer JGF, Marques KMJ, Postmus PE, et al. Effects of Epoprostenol on Right Ventricular Hypertrophy and Dilatation in Pulmonary Hypertension. Chest. 2004 Feb;125(2):572–9.

255. Crawley SF, Johnson MK, Dargie HJ, Peacock AJ, Mbchb SFC, Johnson MK, et al. LA volume by CMR distinguishes idiopathic from pulmonary hypertension due to Hfpef. JACC Cardiovasc Imaging. American College of Cardiology Foundation; 2013;6(10):1120–1.

256. D'Alto M, Romeo E, Argiento P, Pavelescu A, Mélot C, D'Andrea A, et al. Echocardiographic prediction of pre- versus postcapillary pulmonary hypertension. J Am Soc Echocardiogr. 2015;28(1):108–15.

257. Swift AJ, Rajaram S, Condliffe R, Capener D, Hurdman J, Elliot CA, et al. Diagnostic accuracy of cardiovascular magnetic resonance imaging of right ventricular morphology and function in the assessment of suspected pulmonary hypertension results from the ASPIRE registry. J Cardiovasc Magn Reson. 2012 Jan;14(1):40.

258. Whitlock M, Garg A, Gelow J, Jacobson T, Broberg C. Comparison of Left and Right Atrial Volume by Echocardiography Versus Cardiac Magnetic Resonance Imaging Using the Area-Length Method. Am J Cardiol. Elsevier Inc.; 2010 Nov;106(9):1345–50.

259. Vachiéry J-L, Adir Y, Barberà A, Champion H, Coghlan G, Cottin V, et al. Pulmonary hypertension due to left heart diseases. J Am Coll Cardiol. 2013 Dec 24;62(25 Suppl):D100-8.

260. Freed BH, Collins JD, François CJ, Barker AJ, Cuttica MJ, Chesler NC, et al. MR and CT Imaging for the Evaluation of Pulmonary Hypertension. JACC Cardiovasc Imaging. 2016 Jun;9(6):715–32.

261. Leung CC, Moondra V, Catherwood E, Andrus BW. Prevalence and risk factors of pulmonary hypertension in patients with elevated pulmonary venous pressure and preserved ejection fraction. Am J Cardiol. Elsevier Inc.; 2010;106(2):284–6.

262. Tampakakis E, Tedford RJ. Balancing the positives and negatives of the diastolic

pulmonary gradient. Eur J Hear Fail Suppl. 2017;19(1):98–100.

263. Nagy AI, Venkateshvaran A, Merkely B, Lund LH, Manouras A. Determinants and prognostic implications of the negative diastolic pulmonary pressure gradient in patients with pulmonary hypertension due to left heart disease. Eur J Heart Fail. 2017 Jan;19(1):88–97.

264. Bitar A, Selej M, Bolad I, Lahm T. Poor Agreement between Pulmonary Capillary Wedge Pressure and Left Ventricular End-Diastolic Pressure in a Veteran Population. Abbate A, editor. PLoS One. 2014 Jan 31;9(1):e87304.

265. Halpern SD, Taichman DB. Misclassification of Pulmonary Hypertension Due to Reliance on Pulmonary Capillary Wedge Pressure Rather Than Left Ventricular End-Diastolic Pressure. Chest. 2009 Jul;136(1):37–43.

266. Guazzi MDM, Vicenzi M, Arena R, Guazzi MDM. Pulmonary Hypertension in Heart Failure With Preserved Ejection Fraction: A Target of Phosphodiesterase-5 Inhibition in a 1-Year Study. Circulation. 2011 Jul 12;124(2):164–74.

267. Cottin V. Combined pulmonary fibrosis and emphysema: a distinct underrecognised entity. Eur Respir J. 2005;26(4):586–93.

268. Hansell DM, Bankier AA, MacMahon H, McLoud TC, Müller NL, Remy J. Fleischner Society: Glossary of Terms for Thoracic Imaging. Radiology. 2008 Mar;246(3):697–722.

269. Weir-McCall JR, Liu-Shiu-Cheong PS, Struthers AD, Lipworth BJ, Houston JG. Pulmonary arterial stiffening in COPD and its implications for right ventricular remodelling. Eur Radiol. European Radiology; 2018 Feb 27;103(Suppl 1):A21 LP-A21.

270. Wells JM, Bhatt SP, Gupta H, Denney TS, Lloyd SG, Dell'Italia LJ, et al. Cardiac MRI Detects Alterations In Right Ventricular Preload In Subjects With COPD And A PA:A ratio >1. In: B22 CHRONIC OBSTRUCTIVE PULMONARY DISEASE: UNDERSTANDING THE LUNG AND HEART INTERACTION. American Thoracic Society; 2013. p. A2421–A2421. (American Thoracic Society International Conference Abstracts).

271. Kim NH, Delcroix M, Jenkins DP, Channick R, Dartevelle P, Jansa P, et al. Chronic thromboembolic pulmonary hypertension. J Am Coll Cardiol. 2013;62(25 Suppl):D92-9.

272. Reinartz P, Wildberger JE, Schaefer W, Nowak B, Mahnken AH, Buell U. Tomographic imaging in the diagnosis of pulmonary embolism: a comparison between V/Q lung scintigraphy in SPECT technique and multislice spiral CT. J Nucl Med. 2004;45(9):1501–8.

273. Korosec FR, Frayne R, Grist TM, Mistretta CA. Time-resolved contrast-enhanced 3D MR angiography. Magn Reson Med. 1996 Sep;36(3):345–51.

274. McHugh ML. Interrater reliability: the kappa statistic. Biochem Medica. Croatian Society of Medical Biochemistry and Laboratory Medicine; 2012 Oct 15;22(3):276–82.

275. Stein PD, Chenevert TL, Fowler SE, Goodman LR, Gottschalk A, Hales C a, et al. Gadolinium-Enhanced Magnetic Resonance Angiography for Pulmonary Embolism: A Multicenter Prospective Study (PIOPED III). Ann Intern Med. 2010;152(7):434–43.

276. Schiebler ML, Nagle SK, François CJ, Repplinger MD, Hamedani AG, Vigen KK, et al. Effectiveness of MR angiography for the primary diagnosis of acute pulmonary embolism: Clinical outcomes at 3 months and 1 year. J Magn Reson Imaging. 2013 Oct;38(4):914–25.

277. Oudkerk M, van Beek EJ, Wielopolski P, van Ooijen PM, Brouwers-Kuyper EM, Bongaerts AH, et al. Comparison of contrast-enhanced magnetic resonance angiography and conventional pulmonary angiography for the diagnosis of pulmonary embolism: a prospective study. Lancet. 2002;359(9318):1643–7.

278. Nagle SK, Schiebler ML, Repplinger MD, François CJ, Vigen KK, Yarlagadda R, et al. Contrast enhanced pulmonary magnetic resonance angiography for pulmonary embolism: Building a successful program. Eur J Radiol. 2016 Mar;85(3):553–63.

279. Cuenod CA, Balvay D. Perfusion and vascular permeability: Basic concepts and measurement in DCE-CT and DCE-MRI. Diagn Interv Imaging. Elsevier Masson

SAS; 2013;94(12):1187–204.

280. Østergaard L, Weisskoff R, Chesler D, Gyldensted C, Rosen BR. High resolution measurement of cerebral blood flow using intravascular tracer bolus passages. Part I: Mathematical approach and statistical analysis. Magn Reson Med. 1996;36:715–25.

281. Ingrisch M, Dietrich O, Attenberger UI, Nikolaou K, Sourbron S, Reiser MF, et al. Quantitative Pulmonary Perfusion Magnetic Resonance Imaging. Invest Radiol. 2010 Jan;45(1):7–14.

282. Quadery S, Swift A, Billings C, Thompson A, Elliot C, Hurdman J, et al. Impact of patient choice on survival in patients with chronic thromboembolic pulmonary hypertension offered pulmonary endarterectomy. In: British Thoracic Society Winter Meeting 2017. London, UK; 2017.

283. Strange G, Playford D, Stewart S, Deague JA, Nelson H, Kent A, et al. Pulmonary hypertension: prevalence and mortality in the Armadale echocardiography cohort. Heart. 2012 Dec;98(24):1805–11.

284. Ghio S, Gavazzi A, Campana C, Inserra C, Klersy C, Sebastiani R, et al. Independent and additive prognostic value of right ventricular systolic function and pulmonary artery pressure in patients with chronic heart failure. J Am Coll Cardiol. Elsevier Masson SAS; 2001 Jan;37(1):183–8.

285. Abraham WT, Adamson PB, Bourge RC, Aaron MF, Costanzo MR, Stevenson LW, et al. Wireless pulmonary artery haemodynamic monitoring in chronic heart failure: a randomised controlled trial. Lancet (London, England). 2011 Feb 19;377(9766):658–66.

286. Yancy CW, Lopatin M, Stevenson LW, De Marco T, Fonarow GC, ADHERE Scientific Advisory Committee and Investigators. Clinical presentation, management, and in-hospital outcomes of patients admitted with acute decompensated heart failure with preserved systolic function: a report from the Acute Decompensated Heart Failure National Registry (ADHERE) Database. J Am Coll Cardiol. Elsevier Masson SAS; 2006 Jan 3;47(1):76–84.

287. Tribouilloy C, Rusinaru D, Mahjoub H, Soulière V, Lévy F, Peltier M, et al.

Prognosis of heart failure with preserved ejection fraction: a 5 year prospective population-based study. Eur Heart J. 2008 Feb;29(3):339–47.

288. Tsuchihashi-Makaya M, Hamaguchi S, Kinugawa S, Yokota T, Goto D, Yokoshiki H, et al. Characteristics and outcomes of hospitalized patients with heart failure and reduced vs preserved ejection fraction. Report from the Japanese Cardiac Registry of Heart Failure in Cardiology (JCARE-CARD). Circ J. 2009 Oct;73(10):1893–900.

289. Melenovsky V, Hwang S-J, Lin G, Redfield MM, Borlaug BA. Right heart dysfunction in heart failure with preserved ejection fraction. Eur Heart J. 2014;35(48):3452–62.

290. Abraham WT, Stevenson LW, Bourge RC, Lindenfeld JA, Bauman JG, Adamson PB, et al. Sustained efficacy of pulmonary artery pressure to guide adjustment of chronic heart failure therapy: complete follow-up results from the CHAMPION randomised trial. Lancet (London, England). Elsevier Ltd; 2016 Jan 30;387(10017):453–61.

291. Handoko ML, De Man FS, Oosterveer FPT, Bogaard HH, Vonk-Noordegraaf A, Westerhof N, et al. A critical appraisal of transpulmonary and diastolic pressure gradients. Physiol Rep. 2016 Sep 1;4(17):e12910.

292. Behling A, Rohde LE, Colombo FC, Goldraich LA, Stein R, Clausell N. Effects of 5'-phosphodiesterase four-week long inhibition with sildenafil in patients with chronic heart failure: a double-blind, placebo-controlled clinical trial. J Card Fail. 2008 Apr;14(3):189–97.

293. Sueta CA, Gheorghiade M, Adams KF, Bourge RC, Murali S, Uretsky BF, et al. Safety and efficacy of epoprostenol in patients with severe congestive heart failure. Am J Cardiol. 1995 Jan;75(3):34A–43A.

294. Hussain N, Ramjug S, Billings C, Hurdman J, Elliot C, Condliffe R, et al. P168 Reduced Gas Transfer (tlco) Predicts Poor Outcome In Patients With Pulmonary Hypertension And Heart Failure With Preserved Ejection Fraction. Thorax. 2014 Dec 1;69(Suppl 2):A148–A148.

295. Minai OA, Chaouat A, Adnot S. Pulmonary Hypertension in COPD: Epidemiology,

Significance, and Management. Chest. 2010 Jun;137(6):39S–51S.

296. Hyduk A, Croft JB, Ayala C, Zheng K, Zheng Z-J, Mensah GA. Pulmonary hypertension surveillance--United States, 1980-2002. MMWR Surveill Summ. 2005 Nov 11;54(5):1–28.

297. Boerrigter BG, Bogaard HJ, Trip P, Groepenhoff H, Rietema H, Holverda S, et al. Ventilatory and Cardiocirculatory Exercise Profiles in COPD. Chest. 2012 Nov;142(5):1166–74.

298. Hurdman J, Condliffe R, Elliot C a., Swift A, Rajaram S, Davies C, et al. Pulmonary hypertension in COPD: results from the ASPIRE registry. Eur Respir J. 2013 Jun;41(6):1292–301.

299. Andrew Swift, Angela Lungu, Henry Walker, Dave Capener, Charlotte Hammerton, Charlie Elliot, Robin Condliffe, David Kiely JW. Improved diagnostic accuracy of MRI in patients with suspected pulmonary hypertension with combined right ventricle and pulmonary artery metrics. In: ERS international Congress 2015. 2015.

300. DeCamp MM, Lipson D, Krasna M, Minai O a, McKenna RJ, Thomashow BM. The Evaluation and Preparation of the Patient for Lung Volume Reduction Surgery. Proc Am Thorac Soc. 2008 May 1;5(4):427–31.

301. Meyers BF. Chronic obstructive pulmonary disease * 10: Bullectomy, lung volume reduction surgery, and transplantation for patients with chronic obstructive pulmonary disease. Thorax. 2003 Jul 1;58(7):634–8.

302. Swift AJ, Wild JM, Fichele S, Woodhouse N, Fleming S, Waterhouse J, et al. Emphysematous changes and normal variation in smokers and COPD patients using diffusion 3He MRI. Eur J Radiol. 2005 Jun;54(3):352–8.

303. Regan E a, Hokanson JE, Murphy JR, Lynch D a, Beaty TH, Curran-everett D, et al. Genetic Epidemiology of COPD (COPDGene) Study Design. Epidemiology. 2011;7(1):1–10.

304. Hoffman EA, Ahmed FS, Baumhauer H, Budoff M, Jeffrey Carr J, Kronmal R, et al. Variation in the percent of emphysema-like lung in a healthy, nonsmoking

multiethnic sample. The MESA Lung Study. Ann Am Thorac Soc. 2014;11(6):951–5.

305. Matsuoka S, Washko GR, Yamashiro T, Estepar RSJ, Diaz A, Silverman EK, et al. Pulmonary hypertension and computed tomography measurement of small pulmonary vessels in severe emphysema. Am J Respir Crit Care Med. 2010;181(3):218–25.

306. Matsuoka S, Washko GR, Dransfield MT, Yamashiro T, San R, Estepar J, et al. Quantitative CT Measurement of Cross-sectional Area of Small Pulmonary Vessel in COPD: Correlations with Emphysema and Airflow Limitation. Acad Radiol. 2010;17(1):93–9.

307. Suzuki Y, Yoshimura K, Uto T, Sato J, Imokawa S, Suda T. Morphological changes in small pulmonary vessels are associated with severe acute exacerbation in chronic obstructive pulmonary disease. Int J Chron Obstruct Pulmon Dis. 2016 Jun;Volume 11:1435–45.

308. Estépar RSJ, Kinney GL, Black-Shinn JL, Bowler RP, Kindlmann GL, Ross JC, et al. Computed Tomographic Measures of Pulmonary Vascular Morphology in Smokers and Their Clinical Implications. Am J Respir Crit Care Med. 2013 Jul 15;188(2):231–9.

309. Rahaghi F, Come C, Ross J, Harmouche R, Diaz A, Estépar RSJ, et al. Morphologic Response of the Pulmonary Vasculature to Endoscopic Lung Volume Reduction. Chronic Obstr Pulm Dis J COPD Found. 2015;2(3):214–22.

310. Aaron CP, Hoffman EA, Lima JAC, Kawut SM, Bertoni AG, Vogel-Claussen J, et al. Pulmonary vascular volume, impaired left ventricular filling and dyspnea: The MESA Lung Study. PLoS One. 2017;12(4):e0176180.

311. Galbán CJ, Han MK, Boes JL, Chughtai KA, Meyer CR, Johnson TD, et al. Computed tomography–based biomarker provides unique signature for diagnosis of COPD phenotypes and disease progression. Nat Med. Nature Publishing Group, a division of Macmillan Publishers Limited. All Rights Reserved.; 2012 Oct 7;18:1711.

312. Coste F, Dournes G, Dromer C, Blanchard E, Freund-Michel V, Girodet P, et al. CT

evaluation of small pulmonary vessels area in patients with COPD with severe pulmonary hypertension. Thorax. 2016;71(9):830–7.

313. Johns CS, Wild JM, Rajaram S, Swift AJ, Kiely DG. Current and emerging imaging techniques in the diagnosis and assessment of pulmonary hypertension. Expert Rev Respir Med. 2018 Feb 6;12(2):145–60.

314. Lang IM, Madani M. Update on chronic thromboembolic pulmonary hypertension. Circulation. 2014;130(6):508–18.